Institut national de la recherche scientifique
Centre Eau Terre Environnement

Geochemical and petrogenetic comparison between the VMS-endowed Blake River Group and the VMS-poor Stoughton-Roquemaure assemblage, Abitibi greenstone belt

Comparaison géochimique et pétrogénétique entre le Groupe de Blake River et l'assemblage de Stoughton-Roquemaure, ceinture de roches vertes de l'Abitibi

By

Octavio Vite-Sánchez

Thesis submitted for the degree of

Philosophiae Doctor (Ph.D.)

In Earth Sciences

Evaluation jury

President of the jury and internal examiner	Marc Richer-Laflèche INRS-ETE, Canada
External examiner	Jussi Sakari Heinonen Åbo Akademi University, Finland
External examiner	Steven Philip Hollis University of Edinburgh, Scotland
Research supervisor	Pierre-Simon Ross INRS-ETE, Canada
Research co-supervisor	Patrick Mercier -Langevin Agnico Eagle Mines Limited, Canada and associate professor, INRS

ACKNOWLEDGEMENTS

The culmination of this work is the result of a collective effort from many people, more than I can mention here. Even if your contribution was as small as giving support on a single day, I take it as part of the Journey.

First and foremost, I want to express my deepest gratitude to my supervisors. To Pierre-Simon Ross, thank you for giving me the opportunity to pursue my studies. Your professionalism, commitment, efficiency, and depth of knowledge are admirable and will always be part of my academic foundation. The time spent in the field, our stimulating discussions, guidance, and your thoughtful comments on manuscripts constantly pushed me to improve the quality of my work. Your constant support throughout my PhD, especially during personal difficulties, is something for which I am profoundly grateful.

To Patrick Mercier-Langevin, I am equally thankful for welcoming me into this project. Your expertise and thoughtful insights have been a constant source of learning, always bringing clarity and direction that strengthened this research. I deeply appreciate your remarkable patience, support and kind words during difficult moments.

This project is part of the Metal Earth Research Center at Laurentian University, funded by the Canada First Research Excellence Fund and federal/provincial/industry partners, with grants awarded to P.-S. Ross. Their support made possible my conference attendance, scholarships, fieldwork, and analytical work.

Thanks to the entire Metal Earth research group—their feedback during meetings was invaluable for completing this project. I am especially grateful to Taus Jorgensen and Harold Gibson for discussions and for providing GIS data essential to this study. Thanks also to Caroline Bélanger and Enza Magnier for assistance with data compilation, and to Ministère des Ressources naturelles et des Forêts for field support, especially Mélanie Beaudette and Yannick Daoudene. Thanks to Kieran Iles for the validation and support in the modeling and continuation of this work.

I owe special thanks to a critical part of this project: Dana, my wife, my love, my best friend, my pillar, my blessing. This work exists because you are part of my very being. Thank you for taking care of me, for your love, for your immense patience, for always helping me refocus, for your good advice, and for your beautiful voice. After more than a dozen years together, we have faced so much, yet here you are, still supporting me and being my perfect companion. Thank you also

because, during this project, we welcomed our beautiful baby Leonel into the world. You are without doubt a divine gift from God to me.

Thanks to all the people who made us feel at home in Québec: Yeni, Alex, Lemuel, Gisselle, Lemuelito, Mario, Flor, Bárbara, Adrián, Jessica, Charles, Victoria, Isaque, Giordana, and of course the wonderful community of the Quebec Baptist Church. You were all a true blessing for my family.

Thanks also to my colleagues at INRS for their support and for the friendly environment: Guillaume, Paolo, Grégoire, Alexander, Sophie, Zahoor.

I want to express my deep thanks to my family, but I want to do it in Spanish as most of them do not speak English:

Gracias a mi madre Adriana, tu cariño y tu inmensa dedicación para cuidarme desde pequeño es algo tremendamente hermoso y que van siempre conmigo, eres una inspiración en todo lo que hago. Hermano Reynaldo, tu siempre serás mi mejor amigo. En ti siento un apoyo incondicional y mucho de lo que soy es porque tu existes. Gracias.

Gracias a mi abuelita Tomasa quien ha sido como una segunda mama. Tu educación, constancia, apoyo y consejos han sido fundamentales para que yo sea la persona que soy hoy. También agradezco a mis tíos Ray, Óscar y Paola, que siempre me han mostrado su apoyo, especialmente al estar junto a mi mamá y mi abuelita. Cada cosa que hacen por ellas es también una ayuda para mí.

Gracias a la familia de Dana: a mi suegra Areli, quien nos apoya siempre y nos ayudó tanto con nuestro bebé, y a mis cuñados Daniel y Flor junto con sus familias, que siempre nos reciben con cariño cuando los visitamos en México y nos brindan su apoyo.

I want to dedicate this work to my grandfather Coty and my father Octavio, whose recent passing in the last years took a part of me with them.

Grandpa Coty, thank you for teaching me respect and kindness; I will never forget your positivity and how people laughed in your presence.

Dad Octavio, you largely taught me to be the man I am today. Hard work, commitment, respect, and helping others will always guide me. I will never forget the sacrifice you made to educate me; your memory will live on with me and with my descendants. May you both rest in peace.

Finally, I thank God for His grace in my life.

ABSTRACT

The Abitibi greenstone belt is one of the most studied Archean volcanic provinces globally, known for its exceptional endowment in volcanogenic massive sulfide (VMS) deposits. However, the distribution of these deposits is highly uneven among its volcanic assemblages. This thesis investigates the petrological and geochemical factors controlling this differential endowment by comparing two end-member assemblages: the highly fertile Blake River Group (BRG), representing the Blake River Assemblage, and the poorly endowed Stoughton–Roquemaure (S-R) assemblage.

Over 4,000 whole-rock geochemical analyses of volcanic rocks were compiled, and principal component analysis guided the selection of key variables. Those variables were transformed into a classification diagram for volcanic rocks using immobile element ratios (Zr/Ti vs. Th/Yb), resulting in a unified framework of 12 geochemical groups. Petrogenetic models – including fractional crystallization (FC), assimilation-fractional crystallization (AFC), and magma mixing – were developed using the Magma Chamber Simulator.

Despite the presence of similar geochemical groups in both assemblages, their internal distribution differs markedly. The BRG exhibits a bimodal nature with 62.4% mafic, 9.4% intermediate, and 28.2% felsic compositions, by number of samples (with no komatiitic rocks). The S-R assemblage is dominated by mafic rocks (64.7%), with intermediate (21.8%) and felsic (9.9%) compositions decreasing accordingly. Komatiites account for 1% of the samples and komatiitic basalts for 2.6%. Tholeiitic basalts and high-Th basalts are the dominant mafic groups in both assemblages, but tholeiitic basalts are more than twice as abundant in the S-R (37.1%). Conversely, medium-Th basalts are scarce in the S-R (8.1%), indicating two distinct clusters of mafic compositions, unlike the more continuous spectrum observed in the BRG.

The S-R assemblage has a strong presence of calc-alkaline intermediate volcanic rocks, unlike the BRG. While felsic rocks are more abundant and geochemically diverse in the BRG, low-Yb felsic types dominate in both assemblages. Transitional felsic compositions are prominent in the BRG but nearly absent in the S-R, where tholeiitic felsic types are not recorded.

Significant contrasts also emerge between VMS-endowed and VMS-barren areas. In the BRG, VMS-bearing formations are notably depleted in tholeiitic signatures and are instead characterized by transitional to calc-alkaline affinities, interpreted as the result of crustal interaction. The prolonged emplacement of the BRG (~9 m.y.) likely enabled the development of

a mature transcrustal magmatic system, sustaining extensive felsic volcanism. Unlike the S-R, BRG magmatism was concentrated in a more localized area, potentially facilitated by deep transcrustal structures. However, the occurrence of tholeiitic magmas in the majority of the BRG formations indicates a long-lived mantle-derived thermal flux that replenished the magmatic system.

In contrast, the S-R assemblage was emplaced over a shorter timespan (~3 m.y.) but covers a broader area across the Abitibi greenstone belt, although it does not each as far south. Despite being more voluminous overall, the S-R assemblage reveals a north–south geochemical zonation. Tholeiitic magmas dominate the central and southern sectors, while transitional to calc-alkaline compositions become more prominent toward the north – where the only known formal VMS deposit (Estrades) is located. This pattern aligns with the crustal architecture of the region: the central Abitibi rift zone, associated with the proto–Destor-Porcupine fault, facilitated decompression melting and plume-driven magmatism with minimal crustal interaction. In contrast, the northern Abitibi portion, likely underlain by thicker crust, exhibits stronger evidence for crustal interaction with the same mantle-derived magmas. This interaction likely occurred through assimilation–fractional crystallization (AFC) or magma mixing, both modeled using a high-MgO tholeiitic basalt and a TTG-like crustal end-member.

These findings suggest that VMS fertility in the BRG reflects a combination of factors: prolonged magmatic input (not necessarily larger magma volumes), transcrustal structural controls, and sustained felsic volcanism. In contrast, although the S-R assemblage shows voluminous magmatism, its emplacement was likely more comparable to modern oceanic plateaus were abundant mafic magmatism is generated but limited interaction with the crust occurs, reducing the chances to generate complex magmatic systems in the crust. The strong presence of calc-alkaline intermediate rocks, with compositions resembling the TTG end-member, along with the presence of two chemically distinct mafic rock populations, suggests that magma mixing was the dominant differentiation process in the S-R. This contrasts with the BRG, where geochemical trends are more consistent with progressive assimilation–fractional crystallization (AFC).

This study provides a new framework to assess VMS potential in Archean terranes, integrating geochemistry from mafic to felsic compositions and petrology with crustal-scale processes.

Key words: : Basalt, Crustal assimilation, Archean greenstone belt, VMS fertility, magma mixing, petrogenetic modeling

SOMMAIRE RÉCAPITULATIF

CHAPITRE 1 : INTRODUCTION GÉNÉRALE

La ceinture de roches vertes de l'Abitibi (CRA), située dans la Province du Supérieur du Bouclier canadien (Fig. 1.1 dans le Chapitre 1), est parmi les provinces volcaniques archéennes les plus importantes au monde, remarquable à la fois pour sa diversité magmatique (Thurston et al., 2015; Mole et al., 2021) et pour sa dotation métallique exceptionnelle (Mercier-Langevin et al., 2023). L'activité volcanique principale s'est étendue sur près de 100 Ma (2790-2695 Ma; Ayer et al., 2002; Thurston et al., 2008), offrant un offrant une fenêtre sans égale sur l'évolution magmatique, crustale et métallogénique de la période archéenne.

Au sein de la CRA, le Groupe de Blake River (GBR; 2705-2696 Ma) est la séquence volcanique la plus riche en gisements de sulfures massifs volcanogènes (SMV) et constitue le cœur de l'assemblage de Blake River, tandis que l'assemblage plus ancien de Stoughton–Roquemaure (S-R; 2723-2720 Ma) est relativement pauvre en SMV. Ce contraste marqué entre les deux assemblages soulève des questions fondamentales sur les processus contrôlant la dotation métallique des ceintures de roches vertes.

Cette recherche doctorale s'attarde à la question de la fertilité métallique en examinant la géochimie des roches volcaniques et la pétrogenèse des magmas à travers l'ensemble du spectre volcanique, des komatiites aux compositions felsiques. Les études antérieures se sont souvent concentrées sur les roches felsiques en raison de leur association étroite avec les dépôts de SMV (Lesher et al., 1986; Hart et al., 2004), mais ici les roches ultramafiques à intermédiaires sont également incluses pour établir un cadre volcanique complet.

La CRA a été subdivisée en sept assemblages volcaniques sur la base de la stratigraphie et de la géochronologie (Ayer et al., 2002; Thurston et al., 2008) : pré-2750 Ma, Pacaud, Deloro, S-R, Kidd-Munro, Tisdale et Blake River (Fig. 1.2). Deux assemblages dominés par des roches sédimentaires, Porcupine et Timiskaming, ont ensuite été déposés (Corfu, 1993; Thurston, 2015).

Bien que des décennies de recherche et de cartographie aient permi de documenter en détail la nature des roches volcaniques de la CRA, celles-ci ont dans certaines études été regroupées en termes de deux principales associations: (1) les successions komatiite-tholéiite et (2) les successions bimodales basalte–dacite/rhyolite (Anhaeusser, 2014; Thurston, 2015). Cependant, des études soulignent un spectre géochimique plus complexe, révélé par des études conventionnelles (Mole et al., 2021) et des approches d'apprentissage automatique (Fassbender

et al., 2022, 2023). Ces travaux remettent en évidence la diversité du volcanisme de la CRA et les débats en cours concernant ses compositions dominantes et ses contrôles tectonomagmatiques.

Les dépôts de sulfures massifs volcanogènes (SMV)

Les dépôts de type SMV sont des accumulations de sulfures principalement stratiformes a stratoïdes (Fig. 1.3) et représentent d'importantes sources mondiales de Zn, Cu, Pb, Ag, Au, ainsi que d'éléments critiques tels que Mn, Sn et Te (Barrie et Hannington, 1999; Franklin et al., 2005). Ils se forment sur ou près du plancher océanique en association avec le volcanisme sous-marin et la circulation hydrothermale (Franklin et al., 2005; Ross et Mercier-Langevin, 2014).

La classification la plus courante des SMV utilise un schéma lithostratigraphique basé sur les unités volcaniques et sédimentaires formées simultanément ou juste avant les sulfures dans un district donné (Franklin et al., 2005). Ce schéma inclut cinq types (Fig. 1.4) : (1) mafique, (2) bimodal-mafique, (3) bimodal-felsique, (4) felsique-silicoclastique et (5) mafique-silicoclastique. Un sixième type est appelé « bimodal-felsique hybride » pour les dépôts combinant des caractéristiques épithermales et de SMV (Galley et al., 2007). D'autres schémas séparent les gisements en deux types : dominés par des coulées de laves ou par des volcanoclastites (Morton et Franklin, 1987; Gibson et Watkinson, 1990), ou encore par leur association spécifique avec les roches volcaniques (Ross et Mercier-Langevin, 2014).

Problématique

Les processus de formation des SMV sont relativement bien compris aux échelles du gisement et du district (Franklin et al., 2005; Galley et al., 2007; Piercey et al., 2015, 2023). Toutefois, des centres volcaniques présentant des cadres lithologiques et stratigraphiques similaires peuvent montrer des contrastes frappants en termes de dotation en SMV. Ce constat s'observe non seulement dans la CRA – particulièrement entre le GBR et l'assemblage de S-R – mais aussi dans d'autres ceintures de roches vertes de la Province du Supérieur et ailleurs (Fig. 1.5).

Cette disparité peut refléter des différences dans les contextes tectoniques, les processus magmatiques (Piercey, 2011), ou d'autres contrôles tels que des structures transcrustales de longue durée (Jorgensen et al., 2022) et la proximité d'intrusions synvolcaniques agissant comme moteurs thermiques (Galley, 2003). Notre compréhension limitée des processus volcaniques, magmatiques, tectoniques et croûte–manteau archéens génère en partie ces incertitudes (p. ex. Bédard et al., 2018; Palin et al., 2020; Iles et al., 2025).

D'un point de vue géochimique, aucune étude n'a systématiquement comparé l'ensemble du spectre volcanique – des roches ultramafiques à felsiques – à travers plusieurs assemblages de la CRA, ni évalué leur distribution à l'échelle des assemblages et des districts miniers. De plus, la modélisation pétrogénétique des roches volcaniques archéennes à l'aide d'outils modernes reste limitée, en partie à cause des inquiétudes selon lesquelles l'altération hydrothermale et le métamorphisme masqueraient potentiellement les signatures géochimiques primaires.

Objectifs

Cette étude vise à comparer systématiquement le GBR, fortement doté en SMV et représentant l'assemblage de Blake River, avec l'assemblage de S-R, pauvre en SMV, en utilisant une approche géochimique et pétrogénétique intégrée. Ces assemblages ont été sélectionnés comme cas contrastés de fertilité (Fig. 1.5). L'objectif global est de contraindre les processus pétrogénétiques responsables de leurs signatures géochimiques distinctes et de mieux comprendre les contrôles de la dotation différentielle en SMV. Ce cadre fournit des informations sur l'évolution métallogénique de la CRA et contribue à affiner les stratégies d'exploration dans les terrains archéens. Les objectifs spécifiques sont :

- Compilation de jeux de données : assembler un jeu de données complète d'analyses géochimiques de roches volcaniques pour les deux assemblages, incluant les éléments majeurs et en traces, en assurant la qualité et la représentativité des données.
- Classification unifiée : développer un schéma de classification cohérent des roches volcaniques pour comparer directement le GBR et l'assemblage de S-R.
- Modélisation pétrogénétique : appliquer des modèles de cristallisation fractionnée (FC) et de processus ouverts tels que l'assimilation–cristallisation fractionnée (AFC) et le mélange magmatique pour expliquer la diversité géochimique des assemblages étudiés.
- Interprétation de la fertilité : interpréter l'évolution pétrogénétique et volcanique afin d'évaluer le lien avec la dotation en SMV.

Méthodologie

Jeu de données géochimiques

Un jeu de données de 4 528 analyses géochimiques de roches volcaniques a été compilé à partir de SIGÉOM, des rapports de la Commission géologique de l'Ontario, de la littérature scientifique, de thèses académiques et de rapports d'exploration (travaux statutaires). L'accent a été mis sur les analyses publiées après 2000, comprenant les éléments majeurs, les éléments traces à petit rayon et charge élevée (HFSE : Nb, Th, Zr, Y) et certains des éléments des terres rares (La, Ce,

Sm, Gd, Eu, Yb). Après filtrage de qualité (complétude de l'analyse, et fiabilité analytique sur les diagrammes d'éléments en traces étendus), 3 209 échantillons ont été retenus pour le GBR et 1 319 pour l'assemblage de S-R. Des sous-ensembles comprenant les roches les moins altérées ont été définis (GBR = 2 257 ; assemblage de S-R = 979) et sont utilisés pour les diagrammes impliquant des éléments mobiles, par exemple certains éléments majeurs. La base de données complète a toutefois pu être utilisée sur la majorité des diagrammes, incluant pour la classification fondée sur les rapports d'éléments immobiles.

Classification à l'aide d'éléments immobiles

Comme les roches volcaniques archéennes sont souvent altérées, la classification s'est appuyée sur les rapports de HFSE (*high field strenght elements*) et de terres rares (par ex. Th/Yb, Zr/Ti), résistants à la mobilité post-magmatique (Winchester et Floyd, 1977 ; Pearce, 1996). Ces rapports fournissent également des contraintes sur la différenciation magmatique, l'affinité magmatique et l'assimilation crustale.

Analyse en composantes principales (ACP)

L'ACP a été utilisée pour identifier les éléments contribuant le plus à la variance géochimique et identifier des groupes géochimiques préliminaires. Les analyses géochimiques ont été standardisées par transformation log ratio centrée (Aitchison, 1986). Des ACP distinctes ont été réalisées pour le GBR et l'assemblage de S-R à partir d'éléments immobiles (Al, Ce, Eu, Gd, La, Nb, Sm, Th, Ti, Y, Yb, Zr), afin de mettre en évidence les tendances compositionnelles et les signatures magmatiques primaires.

Définition des groupes géochimiques

Les groupes géochimiques ont été définis à l'aide d'un diagramme Zr/Ti vs Th/Yb, dérivé des résultats de l'ACP. Le premier regroupement a été réalisé par k-moyennes, mais les frontières entre les groupes ont ensuite été affinées manuellement pour assurer la cohérence avec d'autres diagrammes géochimiques comme les diagrammes d'éléments en traces étendus, et les données cartographiques (cohérence spatiale). Cette approche a permis d'obtenir un cadre de classification robuste et comparable entre les assemblages.

Magma Chamber Simulator (MCS)

Le logiciel MCS (Bohrson et al., 2014, 2020) modélise l'évolution magmatique en système fermé ou ouvert en intégrant la cristallisation fractionnée (FC), l'assimilation crustale couplée à la cristallisation fractionnée (AFC), et le mélange de magmas ou la recharge magmatique. La plupart

des simulations pétrogénétiques ont été réalisées à 0,3-0,6 GPa, correspondant à des niveaux moyens à supérieurs de la croûte, et suivent l'évolution des températures, et des éléments majeurs et traces dans le magma liquide et les cristaux. Le module MCS-PhaseEQ calcule l'équilibre des phases, les compositions de liquide et les histoires thermiques, tandis que MCS-Traces utilise ces résultats pour modéliser les éléments traces. Les modèles obtenus peuvent ensuite être comparés avec les données géochimiques naturelles.

Modélisations dans PRIMELT3

L'outil PRIMELT3 (Herzberg et Asimow, 2015) reconstruit les magmas primaires issus du manteau à partir de roches volcaniques mafiques primitives (>9 % MgO) et de roches ultramafiques, et estime la température potentielle du manteau (Tp), le degré de fusion partielle (F) et la lithologie résiduelle. Cette étude utilise PRIMELT3-P (Herzberg et al., 2023), qui affine les estimations de pression et valide les compositions primaires utilisées comme intrants pour les simulations MCS.

Organisation de la thèse

Cette thèse de doctorat est présentée dans un format hydride entre la thèse traditionnelle et la thèse par articles. Elle contient cinq chapitres : le Chapitre 1 qui est une introduction générale, deux articles scientifiques multi-auteurs déjà publiés, respectivement sur le GBR et l'assemblage de S-R (Chapitres 2 et 3), un chapitre conventionnel comparant les deux ensembles géologiques et présentant des modèles contrastés de mise en place (Chapitre 4), et un chapitre de conclusions générales (Chapitre 5).

CHAPITRE 2 : GROUPE DE BLAKE RIVER

L'assemblage de Blake River s'étend de Timmins en Ontario (par ex. zones de Kamiskotia et de Swayze) jusqu'à l'est de Val-d'Or au Québec (Fig. 2.1). Il renferme environ 46 % de la dotation totale en SMV (Ayer et al., 2005 ; Monecke et al., 2017) et 92 % de la dotation aurifère liée aux SMV dans toute la CRA (Mercier-Langevin et al., 2011b, 2014). Le cœur de l'assemblage de Blake River est le GBR, sujet ce cette étude (Fig. 2.1). Il s'agit d'une succession volcanique sous-marine dominée par des compositions mafiques à intermédiaires, mais avec une activité felsique importante (Ross et al., 2011a, b ; McNicoll et al., 2014 ; Sutton et al., 2017) (Fig. 2.2a). Les roches volcaniques sont recoupées par des intrusions archéennes mafiques à felsiques, de mise en place synvolcanique à syntectonique, ainsi que par des dykes protérozoïques (Piercey et al., 2008).

Plusieurs schémas de nomenclature stratigraphique ont été proposés pour les formations du GBR. Le plus simple est la subdivision en Blake River inférieur versus Blake River supérieur (Ayer et al., 2005), actuellement appliquée en Ontario (Fig. 2.2b). Au Québec, une tradition riche de subdivisions en formations et membres existe (p. ex. Gélinas et al., 1984 ; Gibson et Watkinson, 1990 ; Pearson et Daigneault, 2009). Le schéma actuellement utilisé par le gouvernement du Québec distingue neuf formations (Fig. 2.2b) : Rouyn-Pelletier, Duprat-Montbray, Noranda, Renault-Dufresnoy, Bousquet, Horne, Hébécourt, Camac et Dupuis (Mercier-Langevin et al., 2011b ; McNicoll et al., 2014 ; SIGÉOM, 2022).

Résultats

Groupes géochimiques

La compilation géochimique du GBR contient 3 209 échantillons allant des compositions mafiques à felsiques. De ce nombre, 2 271 échantillons sont mafiques à intermédiaires et le reste sont felsiques (Figs. 2.3, 2.4). L'ACP sur les éléments immobiles montre que les éléments Th, Yb et Ti expliquent une partie importante de la variabilité géochimique du GBR (Fig. 2.5). Le rapport Th/Yb est utilisé dans la littérature pour définir l'affinité magmatique (Ross et Bédard, 2009) ou la contribution crustale (Pearce 1983, 2008). De plus, Zr est corrélé négativement avec Ti (Fig. 2.5) et est pertinent pour la différenciation magmatique. Un diagramme Ti/Zr versus Th/Yb a donc été construit pour les roches volcaniques mafiques à intermédiaires (Fig. 2.6). Les regroupements géochimiques dominants ont été identifiés par techniques de clustering et raffinés manuellement. Sept groupes géochimiques ont ainsi été définis: basaltes tholéiitiques, basaltes à Th moyen, basaltes à Th élevé, basaltes à faible Zr, roches intermédiaires tholéiitiques, roches intermédiaires transitionnelles et roches intermédiaires calco-alcalines. Ces groupes montrent des caractéristiques variées sur d'autres diagrammes, notamment ceux de Pearce et al. (2021), de O'Neill (2016) et d'Agrawal et al. (2008) (Fig. 2.7) et sur les diagrammes d'éléments en trace étendus (Fig. 2.8), formant un continuum entre des roches mafiques tholéiitiques issues essentiellement du manteau en allant vers un pôle crustal représenté par une composition moyenne de TTG du SE du Supérieur (Mole et al., 2021) avec un rapport Th/Yb élevé.

Distribution des compositions mafiques à intermédiaires

Dans le GBR, les basaltes tholéiitiques, les basaltes à Th moyen et les basaltes à Th élevé sont les groupes géochimiques les plus abondants. Les basaltes à faible Zr et les roches volcaniques intermédiaires sont plus rares mais localement importants (Figs. 2.9, 2.10).

En Ontario, le Blake River inférieur est dominé par des basaltes tholéiitiques, avec des proportions subordonnées de basaltes à Th moyen et basaltes à Th élevé, et quelques roches intermédiaires. Le Blake River supérieur est dominé par les basaltes à Th élevé et contient davantage de compositions intermédiaires.

Au Québec, l'échantillonnage est plus dense et les compositions sont plus variables. A titre d'exemple, la formation d'Hébécourt, qui ne contient pas de SMV, est dominée par le basalte tholéiitique et les roches intermédiaires tholéiitiques. A l'inverse, les formations riches en SMV comme Noranda et Bousquet sont notables par la présence très limitée de basalte tholéiitiques. La formation de Noranda est enrichie en basalte à Th moyen/élevé et quelques roches intermédiaires transitionnelles. La formation de Bousquet, riche en SMV aurifères, a la plus forte proportion de roches intermédiaires, incluant des roches intermédiaires calco-alcalines, et contient une proportion notable de basalte à faible Zr, un type de roche peu communs ailleurs.

Un profil géochimique stratigraphique dans la formation de Noranda montre une base dominée par le basalte à Th moyen, une section médiane enrichie en basalte à Th élevé coïncidant avec la minéralisation en SMV, et une partie supérieure marquée par un retour à la dominance de basalte à Th moyen (Figs. 2.11, 2.12).

Modélisation pétrogénétique

L'ensemble des roches étudiées peut être modélisé en utilisant une source de magma unique, un basalte tholéiitique riche en MgO (l'échantillon 74J1328 provenant du Blake River inférieur en Ontario), interprété comme un magma primitif issu du manteau asthénosphérique archéen. Les caractéristiques de cette source rappellent le manteau primitif ou la source des basaltes de plateaux océaniques du Phanérozoïque (Fig. 2.7).

Pour expliquer la diversité des éléments majeurs dans les unités de basalte tholéiitique du GBR, incluant des tendances variables d'enrichissement en Fe-Ti, des modèles de cristallisation fractionnée (FC) à 0,25 GPa (~10 km de profondeur) montrent que la teneur en eau du magma est un facteur important (Fig. 2.4). Dans des conditions anhydres, la cristallisation tardive des oxydes de Fe-Ti enrichit le magma en $Fe_2O_3{}^t$ et TiO_2 ; le plagioclase se forme à plus haute température, appauvrissant le magma en Al_2O_3. Dans des conditions hydratées, la cristallisation du plagioclase est retardée, augmentant l'Al_2O_3 dans le magma; l'olivine et le pyroxène captent une partie du Fe-Ti, et les oxydes de Fe-Ti cristallisent plus tôt (Fig. 2.4). L'alternance de tholéiites ferrifères et des tholéiites magnésiennes dans les ceintures de roches vertes pourrait donc être due en partie à des variations de teneurs en eau dans le magma.

Les modèles de cristallisation fractionnée expliquent aussi la genèse des roches volcaniques tholéiitiques intermédiaires depuis les basaltes tholéiitiques (Fig. 2.13a, c, d). Toutefois, ces modèles ne peuvent pas expliquer les cinq autres groupes géochimiques, à rapports Th/Yb moyens à élevés. Pour ceux-ci, une contribution crustale est nécessaire. Les modèles d'AFC à 0,25 GPa montrent que l'assimilation de croûte de type TTG explique les unités basaltiques à Th moyen et les unités basaltiques à Th élevé (Fig. 2.13a, b, e, f). Une assimilation de ~1 % produit des basaltes à Th moyen, tandis qu'une assimilation >2,5 % est nécessaire pour générer des basaltes à Th élevé. Une assimilation de l'ordre de 15% mène aux roches intermédiaires calco-alcalines.

L'alternative à la contamination crustale variable serait l'implication d'une zone de subduction, mais les roches tholéiitiques et calco-alcalines sont intercalées à l'échelle des centaines de mètres dans le GBR, rendant cette hypothèse moins probable.

Discussion et conclusion sur le GBR

Historiquement, l'exploration régionale pour les SVM a surtout fait appel aux signatures géochimiques des roches volcaniques felsiques (p. ex. Lesher et al., 1986; Hart et al., 2004). La présente étude montre que les compositions géochimiques des roches volcaniques mafiques à intermédiaires sont aussi pertinentes. Dans le GBR – la zone la plus riche en SMV de la CRA – les formations riches en SMV affichent des signatures de forte assimilation crustale et se distinguent par l'absence ou la rareté de basalte tholéiitiques et de roches intermédiaires d'affinité tholéiitique. Cela suggère un lien entre assimilation crustale et fertilité en SMV, même si toutes les formations enrichies en signatures d'assimilation ne sont pas minéralisées. Ce lien pourrait passer par la maturation thermique de la croûte : une croûte plus chaude favorise l'assimilation crustale, la production de roches felsiques, et ultimement la circulation hydrothermale nécessaire à la formation des SMV.

CHAPITRE 3 : ASSEMBLAGE DE STOUGHTON-ROQUEMAURE

L'assemblage de Stoughton-Roquemaure (S-R), daté entre ~2723 et ~2720 Ma (Barrie, 1999 ; Davis et al., 2005 ; Ayer et al., 2007), est positionné temporellement entre les assemblages de Deloro (~2734–2724 Ma) et de Kidd-Munro (~2720–2710 Ma) (Ayer et al., 2002 ; Thurston et al., 2008) (Fig. 3.1). Il affleure principalement dans le nord et le centre de la CRA, au nord de la zone de faille Destor-Porcupine, mais apparaît aussi dans le sud, couvrant ~16 000 km² (33-34 % des roches volcaniques de la CRA ; Dubé et Mercier-Langevin, 2020; Jorgensen et Gibson, 2024)

(Fig. 3.2). Selon la littérature, l'assemblage de S-R est dominé par d'épais empilements de basalte tholéiitique, avec des unités de komatiite et basalte komatiitique subordonnées, déposés dans un environnement sous-marin formant une vaste plaine de laves (Thurston et al., 2008 ; Dostal et Mueller, 2013). De petits centres volcaniques intermédiaires à felsiques et de minces unités volcanoclastiques sont aussi localement présents (Barrie, 1999 ; Davis et al., 2014). Un résumé détaillé des formations géologiques composant cet assemblage est donné au tableau 3.1.

Jeu de données et groupements géochimiques

Pour l'assemblage de S-R, 1 309 analyses chimiques ont été compilées. Les roches komatiitiques, formant un peu moins de 4% des analyses, ont été distinguées à l'aide du diagramme de Jensen (1976), qui permet de les séparer en unités de komatiite et de basalte komatiitique (Fig. 3.3a). En fonction du rapport Al/Ti, les roches komatiitiques non appauvries en aluminium (AUK) sont plus communes que celles qui le sont (ADK) (Figs. 3.3b, 3.4). Pour les roches volcaniques mafiques à felsiques (Fig. 3.3c), la même approche que celle utilisée au chapitre 2 pour le GBR a été adoptée, à savoir que les échantillons du S-R ont été classés avec le même diagramme Th/Yb vs. Zr/Ti suite à l'ajout de champs pour les roches felsiques (Fig. 3.3e), car une ACP indépendante a révélé les mêmes éléments dominants (Th, Yb, Ti, Zr).

Ceci a donné 11 groupes géochimiques pour l'assemblage de S-R, en plus des roches komatiitiques. Les trois groupes les plus importants sont les basaltes tholéiitiques (~37%), les basaltes riches en Th (~19%) et les roches intermédiaires calco-alcalines (~17%) (Tableau 3.2). Les compositions felsiques représentent légèrement moins de 10% de l'assemblage, tous groupes réunis. Les caractéristiques des groupes géochimiques sont illustrées aux figures 3.5 à 3.7.

Zonation géochimique

L'assemblage de S-R n'est pas homogène sur toute son étendue. Les zones centrales et méridionales, en particulier autour du système de failles de Destor-Porcupine, sont dominées par des unités de basalte tholéiitique et concentrent presque toute l'activité komatiitique, traduisant une forte signature d'origine mantellique. En revanche, les zones septentrionales et nord-ouest présentent davantage de signatures transitionnelles à calco-alcalines, témoignant d'une interaction plus marquée entre le magma et la croûte (Fig. 3.8).

Magmas parents

Les résultats de PRIMELT3 (Fig. 3.9) révèlent deux familles principales de magmas parents en termes l'éléments majeurs (Al, Fe, Mg) et de températures potentielles du manteau (T_P):

- Une famille plus commune associée aux roches komatiitiques AUK et à la plupart des unités de basaltes tholéiitique, avec un MgO moyen de 20% et T_P = 1565 ± 87°C (2σ).
- Une autre famille liée aux roches komatiitiques ADK et à quelques basaltes, avec un MgO moyen de 24% et Tp = 1658 ± 33°C (2σ).

Ces températures élevées, en contexte archéen, suggèrent une influence de panache mantellique. Elles valident aussi les compositions mafiques primaires utilisées comme intrants pour les modèles pétrogénétiques.

Résultats de modélisation

Afin de contraindre l'origine pétrogénétique des roches volcaniques mafiques à felsiques de l'assemblage de S-R, plusieurs modèles ont été testés avec MCS: FC, AFC et mélange magmatique. Un test important était de mieux contraindre à quelle pression (profondeur) les magmas basaltiques tholéiitiques évoluent depuis ~11% MgO jusqu'à ~3% MgO (Fig. 3.10) : les pressions investiguées vont de 0,15 à 2,0 Gpa (environ 6 km à plus de 60 km). Dans les modèles de cristallisation fractionnée (FC), à partir de 0,6 GPa (~18 km), le grenat devient stable, mais comme cette signature est absente dans les données du S-R, cela indique que la cristallisation fractionnée s'est produite à des profondeurs plus faibles. Les effets de la pression contribuent également à expliquer les variations des teneurs en Al_2O_3, en influençant la chronologie relative de la cristallisation du plagioclase et du pyroxène. Les modèles de FC entre 0,15 et 0,3 GPa, voire 0,6 GPa au maximum, avec des teneurs en eau entre 0,1 et 1,0%, sont donc les plus pertinents pour les roches basaltiques tholéiitiques.

Les modèles d'AFC ou de mélange de magmas sont nécessaires pour expliquer la tendance principale des données, allant des basalte tholéiitique aux roches intermédiaires calco-alcalines (Fig. 3.11, 3.12a). Généralement, les modèles d'AFC entre 0,3 et 0,6 GPa et de 0,1 à 1,0% H_2O expliquent assez bien les éléments majeurs et traces pour les roches mafiques à intermédiaires, transitionnelles à calco-alcalines. L'assimilation s'est révélée plus efficace en profondeur, où les encaissants chauds interagissaient rapidement avec les magmas basaltiques, produisant des compositions mafiques fortement contaminées. Par exemple, le modèle AFC à 0,1% H_2O et 0,6 GPa reproduit les patrons d'éléments en traces du basalte à Th moyen avec 4% d'assimilation,

alors que le basalte à Th élevé et les roches intermédiaires calco-alcalines demandent ~16 % and 27% d'assimilation, respectivement (Fig. 3.12e, f).

Une alternative à l'AFC est le mélange magmatique entre un basalte tholéiitique et un liquide de type TTG. Trois proportions ont été testées (Fig. 3.11, 3.12a, b, c, d) :

- 4:1, donnant une andésite basaltique d'affinité transitionnelle dont les éléments traces sont à la limite du basalte à Th moyen et du basalte à Th élevé (Fig. 3.12a, d, f, g);
- 1:1, donnant une andésite calco-alcaline, à la limite supérieure du basalte à Th élevé en termes de rapport Th/Yb (Fig. 3.12a); et
- 4:1, donnant une andésite plus évoluée représentative de la moyenne du groupe des roches intermédiaires calco-alcalines (Fig. 3.12f, g).

De plus, la limite extrême des unités d'andésite calco-alcaline se situe près du pôle TTG en termes d'éléments majeurs et en traces (Figs. 3.11, 3.12). Un mélange de magma allant de 100% basalte tholéiitique à 100% TTG fournit donc possiblement une bonne explication à la diversité des compositions du S-R pour la « tendance principale » des données. En fractionnant par la suite le magma résultant du mélange, on peut expliquer les groupes felsiques de l'assemblage de S-R (Fig. 3.12a, g, h).

Discussion et conclusions sur l'assemblage de S-R

L'assemblage de S-R représente un pic de magmatisme pour l'Abitibi, avec un grand volume de magma mis en place rapidement (environ 3 millions d'années). L'assemblage est surtout connu comme une association komatiite-tholéiite dans la littérature, mais la présente étude montre que des compositions intermédiaires à felsiques sont également présentes, ainsi que des affinités magmatiques transitionnelles à calco-alcalines.

Un panache mantellique peut expliquer la présence de komatiite, l'abondance de basalte tholéiitique, et la production abondante de magma, surtout pour la partie centrale de l'assemblage de S-R. Toutefois, les estimés de T_P et du contenu en MgO des magmas parentaux sont plus faibles que ceux obtenus par d'autres auteurs pour l'assemblage de Kidd Munro (Fig. 3.13). La décompression du manteau assistée par des structures profondes et une croûte possiblement plus mince dans la partie centrale de l'assemblage, et la présence de volatiles mantelliques, pourraient avoir joué un rôle dans la genèse des magmas.

À l'inverse, une croûte plus épaisse au nord a potentiellement favorisé des interactions plus intenses entre le magma et la croûte, générant des signatures plus évoluées, transitionnelles à calco-alcalines, par AFC, et davantage de roches felsiques. Le produit final d'un des modèles

AFC à faible pression ressemble aux groupes des roches felsiques calco-alcalines du S-R (Fig. 3.12a), ce qui montre que de telles roches, tombant dans les champs FI et FII sur le diagramme de Hart et al. (2004) (Fig. 3.7f), ne sont pas nécessairement liées à une fusion partielle de la croûte à grande profondeur (>30 km pour les FI), et que les terres rares ne peuvent pas toujours être utilisées pour contraindre la profondeur de fusion des roches felsiques. Alternativement, le mélange de basalte tholéiitique et de liquide TTG est une alternative viable à la contamination crustale, surtout que des intrusions de TTG contemporaines aux roches volcaniques du S-R sont documentées (p. ex. Legault et al., 2002).

CHAPITRE 4 : COMPARAISON GÉOCHIMIQUE ENTRE LE GBR ET L'ASSEMBLAGE DE S-R : IMPLICATIONS POUR L'EXPLORATION DES SMV

Les assemblages de Blake River et de S-R représentent des cas de fertilité maximale et minimale pour les SMV, respectivement, dans la CRA. Malgré une étendue spatiale (et probablement un volume) plus de deux fois plus importante que celle de l'assemblage de Blake River (Fig. 4.1), l'assemblage de S-R contient un seul gisement, contre une trentaine pour sa contrepartie. Le contexte géologique était donc clairement plus fertile lors de la mise en place de l'assemblage de Blake River, et en particulier pour le GBR. Comment se comparent-ils géochimiquement ? L'application des groupes géochimiques développés pour le GBR à l'assemblage de S-R (Fig. 4.2) permet une comparaison directe.

Comparaison géochimique

Les roches de composition komatiitique sont absentes du GBR mais représentent ~4 % de l'assemblage de S-R, en accord avec les estimations antérieures (Fig. 4.3a, b). Les roches volcaniques mafiques dominent les deux assemblages (>60 %) (Fig. 4.3c, d) mais leur répartition interne diffère. Dans le S-R, les unités de basalte tholéiitique sont les plus abondantes, tandis que dans le GBR elles arrivent en troisième position, après le basalte à Th élevé et le basalte à Th moyen (Fig. 4.9). Le S-R montre deux regroupements géochimiques mafiques distincts, alors que le GBR présente une distribution plus continue (Fig. 4.3). Le basalte à Th élevé est commun dans les deux, mais constitue le groupe le plus abondant du GBR (Fig. 4.9).

Les roches intermédiaires représentent 22 % de l'assemblage de S-R mais moins de 10 % du GBR. Le S-R est fortement enrichi en roches volcaniques intermédiaires calco-alcalines par rapport au GBR (Fig. 4.9). Cela produit une diminution progressive des compositions mafiques vers les felsiques dans l'assemblage de S-R, en contraste avec la nature nettement bimodale

(mafique-felsique) du GBR, où les roches intermédiaires sont subordonnées aux roches felsiques. Malgré ces différences de proportions de groupes géochimiques, une comparaison de la composition moyenne de la plupart des différents groupes mafiques à intermédiaires, entre le GBR et l'assemblage de S-R, montre que ces moyennes sont similaires (Fig. 4.4), justifiant l'utilisation du même diagramme de classification.

Les roches felsiques constituent une distinction majeure entre les deux ensembles étudiés. Dans le GBR, elles représentent ~28 % des échantillons, avec une diversité géochimique dominée par les suites felsiques à faible Yb et transitionnelles, accompagnées de rhyolites à Yb élevé. Dans le S-R, les roches felsiques ne représentent que ~10 %, sont largement dominées par les types à faible Yb, avec très peu de roches transitionnelles ou de rhyolites à Yb élevé, et aucune signature felsique tholéiitique (Fig. 4.9). De plus, les moyennes compositionnelles des groupes géochimiques diffèrent entre le GBR et l'assemblage de S-R (Fig. 4.4).

En résumé, l'assemblage de S-R se caractérise par la présence de komatiite, une abondance de basalte tholéiitique, un développement marqué de roches intermédiaires calco-alcalines et une rareté relative des roches felsiques. Le GBR, en revanche, affiche un volcanisme bimodal, avec des suites mafiques et felsiques volumineuses, et peu de roches volcaniques intermédiaires. Les roches felsiques du GBR sont géochimiquement plus diverses. Ces caractéristiques contrastées reflètent des régimes magmatiques distincts et ont des implications pour la fertilité en SMV.

Signatures géochimiques dans les zones minières

Les formations comprenant des SMV dans le GBR (Noranda, Bousquet, Horne) et dans l'assemblage de S-R (secteur Estrades) se distinguent des compositions des roches volcaniques situées plus loin des zones minéralisées. Ceci révèle des associations sélectives entre les groupes géochimiques dans les roches volcaniques et l'activité hydrothermal à l'origine des SMV. Dans le GBR, les zones à SMV montrent systématiquement un enrichissement felsique : Noranda et Horne contiennent 50 à 60 % d'échantillons felsiques, dominés par des suites transitionnelles, à Yb élevé et à Yb faible, tandis que Bousquet présente des roches felsiques calco-alcalines associées à des roches basaltiques à faible Zr (Fig. 4.10).

Dans l'assemblage de S-R, le gisement d'Estrades présente une proportion felsique plus élevée que l'assemblage dans son ensemble, dominée par des types à Yb faible avec une minorité de roches felsiques à Yb élevé et calco-alcalines, accompagnées de basalte à Th moyen (Fig. 4.10).

Discussion : un modèle pétrogénétique conceptuel pour chaque assemblage

L'assemblage S-R constitue la plus vaste et volumineuse phase magmatique de la CRA (durée de ~3 Ma), marquée par de fortes contributions mantelliques avec un apport crustal limité dans son domaine central, produisant de nombreuses unités de basalte tholéiitique et de roches komatiitiques (Fig. 4.11). En revanche, le nord du S-R présente des affinités transitionnelles à calco-alcalines et une activité komatiitique faible ou absente, traduisant une contamination crustale et un mélange avec des magmas de type TTG; des indices indirects issus des signatures isotopiques du zircon et des données géophysiques suggèrent une croûte plus épaisse dans cette région. Les contrôles structuraux, tels que l'ancêtre de la faille Destor-Porcupine et un possible rifting, ont favorisé la décompression du manteau, et la présence possible de volatiles ont stimulé la production magmatique. Le volcanisme évolué est resté limité par rapport au GBR, car des systèmes magmatiques rapides privilégiaient l'extraction du magma plutôt que la différenciation.

Le GBR représente la dernière grande phase volcanique de la CRA. Il débute par des successions tholéiitiques mais évolue ensuite vers des suites géochimiquement plus diversifiées, incluant une proportion significative de roches felsiques, lui conférant un caractère nettement bimodal. Contrairement à l'assemblage S-R, le BRG est dépourvu de komatiite, contient moins de basalte tholéiitique et présente une abondance plus marquée de basalte à Th moyen, cohérente avec une assimilation progressive d'une croûte de type TTG (voir chapitres 2–3 ; Fig. 4.11). L'abondance de magmas felsiques implique une évolution magmatique complexe au sein de la croûte, facilitée par des structures transcrustales. Sa mise en place sur une période prolongée (~9 Ma) a permis la maturation crustale et le développement d'un système magmatique transcrustal, où les injections mafiques répétées, la contamination et la différentiation ont produit un volcanisme bimodal et des magmas felsiques par extraction de bouillie cristalline (mush magmatique).

CHAPITRE 5 : CONCLUSION GÉNÉRALE

En comparant le GBR et l'assemblage de S-R, cette étude met en évidence des signatures géochimiques contrastées et variables qui soulignent la complexité des systèmes magmatiques archéens. Les différences géochimiques importantes notées entre un assemblage fertile (Blake River) et un assemblage peu fertile (S-R), et les différences géochimiques entre des secteurs minéralisés et peu minéralisés dans le même assemblage, suggèrent que la composition des

roches volcaniques, ou du moins les processus tectoniques et magmatiques responsable de la génération des magmas à l'origine de ces roches volcaniques, peut expliquer en partie la fertilité différentielle en SMV dans les ceintures de roches vertes archéennes.

Dans le GBR, plusieurs facteurs convergent pour expliquer la fertilité exceptionnelle en SMV. Ses près de neuf millions d'années d'activité volcanique, combinées à la présence de structures transcrustales profondes (Jorgensen et al., 2022), ont créé les conditions favorables au développement et au maintien d'un système magmatique mature. Les modèles récents (Cashman et al., 2017 ; Karakas et al., 2017 ; Annen et al., 2025) montrent que le maintien de volcanisme felsique sur une longue période nécessite un système magmatique transcrustal. De tels systèmes évoluent par injections répétées de magma, stockage dans la croûte moyenne, différenciation, puis extraction progressive de magmas felsiques. Dans ce cadre, les magmas felsiques représentent l'aboutissement d'une évolution prolongée, et les intrusions associées ont probablement agi comme moteurs thermiques favorisant la circulation hydrothermale (plutons subvolcaniques). D'un point de vue géochimique, les formations du GBR contenant des SMV affichent systématiquement des affinités transitionnelles à calco-alcalines, tandis que les magmas tholéiitiques en sont remarquablement absents, ce qui montre l'importance de la contamination crustale des magmas mantelliques.

L'assemblage de S-R présente en quelque sorte le cas inverse. Sa mise en place rapide sur trois millions d'années a limité le développement de réservoirs durables de magma dans la croûte. En conséquence, le système est resté dominé par des basaltes tholéiitiques, avec seulement des signatures transitionnelles à calco-alcalines localisées, qui pourraient s'expliquer par un mélange de magma impliquant également un liquide de type TTG. Le seul gisement formel de SMV du S-R est précisément associé à ces roches transitionnelles à calco-alcalines, mais les magmas felsiques sont peu développés dans le S-R, reflétant l'état immature de son système magmatique.

Dans l'ensemble, la fertilité en SMV dans le CRA semble dépendre moins du volume volcanique que de l'établissement de complexes magmatiques évolutifs et de longue durée. Un magmatisme prolongé favorise l'assimilation, la diversité géochimique (si les magmas interagissent avec des croûtes de nature différente) et fournit l'énergie thermique nécessaire pour accroître la fertilité, comme l'illustre le GBR.

TABLE OF CONTENTS

LIST OF FIGURES

LIST OF TABLES

1 GENERAL INTRODUCTION

The Abitibi Greenstone Belt (AGB) of Quebec and Ontario is famous for its abundant volcanogenic massive sulfide (VMS) deposits, including several world-class examples of gold-rich VMS deposits (Mercier-Langevin et al., 2014). In contrast, other greenstone belts in the Superior Province or beyond are much less endowed, although the geological reasons for this remain debated (Gibson et al., 2007; Piercey, 2011; Jorgensen et al., 2022). Within the AGB itself, different volcanic assemblages also have vastly different VMS endowments, and again this raises important questions about the geological controls governing this variability. Although answering these questions will ultimately require a multidisciplinary approach by many workers over a long period, this PhD thesis contributes to the VMS endowment research by focussing on the whole-rock geochemistry and petrogenesis of the VMS-poor to VMS-rich volcanic rocks of the AGB.

Traditionally, geochemical exploration efforts have concentrated on felsic volcanic rocks due to their close association with VMS deposits in the Archean (e.g., Lesher et al., 1986; Hart et al., 2004; Hollis et al., 2015). However, this work adopts a broader perspective by integrating ultramafic to felsic compositions to characterize the geochemical distribution within and between assemblages, and to interpret their origin assisted by petrogenetic modeling. Ultimately, this approach seeks to link the occurrence of VMS deposits with specific petrological processes.

There are seven subalkaline volcanic assemblages within the AGB covering about 100 m.y. of geological history, and over 10 000 whole-rock analyses of volcanic rocks including the required major and trace elements (details below) were initially compiled. Therefore, to keep the scope of the thesis manageable, two contrasting volcanic assemblages in terms of VMS endowment were selected for comparison: the highly endowed Blake River assemblage and the much less endowed Stoughton-Roquemaure assemblage (Monecke et al., 2017; Mercier-Langevin et al., 2023). This still represented over 4000 geochemical analyses to work with.

This chapter begins with a brief description of the geological background and presents some generalities about VMS deposits. It then outlines the problems to be solved, the aims of the thesis, and the methods used. Finally, the structure of the thesis is outlined, and the contribution of the authors to the different publications is explained.

1.1 Geological background

1.1.1 The Superior Province

The Superior Province, which forms the core of the Canadian Shield, is an Archean craton that spans approximately 1,400,00 km^2 in Quebec, Ontario, Manitoba and the USA (Card, 1990). The geological provinces surrounding the Superior Province are mostly Proterozoic orogens (Percival, 2006; Percival et al., 2012). Tectonic trust and strike-slip faults mark the boundaries in the northern, western and south-eastern zones, whereas the southern and northeastern boundaries are unconformably overlain/over-thrusted by Paleoproterozoic sequences (Card, 1990; Card et al., 1998).

The Superior Province comprises 19 subprovinces (Fig. 1.1) with a dominant east-west structural trend (Card and Ciesielski, 1986; Percival et al., 1992; Leclair et al., 2004). Four principal lithologies define the subprovinces: metasedimentary, metamorphic, volcano-plutonic and plutonic (Card, 1990). About half of the Superior Province is located in Quebec, where subprovinces are divided into two major zones, the southern zone and the northern zone. The southern zone is comprised of alternating linear ~east-west trending metasedimentary (Pontiac, Nemiscau and Opinaca), volcano-plutonic (Abitibi, Opatica and La Grande) and metamorphic (Ashuanipi) subprovinces. The Minto Subprovince makes up the northern zone, which is mostly plutonic in origin (Percival, 2007).

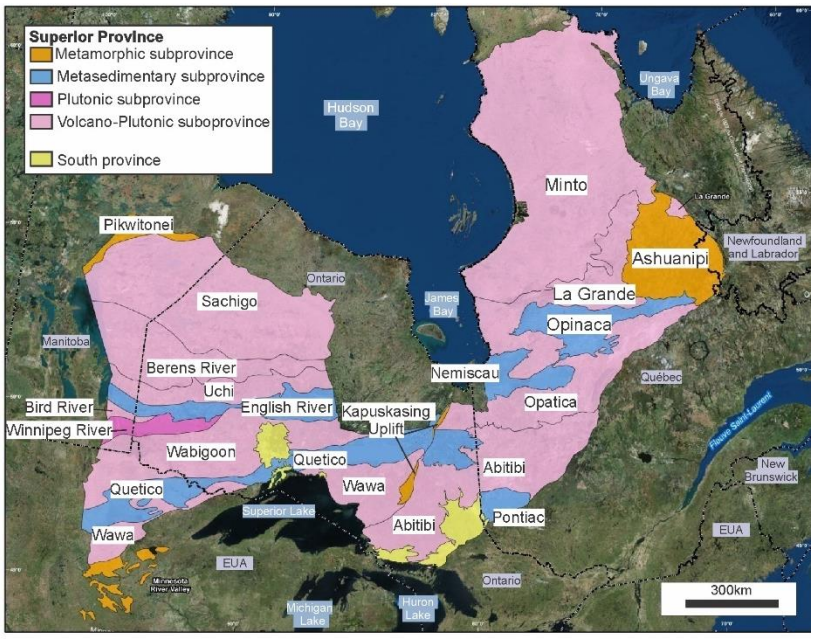

Figure 1.1 The Superior Province divided into 19 subprovinces. Modified from Système d'information Géominière du Québec (SIGÉOM).

1.1.2 The Abitibi Greenstone Belt

The Abitibi Greenstone Belt (AGB) lies in the eastern part of the Abitibi-Wawa Subprovince of the Superior Province (Fig. 1.1) (Thurston et al., 2008) and comprises several mineral deposits, including world-class Archean syngenetic and epigenetic gold deposits, important VMS deposits, and other ore types (Poulsen et al., 2000; Mercier-Langevin et al., 2012; Monecke et al., 2017). It is the largest and one of the best-preserved Neoarchean greenstone belts worldwide (Monecke et al., 2017).

The AGB is generally well preserved, with regional metamorphism mostly at lower-greenschist facies, reaching prehnite–pumpellyite conditions in several southern zones (Gélinas et al., 1982; Morin et al., 1993; Powell et al., 1995). In contrast, the northern part locally experienced slightly higher metamorphic conditions depending on stratigraphic level, structural position, or proximity to intrusive bodies, although greenschist facies still dominates (Allard et al., 1984; Oliver et al., 2012; Daoudene et al., 2022). The AGB is bounded by the Pontiac Subprovince to the south, Kapuskasing structural zone to the west, the Opatica Subprovince to the north, and the Greenville Province to the southeast (Fig. 1.2).

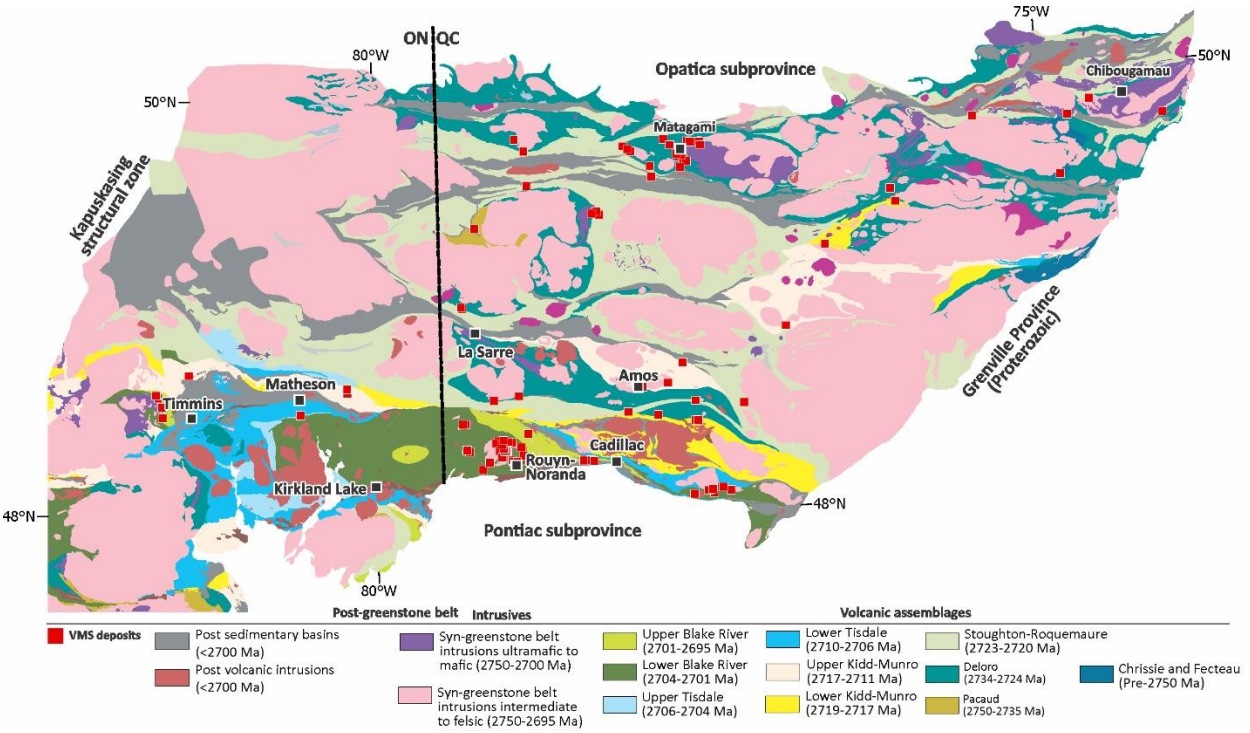

Figure 1.2 Volcanic assemblage map of the Abitibi Greenstone Belt. Modified from Jorgensen and Gibson (2024).

The AGB is composed of east-trending bands of largely volcanic rocks and intervening domes cored by synvolcanic and/or syntectonic plutonic rocks (gabbro-diorite, tonalite, and granite) alternating with east-trending bands of sedimentary rocks (MERN-OGS, 1984; Ayer et al., 2002; Daigneault et al., 2004; Goutier and Melançon, 2007).

Mafic and felsic volcanic units lack laterally persistent marker horizons and the only units with significant lateral persistence are some of the clastic and chemical sedimentary units at the top of volcanic units. Therefore, these sedimentary units mark the stratigraphic limits within the AGB (Ayer et al., 2005; Goutier and Melançon, 2007; Thurston et al., 2008).

The AGB has been divided into seven subalkaline volcanic assemblages or episodes, based on stratigraphic and geochronological data, referred to as the pre-2750 Ma, Pacaud, Deloro, Stroughton-Roquemaure, Kidd-Munro, Tisdale and Blake River assemblages (Fig. 1.2) (Ayer et al., 2002; Ayer, 2005; Thurston et al., 2008). Since geochronology is the deciding factor in assigning rocks to a specific assemblage, ‘episode’ would perhaps be a better term, but in this thesis ‘assemblage’ is used for continuity with previous studies. Some of these assemblages are sometimes divided in lower and upper portions.

The seven volcanic-dominated assemblages extend from about 2790 Ma to 2695 Ma, concluding with the Blake River assemblage deposition. These volcanic rocks were deposited in a subaqueous environment and are generally dominated by basalts, with lesser komatiites and more differentiated products (as presented in the next subsection). Their tectonic setting is controversial, like that of Archean greenstone belts in general. For instance, several volcanic successions in the Abitibi, including the Blake River Group (BRG), have been interpreted as arc-related sequences, primarily on the basis of their geochemical signatures (e.g., Smith, 1980; Laflèche et al., 1992; Scott et al., 2002; Wyman and Kerrich, 2010). However, the calc-alkaline successions of the Abitibi differ markedly from modern arc volcanic facies (Bédard et al., 2013; Thurston, 2015). In contrast, modern arcs are typically long-lived and spatially extensive systems (e.g., Moyen and Laurent, 2018). Alternative explanations for the observed geochemical signatures, such as crustal assimilation or magma mixing, will be further discussed in this study.

Two assemblages dominated by sedimentary rocks, Porcupine and Timiskaming, were deposited after the seven volcanic-dominated ones (Corfu, 1993; Ayer et al., 2002; Thurston, 2015), and these locally contain alkaline to subalkaline volcanic rocks, but these two late assemblages are beyond the scope of this thesis. Supracrustal rocks were affected by tectonic deformation and metamorphism (e.g., Thurston, 2015).

1.1.3 Blake River Group

The Blake River assemblage represents the final major volcanic episode of the AGB, forming between ca. 2704 and 2695 Ma (Ayer et al., 2005; Thurston et al., 2008; McNicoll et al., 2014). It extends from the Timmins–Swayze area in Ontario to east of Val-d'Or in Québec (Fig. 1.2). Within this broader assemblage, the Blake River Group (BRG) forms its core, straddling the Québec–Ontario border between the towns of Cadillac and Matheson (Fig. 1.2). Remarkably, ~46% of the total VMS tonnage of the Abitibi, and more than 90% of its VMS-related gold, is concentrated within the BRG (Ayer et al., 2005; Mercier-Langevin et al., 2011b; Monecke et al., 2017).

Given its exceptional mineral endowment and the high level of preservation, the BRG has been the focus of extensive geological investigations. It is classically described as a submarine volcanic succession dominated by mafic to intermediate lava plains, with lesser but significant bimodal basalt–rhyolite units and local felsic-dominated volcanic centres (de Rosen-Spence, 1976; Goodwin, 1982; Dimroth et al., 1983; Hubert et al., 1984; Gelinas et al., 1984; Laflèche et al., 1992b; Peloquin et al., 2001, 2008; Ross et al., 2011a). This volcanic architecture is intruded by several generations of Archean synvolcanic to syntectonic plutons and by mostly Archean to minor Proterozoic dikes of diverse compositions (Paradis et al., 1988; Galley, 2003; Piercey et al., 2008; McNicoll et al., 2014).

Regionally, BRG rocks record a polyphase deformational history dominated by north–south-directed shortening, later overprinted by oblique dextral shearing (Hubert et al., 1984; Couture and Goutier, 1996; Daigneault et al., 2002). The earliest deformation (D1) is expressed as sinistral to transpressional movement along major regional structures, including the Porcupine–Destor and Larder Lake–Cadillac deformation zones. These zones exerted first-order control on the structural grain and on the distribution of volcanic units (Dimroth et al., 1983; Hubert et al., 1984; Daigneault et al., 2002). A subsequent phase (D2) produced a penetrative, steeply south-dipping east–west-striking regional schistosity (composite S1–S2) and associated folding that transposes stratigraphy, hydrothermal alteration, and sulfide lenses in the Noranda and Doyon–Bousquet–LaRonde camps (Gibson et al., 1983; Tourigny et al., 1988; Mercier-Langevin et al., 2007a; Krushinsky et al., 2022; Yergeau et al., 2022a). Later brittle–ductile deformation (D3 ± D4) is accommodated by conjugate kink bands and reactivation of earlier structures as ENE–WSW to E–W dextral shear zones, fragmenting the volcanic pile and locally remobilizing sulfides (Hubert et al., 1983; Pearson and Daigneault, 2009).

Despite this structural overprint, deformation across the BRG is highly heterogeneous, and primary volcanic textures are generally preserved in many areas. Regional metamorphism ranges from prehnite–pumpellyite to greenschist facies (Jolly, 1978; Dimroth et al., 1983; Powell et al., 1995; Yergeau et al., 2022a). Volcanic architecture remains especially well preserved in the central BRG, whereas stronger strain, pervasive schistosity, and carbonate metasomatism are concentrated along major deformation corridors and at the margins of the assemblage (Hubert et al., 1984; Pearson and Daigneault, 2009).

Several nomenclature schemes have been proposed for the BRG based in lithological and volcanic features (e.g., de Rosen-Spence,1976; Gibson and Watkinson,1990) but also based on geochemical distinctions between tholeiitic and calc-alkaline units that were recognized early (e.g., Smith, 1980; Goodwin, 1982; Capdevila et al., 1982; Gelinas et al., 1984). These works, along with numerous subsequent studies, culminated in the stratigraphic subdivisions used today, which are different in Ontario and Quebec. In Ontario, the BRG is divided into Lower and Upper Blake River (Ayer et al., 2005). In Québec, the provincial scheme recognizes nine formations: Rouyn-Pelletier, Duprat-Montbray, Noranda, Renault-Dufresnoy, Bousquet, Horne, Hébécourt, Camac, and Dupuis (Mercier-Langevin et al., 2011b; McNicoll et al., 2014; SIGÉOM, 2022). Only the Bousquet and Hébécourt formations currently hold formal stratigraphic status (Goutier, 1997; Lafrance et al., 2003).

Interpretations of possible caldera-type structures in the Noranda area (e.g., de Rosen-Spence, 1976; Gibson, 1989), along with the regional arrangement of mafic to intermediate dykes (among other features including the distribution of mafic to intermediate volcaniclastic rocks), motivated the interpretation of the BRG as a large, composite megacaldera system (Pearson and Daigneault, 2009). However, Ross et al. (2011a, b), integrating physical volcanology, geochemistry, and geochronology, showed that the volcaniclastic units were generated by multiple, temporally distinct eruptive events. Their work supports an architecture characterized by several decoupled eruptive centres and magma reservoirs, rather than a single, long-lived caldera system.

Since the 1980s, two contrasting schools of thought have shaped interpretations of BRG and AGB geodynamics. The first applies the framework of modern plate tectonics, invoking extensional regimes to explain tholeiitic signatures (analogous to mid-ocean ridges) and compressional settings to explain calc-alkaline suites (analogous to volcanic arcs), leading to back-arc interpretations (Dimroth et al., 1983; Gelinas and Ludden, 1984; Laflèche et al., 1992a, b). These

models later evolved into more complex scenarios involving multiple accretionary arcs with varying geometries where the BRG normally is interpreted as the last arc in the ABG evolution (Mueller et al., 1996; Daigneault et al., 2002). However, the close temporal overlap of contrasting magmatic signatures (tholeiitic vs. calc-alkaline) and the lack of strong parallels with modern volcanic arc successions have opened the door to alternative interpretations (see Bédard, 2018).

A second school, whose origins can be traced to early works in the AGB by Gorman et al. (1978) and Goodwin and Smith (1980) laid the foundations to a different scenario more recently named as a stagnant lid regime. In this framework, the lithosphere behaves as a thick, immobile outer shell lacking the long-lived subduction and lateral plate motion characteristic of modern plate tectonics. Heat loss and deformation are governed primarily by vertical processes such as mantle plumes, crustal thickening, gravitational instabilities, and drip-style lithospheric foundering. Magmatism is driven by plume upwellings and basaltic underplating, whereas crustal recycling occurs through delamination or sagduction rather than continuous subduction. The recent syntheses of Bédard (2018, 2024, and references therein) formalize this model and frequently use the BRG as a key example due to its exceptional preservation and extensive geological record.

1.1.4 Stoughton-Roquemaure assemblage

The Stoughton-Roquemaure (S-R) assemblage represents all volcanic activity in the AGB between ~2723 and ~2720 Ma (Ayer et al., 2002; Thurston et al., 2008; Dubé and Mercier-Langevin, 2020). It is the largest volcanic episode of the AGB, accounting for approximately 33% of the total volcanic surface area (Mercier-Langevin et al., 2023; Jorgensen and Gibson, 2024). In contrast to the BRG, this assemblage contains only one formal VMS deposit, the Estrades deposit, located in its northern zone (David et al., 2007).

The assemblage derives its name from the Stoughton-Roquemaure Group (Eakins, 1972; Dostal and Mueller, 1997), originally defined in the southern Abitibi where the volcanic succession was first described. In this region, the Stoughton-Roquemaure Group corresponds to a basaltic to basaltic-andesitic tholeiitic succession, locally interlayered with ultramafic flows, cut by intrusions, and metamorphosed from greenschist to amphibolite facies. Reported thicknesses vary substantially, from ~0.2 km to more than 6 km depending on structural position and level of erosion (MRNF, 2022a).

Progressive advances in mapping and U–Pb geochronology expanded recognition of this volcanic assemblage across the entire AGB (Barrie, 1999; Legault et al., 2002; Davis et al., 2005; Ayer et al., 2007; David et al., 2007; Davis et al., 2014), leading to the modern definition of its distribution (Thurston et al., 2008; Dubé and Mercier-Langevin, 2020; Jorgensen and Gibson, 2024).

Although several formations assigned to the S-R assemblage show lithological similarities to the Stoughton-Roquemaure Group – such as the Catherine Group to the south (Corfu, 1993), certain members of the Cartwright Group that reach up to 10 km in thickness (Legault et al., 2002), or the Bruneau Formation in the Chibougamau area (Leclerc et al., 2012) – many other units display markedly different volcanic characteristics. For example, the Deguisier Formation, dated slightly below the lower age limit of the assemblage (2719.4 ± 1 Ma; Pilote et al., 2009), contains significant intermediate to felsic calc-alkaline sequences. Comparable trends toward intermediate–felsic volcanism are also documented in parts of the Cartwright and Vanier-Dalet-Poirier Groups (Legault et al., 2002). In contrast, several formations across the wider AGB are dominated almost entirely by intermediate to felsic calc-alkaline volcanic rocks, such as the Burnbush volcanic complex (Barrett et al., 2013) in the western Abitibi, and the Blondeau (Leclerc et al., 2012; MRNF, 2024b) and Dessuieux formations (Goutier et al., 2004) in the Matagami–Chibougamau region.

For the present study, the distribution of the S-R assemblage follows Jorgensen and Gibson (2024). Detailed descriptions of the geological units included in the S-R assemblage are provided in Chapter 3.

1.2 Volcanic rock geochemistry of the Abitibi greenstone belt

The geochemistry of volcanic rocks in Archean greenstone belts is marked by significant variability and complexity (e.g., Moyen and Laurent, 2018; Bédard, 2018). Several works in the AGB (e.g., Smith, 1980; Goodwin, 1982; Capdevila et al., 1982; Dimroth et al., 1983; Gelinas et al., 1984; Chown et al., 1992; Laflèche et al., 1992a, b; Corfu, 1993; Dostal and Mueller, 1997; Sproule et al., 2002) and other greenstone belts has led to the identification of two major geochemical associations in greenstone belts (Anhaeusser, 2014; Thurston, 2015, and references therein): (1) komatiite-tholeiite sequences, and (2) bimodal basalt-dacite/rhyolite sequences. The former association consists of interlayered komatiitic and tholeiitic basalt flows, with minor volcaniclastic units. Boninites and ferropicrites may also occur, though they are rare (e.g., Kerrich et al., 1998). The latter association comprises alternating mafic and felsic volcanic rocks, ranging from tholeiitic to calc-alkaline (e.g., Leclerc et al., 2011; Bédard et al., 2013). The

term "bimodal" reflects the scarcity of intermediate compositions, which typically represent only ~15% of the volcanic stratigraphy in those successions (Condie, 1986; Anhaeusser, 2014).

In the AGB, assemblages interpreted as komatiite-tholeiite sequences include the Pacaud, Stoughton-Roquemaure, upper Kidd-Munro, and lower Tisdale assemblages (Dostal and Mueller, 1997, 2013; Scott et al., 2002; Thurston et al., 2008; Thurston, 2015). In contrast, the pre-2750 Ma assemblages, Deloro, lower Kidd-Munro, upper Tisdale, and Blake River are generally considered representatives of the bimodal basalt–dacite/rhyolite association (e.g., Kerrich et al., 1998; Polat and Kerrich, 2001; Hart et al., 2004; Ayer et al., 2005; Ross et al., 2011a, b; Bédard et al., 2013). However, interactions between both associations are observed in assemblages such as Pacaud, upper Kidd-Munro, and lower Tisdale (Thurston et al., 2008; Thurston, 2015). In general, komatiite-tholeiite sequences have been interpreted as related to mantle plumes (e.g., Sproule et al., 2002, Dostal and Mueller, 2013) and bimodal sequences have often been interpreted as related to volcanic arcs (e.g., Mueller et al., 1996; Wyman and Kerrich, 2010), although there are issues to applying modern plate tectonics to the Archean as mentioned above and illustrated by a published comment entitled “How many arcs can dance on the head of a plume?” (Bédard, 2013).

Some notable recent works have attempted to generate new geochemical classifications of the volcanic rocks in the AGB to bring petrological insights and further discuss tectonic interpretations. For instance, Mole et al. (2021) and Fassbender et al. (2023, 2024) represent two distinct methodologies in geochemical classification. Mole et al. (2021) applied a classical geochemical approach, using empirically defined thresholds based on major and trace element relationships (e.g., Th vs. TiO_2, MgO vs. SiO_2, Sr/Y vs K_2O/Na_2O). Note that some of the elements used for classification, such as K_2O, Na_2O and SiO_2, are mobile in hydrothermal systems. In contrast, Fassbender et al. (2023, 2024) employed machine learning techniques, specifically principal component analysis (PCA) combined with agglomerative hierarchical clustering, to classify felsic and mafic volcanic samples, respectively, from modern oceanic settings without predefined field boundaries. They then trained random forest algorithms (one for felsic rocks in the 2023 paper, one for mafic rocks in the 2024 paper) to recognize the clusters and applied them to their Abitibi datasets. As for the Mole et al. (2021) classification, some of the elements used in the Fassbender et al. papers are also mobile in hydrothermal systems (Ba, K_2O, SiO_2).

Both studies reached different conclusions regarding the dominant mafic compositions in the AGB. Mole et al. (2021) reported that their low-Th basalts (Table 1.1) represent the most common mafic type, predominantly tholeiitic in magmatic affinity, with flat REE-normalized patterns and

mantle array-like trace element ratios on the Pearce (2008) diagram. In contrast, Fassbender et al. (2024) identified their Cluster C7 (Table 1.2) as the most widespread mafic composition, characterized by negatively sloping REE patterns and higher Th-normalized concentrations, with trace element ratios intermediate between the mantle array and volcanic arc basalts on the Pearce (2008) diagram. However, Fassbender et al. (2024) noted that their algorithm struggled to confidently assign Abitibi samples to any modern tectonic cluster, likely because Archean magmas record different mantle conditions and melting regimes than those represented in the modern training dataset.

Regarding the felsic compositions, Mole et al. (2021) reported that sodic to potassic felsic rocks with low Sr/Y ratios (Table 1.1) are the most common felsic types, broadly comparable to Cluster C5 (Table 1.2) identified by Fassbender et al. (2023).

Table 1.1 Geochemical classification of volcanic rocks in the AGB from Mole et al. (2021).

Composition	Group name	Geochemical characteristics	Tectonic setting / interpretation	Occurrence in the Abitibi (examples)
Ultramafic	Komatiites (AUK, ADK)	High MgO (>18 wt%), low Ti, variable LREE	Mantle plume setting	Mainly Kidd–Munro assemblage (AUK), Deloro assemblage (ADK), Pacaud and Tisdale
Mafic	High-Th basalts	Th-enriched, incompatible trace element enrichment	Arc-related magmatism	Blake River Group, Kidd–Munro
	Medium-Th basalts	Moderate Th, transitional patterns	Transitional arc–back-arc	Blake River Group, Stoughton–Roquemaure
	Low-Th basalts	Low Th, flat REE patterns	Back-arc / MORB-like	Kidd–Munro, Stoughton–Roquemaure
	SHMB	Strongly enriched, high LILE/HFSE	Arc or arc–rift transition	Blake River Group
	LOTI basalts	Low Ti, depleted HFSE	Arc / supra-subduction zone	Kidd–Munro, Stoughton–Roquemaure
	Boninites	Low Ti, high MgO, depleted REE	Forearc / supra-subduction	Kidd–Munro
Intermediate-felsic	Sodic/potasic, High Sr/Y, HP	Sr/Y > 40, high-HREE depletion	Partial melting of thickened basaltic crust at high pressure; deep crustal roots	Blake River Group (mainly)
	Sodic/potasic , High Sr/Y, MP	Sr/Y > 40, medium-HREE depletion	Partial melting of basaltic crust at moderate depth	Blake River Group, Stoughton–Roquemaure
	Sodic/potasic , low Sr/Y, LP	Sr/Y < 40, higher HREE contents	Shallow crustal melting of mafic crust	Blake River Group
	Low-Nb/Yb	Low Nb/Yb and Th/Yb; elevated HREE; TiO_2 > 0.5%	Derived from ultra-depleted mantle sources, possibly boninitic affinity	Stoughton–Roquemaure

Abbreviations: ADK = aluminum-depleted komatiites; AUK = aluminum-undepleted komatiites; HFSE = high field strength elements; HREE = heavy rare earth elements; HP = high pressure; LILE = large ion lithophile elements; LOTI = low-Ti basalts; LP = low pressure; LREE = light rare earth elements; MP = medium pressure; MORB = mid-ocean ridge basalts; SHMB = siliceous high-magnesium basalts.

Table 1.2 Geochemical classification of volcanic rocks in the AGB from Fassbender et al. (2023, 2024).

Fassbender et al. (2023)				
Composition	**Group name**	**Geochemical characteristics**	**Tectonic setting / interpretation[1]**	**Occurrence in the Abitibi**
Felsic	C3 / FIIIb (dominant)	Flat REE pattern, HREE enrichment, slight negative Nb-Ta anomaly, intermediate negative Eu anomaly	Mid-ocean ridges and mature back-arc spreading centers	Matagami, Krist and Deloro, Quévillon
	C5 / FII, FIII fields	Flat to slightly LREE-rich REE pattern, negative Nb-Ta anomaly, weak negative Eu anomaly	Intraoceanic back arc and arc-related rifts	Noranda, Western Blake River, Kamiskotia, Normétal, Joutel, Selbaie
	C8 / FI, FII	High La/Sm, high La/Yb, intermediate negative Eu anomaly, intermediate negative Nb-Ta anomaly	Intracontinental back-arc spreading centers	Dumagami, Bousquet, Hunter, Lac Herbert
	C9 / FI, FII	High La/Sm, high La/Yb, intermediate negative Eu anomaly, intermediate negative Nb-Ta anomaly, strong HREE depletion	Intracontinental arc-related rift	Western Blake River, Hunter, Géant Dormant, Gemini
Fassbender et al. (2024)				
Mafic	C1	Very low La/Sm, very low Th/Yb; no Nb–Ta anomaly	MORB & mature back-arc spreading centers	Rare/absent in Abitibi (no confident C1 assignments; ~0.2% overall)
	C2	Low La/Sm, Th/Yb; no Nb-Ta anomaly	MORB & back-arc spreading	Common (~30% overall). Enriched in Kidd–Munro and Stoughton–Roquemaure
	C3	Intermediate La/Sm, Th/Yb; no Nb-Ta anomaly	Enriched MOR & mature back-arc spreading centers	Present (~7%). Strong in Kidd–Munro and Stoughton–Roquemaure
	C5	Intermediate La/Sm, Th/Yb; moderate negative Nb-Ta anomaly	Back-arc & arc-related rifts	Minor (~1–2% overall) but occurs with C6–C7 in Bousquet and Val-d'Or districts.
	C6	Intermediate La/Sm, high Th/Yb; strong negative Nb-Ta anomaly	Arc fronts & arc-related rifts	Present (~5%). Elevated in Tisdale (also C7), and in Bousquet/Val-d'Or.
	C7	High La/Sm, Th/Yb; moderate negative Nb-Ta anomaly	Nascent back-arc rifts & continental margins	Dominant (~56%). High in Blake River (Noranda) and Deloro; also strong in Tisdale and parts of Val-d'Or/Noranda

Abbreviations: FI to FIII = Felsic rock classification from Hart et al. (2004).
1. Based on the presence of geochemically similar rocks in these tectonic settings on the modern ocean floor.

1.3 VMS deposits

Volcanogenic massive sulfide (VMS) deposits are strata-bound accumulations of sulfide minerals and important sources of Zn, Cu, Pb, Ag, and Au, as well as several critical and strategic elements (e.g., Mn, Sn, Te) (Barrie and Hannington, 1999; Franklin et al., 2005; Galley et al., 2007). These deposits form at or near the seafloor in association with submarine volcanic activity and hydrothermal fluid discharge (Franklin et al., 2005; Ross and Mercier-Langevin, 2014). Modern analogues include more than 300 hydrothermal sites, primarily located along mid-ocean ridges, back-arc basins, and submarine arcs (Hannington et al., 2005; Shanks and Thurston, 2012).

VMS deposits are considered "exhalative" because they are formed by a focussed continuous to episodic discharge of hot metal-rich hydrothermal fluid at the seafloor (Eckstrand et al., 1995; Galley et al., 2007). The hydrothermal fluids in VMS deposits can reach temperatures of 350-450°C (Spooner and Bray, 1977). The typical mound-shaped to tabular massive sulfide lens contains ~40% sulfides, quartz, subordinate phyllosilicates, iron oxide minerals and altered silicate wall-rock (Galley et al., 2007). Usually, the lens is underlain by discordant to semi-concordant stockwork (stringer) veins and disseminated sulfides. This stockwork vein system has a distinctive alteration halo, with chlorite-quartz-sulfide±sericite±talc in the core grading outward to sericite-rich mineral assemblages (Galley et al., 2007) (Fig. 1.3).

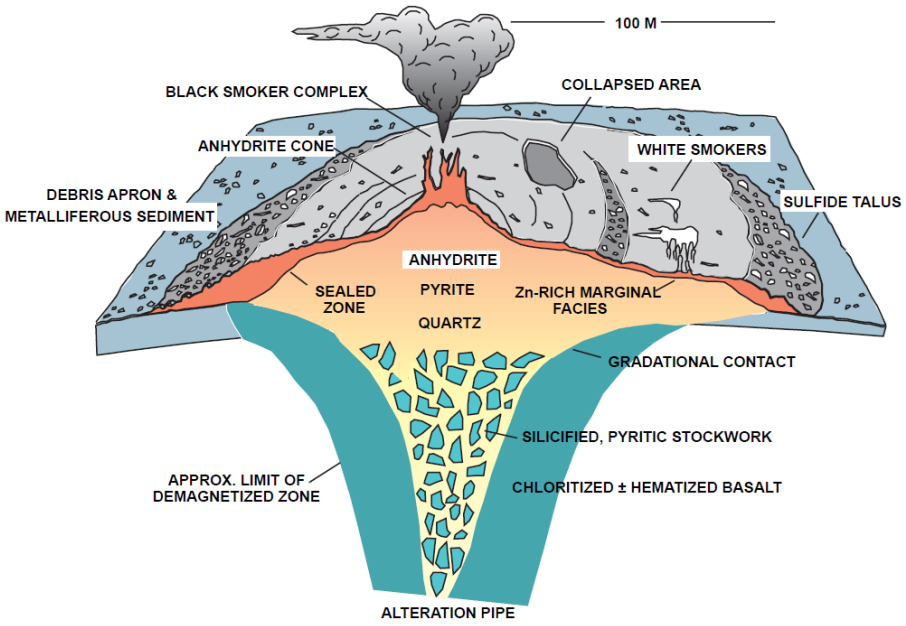

Figure 1.3 Schematic diagram of a sulfide deposit on the Mid-Atlantic Ridge. This figure represents a classic cross-section of a VMS deposit, with a concordant semi-massive to massive sulfide lens underlain by a discordant stockwork vein system and associated alteration halo, or "pipe" (Hannington et al., 1998).

The most common VMS classification uses a lithostratigraphic scheme based primarily on the volcanic and sedimentary lithological units formed concurrently with (Table 1.3, Fig. 1.4), or just before, the deposits in a given district that also show a common metal association (Franklin et al., 2005, Galley et al., 2007; Piercey, 2011; Piercey et al., 2023). Alternatively, their host volcanic rocks can separate VMS deposits into two types: lava flow-dominated and volcaniclastic-dominated (Morton and Franklin, 1987; Gibson and Watkinson, 1990).

Table 1.3 VMS deposits subtypes based on lithologic association (see text).

Subtype / lithologic Association	Common metal associations	Representative traditional name(s)
Mafic	Cu and/or Cu-Zn dominated	Cyprus
Bimodal-Mafic	Cu and/or Cu-Zn dominated	Noranda
Bimodal-Felsic	Zn–Cu–Pb	Kuroko
Felsic-Siliciclastic	Zn–Cu–Pb	Bathurst / Iberian Pyrite Belt
Mafic-Siliciclastic	Cu-Zn-Co	Besshi
Hybrid Bimodal–Felsic (Epithermal–VMS)	Zn-Pb > Cu	-

In terms of association with specific volcanic rocks, Ross and Mercier-Langevin (2014) distinguish VMS deposits related to (1) felsic dome complexes and lavas, (2) pumiceous felsic pyroclastic rocks (including those formed by submarine calderas) and (3) basaltic volcanic rocks and sills. Some deposits are associated with other volcanic settings, although these three categories cover a large proportion of deposits (Ross and Mercier-Langevin, 2014).

VMS deposits are globally distributed and range in age from the Paleoarchean to modern seafloor systems. In Canada, they are found in every geographic province except Alberta and Prince Edward Island, with the highest concentration in Quebec (~33%) (Galley et al., 2007). Globally, most VMS deposits occur in Phanerozoic terranes (72%), followed by Proterozoic (20%) and Archean (8%) belts (Mercier-Langevin et al., 2014).

1.4 Problem to be solved

The processes responsible for the formation of VMS deposits are relatively well understood at the scale of individual deposits, and districts (e.g., Gibson and Watkinson, 1990; Barrie and Hannington, 1999; Franklin et al., 2005; Galley et al., 2007; Mercier-Langevin et al., 2014; Monecke et al., 2014; Ross and Mercier-Langevin, 2014, Piercey et al., 2015, 2023). However, volcanic centers with similar lithological and stratigraphic characteristics can display striking contrasts in VMS endowment. Within the AGB, different volcanic assemblages have very different endowments (Fig. 1.5); within the Superior Province, different greenstone belts have variable endowments. This disparity may be linked to differences in tectonic setting or magmatic processes (e.g., Piercey, 2011). Other studies have proposed that the presence of long-lived transcrustal structures (Jorgensen et al., 2022) or proximity to thermal engines such as synvolcanic intrusions (Galley, 2003) may play a key role in controlling regional VMS fertility.

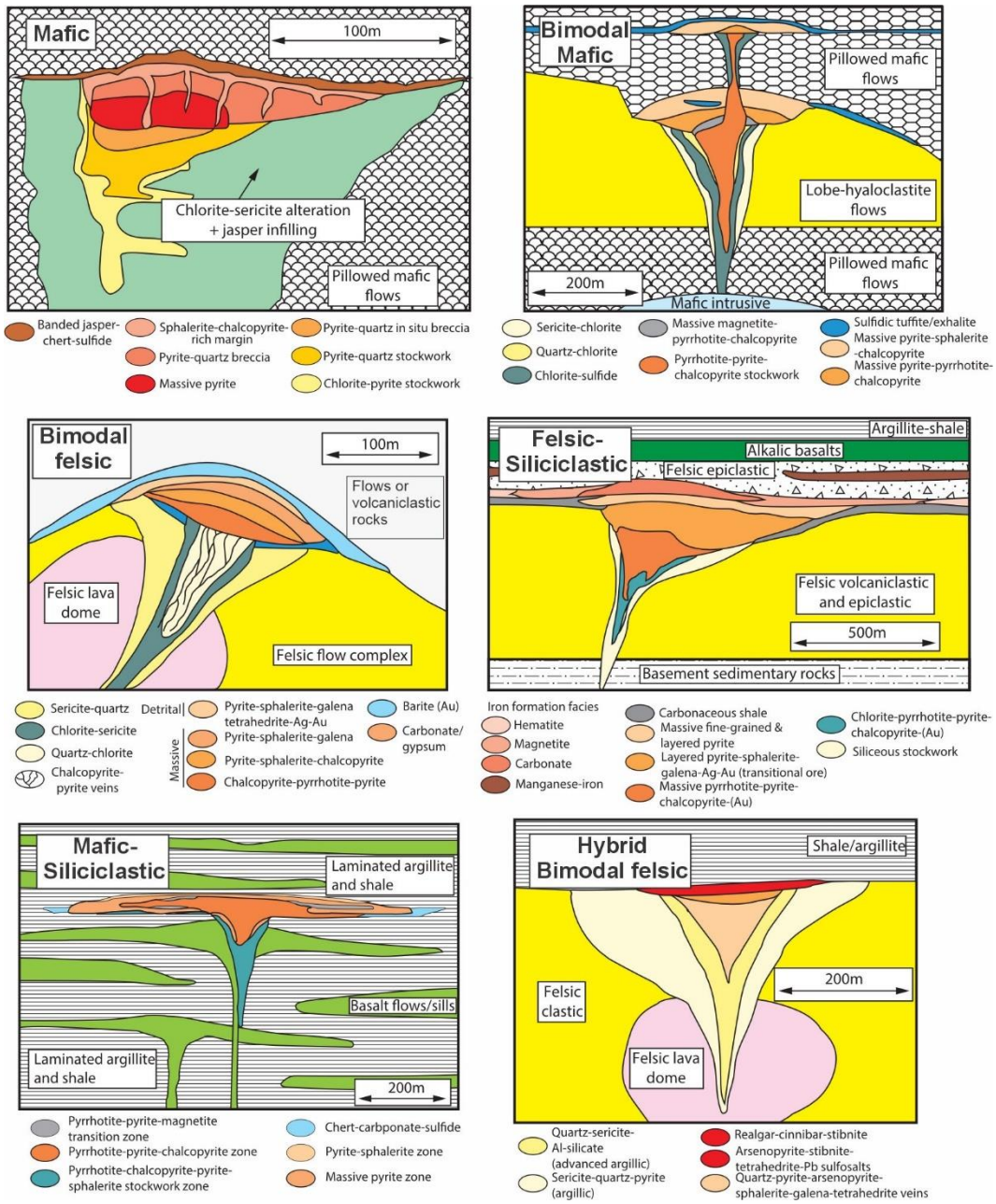

Figure 1.4 Sub-classes of volcanogenic massive sulfide deposits. Modified from Galley et al. (2007) and Piercey et al. (2023).

Our limited understanding of the causes of variable VMS fertility at the assemblage, greenstone belt and craton scales reflects, in part, uncertainty regarding Archean volcanic, magmatic, tectonic and crust-mantle processes (e.g., Bédard, 2018; Palin et al., 2020; Iles et al., 2025). There has been only limited research done at these scales with the appropriate tools, to resolve this fundamental question. A comparison of the geology, geochemistry, geophysics and geochronology of variably VMS endowed assemblages within the AGB could bring a better

understanding on the controls on VMS endowment during the evolution and assembly of greenstone belts.

Looking at geochemistry specifically, no previous study has systematically compared the full range of volcanic compositions between assemblages in the AGB, nor assessed their distribution at the scale of entire assemblages and mining districts considering the whole volcanic compositional spectrum, from ultramafic to felsic. Also, petrogenetic modelling of Archean volcanic rocks using modern modeling tools has been rather limited, partly because of the fear that hydrothermal alteration and metamorphism may have completely obscured the primary signatures of those rocks.

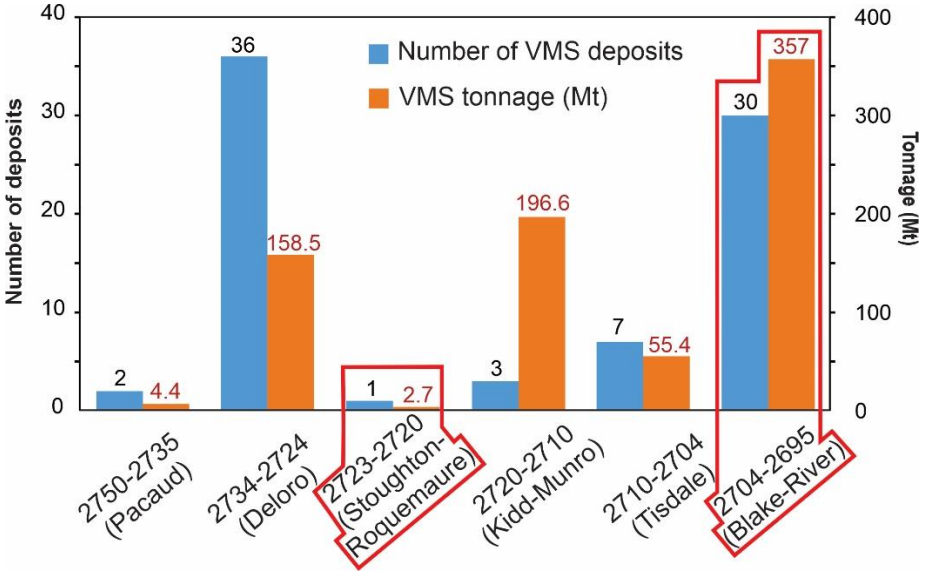

Figure 1.5 Distribution of VMS deposits by number and tonnage. Modified from Monecke et al. (2017).

1.5 Aims

This study aims to systematically compare the highly VMS-endowed Blake River Group (BRG), representing the Blake River assemblage, with the poorly endowed Stoughton-Roquemaure (S-R) assemblage in the AGB, through an integrated geochemical and petrogenetic approach. These assemblages were chosen as representative endmembers in terms of VMS fertility (Fig. 1.5). The overarching goal is to better understand the controls on the differential VMS endowment between these two contrasting assemblages by constraining the petrogenetic processes underlying the observed geochemical signatures. This approach offers a more comprehensive framework to understand the metallogenic evolution of the AGB and might improve exploration strategies both regionally and in other Archean terranes.

To achieve this, four specific objectives are proposed:

1. Compile a comprehensive geochemical database of volcanic rocks from both assemblages, including major and key trace elements, ensuring adequate data quality and representativeness.
2. Develop a unified classification scheme to group volcanic rocks from both the BRG and the S-R assemblage, enabling a consistent geochemical comparison.
3. Apply petrogenetic modeling to explain the geochemical diversity, using both closed-system fractional crystallization (FC) and open-system processes such as assimilation–fractional crystallization (AFC) and magma mixing.
4. Interpret the petrogenetic evolution within and between assemblages to assess their link with VMS fertility.

1.6 Overview of the methods

1.6.1 Database compilation

More than 5,000 analyses of BRG and S-R assemblage rocks were collected for this work, from which the final database was reduced to 4,528. The reduction was made according to the completeness of the data for major elements, as well as presence of loss on ignition (LOI) and sufficient trace elements, especially the petrologically canonical high field strength elements (HFSE; Nb, Th, Zr, Y) and rare earth elements (REE; La, Ce, Sm, Gd, Eu, Yb). These compiled analyses come mostly from the "Système d'information géominière" (SIGÉOM) of the Ministère des Ressources naturelles et des Forêts (Québec), and from the Geological Survey of Ontario reports from which reports newer than the year 2000 were prioritized. The remaining data was sourced from scientific publications, academic theses, mineral exploration reports, and unpublished data. 3209 analyses are from the BRG and 1319 are from the S-R assemblage.

In chapters 2 and 3, least-altered subsets are introduced for the BRG (n = 2257) and the S-R assemblage (n = 979). These least-altered subsets are only used on geochemical plots involving mobile elements, such as Harker diagrams, which are important for modelling. Most of the work however, including the geochemical grouping exercise, was done on the full datasets using immobile element ratios, as explained in the next section.

1.6.2 Ratios of immobile elements

Secondary processes such as diagenesis, metamorphism, and hydrothermal alteration are common in Precambrian greenstone belts, particularly in and around VMS systems (MacLean and Barrett, 1993). In such contexts, mobile elements – including Na_2O, K_2O, and SiO_2 (the main constituents of the total alkali-silica or TAS diagram) – can be significantly affected. This issue is well documented in VMS-bearing environments in the Abitibi, where pervasive alteration can completely mask the original geochemical character of the rocks (e.g., MacLean and Kranidiotis, 1987; Barret and MacLean, 1994; Rogers et al., 2014; Debreil et al., 2014). Relying solely on major elements in such settings would lead to misclassification if altered rocks are considered in the dataset. Alternatively, screening out altered rocks from the dabase in order to use mobile elements would lead to the omission of important VMS-related volcanic units. For example, the Watson Lake Group, the footwall of the Matagami VMS deposits in the Deloro assemblage, would be almost completely removed from a classification of AGB volcanic rocks (Debreil, 2014), if altered rocks were screened out before classification (Fig. 1.6).

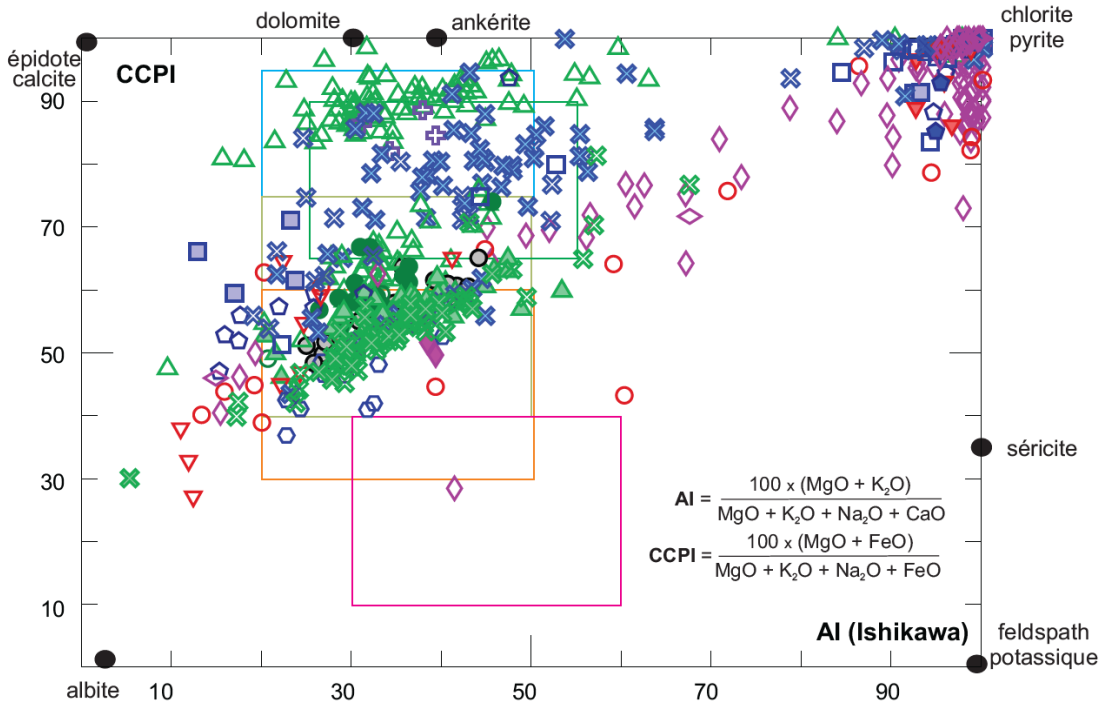

Figure 1.6 Figure from Debreil (2014) from the Matagami VMS camp volcanics. It displays that nearly all samples from the Watson Lake Group (purple diamonds), which is the footwall of the VMS deposits, are strongly altered, largely plotting near the chlorite–pyrite alteration pole. These samples would be removed if a database was screened for alteration before classifying the volcanic rocks.

To minimize these large sources of error or bias, this work adopts a classification based on ratios of immobile elements, particularly those involving trace elements such HFSE and REE, which are generally considered robust against post-magmatic mobilization (e.g., Winchester and Floyd, 1977; Pearce, 1996; Rollinson and Pease, 2021). This approach is especially suitable for Archean terranes, where seafloor alteration, and greenschist- to amphibolite-facies metamorphism are pervasive (see section 1.1). Using immobile-element ratios allows altered samples to be meaningfully compared to less altered equivalents.

A key advantage of using trace elements is that ratios of immobile elements remain relatively constant even when rocks undergo mass gains or losses during alteration (Pearce, 1996). Ratios such as Zr/Ti and Th/Yb therefore provide a robust framework for classifying volcanic rocks, monitoring fractionation (e.g., Zr/Ti; Winchester and Floyd, 1977), and evaluating petrogenetic processes such as crustal assimilation or mantle enrichment (e.g., Nb–Yb–Th systematics; Pearce, 2008; Ross and Bédard, 2009; Pearce et al., 2021).

Despite their utility, immobile-element diagrams have inherent limitations. For example, the Zr/Ti ratio is not a perfect substitute for SiO_2 when naming volcanic rocks. Pearce (1996) explicitly recognized this when revising the Winchester and Floyd (1977) diagram, broadening the fields and introducing 90% probability contours to capture natural variability. Even with these refinements, field overlap persists. Rock classifications using the Zr/Ti ratio have a success rate in the 70–80% range for volcanic rocks in modern settings (Lang et al., 2023).

Overall, while immobile trace-element ratios provide the most reliable means of classifying altered Archean volcanic rocks, they should not be interpreted in isolation. In this study, diagrams derived from Winchester and Floyd (1977), Pearce (1996) and Ross and Bédard (2009), are used as supporting tools integrated with PCA results, extended trace-element patterns, and petrological context to refine interpretations of volcanic composition and magmatic processes.

1.6.3 Principal component analysis

In order to define the most representative set of elements of the dataset, a principal component analysis (PCA) is applied as it has wide acceptability and application in earth sciences (e.g., Rollinson and Pease, 2021). PCA is a multivariate statistical technique used to reduce the dimensionality of complex datasets while preserving most of the original variability. It identifies new, uncorrelated variables called principal components (PCs), which are linear combinations of the original variables (e.g., Albarède, 1995).

The first principal component (PC1) captures the largest amount of variance in the dataset, followed by PC2, and so on. Each subsequent component is orthogonal to the previous ones, ensuring that no redundant information is included. The number of PCs retained typically depends on the proportion of variance explained.

In geochemistry, PCA is particularly useful for handling large datasets involving multiple major, trace, and rare earth elements. By projecting samples into a lower-dimensional space defined by a few PCs, PCA highlights compositional trends, major clusters, and outliers that might be obscured in raw data tables. Moreover, the loadings of each element on the PCs provide insights into the variables driving the geochemical variance (e.g., Rollinson and Pease, 2021).

PCA assumes linear relationships and is sensitive to the scaling of variables; therefore, geochemical data are typically standardized. This work uses the centered log-ratio from Atchinson (1986).

Separate PCAs are presented for the BRG and S-R assemblage in subsequent chapters. Because the goal of the exercise was to identify primary geochemical signatures, only the following immobile elements were included in the PCAs: Al, Ce, Eu, Gd, La, Nb, Sm, Th, Ti, Y, Yb, Zr.

1.6.4 Geochemical grouping

The geochemical grouping used in this study was initially developed for the BRG by constructing a classification diagram based on two immobile-element ratios: Zr/Ti and Th/Yb. These ratios were selected using PCA, which identified the elements contributing most strongly to the observed geochemical variability. The Zr/Ti ratio primarily reflects magmatic fractionation processes (e.g., Winchester and Floyd, 1977, employ it as a substitute for SiO_2), whereas the Th/Yb ratio is sensitive to magmatic affinity and can also record processes such as crustal assimilation or subduction-related inputs (e.g., Ross and Bédard, 2009; Pearce, 2008).

To define compositional groups, clustering techniques such as k-means were first applied to identify major trends in the Zr/Ti vs. Th/Yb space. However, the final group boundaries were refined manually to ensure that groups made sense on other geochemical diagrams (employing other elements) and on the geological map (spatial consistency). A detailed explanation of this geochemical classification methodology is provided in Chapter 2 (Vite-Sánchez et al., 2024).

1.6.5 Magma Chamber Simulator

The Magma Chamber Simulator (MCS) is a thermodynamic tool designed to model the close- to open-system evolution of magmatic systems (Bohrson et al., 2014, 2020). It integrates mass and energy balance with phase equilibria to simulate the evolving major and trace element compositions, isotopic ratios (if required; not used in this work), and thermal conditions of a magma body. The model considers four interacting subsystems: the resident magma, the cumulate reservoir, the wallrock, and the recharge reservoirs. Within this framework, MCS can model fractional crystallization (FC), assimilation of anatectic melts or stoped wallrock blocks (AFC), and magma recharge/mixing events.

The resident magma, initially defined as a finite mass in a well-constrained thermodynamic state, is coupled to its host wallrock under adiabatic and semipermeable conditions. During AFC, both sensible heat (magma cooling) and latent heat (crystallization and cumulate formation) are transferred across the magma-wallrock boundary. When partial melting of the wallrock occurs and the melt fraction exceeds a critical percolation threshold, the resulting anatectic melt is transferred into the magma reservoir, where it equilibrates with the resident magma, generating a new hybrid composition.

MCS operates through incremental temperature decrements, resolving at each step the redistribution of mass and enthalpy among all subsystems while simultaneously tracking phase equilibria and the evolving major, trace, and isotopic compositions. Calculations are carried out in two modules. The first, MCS-PhaseEQ, computes phase equilibria, major element compositions, and the thermal evolution of all subsystems. User-defined parameters include initial masses, pressure, oxygen fugacity buffers, the percolation threshold, the number of recharge events, and optional suppression of specific phases. These computations employ the MELTS thermodynamic engines (Ghiorso and Sack, 1995; Asimow and Ghiorso, 1998; Ghiorso et al., 2002; Gualda et al., 2012; Ghiorso and Gualda, 2015), and this study uses version 1.2.0. The resulting ‘RunSummary’ output is then used by the second module, MCS-Traces (Heinonen et al., 2020), which calculates the evolution of trace elements and isotopic systems based on user-defined initial concentrations and partition coefficients.

Both modules share a Visual Basic interface and generate a comprehensive Excel-based multitab output. Results include major element compositions, phase proportions, and the thermal histories of all subsystems, along with trace element trajectories, isotopic evolution, and prebuilt graphs for rapid comparison with natural geochemical datasets.

This work used the MCS to evaluate FC, AFC and magma mixing in chapter 2 and 3. The compositions used in the models and a summary of the conditions are summarized in tables 1.4 and 1.5, respectively.

Table 1.4 Compositions used for the MCS models.

Sample	Tholeiitic basalt endmember: sample 74J1328 (BRG)	Tholeiitic basalt endmember: sample 1992005106 (S-R)	Average of SE Superior Province TTGs (Mole et al., 2021)
SiO_2	49.0	48.5	68.6
TiO_2	0.8	0.7	0.3
Al_2O_3	13.3	13.8	15.4
Fe_2O_3t	11.7	12.3	2.7
MnO	0.2	0.1	0
MgO	11.1	11.1	1.0
CaO	11.1	11.4	3.0
Na_2O	1.5	1.3	4.8
K_2O	0.6	0.2	1.8
P_2O_5	0.1	0.1	0.1
Th	0.21	0.24	3.9
Nb	1.74	3.2	19.3
La	2.49	3.75	21.7
Ce	6.5	10	44.9
Nd	5.2	8.3	19.3
Sm	1.71	2.54	3.48
Zr	35	50	114
Hf	1.1	1.3	3.0
Eu	0.5	0.72	0.85
Gd	2.13	2.81	2.5
Dy	2.70	3.32	1.21
Y	16.8	19.3	6.2
Yb	1.84	2.06	0.52
Lu	0.283	0.289	0.09

Table 1.5 Parameters for the MCS models.

Magma initial temperature	Wall rock or melt	Pressure (kbars)	Water content (initial composition)	Oxygen buffer
Fractional crystallization				
BRG				
1286 ºC	-	2.5	0.0%	fmq*
1277 ºC	-	2.5	0.5%	fmq*
1258ºC	-	2.5	1.2%	fmq*
S-R				
1250 ºC	-	1.5	0.1%	fmq +1
1300 ºC	-	3	0.1%	fmq +1
1350 ºC	-	6	0.1%	fmq +1
1430 ºC	-	10	0.1%	fmq +1
1550 ºC	-	20	0.1%	fmq +1
1240 ºC	-	1.5	1.0%	fmq +1
1260 ºC	-	3	1.0%	fmq +1
1300 ºC	-	6	1.0%	fmq +1
1375 ºC	-	10	1.0%	fmq +1
1535 ºC	-	20	1.0%	fmq +1
Assimilation fractional crystallization				
BRG				
1286 ºC	400 ºC (90 g)	2.5	0.0%	fmq*
1277 ºC	400 ºC (70 g)	2.5	0.5%	fmq*
1258ºC	400 ºC (70 g)	2.5	1.2%	fmq*
S-R				
1287 ºC	300 ºC (100 g)	3	0.1%	fmq +1
1343 ºC	600 ºC (100 g)	6	0.1%	fmq +0.5
1243 ºC	300 ºC (100 g)	3	1.0%	fmq +1
1294 ºC	600 ºC (100 g)	6	1.0%	fmq +0.5
Magma mixing				
S-R				
1249 ºC	1000 ºC (1-1 ratio)	3	1.0%	fmq
1249 ºC	1000 ºC (1-4 ratio)	3	1.0%	fmq
1249 ºC	1000 ºC (4-1 ratio)	3	1.0%	fmq

* The actual oxygen buffer used for the BRG models was hm -5 (Chapter 2), which is approximately equivalent to fmq (Frost et al., 1988).

Some important limitations are that MCS does not include a module for generating primary mantle melts (like pMELTS, Ghiorso et al., 2002) meaning that initial mafic magma compositions must be validated or constrained using external tools such as PRIMELT, experimental data, or independent geochemical criteria. In addition, the simulator operates as a zero-dimensional

equilibrium model which is effective for capturing first-order open-system processes but cannot reproduce finer aspects of crustal architecture, such as vertical or lateral heterogeneities. The stability of amphibole- and biotite-rich, hydrous mafic to intermediate magmas is also imperfectly represented because the underlying MELTS engines do not fully capture their phase relations (Gualda et al., 2012), which directly impacts modeled water budgets, phase proportions, and trace-element behaviour. Furthermore, MELTS incorporates only a limited set of accessory phases (mainly apatite and some oxides), while several key trace-element hosts – such as zircon, titanite and monazite – are not explicitly modelled (Ghiorso and Sack, 1995; Iles et al., 2022).

1.6.6 PRIMELT3

PRIMELT3 (Herzberg and Asimow, 2015) is an inverse modeling tool designed to reconstruct the primary magma compositions of primitive mafic to ultramafic rocks (typically >9 wt.% MgO). It calculates the composition of the melt in equilibrium with a fertile peridotite source under nominally anhydrous conditions and estimates key mantle melting parameters, including the mantle potential temperature (Tp), degree of partial melting (F), and residual lithology of the source. The algorithm incrementally adds or subtracts equilibrium olivine in 1 wt.% steps to back-calculate the composition of the parental melt, using projections in the olivine–anorthite–quartz (Ol–An–Qz) and FeO–MgO spaces (Herzberg and O'Hara, 2002). The reconstructed primary melt represents the volatile-free parental magma generated by adiabatic decompression melting of a fertile peridotite source.

PRIMELT3 simulates accumulated fractional melting during adiabatic decompression of a peridotitic mantle source, using experimental calibrations on fertile peridotite KR-4003 (Walter, 1998). Unlike batch melting, where melts remain in equilibrium with the residue, accumulated fractional melting assumes that small increments of melt are extracted continuously and mixed during ascent, producing an aggregate melt that is not in equilibrium with the final residue. This behavior better reflects natural mantle melting regimes, where melts segregate rapidly into channels or porous networks and migrate without extensive re-equilibration. These results are preferred over batch melting as better reflects natural systems (Herzberg and Asimow, 2015).

In this work we use PRIMELT3-P (Herzberg et al., 2023) that has the same strength and methods of PRIMELT3 (Herzberg and Asimow, 2015). Here, we focus on validating the reconstructed primary magma compositions for the MCS models and exploring the thermal conditions and compositional characteristics of the potential primary magmas. One limitation is that PRIMELT operates under volatile-free assumptions, which may not fully represent natural magmas

containing dissolved H_2O or CO_2. In addition, alteration or mobilization of major elements can affect the accuracy of primary magma estimates and should be considered when interpreting results.

1.7 Thesis organization

This thesis is presented with a hybrid format, intermediate between a classical dissertation and a thesis by publication. It contains three traditional chapters (1, 4, 5), written by the PhD candidate and revised by the thesis supervisors. The thesis also contains two published papers (chapters 2 and 3) and the roles of each author in these chapters are presented in the next section.

Chapter 1 serves as the general introduction. Chapter 2 focuses on the VMS-rich BRG and presents the initial development of the geochemical classification system, which in this case is applied to volcanic rocks with mafic and intermediate compositions. This chapter also contains petrogenetic models done in MCS, including work on variable water contents in FC models to explain the tholeiitic series, as well as initial AFC modeling to explain the transitional to calc-alkaline affinities in the BRG. Finally, chapter 2 presents a geochemical comparison between the well-endowed and less-endowed formations of the BRG with regards to VMS deposits and discusses metallogenic implications.

Chapter 3 applies the same classification framework, expanded to include felsic volcanic rocks, to the VMS-poor S-R assemblage. Petrogenetic modeling in MCS presented in chapter 4 includes refining the relevant depth (pressure) applied to FC models and introducing magma mixing models as a possible alternative to AFC models to explain the crustal input in some geochemical groups. This chapter also presents estimates of primary magma compositions and mantle potential temperatures, for komatiitic rocks and tholeiitic basalts, using PRIMELT3. The geographic distribution of the geochemical groups in the S-R assemblage is explored and the petrogenetic implications are discussed.

Chapter 4 aims to compare the geochemical characteristics and petrogenetic evolution of the S-R assemblage and the BRG. The chapter starts by presenting the felsic geochemical groups from the BRG, which were not introduced and described in chapter 2 due to a lack of space in the paper. Chapter 4 then synthesizes and compares the geochemical trends and petrogenetic process between the two assemblages. Comparisons between endowed and less endowed portions of assemblages are also made. Finally, based on petrological interpretations and the identified differences, hypotheses about the factors controlling the contrasting metal endowments of these volcanic successions are proposed.

Finally, Chapter 5 provides a general discussion, concluding remarks, and recommendations for future work, based on the findings of the preceding chapters.

1.8 Contribution of the authors to the publications

This section outlines the roles of different people in the multi-author publications inserted as chapters 2 and 3.

Chapter 2: Published by O. Vite-Sánchez, P.-S. Ross, and P. Mercier-Langevin in Precambrian Research, in 2024, with the title of “Mafic to intermediate volcanic rocks of the Blake River Group, Abitibi greenstone belt, Canada: Geochemistry, petrogenesis and relation with VMS deposits” (volume 404, article 107331).

- O. Vite-Sánchez: Writing – original draft, Visualization, Validation, Software, Investigation, Formal analysis, Data curation, Conceptualization.
- P.-S. Ross: Conceptualization, Methodology, Validation, Resources, Writing – review & editing, Resources, Supervision, Project administration, Funding acquisition.
- P. Mercier-Langevin: Writing – review & editing, Validation, Supervision, Project administration, Methodology, Conceptualization.

Chapter 3: Published by O. Vite-Sánchez, P.-S. Ross, P. Mercier-Langevin and K. Iles in Canadian Journal of Earth Sciences, in 2025, with the title of “Petrogenetic insights on the largest volcanic pulse in the Archean Abitibi greenstone belt, Canada: the Stoughton-Roquemaure assemblage” (e-First).

- O. Vite-Sánchez: Writing – original draft, Visualization, Validation, Software, Investigation, Formal analysis, Data curation, Conceptualization.
- P. S. Ross: conceptualization, Methodology, Validation, Resources, Writing – review & editing, Resources, Supervision, Project administration, Funding acquisition.
- P. Mercier-Langevin: Writing – review & editing, Validation, Supervision, Project administration, Methodology, Conceptualization.
- K. Iles: Writing – review & editing, Validation.

2 FIRST ARTICLE: BLAKE RIVER GROUP

Mafic to intermediate volcanic rocks of the Blake River Group, Abitibi greenstone belt, Canada: Geochemistry, petrogenesis and relation with VMS deposits

Roches volcaniques mafiques à intermédiaires du Groupe de Blake River, ceinture de roches vertes de l'Abitibi, Canada : géochimie, pétrogenèse et relation avec les gisements de SMV

Authors :

Octavio Vite-Sánchez[a], Pierre-Simon Ross[a], Patrick Mercier-Langevin[b, c]

a.- Institut national de la recherche scientifique, 490 rue de la Couronne, Québec (Qc), G1K 9A9, Canada

b.- Geological Survey of Canada, 490 rue de la Couronne, Québec, G1K 9A9, Canada

c.- Now at: Agnico Eagle Mines Ltd, 145 King St. East, Suite 400, Toronto, Ontario, M5C 2Y7, Canada.

Title of the journal:

Precambrian Research

Accepted: 14 February 2024

DOI: 10.1016/j.precamres.2024.107331

This chapter is the accepted version of the research article:

Vite-Sánchez, O., Ross, P.S. and Mercier-Langevin, P., 2024. Mafic to intermediate volcanic rocks of the Blake River Group, Abitibi greenstone belt, Canada: Geochemistry, petrogenesis and relation with VMS deposits. Precambrian Research, 404, article 107331

2.1 Abstract

Volcanogenic massive sulfide (VMS) deposits, prevalent since the Archean, constitute a well-explored ore deposit type. Nonetheless, the factors contributing to variations in fertility among volcanic centers, assemblages within greenstone belts, or entire greenstone belts remain unclear. For instance, the Blake River Group (BRG) of Ontario and Quebec, Canada, hosts almost half of the total VMS tonnage of the entire Abitibi greenstone belt, yet represents less than 10 % of its map surface. This study utilizes a large dataset (n = 2271) of whole-rock geochemistry for mafic to intermediate volcanic rocks to understand the BRG petrogenesis, and its implications for VMS endowment in the Abitibi. Principal Component Analysis shows that Ti, Th, and Yb are the primary contributors to the dataset's variation.

This yields a two-ratio diagram (Th/Yb versus Zr/Ti) revealing seven geochemical groups with coherent map patterns referenced as tholeiitic basalts, tholeiitic intermediate rocks, medium-Th basalts, transitional intermediate rocks, high-Th basalts, calc-alkaline intermediate rocks and low-Zr basalts. A least altered subset of the data is used to analyze major element patterns. BRG mafic to intermediate magmas show variable degrees of Fe-Ti enrichment/depletion during their evolution, with simultaneous Al2O3 depletion or lack thereof. Utilizing a single parental mafic tholeiitic magma, the Magma Chamber Simulator enables the modeling of major and trace element compositions for each geochemical group. Fractional crystallization (FC) models with variable initial water contents can explain the range of the tholeiitic basalt and tholeiitic intermediate compositions. Assimilation fractional crystallization (AFC) models successfully replicate most of the geochemical groups using a TTG average composition for the assimilant. While mafic-intermediate host rock geochemical signatures are not the sole factor influencing VMS endowment in volcanic belts, regional analysis reveals that the vast majority of volcanic rocks in geological formations bearing VMS deposits in the BRG are crustally contaminated lacking tholeiitic geochemical groups. Conversely, poorly endowed formation consistently contains samples from these groups. Moreover, the Bousquet formation, which hosts several world-class gold-rich VMS deposits, displays the highest rates of crustal assimilation, further suggesting that petrogenesis of mafic-intermediate volcanic rocks is linked to VMS metallogenesis in the BRG.

2.2 Introduction

Volcanogenic massive sulfide (VMS) deposits have been subdivided using several classification schemes, including host-rock lithologies, base and precious metal contents, and tectonic settings (e.g., Franklin et al., 1981, 2005; Cox and Singer, 1986; Barrie and Hannington, 1999; Galley et al., 2007; Mosier et al., 2009; Mercier-Langevin et al., 2011a; Ross and Mercier-Langevin, 2014). VMS mineralization occurs in submarine volcanic and volcano-sedimentary successions related to mid-ocean ridges, back-arc basins, volcanic arcs, and continental margins (Franklin et al., 2005; Hannington et al., 2005; Galley et al., 2007).

VMS ores occur in terranes from 3.4 Ga to the present, as they are actively forming in modern seafloor environments (Hannington et al., 2005; Galley et al., 2007). The Superior Province of Canada hosts 80% of the total tonnage of Archean VMS deposits (Mercier-Langevin et al., 2014), despite covering a much smaller portion of preserved Archean crust. The 2740–2690 Ma period marked the peak of VMS generation in the Archean (Huston et al., 2010), primarily within the Abitibi greenstone belt (Fig. 2.1), which includes notable gold-rich VMS deposits (Ayer et al., 2005; Thurston et al., 2008; Mercier-Langevin et al., 2011a, 2011b; Monecke et al., 2017). The Blake River assemblage represents the youngest sub-alkaline volcanic episode in the Abitibi greenstone belt, making up about 11% of Abitibi volcanic rocks, but hosting nearly half of the total VMS tonnage of the belt (Monecke et al., 2017; Mercier-Langevin et al., 2023). Within the Blake River assemblage, the richest portion is known as the Blake River Group (BRG), with specific stratigraphic intervals hosting important VMS deposits (McNicoll et al., 2014).

The reasons for the highly variable VMS endowment at different scales (formation, group, assemblage, greenstone belt, craton) are not fully understood. Existing explanations include tectonic setting, rock types, permeability, thermal history, rhyolite geochemistry, syn-volcanic structures, water depth, or contributions from magmatic-hydrothermal fluids (e.g., Lesher et al., 1986; Lydon, 1996; Gibson et al., 1999; Franklin et al., 2005; Hannington et al., 2005; Gibson et al., 2007; Mercier-Langevin et al., 2011b; Piercey, 2011). These factors mostly explain endowment differences at the mining district scale, but less so at larger scales. What are the major differences in assemblage-scale tectonic, magmatic, and crust-mantle processes that impact VMS endowment in Archean greenstone belts? To answer this, we need to compare well-endowed with less-endowed areas at the appropriate scale.

This paper presents a regional whole-rock geochemical study of the mafic to intermediate volcanic rocks in the BRG, the best endowed area of the best endowed assemblage in the best endowed greenstone belt within the best endowed Archean craton. Our focus on mafic to intermediate

compositions is due to their abundance within all Abitibi assemblages. Additionally, mafic to intermediate volcanic compositions are not conventionally used for VMS exploration, despite the fact they are more abundant than felsic volcanic rocks, and therefore may represent an underdeveloped exploration vectoring tool. Furthermore, the composition of basalts in particular provides more direct insights about their magmatic sources. The objectives of the study are to understand geochemical variations through the BRG, interpret their petrological causes, and identify volcanic compositions and processes associated with VMS deposits in a very well-endowed succession.

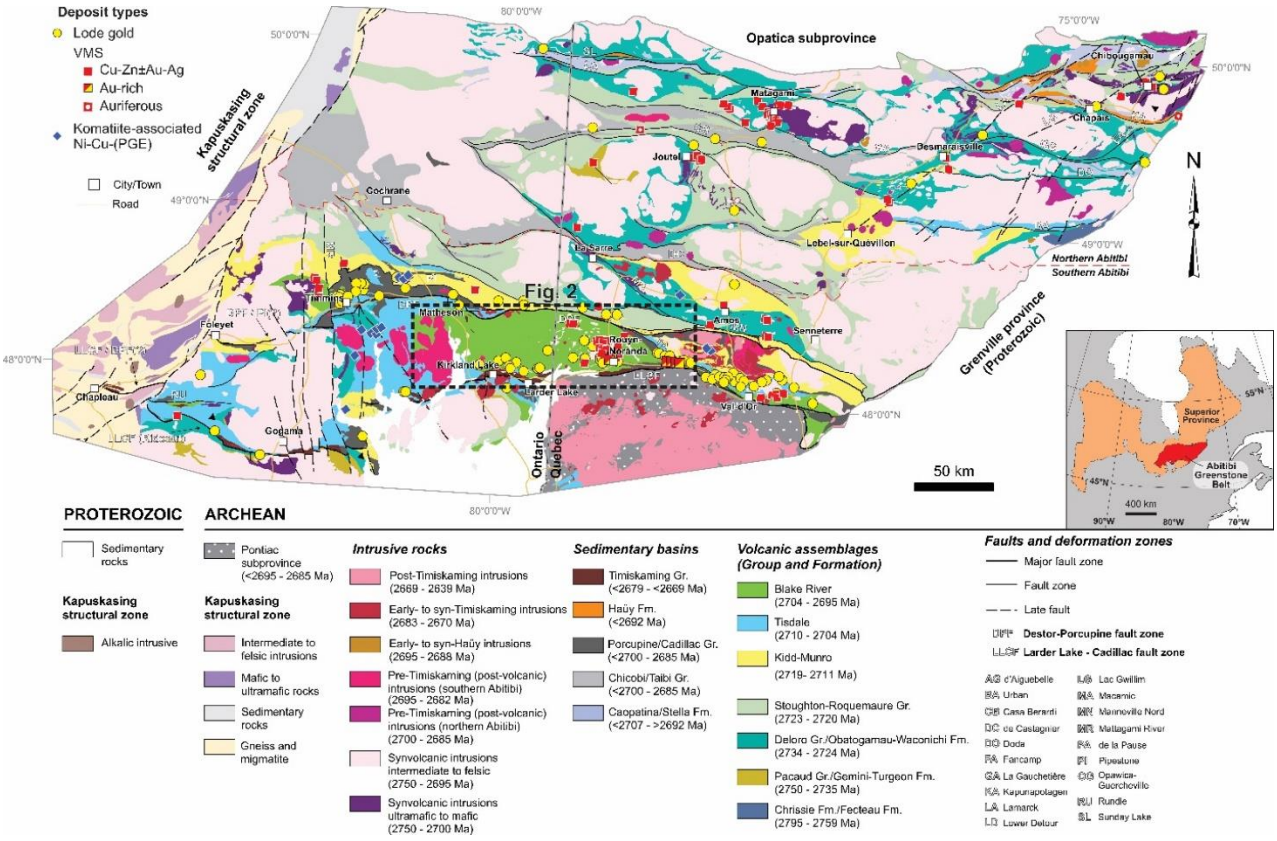

Figure 2.1 Geological map of the Abitibi greenstone belt illustrating the volcanic assemblages, the intrusive rocks, sedimentary basins, and main structures (modified from Dubé and Mercier-Langevin, 2020).

2.3 Geological context

2.3.1 Abitibi Greenstone Belt

The Abitibi greenstone belt is located in the southeastern part of the Superior Province (Fig. 2.1). This well-studied belt is known for its abundant mineral wealth, including world-class Archean syngenetic and epigenetic gold deposits, significant VMS deposits, and other ore types (Poulsen et al., 2000; Mercier-Langevin et al., 2014, 2023; Monecke et al., 2017). It is bounded by the Kapuskasing structural zone to the west, the Opatica Subprovince to the north, the Grenville Province to the southeast, and the Pontiac Subprovince to the south (Fig. 2.1). The Abitibi greenstone belt comprises east-trending bands of largely volcanic rocks alternating with bands of sedimentary rocks and intervening domes cored by synvolcanic and/or syntectonic plutonic rocks (Ayer et al., 2002; Goutier and Melançon, 2007). Volcanic rocks comprise about one-third of the belt (~36 %), whereas sedimentary and plutonic rocks represent ~11 and ~53 % of the belt, respectively (Mercier-Langevin et al., 2023). The Abitibi greenstone belt comprises seven different sub-alkaline volcanic assemblages, mainly based on geochronological constrains, referred to as the pre-2750 Ma (or Chrissie-Fecteau), Pacaud (2750-2735 Ma), Deloro (2734-2724 Ma), Stoughton-Roquemaure (2723-2720 Ma), Kidd-Munro (2719-2711 Ma), Tisdale (2710-2704 Ma), and Blake River (2704-2695 Ma) assemblages (Ayer et al., 2002, 2005; Thurston et al., 2008; Dubé and Mercier-Langevin, 2020). After the sub-alkaline volcanic activity, two sedimentary-dominated assemblages, Porcupine and Timiskaming, were formed and are interpreted as successor basins that locally contain calc-alkaline and younger alkaline volcanic rocks (Ayer et al., 2002; Thurston, 2015; Dubé and Mercier-Langevin, 2020).

2.3.2 Blake River Group

The Blake River assemblage represents all volcanic rocks deposited in the Abitibi greenstone belt between 2704 and 2695 Ma (Ayer et al., 2005; Thurston et al., 2008; McNicoll et al., 2014). It extends from Timmins in Ontario (e.g., Kamiskotia and Swayze areas) to the east of Val-d'Or in Quebec (Fig. 2.1). The Blake River Group (BRG) constitutes a major portion of this assemblage (Fig. 2.1 dotted rectangle), hosting several types of ore deposits. The BRG contains approximately 46% of the total VMS tonnage (Ayer et al., 2005; Monecke et al., 2017) and 92% of the VMS-related gold endowment in the entire Abitibi greenstone belt (Mercier-Langevin et al., 2011b, 2014). The BRG is a submarine volcanic succession dominated by mafic to intermediate compositions, with minor felsic activity (Ross et al., 2011a, b; McNicoll et al., 2014; Sutton et al.,

2017) (Fig. 2.2a). The volcanic rocks are cut by Archean mafic to felsic intrusions of synvolcanic to syntectonic timing, as well as Proterozoic dikes (Piercey et al., 2008, and references therein).

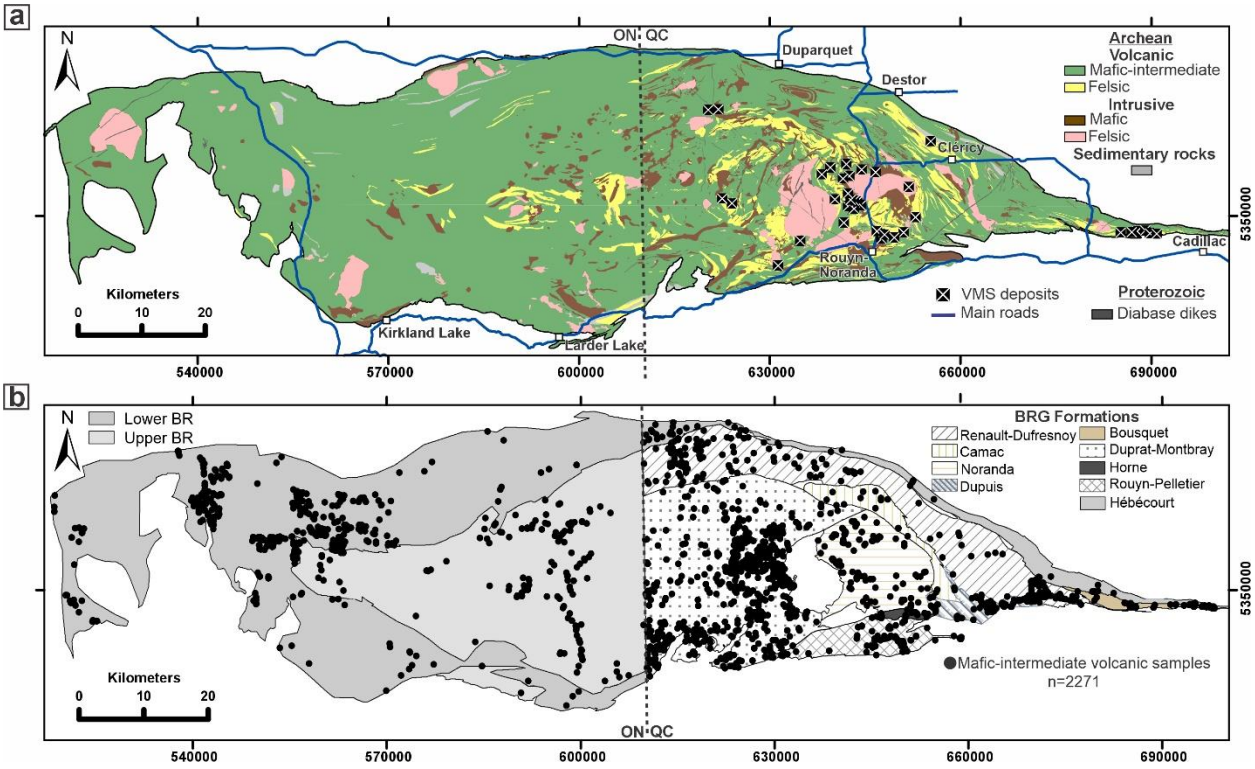

Figure 2.2 Geology, formations, and sample distribution of the Blake River Group. (a) Simplified geological map illustrating the distribution of mafic to intermediate volcanic rocks, felsic volcanic rocks and intrusive rocks. Geology layers from SIGEOM (2022) and the Ontario Geological Survey (2011). (b) Geological formation nomenclature for the Blake River Group and sample distribution used for this work. The Ontario side uses the Ayer et al. (2005) subdivision and the Quebec side the current provincial geology (SIGEOM, 2022).

Several nomenclature schemes have been proposed for the BRG formations. The most elementary is the Lower Blake River versus Upper Blake River subdivision from Ayer et al. (2005) and this scheme is currently applied in Ontario (Fig. 2.2b). On the Quebec side there is a rich history of subdividing the BRG into formations and even members (e.g., Gélinas et al., 1984; Gibson and Watkinson, 1990; Pearson and Daigneault, 2009; and references therein). The current scheme used by the Quebec provincial government contains nine formations (Fig. 2.2b): Rouyn-Pelletier, Duprat-Montbray, Noranda, Renault-Dufresnoy, Bousquet, Horne, Hébécourt, Camac, and Dupuis (Mercier-Langevin et al., 2011b; McNicoll et al., 2014; SIGÉOM, 2022). Only the Bousquet and the Hébécourt formations have formal status (Goutier, 1997; Lafrance et al., 2003). However, for the sake of brevity, only informal names will be used.

The mafic to felsic Noranda formation (Fig. 2.2b) represents one of the most VMS-endowed formations in the BRG (Gibson et al., 2007; Mercier-Langevin et al., 2011b). It possesses an apparent stratigraphic thickness of 7.5-9 km (Gibson and Watkinson, 1990) forming a NE-younging homoclinal package with dips ranging between 5 and 55º from horizontal, but typically in the 35-55º range (e.g., Gibson, 1989; Gibson and Watkinson, 1990; Monecke et al., 2008). VMS ores in the Noranda formation are typically Cu-Zn-rich and characterized by a mound-shaped sulfide deposit; they are classified as bimodal-mafic (Gibson et al., 2007). In the southern part of the Noranda formation, the Quemont deposit contains the eight largest gold endowment in the world for a VMS deposit (Mercier-Langevin et al., 2011a).

The Bousquet formation is another important stratigraphic unit in terms of VMS production, having a quarter of the total production in the whole BRG (Mercier-Langevin et al., 2007a, b, 2011a, b; Galley and Lafrance, 2014). In the easternmost part of the BRG, the Bousquet formation overlies the Hébécourt formation in the Doyon-Bousquet-LaRonde mining camp (Fig. 2.2b). The Bousquet formation is subdivided into the lower and upper members (Lafrance et al., 2003). The lower member includes mafic to intermediate volcanic rocks cut by felsic dikes and sills (Lafrance et al., 2003). The upper member comprises intermediate to felsic volcanic rocks intruded by basaltic dikes and sills, and by quartz- and feldspar-phyric rhyolite sills, dikes, and cryptodomes (Lafrance et al., 2003; Mercier-Langevin et al., 2007a, b). Dips of strata are almost vertical and the stratigraphic polarity points towards the south (Lafrance et al., 2003). VMS deposits within the Bousquet formation are notably rich in gold and are closely associated with felsic domes and/or cryptodomes, often linked to extensive volcaniclastic rocks of the upper Bousquet member (Dubé et al., 2007a, b, 2014; Mercier-Langevin et al., 2007b, 2011a, b; Yergeau et al., 2022a, b). This formation hosts the LaRonde-Penna, Bousquet 2-Dumagami, and Westwood deposits (Mercier-Langevin et al., 2007a, b; Dubé et al. 2014; Yergeau et al., 2022a, b).

Another particularly important area for VMS deposits is the Horne formation, which contains the giant Horne gold-rich VMS deposit (Hannington et al., 1997; Dubé et al., 2007b; Galley et al., 2007; Mercier-Langevin et al., 2011b) and the Horne 5 deposit (Sinclair, 1971; Krushnisky et al., 2023). The Horne formation is primarily composed of felsic volcanic rocks. Unfortunately, mafic-intermediate compositions are not well represented in our database and this formation is, therefore, not covered in this work.

2.4 Methods

2.4.1 Lithogeochemical databases

2.4.1.1 BRG dataset

The BRG geochemical dataset includes mafic to felsic volcanic rock samples. It is a compilation of 3209 analyses for which major oxides, loss on ignition (LOI), and trace elements are available. The data from the Quebec side derives primarily from the previous compilation by Sterckx (2018), supplemented by additional compilation. Approximately 73% of those analyses were sourced from the "Système d'information géominière" (SIGÉOM) of the Ministère des Ressources naturelles et des Forêts (Québec), with the remaining 27% sourced from scientific publications, academic theses, and unpublished data. Data for the Ontario side was gathered from the Geological Survey of Canada and the Ontario Geological Survey reports and merged with those from Quebec. Most of the data come from the year 2000 or more recent to minimize potential analytical issues. The BRG dataset is used briefly below (section 2.4.2) and then we focus on mafic to intermediate volcanic rocks, as the data for felsic rocks will not be discussed further in this manuscript.

2.4.1.2 Mafic to intermediate rocks dataset

Mafic to intermediate volcanic compositions were isolated on the Pearce (1996) version of the Winchester and Floyd (1977) classification diagram (Fig. 2.3a). This resulted in 2271 mafic to intermediate samples (Fig. 2.2b). The mafic to intermediate dataset is available as Online Supplement 1.

2.4.1.3 Least altered samples

A subset of the mafic to intermediate dataset containing only the least altered samples was created to enable the use of more mobile elements on certain diagrams (e.g., Harker diagrams). The selection process involved keeping only those samples that plotted in the least altered boxes of the Large et al. (2001) alteration box plot, as modified by Rogers et al. (2014) (Fig. 2.3b), which include the Chlorite-Carbonate-Pyrite (CCPI, Large et al., 2001) and the Ishikawa alteration indexes (AI, Ishikawa et al., 1976). Furthermore, samples with >62.5% silica (upper limit for andesite on the TAS diagram) were discarded after recalculating the major oxides to 100% (anhydrous basis). These steps together resulted in a reduction of nearly one-third, leaving a total of 1611 least altered mafic to intermediate samples.

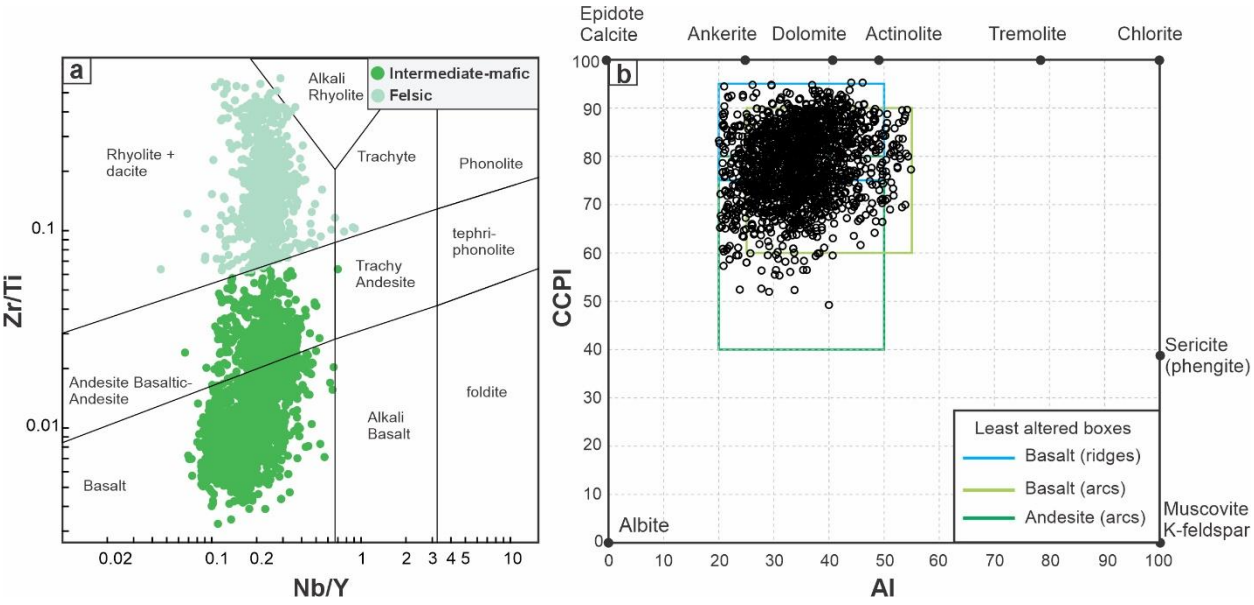

Figure 2.3 Mafic, intermediate and felsic BRG compositions and least altered samples. (a) Subdivision of the BRG complete dataset into mafic-intermediate and felsic compositions using the Zr/TiO2 vs Nb/Y boundaries from Pearce (1996). (b) Al-CCPI alteration box plot (after Large et al., 2001), for the least altered mafic to intermediate samples only. Al = 100*(K2O + MgO) / (K2O + MgO + Na2O + CaO); CCPI = 100*(MgO + FeOt) / (MgO + FeOt + Na2O + K2O). The box for unaltered ridge basalts is from Rogers et al. (2014) whereas boxes for arc basalts and arc andesites are from Gifkins et al. (2005).

2.4.2 Geochemical grouping

Considering that the mafic to intermediate dataset comprises over 2000 samples analyzed in various laboratories using different methods over a period exceeding 20 years, it is perhaps not surprising to get a continuum of data points on most geochemical diagrams. The task of splitting the BRG mafic to intermediate volcanic rocks into different chemical groups is, therefore, not a trivial exercise and required several iterations. We only present our final methodology here.

2.4.2.1 Element selection

The datasets contain tens of different chemical elements, but for placing the volcanic rocks into groups we relied mostly on Al, Ce, Eu, Gd, La, Nb, Sm, Th, Ti, Y, Yb, and Zr. These elements are relatively straightforward to analyze, petrologically relevant, and known for their relative immobility during geological processes such as metamorphism and alteration, including the impact of hydrothermal fluids in VMS systems (Jenner, 1996). This last characteristic makes them particularly valuable in rock classification and petrological examinations (Winchester and Floyd, 1977; Pearce, 2008; Ross and Bédard, 2009). Notably, ratios of immobile elements (e.g., MacLean and Barrett, 1993) remain relatively constant during hydrothermal alteration, making them favorable for this study, as altered rocks near VMS deposits are included in the BRG dataset.

Besides, most of the selected elements are incompatible during low-pressure fractional crystallization (e.g., Sun and McDonough, 1989).

2.4.2.2 Principal Component Analysis

Before calculating principal components for the BRG dataset, compositional data underwent a centered log-ratio transformation (Aitchison, 1986) to avoid closure problems. This transformation converts the data into a real vector space by taking the logarithm of each component and centering the values by subtracting their geometric mean. This transformation allows meaningful statistical analysis, reduces spurious correlations, and enhances visualization (Pawlowsky-Glahn and Egozcue, 2006).

Principal Component Analysis (PCA), initially developed by Hotelling (1933), is a statistical technique that identifies patterns and relationships in data by reducing its dimensionality. PCA aims to capture maximum variance with a reduced number of variables called principal components (PCs) (e.g., Jolliffe and Cadima, 2016). Typically, two or three principal components effectively summarize a multivariate dataset, explaining a significant portion of its variance. The principal components in this study were calculated using the Python library Scikit-learn (Pedregosa et al., 2011).

2.4.2.3 Main diagrams used for groupings and classification

As will be illustrated below, PC1-PC2 variations are captured by two ratios of immobile elements, Zr/Ti and Th/Yb. This allowed the creation of a simple geochemical diagram that facilitates the subdivision of mafic to intermediate compositions within the BRG. The volcanic rock names were assigned using the Pearce (1996) diagram, while magmatic affinities were determined using the Ross and Bédard (2009) diagram. Additionally, extended trace element diagrams were utilized to verify the geochemical groups.

2.4.3 Petrological modeling

Limited petrological modeling was carried out using the Magma Chamber Simulator (MCS) (Bohrson et al., 2014) to model Fractional-Crystallization (FC) and Assimilation-Fractional-Crystallization (AFC) processes. MCS uses the MELTS code provided by Ghiorso and Sack (1995) as a thermodynamic engine. To establish an initial composition for the modeling, several of the most primitive basalts (>10% MgO) from the least altered dataset were assessed. The

sample bearing the “74J1328” identifier, which is a basalt from the lower Blake River formation in Ontario, was selected based on its ability to reproduce the BRG major element trends during modeling in MCS. The PRIMELTS3 algorithm developed by Herzberg and Asimow (2015) was employed to confirm that 74J1328 is compatible with a primary melt composition from a peridotitic mantle.

The assimilant or wall rock was modelled based on the average composition of tonalite–trondhjemite–granodiorite (TTG) in the SE Superior Province from Mole et al. (2021). A slight adjustment was made to the SiO_2 and MgO values, and 1.4% H_2O was introduced to enhance MCS calculations.

2.5 Major oxides

The BRG mafic to intermediate rocks are separated into seven geochemical groups (tholeiitic basalt, tholeiitic intermediate, medium-Th basalt, transitional intermediate, high-Th basalt, calc-alkaline intermediate and low-Zr basalt) based mostly on trace elements, as will be explained in the next section (Table 2.1 summarizes the most important aspects of the groups). In the current section, we employ these groups to examine variations in terms of major elements within the least altered samples dataset. MgO is employed as the fractionation monitor due to its higher sensitivity to the fractionation of phases such as olivine in ultramafic to mafic magmas (e.g., Juster et al 1989). Generally, lower contents of MgO represent more evolved compositions, from right to left on the diagrams (Fig. 2.4). On the vertical axis of the Harker diagrams, TiO_2, Al_2O_3, $Fe_2O_3^t$, SiO_2 and CaO are displayed (Fig. 2.4), excluding the more mobile alkali elements.

Rocks with MgO contents larger than 8 wt. % have a restricted range of TiO_2 (mostly 0.5-1.5 wt. %), $Fe_2O_3^t$ (mostly 10-13 wt. %), and SiO_2 (mostly 47-53 wt. %) (Fig. 2.4). In contrast, rocks with MgO contents between 8% and 2.5% exhibit considerable spread in these elements. For example, at 5.0% MgO, $Fe_2O_3^t$ ranges from 5 to 20 wt. % and TiO_2 from 0.5 to 3%, representing behavior ranging from Fe-Ti depletion to Fe-Ti enrichment (Figs. 2.4a, 2.4c). The behavior of Al_2O_3 is mostly similar to that of the other mentioned oxides, with the largest spread in Al_2O_3 in the 6-3% MgO region (Fig. 2.4b). CaO diminishes along with MgO, broadly displaying a positive correlation (Fig. 2.4e).

Table 2.1 Summary of the geochemical groups for the BRG.

Geochemical group	Magmatic affinity	Geochemical characteristics
Tholeiitic basalts	Tholeiitic	Low Th/Yb ratio (up to 0.2), flat REE profile
Tholeiitic intermediate group	Tholeiitic	Low Th/Yb ratio (up to ~0.2), flat REE profile, negative Ti-Eu anomaly
Medium-Th basalts	Tholeiitic to transitional	Moderate Th/Yb ratio (>0.2, up to ~0.5), small negative Nb anomaly, slight enrichment in LREE
High-Th basalts	Transitional to calc-alkaline	High Th/Yb ratio (>0.5), pronounced negative Nb anomaly, moderate to high enrichment in LREE, slight depletion in HREE, small negative Ti anomaly, small positive Zr-Hf anomalies
Low-Zr basalts	Transitional to calc-alkaline	High Th/Yb ratio (>0.5), negative Nb anomaly, moderate to high enrichment in LREE, slight depletion in HREE, negative Zr-Hf anomalies
Transitional intermediate group	Transitional	Moderate to high Th/Yb ratio (0.2-0.7), small negative Nb anomaly, slight enrichment in LREE
Calc-alkaline intermediate group	Calc-alkaline	High Th/Yb ratio (>0.9), large negative Nb anomaly, high enrichment in LREE and slight to moderate depletion in HREE

Several tendencies are evident when examining geochemical trends by compositional group. For example, tholeiitic basalt samples typically display Fe-Ti enrichment trends and the lowest contents in SiO_2 (Fig. 2.4d) and $Al2O_3$ (with Al_2O_3 decreasing along with MgO). However, some samples of this group display Fe-Ti depletions. High-Th basalt samples display Fe-Ti depletion (or flat trends) and have higher concentrations of SiO_2 and $Al2O_3$ than the tholeiitic basalt samples. The medium-Th basalt group tend to plot between these two geochemical groups (Fig. 2.4). The rest of the groups are less abundant and do not show such clear trends.

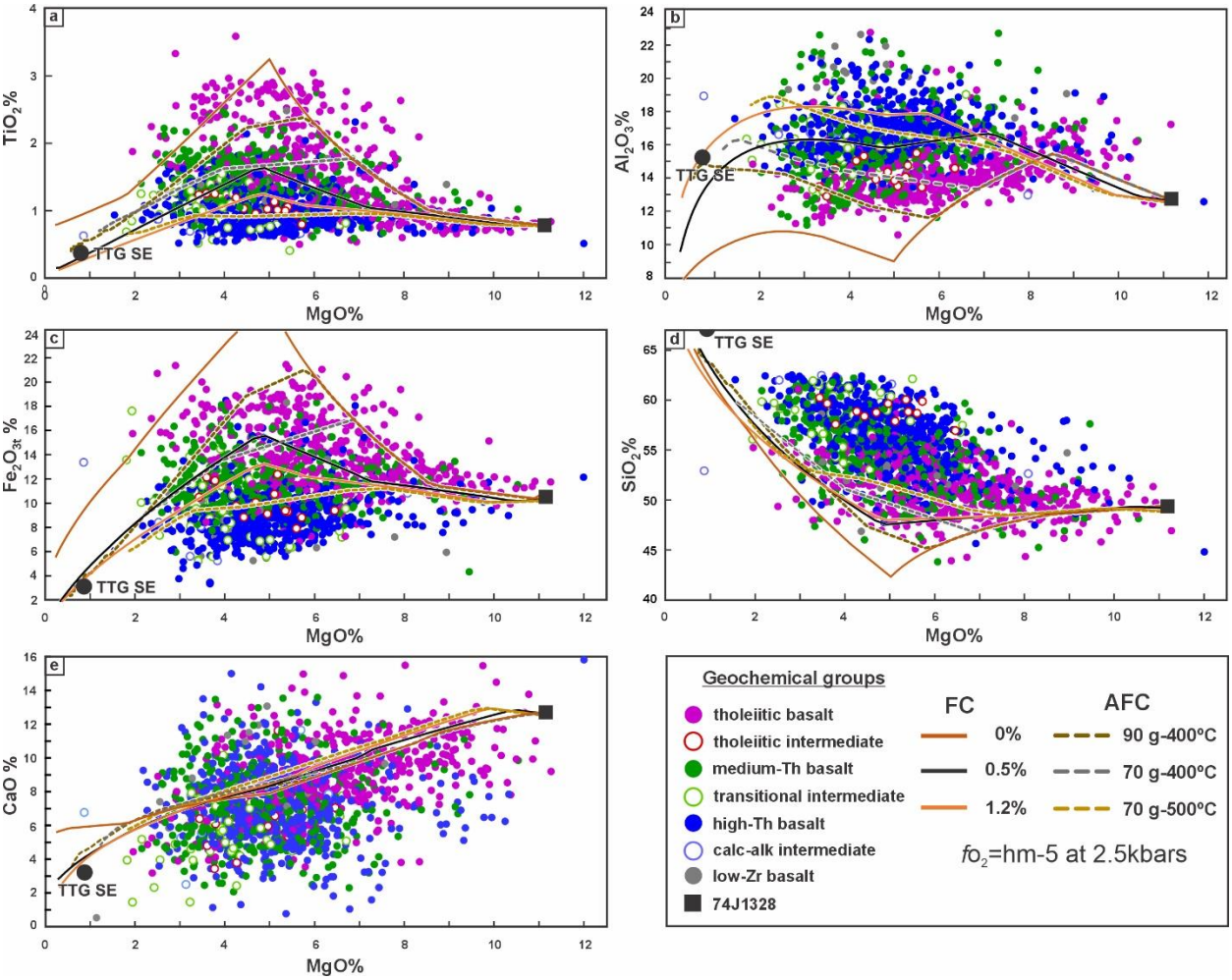

Figure 2.4 Major oxide variation diagrams for the least altered BRG samples. (a)-(e) TiO2, Al2O3, Fe2O3t, SiO2 and CaO versus MgO. Several models of LLD for FC (continuous lines) and AFC (dotted lines) are shown. The models were better constrained using a magnetite-hematite *f*O2 offset of -5 (hm-5). The FC models represent 5ºC decrements and their initial temperatures are as follows: 1264ºC for 0%, 1254ºC for 0.5% and 1250ºC for 1.2% model. AFC LLD are shown in 5ºC decrements (90 g-400ºC and 70 g-400ºC) and 8ºC (70 g-500ºC) decrements. The legend "00 g-000ºC" represent the wall rock mass involved on the AFC model, in grams, and its initial temperature. For the 90 g-400ºC and the 70 g-400ºC models, the initial mafic magma contains 0% dissolved water. In the 70 g-500ºC model, the initial magma contains 1.2% dissolved water. "TTG SE" = average TTG composition of the SE Superior Province from Mole et al. (2021).

2.6 Geochemical groupings

2.6.1 PCA results on the BRG dataset

The application of PCA on the entire BRG dataset (mafic to felsic volcanic rocks) provides a basis for determining the elements that capture the highest variance and can be used for geochemical grouping. Figure 2.5 displays the importance of each element represented by its loading, which is delineated by the red vectors. The first principal component (PC1) accounts for 69% of the total variance in the dataset (Fig. 2.5). PC1 exhibits positive loadings for Zr and Nb, and negative

loadings for Ti and Al. When two or more elements have similar vector directions, it means they are highly correlated. Conversely, if two elements have opposite loadings (one positive and the other negative), it suggests a negative correlation between them, such as in the case of Ti and Zr. The elements aligned along the PC1 component, namely Ti, Al, and Zr, are typically associated with crystal fractionation. On figure 2.5, mafic-intermediate compositions plot to left, while felsic compositions plot to the right.

The second principal component (PC2) accounts for 19% of the total variance. Th, La, and Ce exhibit positive loadings and display a high correlation among themselves. Sm, Gd, Y, and Yb exhibit negative loadings, with the latter three showing a strong correlation. The PC2 axis seems to mostly represent the overall slope of the pattern on an extended trace element diagram (from Th to Yb), and/or the slope of the rare earth elements (REE).

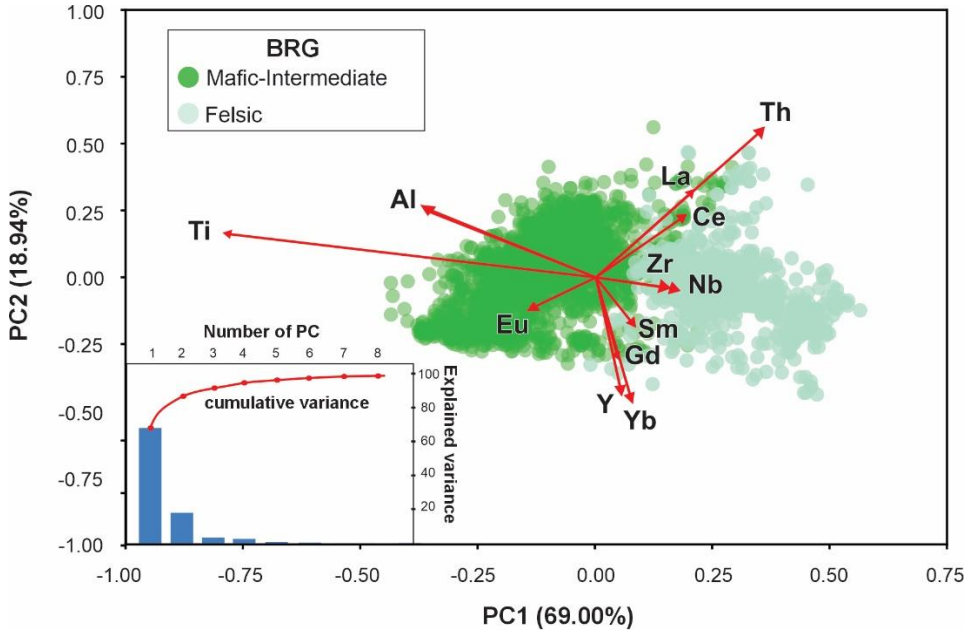

Figure 2.5 PC1 vs PC2 from the analysis in the complete BRG dataset. Red arrows display the loads of each element. The inset shows the variance captured by each PC, and the cumulative variance marked by the red line.

2.6.2 Ti/Zr vs. Th/Yb diagram for mafic to intermediate volcanic rocks

The PC1-PC2 diagram can be simplified into a binary diagram featuring two ratios of immobile elements, which is easier to interpret and facilitates petrological modeling. Zr/Ti approximates PC1, and Th/Yb represents PC2, forming the Zr/Ti vs. Th/Yb diagram used to establish geochemical groups for mafic to intermediate volcanic rocks in the BRG (Fig. 2.6).

The Zr/Ti ratio is widely used in the literature to identify magma composition (e.g., Winchester and Floyd, 1977; Pearce, 1996). The Th/Yb ratio is a well-known petrogenetic ratio popularized by the works of Pearce (1983, 2008). Th is enriched in the metasomatized mantle above subduction zones and is also enriched in crustal rocks, typically accompanied by light rare earth element (LREE) enrichments. Yb, on the other hand, tends to stay behind in residual garnet or amphibole at high pressures. The resulting ratio is typically interpreted as a proxy for crustal assimilation or subduction processes (Pearce, 2008; Pearce et al., 2021). It is also used to separate tholeiitic from calc-alkaline magmas (Ross and Bédard, 2009).

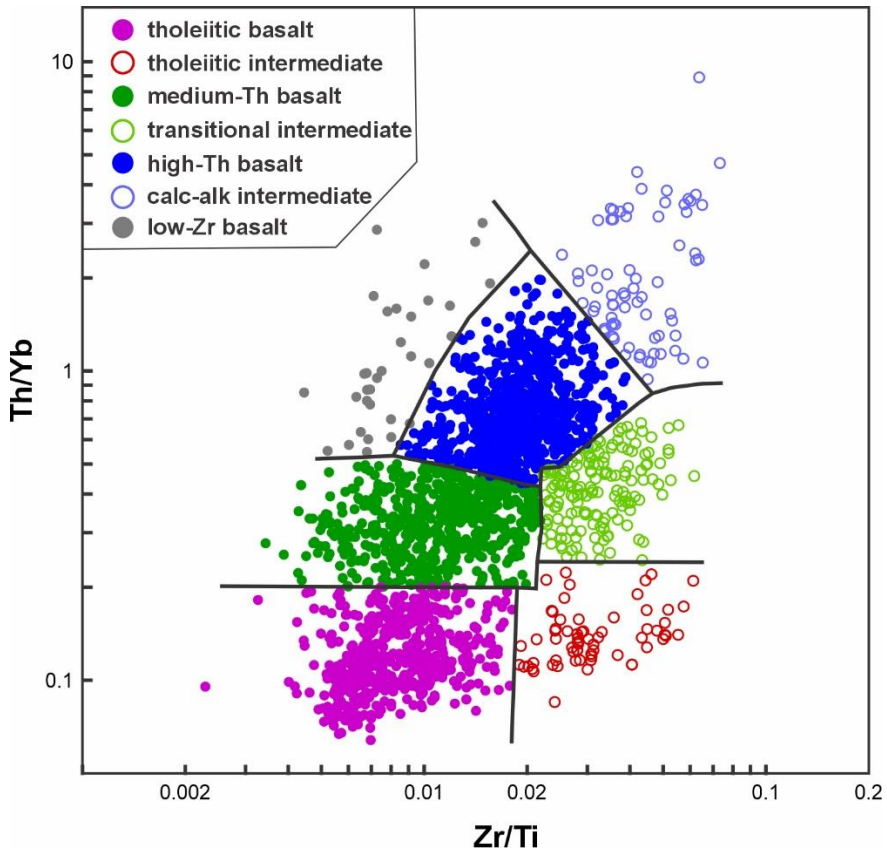

Figure 2.6 Zr/Ti (ppm/ppm) vs Th/Yb (ppm/ppm) diagram. Seven mafic to intermediate geochemical groups are delineated in the BRG.

The Zr/Ti vs. Th/Yb diagram reveals seven geochemical groups as illustrated in Figure 2.6 and summarized in Table 2.1. The number of groups was kept low enough to ensure mappable units and capture the overall geochemical diversity within tight clusters. While drawing general inspiration from automated clustering algorithms (Online Supplement 2), the final thresholds were meticulously performed manually, as illustrated in Figure 2.6. To maintain consistency of the

geochemical groups, verification was conducted on the diagrams of Figure 2.7 (Agrawal et al., 2008; Ross and Bédard, 2009; O'Neill, 2016; Pearce et al., 2021) and extended trace elements (Fig. 2.8). The individual characteristics of each group are discussed below.

2.6.3 Geochemical groups

2.6.3.1 Tholeiitic basalt group and tholeiitic intermediate group

The tholeiitic basalt group and the tholeiitic intermediate group primarily plot within the array for Mid-Ocean Ridge Basalt (MORB), Oceanic Plateau Basalt (OPB) and Ocean Island Basalt (OIB), i.e. the MORB-OPB-OIB mantle array, on the Pearce et al. (2021) plot (Fig. 2.7a). The centroid of the tholeiitic basalt group is located near the composition of the Primitive Mantle (PM) on this diagram, but the samples are distributed towards a more depleted source, the modern N-MORB pole. This behavior is consistent on the λ1-λ2 O'Neill (2016) diagram (Fig. 2.7b). Samples of these two groups are restricted to the MORB field in the tectonic discriminant plot from Agrawal et al. (2008) (Fig. 2.7c) and confined in the tholeiitic magmatic affinities on the Ross and Bédard (2009) diagram (Fig. 2.7d). Upon examining the extended trace element diagrams, tholeiitic basalt samples display nearly flat profiles with low Th-Nb concentrations compared to other elements (Fig. 2.8a), whereas the tholeiitic intermediate group exhibits higher trace element concentrations and a negative Ti anomaly (Fig. 2.8b).

2.6.3.2 Medium-Th basalt group

Medium-Th basalt samples have similar to slightly higher Zr/Ti ratios relative to the tholeiitic basalt group, but with higher Th/Yb ratios (Fig. 2.6). On the extended trace element profiles, these samples show increased Th and LREE concentrations, while the Nb content remains relatively unchanged compared to tholeiitic basalt samples (Fig. 2.8c), which creates a small negative Nb anomaly. Medium-Th basalt samples occupy an intermediate position between the MORB-OPB-OIB and Island Arc Basalt (IAB) arrays on the Pearce et al. (2021) diagram (Fig. 2.7a). Based on the λ1 and λ2 values, they have a similar composition to the modern E-MORB average, but also plotting along a crustal assimilation vector, away from the tholeiitic basalt group (Fig. 2.7b). The medium-Th basalt samples form a cluster between the MORB and IAB fields on the tectonic discriminant diagram (Fig. 2.7c). According to the magmatic affinity diagram, they range from tholeiitic to transitional, with most of the samples plotting as transitional (Fig. 2.7d).

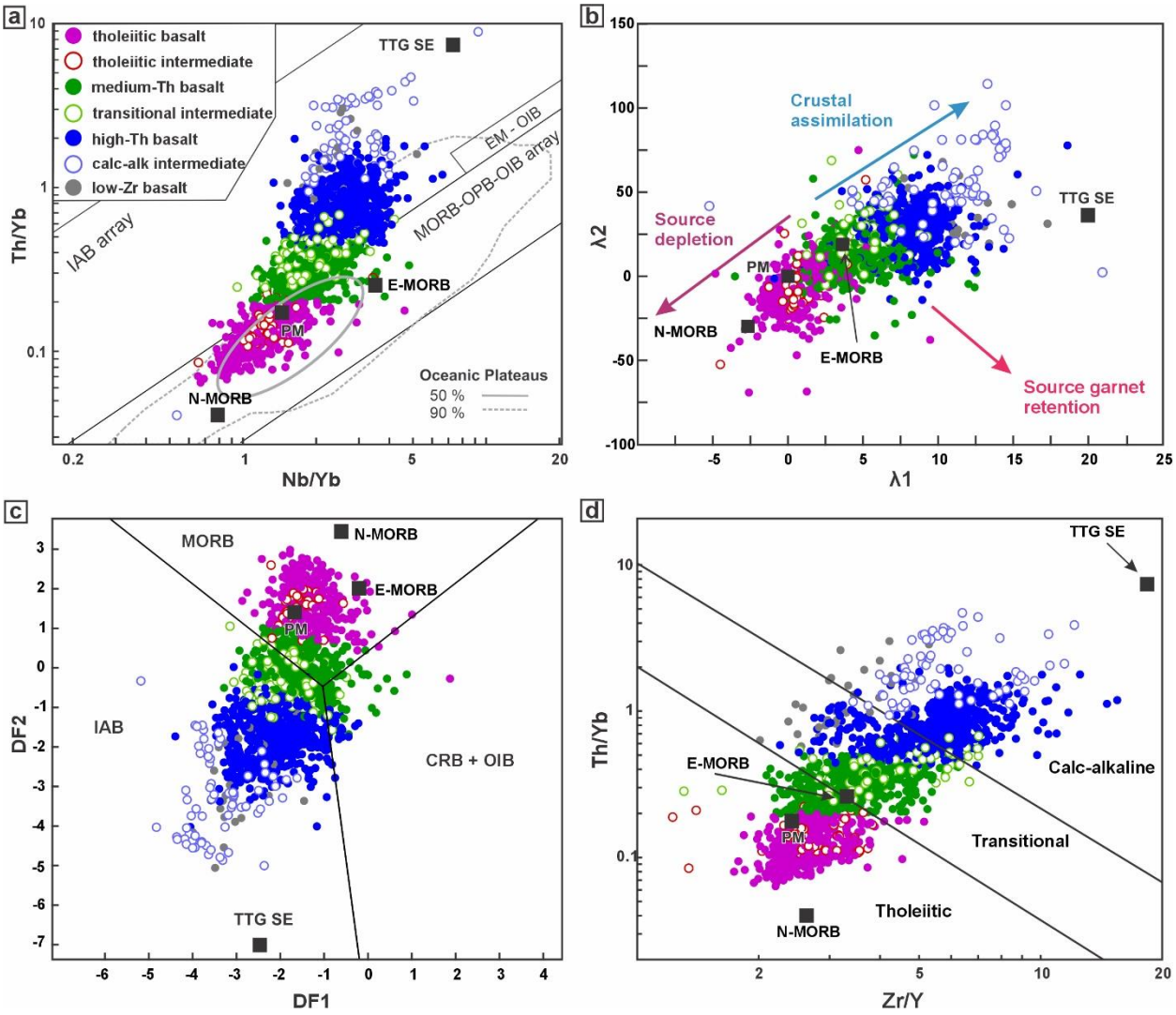

Figure 2.7 Trace element diagrams showing the various mafic to intermediate geochemical groups. (a) Th/Yb vs Nb/Yb diagram from Pearce et al. (2021), modified from Pearce (2008). Oceanic Plateau data compilation from Barnes et al. (2021). (b) λ1 vs λ2 plot from O'Neill (2016). Colored arrows show generalized vectors for significant geochemical processes. (c) Tectonic discrimination diagram from Agrawal et al. (2008). DF1 = 1.7517 loge (Sm/Th) – 1.9508 loge (Yb/Th) + 1.9573 loge (Nb/Th) – 5.0928; DF2 = –2.2412 loge (Sm/Th) + 2.2060 loge (Yb/Th) + 1.2481 loge (Nb/Th) – 0.8243. (d) Zr/Y vs Th/Yb magmatic affinity diagram from Ross and Bédard (2009). E-MORB, N-MORB, and OIB compositions from Sun and McDonough (1989). TTG-SE = average TTG composition of the SE Superior Province from Mole et al. (2021).

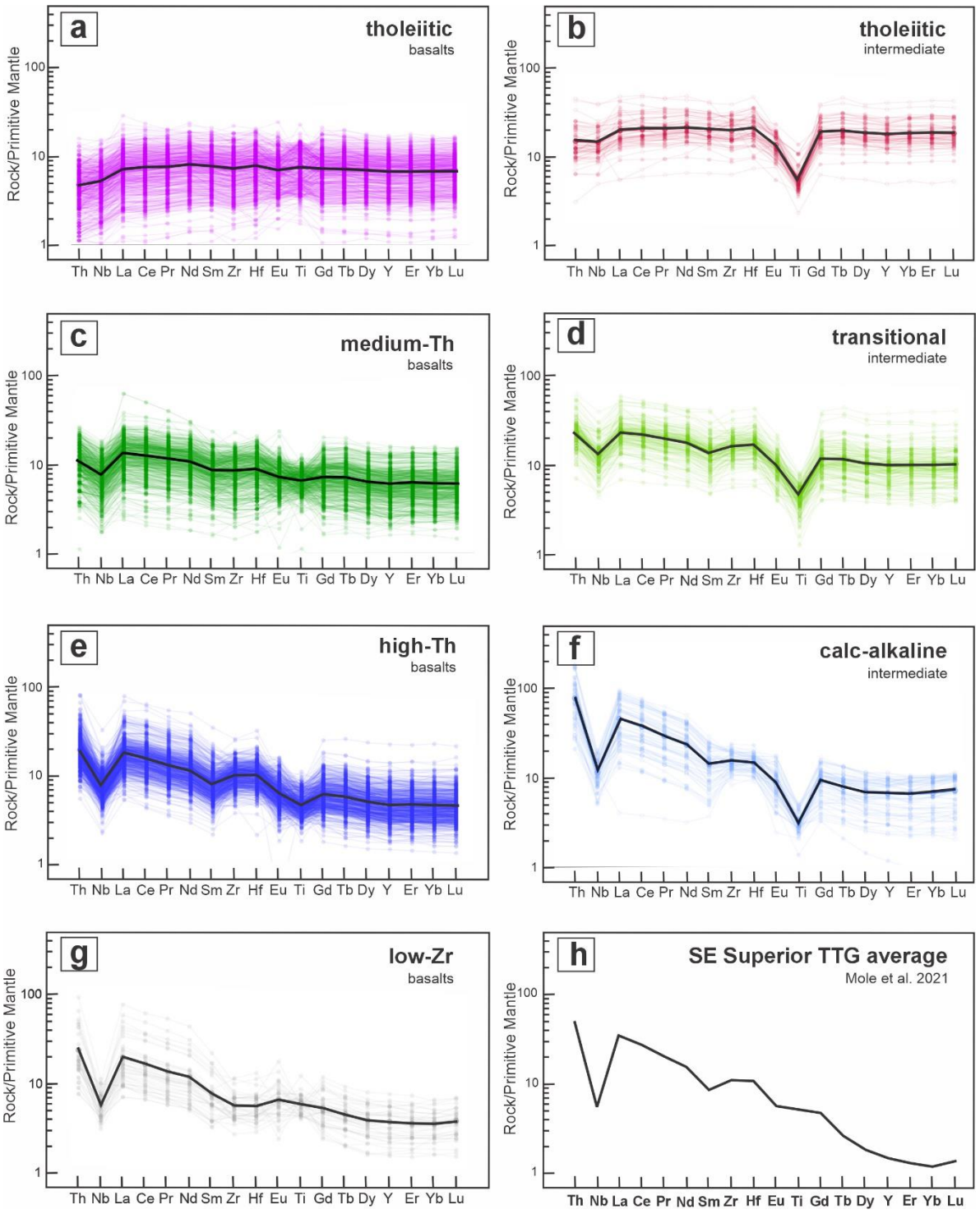

Figure 2.8 Extended trace element profiles for the mafic and intermediate geochemical groups (a-g). Black lines represent the averages of each group. (h) Average TTG composition for the SE Superior Province from Mole et al. (2021). Primitive mantle normalization values from Sun and McDonough (1989).

2.6.3.3 Transitional intermediate group

The transitional intermediate samples have similar to slightly higher Th/Yb ratios than the medium-Th basalt samples, but with higher Zr/Ti ratios (Fig. 2.6). They are predominantly confined to the transitional field in the magmatic affinity diagram (Fig. 2.7d). This group of rocks exhibits characteristics similar to that of medium-Th basalt group in the tectonic discriminant diagram (Fig. 2.7c). Certain transitional intermediate samples display higher Th/Yb ratios in the Pearce et al. (2021) plot (Fig. 2.7a) and higher λ1 and λ2 values following the crustal assimilation vector (Fig. 2.7b). On extended trace element diagrams, they demonstrate a similar profile to the medium-Th basalt samples, but with higher trace element concentrations and a negative Ti anomaly (Fig. 2.8d).

2.6.3.4 High-Th basalt group

Elevated Th concentrations, negative Nb anomalies and a negative REE slope on the extended trace elements diagram (Fig. 2.8e) characterize the high-Th basalt samples. Additionally, these rocks show Zr and Hf positive anomalies (Fig. 2.8e). They plot mostly in the IAB array on the Pearce et al. (2021) diagram (Fig. 2.7a) and in the same field on the tectonic discriminant diagram (Fig. 2.7c). Their magmatic affinity spans from transitional to calc-alkaline (Fig. 2.7d). This group continues the trend of increasing crustal assimilation on the λ1-λ2 diagram (Fig. 2.7b).

2.6.3.5 Calc-alkaline intermediate group

Samples from the calc-alkaline intermediate group occupy the upper right corner on the Zr/Ti versus Th/Yb diagram (Fig. 2.6). They are primarily restricted to the calc-alkaline field on the magmatic affinity diagram (Fig. 2.7d). They show the highest Th/Yb ratios of the studied samples, occupying the IAB array on the Pearce et al. (2021) plot (Fig. 2.7a) and the IAB field on the tectonic discriminant diagram (Fig. 2. 7c). Based on their λ1-λ2 values, calc-alkaline intermediate rocks show high rates of crustal assimilation (Fig. 2.7b). In the extended trace element profiles, they reflect the highest Th values, demonstrate a steeper profile, particularly in the LREE, and show significant negative Nb and Ti anomalies. The Zr-Hf positive anomalies are not as evident as in the high-Th basalt samples (Fig. 2.8f).

2.6.3.6 Low-Zr basalt group

This minor group has Th/Yb ratios similar to the high-Th basalt samples, but at lower Zr/Ti ratios (Fig. 2.6). This creates negative Zr and Hf anomalies on the extended trace element diagram (Fig. 2.8g) and the samples overlap with the previous two groups on the diagrams of figure 2.7.

2.6.4 Geographical distribution of geochemical groups and stratigraphic differences

Tholeiitic, medium-Th, and high-Th basalt samples are the most abundant geochemical groups in the BRG formations (Figs. 2.9, 2.10). Tholeiitic, transitional and calc-alkaline intermediate groups, along with low-Zr basalt samples, are less common overall, but are more prevalent in certain areas or volcanic sequences.

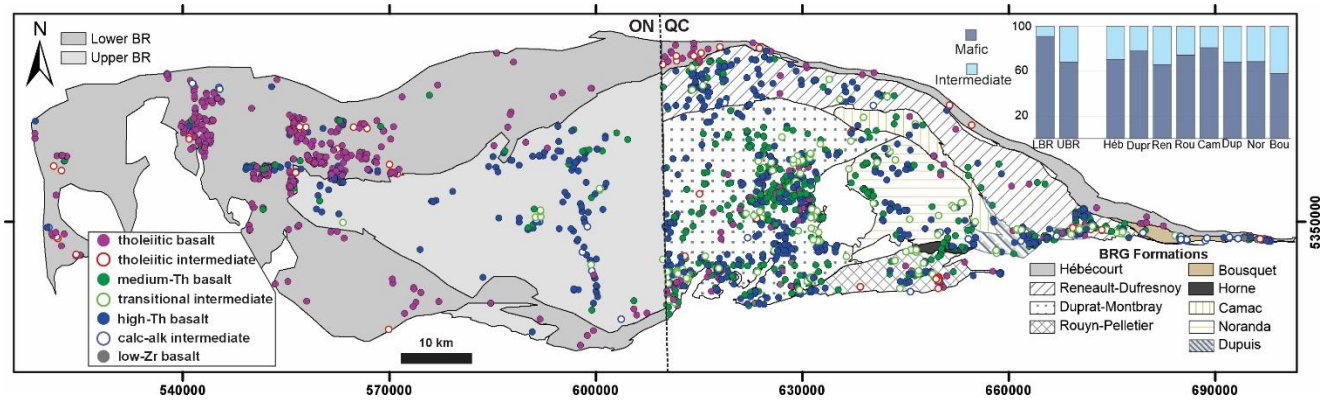

Figure 2.9 Geographic distribution of the geochemical groups in the BRG. Inset figure shows a histogram of the percentage of basalts versus intermediate volcanic rocks for each formation.

2.6.4.1 Ontario

In Ontario, the Lower and Upper BRG subdivisions are clearly distinguished by their geochemical groupings (Figs. 2.9, 2.10). The Lower subdivision mainly consists of mafic rocks, with minor intermediate compositions (Fig. 2.9, inset). Tholeiitic basalt samples are the predominant signature, with smaller proportions of high-Th and medium-Th basalt samples, as well as tholeiitic and calc-alkaline intermediate compositions (Figs. 2.9, 2.10). In contrast, the Upper BRG has a larger proportion of intermediate samples (Fig. 2.9, inset), with the high-Th basalt group being predominant (Fig. 2.10). The medium-Th basalt and calc-alkaline intermediate rocks also occur in lesser proportions while there are no occurrences of low-Zr basalt samples (Fig. 2.10).

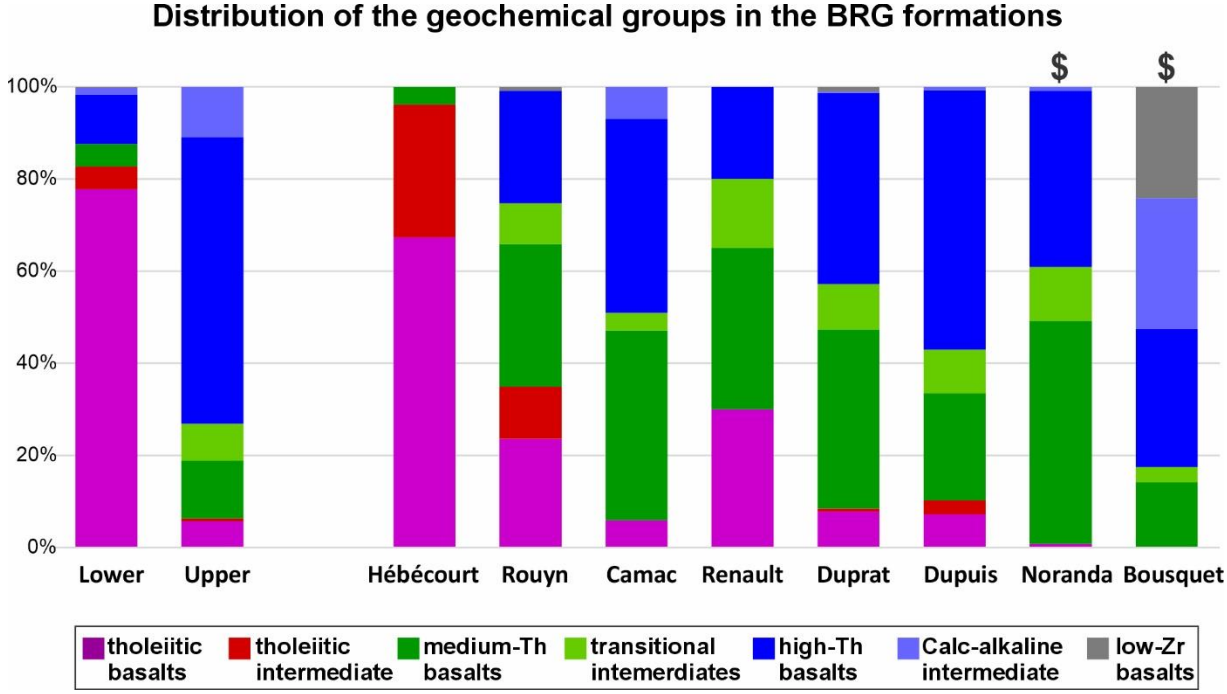

Figure 2.10 Histogram showing the proportions of each geochemical group in the BRG formations. VMS-endowed formations are marked with '$'.

2.6.4.2 Quebec

The Quebec side of the BRG exhibits a more complex distribution of geochemical groups due to a higher number of samples and increased variability (Fig. 2.9). However, a closer examination of histograms (Fig. 2.10) and detailed maps (e.g., Fig. 2.11) reveals several patterns. In the NW portion of Quebec's BRG, the trends present in the Lower/Upper subdivisions in Ontario persist within the Hébécourt and Renault-Dufresnoy formations (Fig. 2.9). The Hébécourt formation is mainly composed of tholeiitic basalt and tholeiitic intermediate rocks, while the northern part of the Renault-Dufresnoy formation is characterized by a prevalence of high-Th basalt samples (Figs. 2.9, 2.10). In the Duprat-Montbray area, where sample density is high, distinct geographic clusters of the same geochemical groups are present, particularly for the medium-Th basalt and high-Th basalt rocks (Fig. 2.9).

Formations hosting large and/or abundant VMS deposits like the Noranda and Bousquet formations contain almost no samples of tholeiitic basalt and tholeiitic intermediate rocks (Figs. 2.9, 2.10). The Noranda formation shows a larger proportion of medium-Th basalt and high-Th basalt samples with minor proportions of transitional intermediate compositions. The Bousquet formation, which contains important gold-rich VMS deposits, exhibits the greatest abundance of

intermediate samples in our database (Fig. 2. 9, inset) featuring calc-alkaline intermediate rocks and low-Zr basalt compositions (Fig. 2.10) not seen in the same proportions elsewhere.

2.6.4.3 Noranda formation

There are variations in geochemical compositions between BRG formations, but also stratigraphic evolutions within specific formations. To illustrate this, the Noranda formation is used as an example. It consists of a homoclinal volcanic succession with a stratigraphic polarity, or younging direction, oriented to the NE (Fig. 2.11). A stratigraphic profile (Figs. 2.11, 2.12) was drawn along section A-A' with an apparent thickness of 12 km, but a true thickness of about ~6 km. Samples up to 2.5 km away on either side of the section line were projected back to the section, which also crosses six Cu-Zn VMS deposits and showings. The objective of this exercise is to observe the variations along the volcanic succession ranging from the base to the top.

The geochemical profile shows variations in both differentiation (Zr/Ti, Fig. 2.12a) and crustal input (Th/Yb, Fig. 2.12b) along with stratigraphic position. The base of the sequence comprises medium-Th basalt samples. No former mines are found in this sequence, but two developed mineral showings (Bedford Hill and West Ansil) occur (Fig. 2.12), with an aggregate ore estimation of less than <0.5 Mt (SIGEOM, 2022).

Higher in the sequence, from the Old Waite to the Newbec mine positions there is a discernible trend of increasing Th/Yb ratios, accompanied by a subtle rise in the Zr/Ti ratio. VMS deposits occurring in this part of the sequence were mined, with productions >1 Mt (Monecke et al., 2017) with the exception of the Newbec mine with <0.3 Mt (SIGEOM, 2022). Although samples are sparse, there is a discernible trend towards more mafic magmas stratigraphically above the Newbec mine position, with the presence of medium-Th basalt samples and lower Th/Yb ratios, resembling the compositional characteristics at the base of the sequence (Fig. 2.12). The Noranda formation contain only one sample classified as tholeiitic basalt (Figs. 2.10, 2.11).

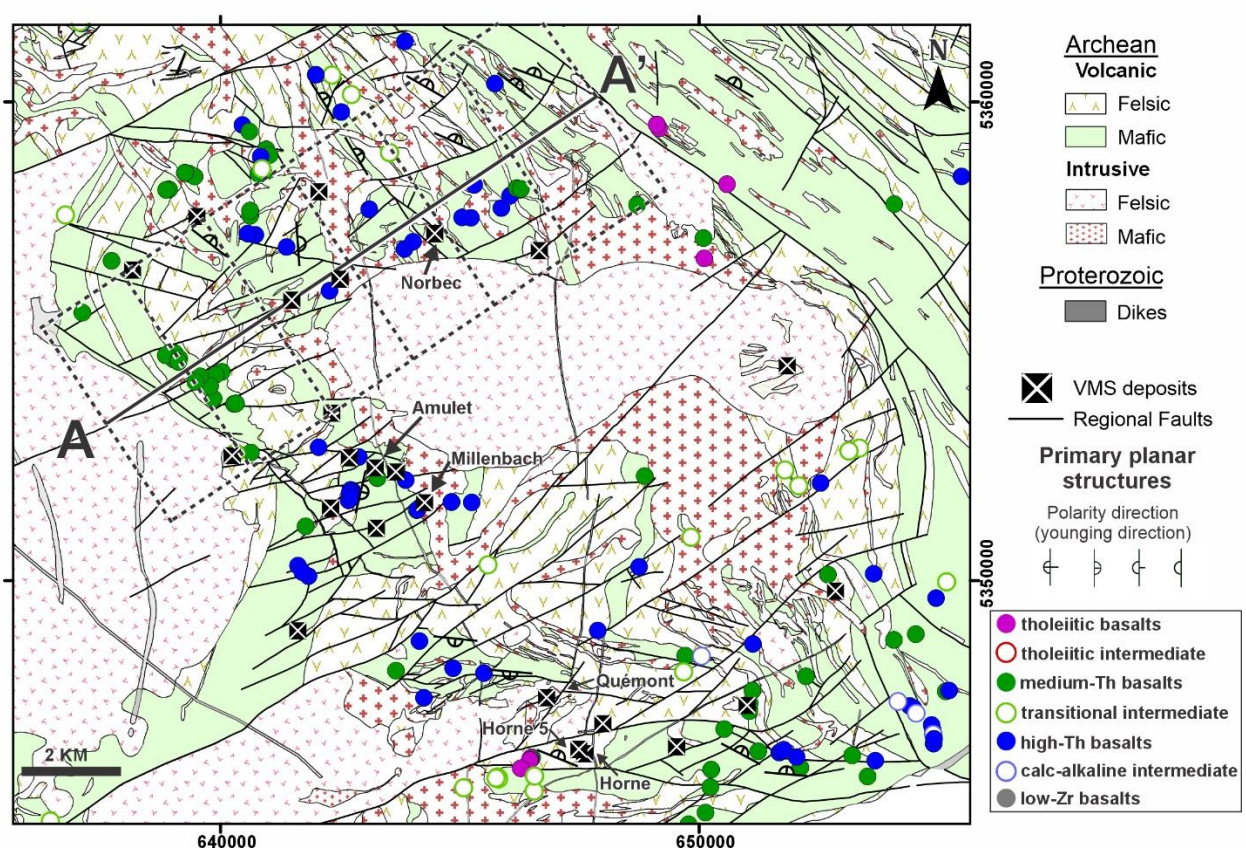

Figure 2.11 Simplified geological map of the Noranda camp portion of the BRG. The figure shows geochemical profile A-A' and the distribution of the mafic to intermediate geochemical groups. Geology simplified from SIGEOM (2022). All geochemical data within the dotted rectangle are projected in the central continuous line to observe the geochemical variations across the volcanic sequence as show in Figure 2.12.

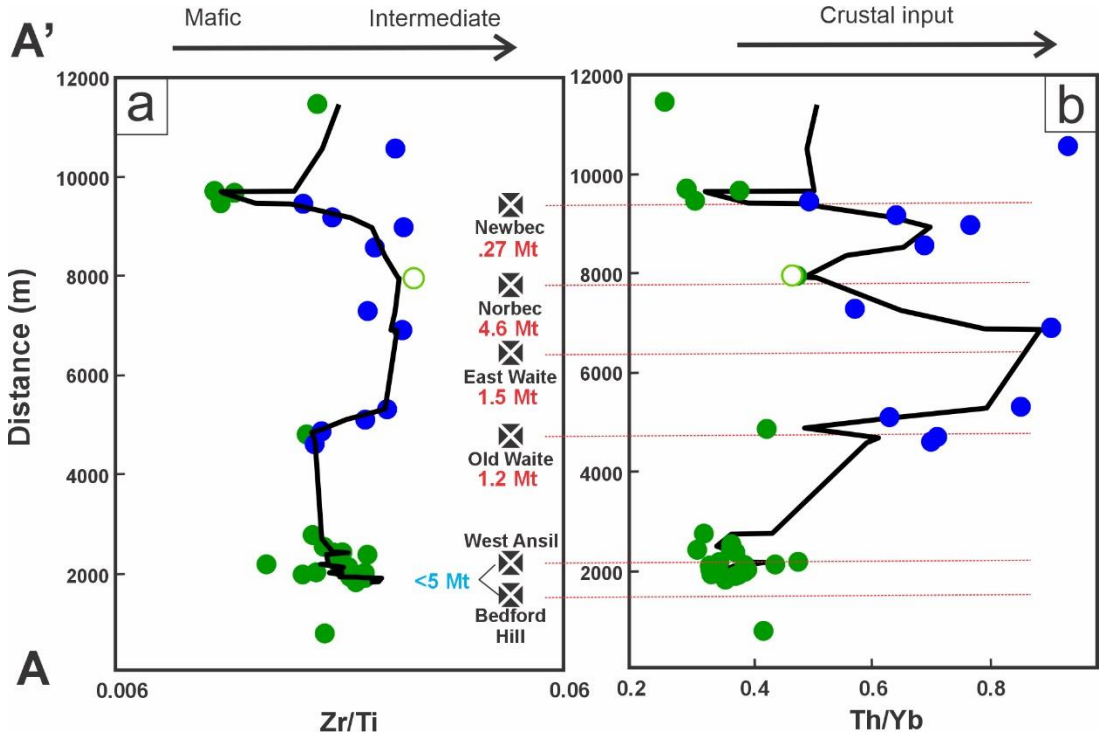

Figure 2.12 Geochemical profile A-A' in the Noranda formation (Fig. 2.11). (a) Magma fractionation is based on the ratio Zr/Ti (ppm/ppm). (b) Crustal assimilation based on the ratio Th/Yb (ppm/ppm). Total mine production are marked in bold red while estimated resources in bold blue. See section 2.6.4.3 for references and description.

2.7 BRG petrogenesis

This section is primarily focused on discussing the petrogenetic aspects of the BRG and the results of the modeling with the Magma Chamber Simulator.

2.7.1 Mantle source

The tholeiitic basalt group is interpreted to closely resemble the mantle source beneath the BRG in Archean times, given the minimal crustal assimilation displayed by those samples (discussed below). These magmas represent shallow asthenospheric melts with trace element characteristics similar to the Primitive Mantle or to Phanerozoic oceanic plateaus (Fig. 2.7). Several samples of the tholeiitic basalt group come from a more depleted mantle, trending towards the Phanerozoic N-MORB pole on several diagrams (Fig. 2.7). Similar samples to those from the tholeiitic basalt group are present in the other Abitibi assemblages (unpublished results) and other Archean greenstone belts like those of the Yilgarn craton (e.g., Barnes et al., 2021).

2.7.2 Fractional crystallization models

Three distinct Liquid Lines of Descent (LLD) or fractionation lines were modeled (Fig. 2.4), for initial dissolved water contents of 0%, 0.5%, and 1.2%. All simulations were conducted at 2.5 kbars (representing a magma chamber at ~10 km crustal depth), using the hematite-magnetite oxygen buffer with an offset ($fO2$=hm-5), and slightly different initial temperatures depending on the water content (Fig. 2.4).

2.7.2.1 Major oxides

Special attention was given to constraining TiO_2 and Al_2O_3 (Fig. 2.4a, b), as these elements exhibit greater sensitivity to water concentration (e.g., Sisson and Grove, 1993; Feig et al., 2006) and are typically immobile. $Fe_2O_3^t$ also exhibits sensitivity to water concentrations (Fig. 2.4c), although it may be more prone to mobility due to hydrothermal alteration and metamorphism.

Liquid evolution from the starting composition (~11.2% MgO) to ~8% MgO is related to olivine and pyroxene fractionation (~20% of the mass removed). What happens next depends on the water content. For the anhydrous composition, plagioclase starts to crystallize at ~8.2% MgO, which decreases Al_2O_3 in the melt but allows $Fe_2O_3^t$ and TiO_2 to rise quickly, peaking at 5% MgO, by which time ~27% of plagioclase has been removed (Fig. 2.4a, b, c). Iron and Ti then decrease quickly due to crystallization and removal of 5% Fe-Ti oxide minerals. In this anhydrous case, silica decreases slightly from high-MgO values to about 5% MgO, before increasing again. In contrast, progressively higher water contents, like in the 0.5% and 1.2% models, promote earlier crystallization of Fe-Ti oxides and delay plagioclase growth, thereby suppressing the Fe-Ti enrichment trend while rising Al_2O_3 contents. Taken together, the three fractional crystallization models generally reproduce the behavior of the tholeiitic basalt and tholeiitic intermediate rocks in terms of TiO_2, Al_2O_3, Fe_2O_3t, and CaO. However, our models do not reproduce silica contents well, particularly for tholeiitic basalt and intermediate samples with elevated silica concentrations.

Several authors have described Fe-Ti enrichments as “Fe-tholeiites” in the Kinojevis Group (now lower Blake River in Ontario) whereas “Mg-tholeiites” were attributed to Fe-Ti depletions (Fowler and Jensen, 1989; Kerrich et al., 1999, 2008). Fe-tholeiites and Mg-tholeiites are intimately intercalated in the lower BRG. Fowler and Jensen (1989) interpreted Fe-Ti oxide behavior to be responsible for the enrichment/depletion patterns. The advancements in understanding the impact of water on the evolution of modern magmas (e.g., Sisson and Grove, 1993; Feig et al., 2006; Zimmer et al., 2010), as well as modeling approaches similar to those presented in this

work (e.g., MacLeod et al., 2013) have revealed that water is the primary driver of these trends affecting the evolution for the mineral phase fractionation.

2.7.2.2 Trace elements

Tholeiitic basalt and tholeiitic intermediate samples show similarities in their trace element profiles (Figs. 2.8a, b). Intermediate compositions simply show higher concentrations in all elements displayed except Ti. The likeliest way to get from basalt to andesite here is the fractionation of major crystal phases (e.g., Juster et al., 1989). Using the 0.5% H2O FC model as an example, crystallizing olivine, pyroxene, Fe-Ti oxides and plagioclase progressively rises the Zr/Ti ratio without significantly affecting the Th/Yb ratio (Fig. 2.13a). On the extended trace element diagram (Figs. 2.13c), the progressive removal of crystallizing phases enriches the melt in incompatible trace elements. The tholeiitic basalt average group composition is reached after ~40% crystallization from the 74J1328 sample; whereas the tholeiitic intermediate average group composition is reached after approximately 80% (Fig. 2.13c, d). The cumulated mineralogy after 80% crystallization includes olivine (~2%), pyroxene (~52%), plagioclase (~21%) and Fe-Ti oxides (~5%). The negative anomaly in Eu is due to its compatibility with plagioclase, replacing Ca cations. In some parts of the Hébécourt formation (Rogers et al., 2014) and the lower BRG, tholeiitic basalt and tholeiitic intermediate rocks are intercalated with each other (Fig. 2.9), suggesting FC in a relatively shallow storage zone to produce tholeiitic intermediate compositions, followed by resupply of tholeiitic basalt.

2.7.3 Assimilation-Fractional Crystallization models

Fractional crystallization alone cannot suffice to explain the overall geochemical patterns in the BRG, especially for trace elements, and for some major elements. In this section we model simultaneous assimilation and fractional crystallization (AFC) involving a Th-rich assimilant, possibly originating from an older TTG crust underneath the greenstone belt. The MCS allows the evaluation of several parameters concerning the initial magma composition and the wall rock. Diverse initial dissolved water contents were evaluated for the initial composition, similar to the FC exercise. We also kept the same initial magma temperatures, pressure and oxygen fugacity as in the FC models. The wall rock was evaluated at various initial temperatures and masses. When a partial melt is added from the wall rock to the system, the MCS assumes magma homogenization and hybridization.

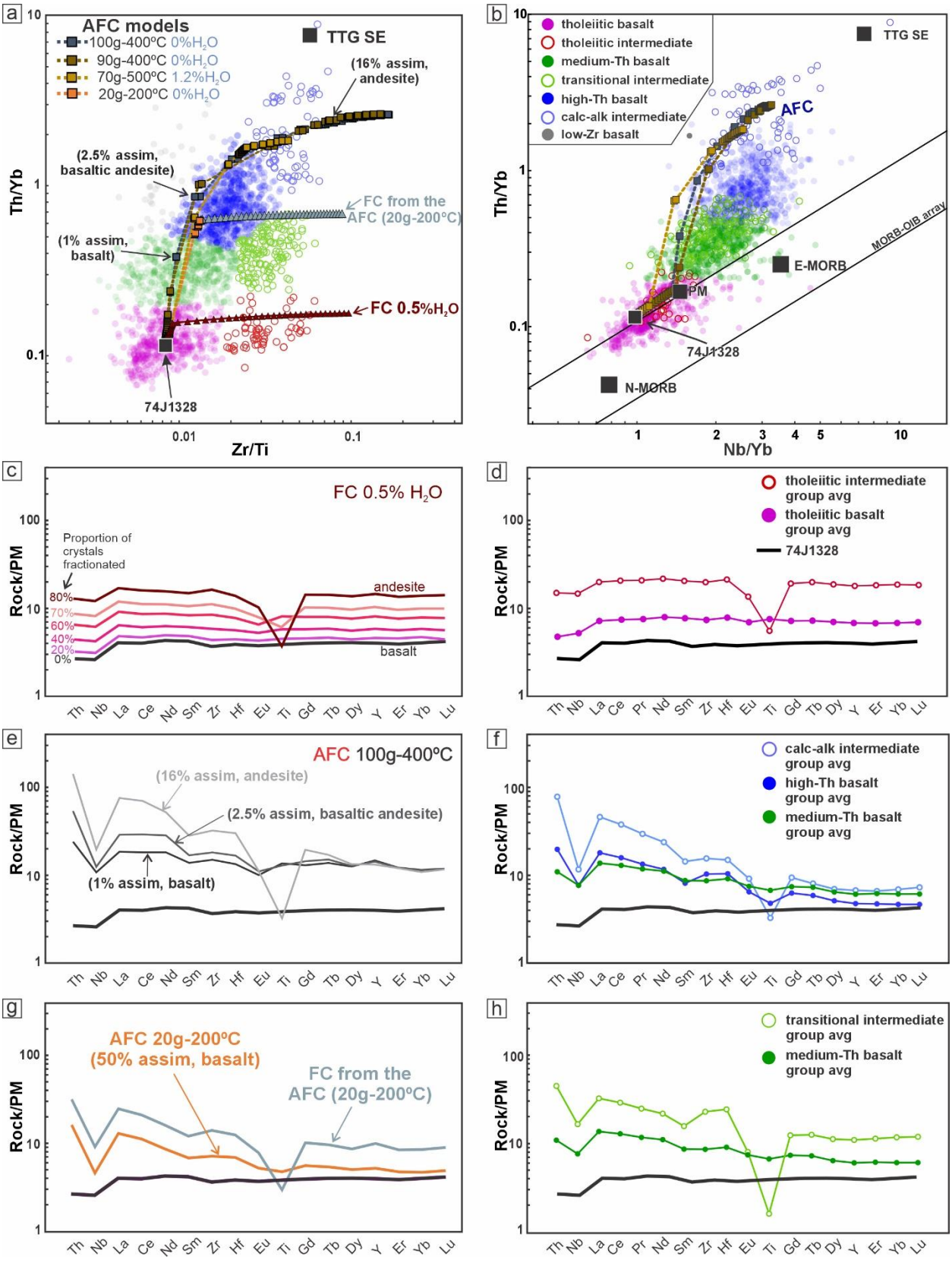
a
AFC models
100g-400ºC 0%H2O
90g-400ºC 0%H2O
70g-500ºC 1.2%H2O
20g-200ºC 0%H2O
TTG SE
(16% assim, andesite)
(2.5% assim, basaltic andesite)
FC from the AFC (20g-200ºC)
(1% assim, basalt)
FC 0.5%H2O
74J1328
Th/Yb
Zr/Ti
b
tholeiitic basalt
tholeiitic intermediate
medium-Th basalt
transitional intermediate
high-Th basalt
calc-alk intermediate
low-Zr basalt
TTG SE
AFC
E-MORB
PM
MORB-OIB array
74J1328
N-MORB
Th/Yb
Nb/Yb
c
FC 0.5% H2O
Proportion of crystals fractionated
80%
70%
60%
40%
20%
0%
andesite
basalt
Rock/PM
d
tholeiitic intermediate group avg
tholeiitic basalt group avg
74J1328
e
AFC 100g-400ºC
(16% assim, andesite)
(2.5% assim, basaltic andesite)
(1% assim, basalt)
f
calc-alk intermediate group avg
high-Th basalt group avg
medium-Th basalt group avg
g
AFC 20g-200ºC (50% assim, basalt)
FC from the AFC (20g-200ºC)
h
transitional intermediate group avg
medium-Th basalt group avg
Th Nb La Ce Pr Nd Sm Zr Hf Eu Ti Gd Tb Dy Y Er Yb Lu

Figure 2.13 (previous page) MCS modeling results. (a)-(b) Zr/Ti (ppm/ppm) vs Th/Yb (ppm/ppm) and Nb/Yb vs. Th/Yb diagrams with four AFC models, all plotting along the "main trend" of BRG compositions extending from the tholeiitic basalt group to the calc-alkaline intermediate group. First number in the AFC model list is the amount of wall rock in grams (for 100 g of initial magma in the chamber) and second number is the initial wall rock temperature. Panel (a) also includes two FC models, one starting from the tholeiitic basalt composition and the other from the end of an AFC model. (c)-(h) Extended trace elements diagrams normalized to the primitive mantle, comparing certain models with BRG group compositions. (c) Simulated liquids with increasing degrees of crystal fractionation, from 0% to 80%, based on the FC model with 0.5% H2O. (d) Average compositions of the tholeiitic basalt group and the tholeiitic intermediate group, for comparison with (c). (e) AFC model starting with 100 g of 400°C wall rock, showing the starting magma and evolving liquid compositions for 1%, 2.5% and 16% assimilation. (f) Average compositions for the medium-Th basalts, high-Th basalts, and calc-alkaline intermediate group, for comparison with (e). (g) Two-step model starting with AFC (orange line) and ending with FC (grey line); see text for details. (h) Average compositions for the medium-Th basalts and transitional intermediate group, shown for comparison with (g).

2.7.3.1 Major oxides

The MCS normally simulates 100 g of initial magma interacting with a certain mass wall rock (normally up to 100 g). In cases when the initial mass of the wall rock is reduced, the model requires less energy to heat up the wall rock enough to trigger partial melting. This process is exemplified in Figure 2.4, where an anhydrous magma (74J1328 sample) undergoes an AFC process with 90 g or 70 g of wall rock, and initial temperatures of 400°C, which are typical for high geothermal gradients (e.g., Holder et al., 2019). The anhydrous FC (0% orange line) and AFC models (90g-400ºC and 70g-400ºC dotted lines) are initially similar, primarily because the initial magma undergoes only FC (~11-7% MgO) (Fig. 2.4). However, the AFC models diverge as they elevate the temperature of the adjacent wall rock, resulting in the initiation of partial melting at approximately 7-5% MgO. In the case of AFC, the process leads to the suppression of Fe-Ti enrichment and a reduction in Al_2O_3 depletion, as illustrated in Figure 4. This effect becomes more pronounced when the magma assimilates 70 g of wall rock, triggering earlier partial melting, particularly at higher MgO values, compared to assimilating 90 g. Notably, certain major element compositions of medium-Th basalt are reasonably replicated by these anhydrous AFC models, presented as an end-member possibility. However, adding some water to the initial magma would likely enhance the modeling of other medium-Th samples.

To reproduce the behavior of high-Th basalt rocks, a water-rich tholeiitic basalt (1.2% H2O) is employed in an AFC model with 70 g of wall rock at an initial temperature of 500°C. Elevated temperatures in the wall rock trigger partial melting at even earlier stages of the system. In combination with the higher initial water concentration, this leads to Fe-Ti depletions and rising concentrations in Al_2O_3 and SiO_2 as MgO decreases (Fig. 2.4). The outcomes are generally similar to the calc-alkaline magmas series described in the literature (e.g., Irvine and Baragar,

1971) and explain the trends in the high-Th basalt and the calc-alkaline intermediate groups described in this work.

2.7.3.2 Trace elements

On the Zr/Ti vs Th/Yb (Fig. 2.13a) and the Pearce et al. (2021) diagrams (Fig. 2.13b) we show four AFC models, with initial wall rock temperatures ranging from 200°C to 500°C, initial wall rock amounts of 20-100 g and initial magma water contents of 0-1.2%. This set of conditions is broader than, but includes, those illustrated for major elements in Figure 2.4. These AFC models are collectively able to reproduce the “main trend” from tholeiitic basalt to calc-alkaline intermediate compositions, especially in Figure 2.13a.

The AFC model where the initial magma interacts with 100 g of wall rock at 400°C illustrates how trace element composition evolves during an AFC progression (Fig. 2.13a, e, f). Only ~1% of wall rock assimilation is necessary to move from tholeiitic basalt to medium-Th basalt. At 2.5% assimilation, Th and LREE concentrations become more pronounced, producing trace element profiles and Th/Yb ratios similar to those of high-Th basalt samples. With 16% assimilation, the magmatic system has evolved to andesitic compositions displaying high Th/Yb ratios and a steeper extended trace element profile, resembling calc-alkaline intermediate compositions.

Transitional intermediate compositions do not fit in the “main trend” in Figure 2.13a, since they have higher Zr/Ti ratios for the same Th/Yb. We interpret this “sideways” trend, off the main trend, as AFC followed by FC. Conceptually, the initial magma might acquire a small degree of contamination, such as 1-2%, from a TTG crust, leading to a quick increase in the Th/Yb ratio (see the first three models in Fig. 2.13a). Then continue its journey in the crust and fractionate within a secondary chamber perhaps hosted by existing basalts, yielding the increase in Zr/Ti to produce the transitional intermediate group. Single chamber scenarios can also be envisaged, for example we show an AFC run with only 20 g of wall rock and relatively cold initial temperatures of 200°C (grey triangles on Fig. 2.13a). After assimilating ~50% (10 g) of wall rock, the MCS automatically halted the process, as the temperature of the wall rock and the system are now the same and no more AFC process continues. The remaining magma was subjected to FC, yielding the sideways trend (Figs. 2.13a), including the Ti anomaly (Fig. 2.13g). The result partly resembles the average composition of the transitional intermediate group (Fig. 2.13h).

The low-Zr basalt group also plot away from the main trend and might require a different wall rock or initial magma to model their compositions. We have not specifically tried to model this volumetrically minor group.

2.7.4 Crustal assimilation or subduction?

2.7.4.1 Support for crustal assimilation

Crustal assimilation has been widely proposed as a significant petrogenetic process in various Archean volcanic and intrusive sequences, such as the Superior Province (e.g., Sproule et al., 2002; Bédard et al., 2013; Thurston, 2015), the Yilgarn craton in Australia (e.g., Arndt and Jenner, 1986; Barnes and Van Kranendonk, 2014), and in general petrogenetic studies on Archean magmas (e.g., Pearce, 2008; Moyen and Laurent, 2018; Barnes et al., 2021). This process may account for features such as high Th values, LREE enrichments, negative Nb anomalies, and distinctive radiogenic isotope patterns (Bédard, 2018 and references therein). We have illustrated this for the BRG using AFC models where a tholeiitic basaltic magma interacts with a TTG crust. However, is there evidence for such an older Th-rich crust underneath the greenstone belt?

Geophysical surveys in the Abitibi have revealed evidence for the presence of a potentially fusible middle (or lower) crust (e.g., Benn, 2006; Haugaard et al., 2021; Jorgensen et al., 2022) and zircons studies in the Abitibi volcanic rocks provide compelling evidence for an older crust component beneath the Abitibi greenstone belt. A comprehensive analysis of trace elements in zircons of the SE Superior Province by Mole et al. (2021) indicates a crustal component for various zones in the Abitibi greenstone belt, including the Blake River assemblage. Locally, geochronological studies have detected groups of zircons interpreted as inherited in several localities in the BRG for felsic volcanic and intrusive rocks (Mercier-Langevin et al., 2007a; McNicoll et al., 2014; Rogers et al., 2014).

Another scenario to explain the crustal input is magma mixing. Instead of the TTG component representing older crust, it could be a second magma which would mix with the mantle-derived basaltic magma in a crustal magma chamber. A magma mixing process has been invoked in some Phanerozoic arc settings with thick crust (e.g., Hildreth and Moorbarth, 1988; Dufek and Bergantz, 2005). Potentially, magma mixing – not necessarily in an arc setting – might produce similar trends to the AFC models presented here and we will reexamine this idea in a future publication related to the petrogenetic evolution of other Abitibi volcanic assemblages.

2.7.4.2 Archean subduction?

Another possible explanation for some of these geochemical signatures is the involvement of Archean subduction, which may include complex plume/arc/back-arc interactions proposed within the Abitibi by some authors (e.g., Wyman, 1999; Wyman and Kerrich, 2010). However, tholeiitic and calc-alkaline rocks are intercalated on the scale of hundreds of meters in the BRG. If calc-alkaline rocks (e.g., high-Th basalt or calc-alkaline intermediate rocks) were produced in a different tectonic setting (e.g., volcanic arc) than the tholeiitic basalt rocks (e.g., ridge or back-arc basin), it suggests a very dynamic history marked by rapid fluctuations in the tectonic conditions within the BRG. Some authors find this scenario improbable, as the question of how quickly a tectonic setting can transition from one state to another and then revert to the previous setting remains unclear (e.g., Bédard et al., 2013; Bédard and Harris, 2014; Thurston, 2015; Bédard, 2018). Research in the modern Lau Basin back-arc, however, indicates that major geochemical contrasts can exist in volcanic rocks formed simultaneously and in proximity because of very complex tectonics (Stewart et al., 2022; Fassbender et al., 2023). Since much more research is necessary to fully understand controls on petrogenesis in ancient settings, as well as Archean tectonics, we opted for a single main magma source in the mantle, with variable crustal input, to explain the petrogenetic evolution of the BRG in the simplest way possible.

2.8 Mafic to intermediate volcanic rocks and VMS deposits

Historically, the use of lithogeochemistry/petrology for VMS exploration has focused on felsic volcanic rocks (Lesher et al., 1986; Hart et al., 2004). However, Piercey (2010) has demonstrated that certain types of mafic to intermediate volcanic rocks can be preferentially associated with VMS deposits. While felsic rocks provide valuable insights on VMS exploration, mafic to intermediate volcanic rocks are more widespread in greenstone belts, and offer more direct insights into the magmatic source of the volcanic sequence. Therefore, it is worth exploring their potential to serve as aids to exploration.

Upon analyzing geochemical group abundances in every BRG formation, patterns emerge concerning VMS hosting formations. At the scale of BRG, the well-endowed Noranda and Bousquet formations are associated with medium-Th, high-Th and low-Zr basalt samples, alongside transitional and calc-alkaline intermediate rocks. Notably, there is a scarcity of tholeiitic basalt and tholeiitic intermediate rocks within these formations (Fig. 2.10). This observation suggests that the erupting magma for these formations consistently experienced some degree of crustal assimilation.

In the Bousquet formation in particular, a large proportion of samples come from the high-Th basalt, low-Zr basalt and calc-alkaline intermediate groups, indicating significant degrees of crustal assimilation (Fig. 2.10). In more detail, VMS deposits are hosted in the upper member of the Bousquet formation, which is more strongly influenced by crustal assimilation than the lower member (Mercier-Langevin et al., 2007b; Yergeau et al., 2022a). Within the northern Noranda formation, we have also shown a potential spatial correlation between volcanic mafic-intermediate compositions featuring high Th/Yb ratios and the presence of economically significant VMS occurrences (Figs. 2.11, 2.12).

Therefore, the spatial association between VMS deposits and crustally contaminated mafic to intermediate volcanic rocks appears to apply both at the scale of the BRG and within specific formations, suggesting a potential genetic link, further discussed below. Nevertheless, other BRG formations, like the Dupuis formation on the Quebec side, or the upper BRG on the Ontario side, also exhibit large amounts of crustally contaminated rocks but lack significant VMS discoveries. This implies that the abundance of such geochemical signatures is not the sole factor controlling VMS endowment. For example, recent integrated geophysical studies suggest the presence of ancestral transcrustal structures beneath the Noranda district, that potentially influenced the localization and optimization of magmatic and ore processes (Jorgensen et al., 2022). Another caveat is that a detailed analysis at the scale of tens or hundreds of meters, typical for VMS occurrences, is essential to comprehend the nuances of geochemical variation along the volcanic sequence. Presently, our observations primarily apply to a regional scale.

So what could explain a possible genetic link between VMS deposits and crustal assimilation? Thermal models posit that achieving a diverse range of volcanic products, ranging from mafic to felsic, as seen in the BRG, requires thermal maturity in the crust over an extended temporal span, potentially several million years (e.g., Annen, 2009; Karakas et al., 2017). A thermally mature system may facilitate partial crustal melting, leading to the assimilation and homogenization of contaminated signatures (Dufek and Bergantz, 2005). Furthermore, such a thermal system enhances the generation of felsic volcanic products (Annen, 2009; Karakas et al., 2017) and may contribute to the sustenance of long-lived thermal anomalies essential for VMS generation and endowment.

2.9 Conclusions

The Blake River Group (BRG) stands out as the most VMS-endowed area within the Abitibi greenstone belt. This paper uses a large whole-rock geochemistry dataset to examine

petrogenetic controls of the mafic to intermediate volcanic rocks on a regional scale, including hydrothermally altered samples spatially associated with VMS deposits.

Principal component analysis of immobile elements identifies Th, Yb, and Ti as main contributors to the dataset's variance. Integrating these elements along with Zr into geochemical ratios, a Th/Yb vs Zr/Ti diagram was constructed, revealing seven distinct geochemical groups: tholeiitic basalt, tholeiitic intermediate, medium-Th basalt, transitional intermediate, high-Th basalt, calc-alkaline intermediate and low-Zr basalt.

Through modeling with the Magma Chamber Simulator (MCS), we successfully replicated the geochemical patterns of most groups. Utilizing a high MgO sample from the BRG dataset as a starting point, Fractional Crystallization models were employed to elucidate major oxides and trace element patterns of the uncontaminated groups, namely tholeiitic basalt and tholeiitic intermediate rocks.

For the remaining geochemical groups, Assimilation-Fractional-Crystallization models were applied. Medium-Th basalt and transitional intermediate samples represent lower assimilation rates (averaging ~1%) while high-Th basalt and calc-alkaline intermediate rocks indicate moderate to high assimilation rates ranging from 2.5% to ~23%.

Geological formations hosting VMS deposits in the BRG display a dominance of geochemical signatures indicative of crustal assimilation. Notably, these VMS-endowed formations lack tholeiitic basalt or tholeiitic intermediate samples. This hints at a potential link between crustal assimilation and VMS endowment, although not all formations characterized by signatures with crustal assimilation display VMS endowment. This implies that while the geochemical composition of mafic to intermediate volcanic rocks might play a role in VMS fertility, it is not the sole determinant. Future work will explore whether analogous patterns are discernible in other regions of the Abitibi greenstone belt, explore potential genetic explanations, and assess how these patterns could evolve into effective vectoring tools. Mafic to intermediate volcanic rocks emerge as crucial indicators for identifying the processes associated with VMS fertility.

2.10 Acknowledgments

We thank Taus Jorgensen and Harold Gibson for relevant discussions on the geology and structures in the Blake River Group and for providing GIS data on the Abitibi greenstone belt.

3 SECOND ARTICLE : STOUGHTON-ROQUEMAURE

Petrogenetic insights on the largest volcanic pulse in the Archean Abitibi greenstone belt, Canada: the Stoughton-Roquemaure assemblage

Compréhension pétrogénétique du plus grand pulse volcanique de la ceinture de roches vertes archéennes de l'Abitibi, Canada : l'assemblage de Stoughton-Roquemaure

Authors :

Octavio Vite-Sánchez[a], Pierre-Simon Ross[a], Patrick Mercier-Langevin[b, c], Kieran Iles[a]

a.- Institut national de la recherche scientifique, 490 rue de la Couronne, Québec (Qc), G1K 9A9, Canada

b.- Geological Survey of Canada, 490 rue de la Couronne, Québec, G1K 9A9, Canada

c.- Now at: Agnico Eagle Mines Ltd, 145 King St. East, Suite 400, Toronto, Ontario, M5C 2Y7, Canada.

Title of the journal:

Canadian Journal of Earth Sciences

Accepted: 28 July 2025

DOI: doi.org/10.1139/cjes-2025-0019

This chapter is the accepted version of the research article:

Vite-Sánchez, O., Ross, P.S., Mercier-Langevin, P. and Iles, K., 2025. Petrogenetic insights on the largest volcanic pulse in the Archean Abitibi greenstone belt, Canada: the Stoughton-Roquemaure assemblage. Canadian Journal of Earth Sciences, e-First.

3.1 Abstract

The Stoughton-Roquemaure (S-R) assemblage represents the largest and most rapidly emplaced (~3 m.y.) volcanic sequence within the Abitibi greenstone belt, yet much of its petrogenetic history remains unexplored. To address this, we compile 1,319 whole-rock geochemical analyses, comprising 1.0% komatiites, 2.6% komatiitic basalts, 37.1% tholeiitic basalts, 0.5% tholeiitic intermediate volcanics, 8.1% medium-Th basalts, 19.1% high-Th basalts, 0.4% low-Zr basalts, 4.2% transitional intermediate volcanic rocks, 17.1% calc-alkaline intermediate volcanic rocks, and 9.9% felsic volcanic rocks. Primary magma estimates for komatiites and tholeiitic basalts reveal two clusters of mantle potential temperatures (TP) of $1637 \pm 65\,^{\circ}C$ and $1575 \pm 105\,^{\circ}C$, suggesting a mantle plume influence. Fractional crystallization (FC) models, under varying pressures and H_2O contents, explain the evolution of the tholeiitic suite. However, more than half of the S-R samples exhibit transitional to calc-alkaline affinities, modeled as the result of assimilation–fractional crystallization (AFC) or magma mixing between tholeiitic basalt and a TTG-like crustal end-member. The generation of these volcanic rock signatures implies the development of complex crustal magmatic systems. Spatial analysis reveals that these signatures are prevalent in the north whereas ultramafic and tholeiitic rocks dominate central and southern zones, defining a north-south geochemical zonation. This likely reflects rapid ascent through a thinner crust in the south versus enhanced crustal interaction in the north. Our results underscore the interplay between the mantle-derived magmas and crustal architecture in controlling volcanic evolution. These results offer new insights into the geochemical diversity and voluminous magmatism of the S-R assemblage and contribute to our understanding of Archean lithospheric development.

3.2 Introduction

Greenstone belts are assemblages of supracrustal volcanic rocks that are key components of preserved Archean crust. They consist of metamorphosed, mostly mafic volcanic rocks, typically deposited in a submarine environment, as well as various intrusive and sedimentary rocks (Thurston, 2015). The Abitibi greenstone belt in Canada represents the largest exposed Archean example of a greenstone belt and is one of the most studied, largely due to its exceptional mineral wealth (e.g., Monecke et al., 2017; Mercier-Langevin et al., 2023). However, the detailed geochemical evolution of the Abitibi volcanic assemblages remains understudied.

This study aims to provide new insights into the petrogenesis of the Stoughton-Roquemaure (S-R) assemblage, which constitutes the largest volcanic pulse in the Abitibi greenstone belt, based

on its surface extent of ~16 000 km^2 (or 34% relative to volcanic assemblages; Mercier-Langevin et al., 2023; Jorgensen and Gibson, 2024) and brief emplacement over approximately 3 m.y (Ayer et al., 2002; Thurston et al., 2008; Dubé and Mercier-Langevin, 2020). The S-R assemblage has traditionally been classified as a komatiite–tholeiite association, and previous authors have focused their studies on central areas of the assemblage, which do exhibit these characteristics (e.g., Dostal and Müller, 1997, 2013; Sproule et al., 2002).

However, our compilation of whole-rock geochemical data reveals significant compositional variability in the S-R assemblage. The variability is addressed by grouping the samples into geochemical groups to simplify their interpretation, calculate their relative abundances and to easily illustrate their distribution within the assemblage. In addition, thermodynamic-geochemical modeling is used to investigate key petrogenetic process, including fractional crystallization (FC), fractional crystallization coupled with wall rock assimilation (AFC), and magma mixing. Estimates of mantle potential temperatures for ultramafic and mafic compositions suggest the presence of a significant thermal anomaly, likely related to plume activity, that contributed to the voluminous magmatism of the S-R assemblage. Although a substantial portion of the volcanic rocks are mantle-derived and evolved through fractional crystallization, over half of the samples require a crustal input, modeled as either through AFC or magma mixing.

3.3 Geological background

The Superior Province of Canada (Fig. 3.1, inset) is a series of dominantly east-trending Mesoarchean to Neoarchean terranes or subprovinces (Percival et al., 2012). The Abitibi greenstone belt is located in the southeastern portion of the Superior Province and is part of the Abitibi-Wawa Subprovince (Fig. 3.1). The volcanic rocks of the Abitibi greenstone belt have been subdivided into seven subalkaline assemblages ranging in age from 2795 Ma to 2695 Ma (Ayer et al., 2002; Thurston et al., 2008; Dubé and Mercier-Langevin, 2020). The majority of the preserved volcanic rocks were emplaced within the last five assemblages, spanning approximately 40 m.y., from ~2734 Ma to ~2695 Ma. The S-R assemblage is situated temporally between the Deloro (~2734-2724 Ma) and Kidd-Munro (~2720-2710 Ma) assemblages (Ayer et al., 2002; Thurston et al., 2008; Dubé and Mercier-Langevin, 2020) (Fig. 3.1). The stratigraphic units assigned to the S-R assemblage have been dated by U-Pb on zircons as having an age range between ~2723 and ~2720 Ma (Barrie, 1999; Legault et al., 2002; Davis et al., 2005; Ayer et al., 2007; David et al., 2007; Davis et al., 2014) but some units remain undated (Table 3.1).

Volcanic rocks of the S-R assemblage crop out mostly in the northern part of the Abitibi greenstone belt (Thurston et al., 2008), but they also occur in the southern zone, mainly between the Destor-Porcupine, the Manneville Nord and Macamic fault zones (Dubé and Mercier-Langevin, 2020) (Fig. 3.2). Overall, the S-R assemblage covers ~16,000 km2, representing ~33% of volcanic rocks in the Abitibi greenstone belt within the compilations of Dubé and Mercier-Langevin (2020), Mercier-Langevin et al. (2023) and Jorgensen and Gibson (2024). Representative stratigraphic units assigned to the S-R assemblage by previous works are summarized in Table 3.1. In the literature, the S-R assemblage is predominantly characterized by a thick succession of tholeiitic basalts, accompanied by less abundant komatiites and komatiitic basalts, which were deposited in a submarine environment, likely forming an extensive lava plain (Thurston et al., 2008; Dostal and Mueller, 2013, and references therein). Minor intermediate to felsic volcanic centers, along with thin volcaniclastic units interbedded with the mafic to ultramafic units, have also been documented (Barrie, 1999; Legault et al., 2002; Davis et al., 2005; Ayer et al., 2007; David et al., 2007; Davis et al., 2014).

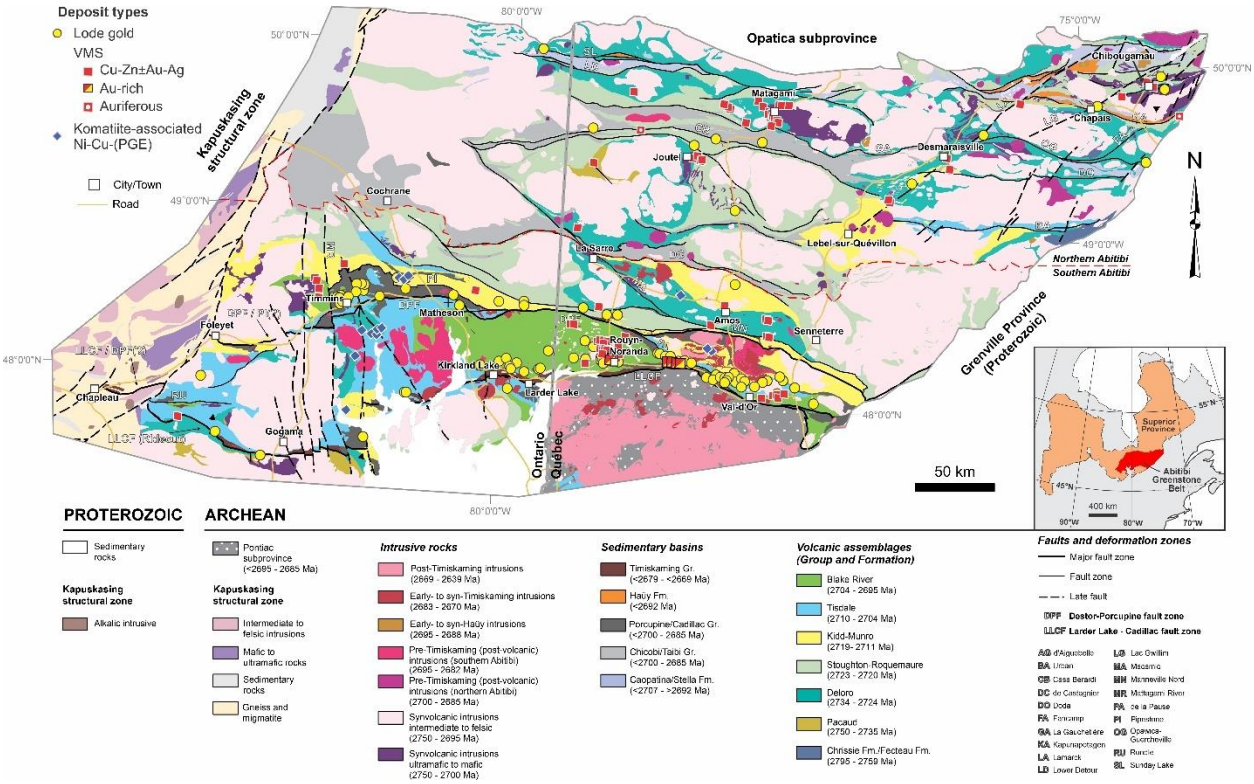

Figure 3.1 Geological map of the Abitibi greenstone belt illustrating the volcanic assemblages, the intrusive rocks, sedimentary basins, and main structures (modified from Dubé and Mercier-Langevin, 2020).

Table 3.1 Representative stratigraphic units in the Stoughton-Roquemaure assemblage.

Stratigraphic unit	Location	True thickness	Lithologies	Ages (U-Pb on zircons)
Stoughton-Roquemaure Group	Near Quebec-Ontario provincial border, north of the Destor-Porcupine fault zone	0.2-6 km (Dostal and Mueller, 1997; MRNF, 2022a)	- Tholeiitic basaltic lavas (massive to pillowed), limited fragmental facies (MRNF, 2022a, and references therein) - Intercalated komatiites & komatiitic basalts (also massive to pillowed; Dostal and Mueller, 1997, 2013)	2721.1 ± 1 Ma and 2723.2 ± 2 Ma (Barrie, 1999)
No specific name assigned, although several ages reported	S-R assemblage between Timmins and Cochrane in Ontario	-	Massive to pillowed basalts with minor felsic volcanic components (1%)	2721.6 ± 1.4 Ma (Barrie, 1999), 2719.5 ± 1.7 Ma (Ayer et al., 2002), 2722 ± 1.7 Ma (Berger et al., 2007)
Deguisier Formation (Kinojévis Group)	North of the Destor-Porcupine fault zone in Quebec	1-7 km (MRNF, 2019 and references therein)	- Pillowed to massive tholeiitic basalts - Various minor lithologies ranging up to felsic ones (MRNF, 2019, and references therein)	2719.4 ± 1 Ma, 2718 ± 1.3 Ma (Pilote et al., 2009) and 2720.7 ± 1.2 Ma (David et al., 2011)*
Catherine Group	Kirkland Lake area	Not provided	Pillow basalts with minor massive flows and sills (Corfu, 1993)	2720 ± 2 Ma (Corfu, 1993)
Vanier-Dalet-Poirier Group	Southeast of Joutel	~10 km (Legault et al., 2002)	Effusive sequence of basalt to andesite, interlayered with volcaniclastic units (Legault et al., 2002)	2722 ± 2 (Gaboury and Daigneault, 1999)
Collines de Cartwright Group	Northwest of Joutel	~5 km (Legault et al., 2002)	-Mafic volcanics occurring as massive, pillowed and locally brecciated flows -Minor intercalations with ultramafic rocks (Legault et al., 2002)	2721 ± 3 Ma (Legault et al., 2002) and 2720 ± 3 Ma (David et al., 2007)
Burntbush volcanic complex	Northwest of La Sarre in Ontario side	Not provided	-Basaltic to intermediate massive flows, with minor pillow lavas and mafic volcaniclastic intercalations -less abundant felsic volcanic rocks (Ordóñez-Calderón, 2013)	2720.1 ± 1.6 Ma (Barret et al., 2013)

Desboues formation	East of La Sarre	100s of m to ~10 km (MRNF, 2022b)	Mainly composed of basalts and andesites, locally pillowed, with gabbroic sills (MRNF, 2022b and references therein)	Stratigraphically related to S-R (Thurston et al., 2008), but no absolute age available
Beaupré Formation	North of La Sarre	~1.8 km (Lafrance et al., 2000)	Basalts (pillowed to massive) with a massive sodic rhyolite complex (Lafrance et al., 2000)	2722 ± 3 Ma (Zhang et al., 1993)
Clermont-Disson Formation	North of La Sarre	~2-10 km (MRNF, 2022c)	-Mainly mafic-intermediate massive and pillowed flows with local undifferentiated tuff. -Includes minor felsic, tuff and sedimentary successions	Stratigraphically related to the S-R (Jorgensen and Gibson, 2024), but no absolute age available
Enjalran-Bapst Group	Northernmost part of the S-R assemblage between Ontario and Quebec	Not provided	Basaltic dominated featuring massive, pillowed and brecciated facies, intercalated with fined gabbroic sills (Lacroix, 1994)	2721.2 ± 1.7 Ma (Ayer et al., 2007)
Bruneau Formation	Chapais-Chibougamau area	2-3 km (MRNF, 2024a and references therein)	90% of the formation consists of tholeiitic basalts, which are pillowed, massive and fragmental (MRNF, 2024a and references therein)	2724.4 ± 1.2 Ma (Davis et al., 2014); slightly older than the established age for the assemblage
Blondeau Formation	Chapais-Chibougamau area	Not provided	Intermediate to felsic volcanic rocks with minor sedimentary successions (MRNF, 2024b)	Maximum depositional age of <2721 Ma (Leclerc et al., 2012)
Dussieux formation	Matagami area	Not provided	Intermediate to felsic volcanic rocks (Goutier et al., 2004)	2720 ± 1 Ma (Davis et al., 2005)

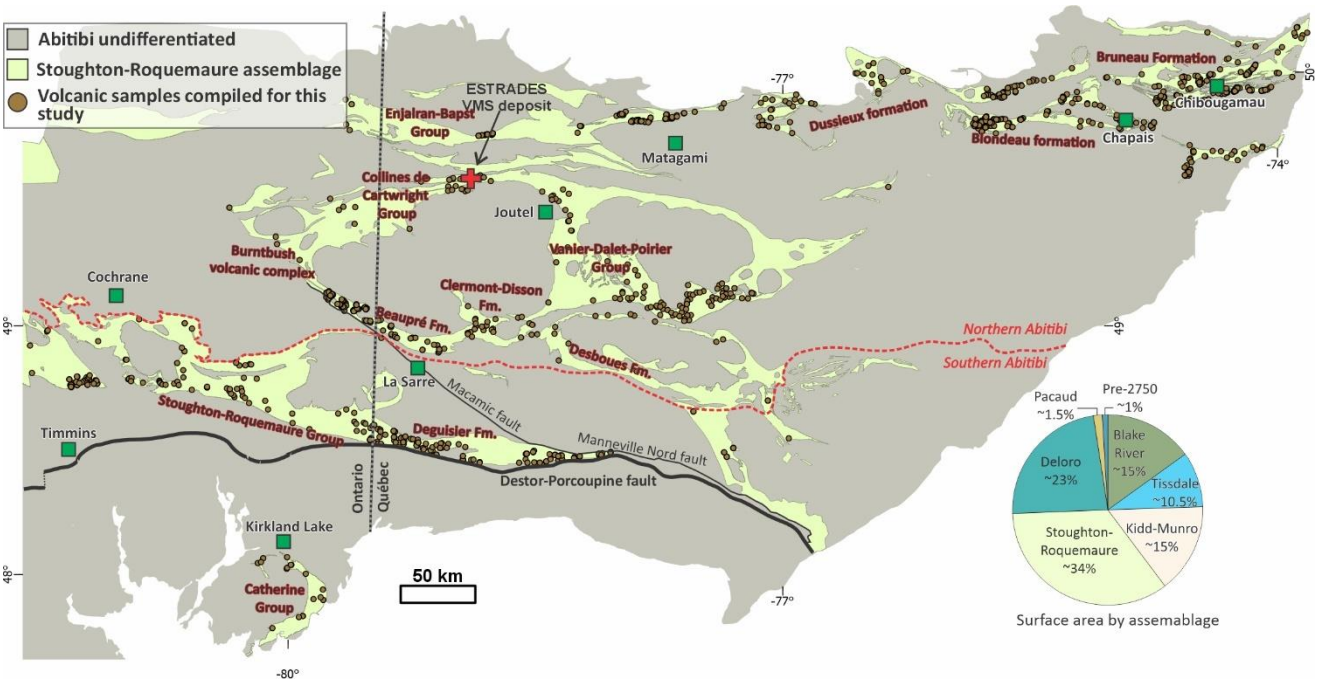

Figure 3.2 Distribution of the Stoughton-Roquemaure (S-R) assemblage from Jorgensen and Gibson (2024) base map. Formations and stratigraphic group names indicate their approximate locations (see Table 1). Surface area information from Jorgensen and Gibson (2024). Samples information in 'cjes-2025-0019suppla'. Map projection: Lambert Conformal Conic. Datum: North American 1983 CSRS. Coordinate system: Lat-Lon.

3.4 Methods

3.4.1 Dataset

A large dataset of whole-rock geochemistry for volcanic rocks in the S-R assemblage was compiled. The dataset primarily utilized publicly available sources, with the majority (98%) derived from the provincial geological surveys of Quebec (*´Système d'information géominière',* SIGÉOM) and Ontario (Open File Reports from the Ontario Geological Survey, OGS), including publicly accessible industry data. The remaining 2% of the data originated from academic studies. Detailed source information is provided in 'cjes-2025-0019suppla'. To ensure a minimum standard of data quality, only analyses conducted after the year 2000 were included. The selection criteria required samples to contain measurements of major oxides, loss on ignition, and key trace elements, specifically Ce, Eu, Gd, La, Nb, Sm, Th, Y, Yb, and Zr. After applying these criteria, 1,319 analyses were retained for the final dataset.

3.4.2 Element mobility and the 'least-altered' samples

In Precambrian greenstone belts, secondary processes such as diagenesis, metamorphism and hydrothermal alteration create issues with element mobility (MacLean and Barrett, 1993);

therefore, mobile oxides such as Na_2O, K_2O, SiO_2 (the constituents of the TAS diagram) must be used with great caution in these settings. Among major oxides, only Al_2O_3 and TiO_2 are typically considered immobile (Winchester and Floyd, 1977). Similarly, many trace elements, especially high field strength elements (HFSE), are considered robust against mobilization (e.g., Winchester and Floyd, 1977; Pearce, 1996; Rollinson and Pease, 2021). The rare earth elements (REE) are commonly considered within this group, although under focused hydrothermal conditions they may still be mobilized (e.g., Migdisov et al., 2016).

Given these constraints and following the methodology of Vite-Sanchez et al. (2024), this work uses immobile element ratios to classify rocks from mafic to felsic compositions. These ratios tend to remain constant even when the rocks undergo mass changes in processes such as silicification or leaching (e.g., Pearce, 1996). In addition, these immobile element ratios serve as useful proxies for petrogenetic interpretation, such as Zr/Ti for monitoring fractionation (Winchester and Floyd, 1977) or the Nb-Yb-Th systematics to interpret the tectonic and magmatic process (e.g., Pearce, 2008; Condie, 2005; Pearce et al., 2021).

Komatiites and komatiitic basalts are identified separately on the Jensen (1976) plot. Since this employs major elements, we follow the approach of Sproule et al. (2002), which employs MgO content versus loss on ignition (LOI) to exclude samples largely affected by chloritization and serpentinization. Although this method is not infallible, the ultramafic samples included here are considered to exhibit low degrees of alteration.

To improve the reliability of major element visualizations (e.g., Harker diagrams), a subset of ‘least-altered’ samples was defined across the mafic to felsic range. This subset was used exclusively for visualization and modeling purposes, not for classification. Least-altered samples were identified using alteration indices, specifically the Chlorite–Carbonate–Pyrite Index (CCPI; Large et al., 2001) and the Ishikawa Alteration Index (AI; Ishikawa et al., 1976), using the modified boxplot of Rogers et al. (2014). This filtering procedure excluded approximately 27% of the dataset, retaining 979 samples in the final least-altered subset. Once selected they were normalized to 100% on a volatile-free basis for plotting purposes.

3.4.3 Geochemical subdivision

The first step in classifying the samples was to use the Jensen (1976) cation plot to identify komatiitic basalts and komatiites (Fig. 3.3a). In general, true komatiites contain over 18% MgO while komatiitic basalts range between 12 and 18% MgO (Arndt, 1994) but using the Jensen plot creates slightly broader MgO ranges. We later classified them into aluminum undepleted

komatiites (AUK, Al/Ti >13) and aluminum depleted komatiites (ADK, Al/Ti<13) (Fig. 3.3b). Rocks with more than 35% MgO were discarded to avoid olivine-rich cumulates, although some of the remaining samples are likely cumulative.

Mafic to felsic compositions were subdivided using the approach of Vite-Sánchez et al. (2024) that uses the Pearce (1996) diagram (Fig. 3.3c) to broadly separate mafic, intermediate and felsic compositions, the Ross and Bédard (2009) diagram (Fig. 3d) to assign magmatic affinities, and a custom Th/Yb versus Zr/Ti diagram to generate the final geochemical groups (Fig. 3.3e). This diagram, developed and optimized for the Blake River Group by Vite-Sánchez et al. (2024), is applied here without modification to the S-R assemblage.

To simplify the description of the geochemical groups in certain geochemical diagrams, we constructed three distinct distribution ellipsoids using the Mahalanobis distance (Mahalanobis, 1936). Each ellipsoid encompasses several geochemical groups with similar magmatic affinities, as guided by the Ross and Bedard (2009) diagram (Fig. 3.3d). The ellipsoids represent distributions at the 0.5 and 0.95 levels. The geochemical groups within each ellipsoid are as follows:

Tholeiitic affinity ellipsoid: Komatiites, komatiitic basalts, tholeiitic basalts, tholeiitic intermediate volcanic rocks.

Transitional affinity ellipsoid: Medium-Th basalts, transitional intermediate volcanic rocks, transitional felsic volcanic rocks, and high-Yb rhyolites.

Calc-alkaline affinity ellipsoid: High-Th basalts, low-Zr basalts, calc-alkaline intermediate volcanic rocks, low-Yb felsic volcanic rocks, and calc-alkaline felsic volcanic rocks.

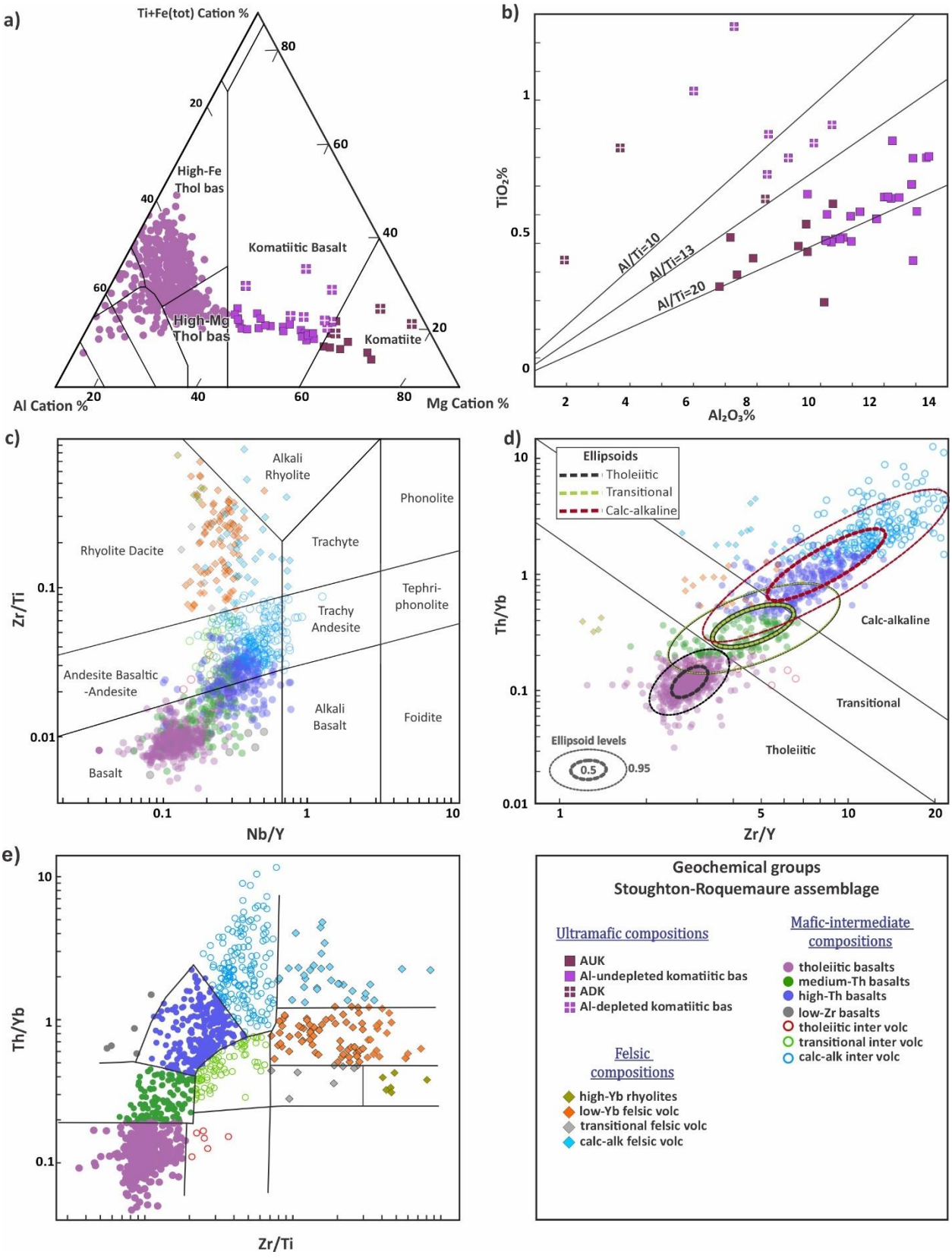
a)
Ti+Fe(tot) Cation %
Al Cation %
Mg Cation %
High-Fe Thol bas
Komatiitic Basalt
High-Mg Thol bas
Komatiite
b)
TiO2%
Al2O3%
Al/Ti=10
Al/Ti=13
Al/Ti=20
c)
Zr/Ti
Nb/Y
Alkali Rhyolite
Phonolite
Rhyolite Dacite
Trachyte
Tephri-phonolite
Trachy Andesite
Andesite Basaltic -Andesite
Alkali Basalt
Foidite
Basalt
d)
Ellipsoids
Tholeiitic
Transitional
Calc-alkaline
Th/Yb
Zr/Y
Calc-alkaline
Transitional
Tholeiitic
Ellipsoid levels
0.5
0.95
e)
Th/Yb
Zr/Ti
Geochemical groups
Stoughton-Roquemaure assemblage
Ultramafic compositions
AUK
Al-undepleted komatiitic bas
ADK
Al-depleted komatiitic bas
Mafic-intermediate compositions
tholeiitic basalts
medium-Th basalts
high-Th basalts
low-Zr basalts
tholeiitic inter volc
transitional inter volc
calc-alk inter volc
Felsic compositions
high-Yb rhyolites
low-Yb felsic volc
transitional felsic volc
calc-alk felsic volc

Figure 3.3 (previous page) Classification and geochemical grouping of the S-R assemblage volcanic rocks. (a) Jensen's cation plot (Jensen, 1976) for the least-altered samples. (b) Al_2O_3 vs. TiO_2 diagram, with the Al/Ti = 13 line distinguishing Al-depleted from Al-undepleted komatiites and komatiitic basalts, after Nesbitt et al. (1979). (c) Zr/Ti vs. Nb/Y classification plot (Pearce, 1996) showing S-R mafic to felsic compositions. (d) Th/Yb vs. Zr/Y diagram (Ross and Bédard, 2009) displaying magmatic affinity ellipsoids for S-R geochemical groups. (e) Th/Yb vs. Zr/Ti classification diagram for mafic to felsic compositions (Vite-Sánchez et al., 2024). Panels (c) to (e) show the whole S-R dataset (including hydrothermally altered samples), except komatiitic rocks.

3.4.4 Magma Chamber Simulator (MCS)

The Magma Chamber Simulator (MCS, Bohrson et al., 2014, 2020) uses the thermodynamic MELTS engine (Ghiorso and Sack, 1995; Ghiorso et al., 2002; Gualda et al., 2012) to calculate phase equilibria in a magmatic system, and thereby track the geochemical evolution of the magma. MCS evaluates major and trace elements, as well as certain isotopic systems (Bohrson et al., 2014; Heinonen et al., 2020); the latter are not considered in this work. Processes such as magma recharge, assimilation of partial melts, and fractional crystallization can be modeled. The processes explored for understanding the S-R magmas are briefly outlined below.

3.4.4.1 Fractional crystallization (FC) models (MCS)

Fractional crystallization (FC) models are designed to understand the evolution of tholeiitic basalts and intermediate compositions under varying conditions. For this purpose, liquid lines of descent (LLDs) are displayed representing fractional crystallization models under varying pressures (0.15, 0.3, 0.6, 1.0, and 2.0 GPa, equivalent to crustal depths of about 6, 12, 18, 34, 64 km, respectively) and water contents (0.1% and 1.0%). Models are built under the fayalite-magnetite-quartz buffer (FMQ +1) to best match the element variability present in the S-R magmas. The temperature decrement for all FC models is 5º C. Sample 1992005106 is employed as the initial magma composition as it represents a high-MgO basalt (11.3 wt. % MgO) compatible with a primary magma composition from PRIMELT3 parameters (see below).

3.4.4.2 Assimilation-fractional crystallization (AFC) models (MCS)

Assimilation-fractional crystallization (AFC) and mixing models test the hypothesis that the geochemical diversity of the S-R assemblage can be derived from two end-members: a primitive mafic magma (sample 1992005106) and the average composition of the Southeast Superior Tonalite-Trondhjemite-Granodiorite (TTG-SE) (Mole et al., 2021). AFC, as modeled in MCS,

represents assimilation of wall rock-derived partial melt rather than wholesale incorporation of stopped blocks.

AFC models set wall-rock temperature using a thermal gradient of 100 ºC/0.1 GPa (Holder et al., 2019). We used two different pressures, 0.3 and 0.6 GPa, since these give the most convincing FC models for tholeiitic basalts (see below). Two water contents (0.1% and 1.0%) are modeled. In all cases, one unit of tholeiitic basalt interacts with one unit of wall rock (100 g) with temperature decrements of 10–20°C.

3.4.4.3 Magma mixing (MCS)

Numerical models and experimental studies suggest that hybrid compositions can be achieved by mixing different end-member magmas (e.g., De Campos et al., 2011; Laumonier et al., 2014) and can occur at various stages of the magmatic system (Perugini and Poli, 2012). However, some authors suggest that mixing efficiency or magma hybridization is maximized when the rheological properties of the end-members, particularly viscosity, are similar, and certain turbulence conditions are met (e.g., Sparks and Marshall, 1986; Laumonier et al., 2014). Common scenarios for magma mixing include the replenishment of a felsic reservoir by a mafic magma (Laumonier et al., 2014) or when different melts crosscut their trajectories in channels *en route* to the surface (Perugini and Poli, 2012).

In this study, magma mixing is evaluated using the recharge module within the MCS (e.g., Spera et al., 2016), which assumes complete hybridization of the two end-members upon interaction. To establish the conditions for magma mixing, experimental and numerical data outlined by Laumonier et al. (2014) were used as a guide. According to these criteria, hybridization might occur when a partially molten felsic magma interacts with a partially crystallized mafic magma (within 10–30% crystallization). Under these conditions, the viscosities of the felsic and mafic melts become similar, facilitating the hybridization process.

The mixing models presented here simulate three different proportions: one where the mafic end-member dominates in a 4:1 ratio, another with equal contributions of both end-members in a 1:1 ratio, and a third where the felsic magma is dominant in a 1:4 ratio. The mafic and felsic end-members used match those employed in the FC and AFC models, with pressures constrained to 0.3 GPa and the mafic end-member containing 1.0% H_2O, as this water content provided the best fit for our models.

3.4.5 PRIMELT3

PRIMELT3 (Herzberg and Asimow, 2015) is an inverse modeling tool that reconstructs primary magma compositions from primitive mafic to ultramafic rocks (>9 wt% MgO). In addition, it estimates mantle potential temperature[1] (T_P), melt fractions, residual lithology, among other parameters. The model incrementally adds olivine in 1% steps to back-calculate a fertile peridotite composition, using projections in the olivine-anorthosite-quartz and FeO-MgO systems (Herzberg and O'Hara, 2002). The reconstructed fertile peridotite represents the mantle source of volatile-free primary magma compositions. PRIMELT3 provides two melting models: accumulated fractional melting and batch melting. The former is preferred because mantle melts typically segregate and migrate through grain boundaries or porous channels shortly after formation, rather than remaining in equilibrium with the residue. This behavior is better captured by accumulated fractional melting, which reflects progressive melt extraction and depletion of the source (Herzberg and Asimow, 2015; Herzberg et al., 2023). Accordingly, this study emphasizes results based on this model. Samples that fail to produce valid solutions are marked as 'unsuccessful', likely due to processes such as augite fractionation, a pyroxenite source, or volatiles. Additionally, PRIMELT3 is used to validate the chosen initial composition in MCS models.

3.5 Results

3.5.1 Major oxides

Decreasing MgO is used as a differentiation monitor since the dataset contains ultramafic to felsic samples (Fig. 3.4). Al-undepleted komatiites and komatiitic basalts show slight enrichments in TiO_2, Al_2O_3 and SiO_2 as MgO decreases, while $Fe_2O_3^T$ concentrations remain around 10% (Fig. 3.4a, b, c, d). Al-depleted komatiitic rocks exhibit higher TiO_2 concentrations and lower Al_2O_3, reflected in their lower Al/Ti ratios (Fig. 3b).

Mafic compositions (10–4 wt% MgO) display varying Al_2O_3, $Fe_2O_3^T$, and TiO_2 concentrations, with the largest variations at ~6–4 wt% MgO. Intermediate samples (5-2 wt% MgO) have large variations in Al_2O_3 but start to converge for other displayed oxides. Felsic samples (<2.5 wt% MgO) exhibit the lowest FeO, TiO_2, and MgO, and the highest SiO_2 contents (Fig. 3.4).

[1] Mckenzie and Bickle (1988) defined 'Mantle potential temperature' as the temperature that mantle would have if it were brought to the Earth surface adiabatically.

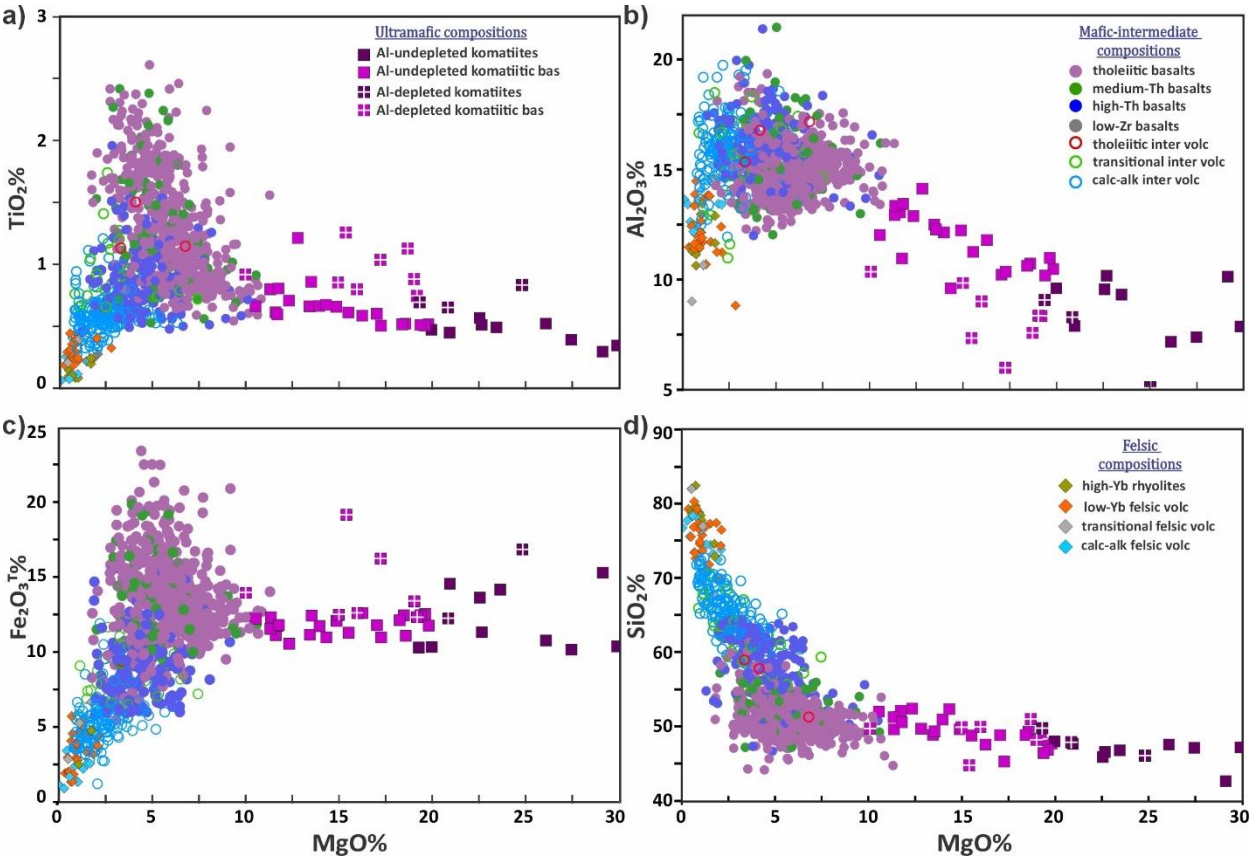

Figure 3.4 Major oxide variation diagrams for the least altered S-R samples (see text). (a)-(d) TiO2, Al2O3, Fe2O3T, SiO2 versus MgO.

3.5.2 Geochemical groups

Mafic to felsic compositions were classified into 11 groups (Fig. 3.3e, Table 3.2) and are described according to their magmatic affinity ellipsoid (see section 3.4.3). Although komatiites and basaltic komatiites are not included in figure 3.3e, they are also included in the following description based on their magmatic affinity.

3.5.3 Tholeiitic affinities

Komatiites and komatiitic basalts constitute 3.6% of the dataset, with komatiites (~1%) being less abundant than komatiitic basalts (2.6%). Among komatiitic rocks, Al-undepleted compositions (AUK) dominate (~2.5%) over Al-depleted compositions (ADK). AUK samples consistently plot within tholeiitic affinity ellipsoids across different diagrams (Fig. 3.5a, b, c, d, e). In contrast, ADK samples exhibit higher Zr/Y, Nb/Yb, and TiO_2/Yb ratios often plotting outside these ellipsoids. Furthermore, ADK samples exhibit a slight depletion in heavy rare earth elements (HREE) relative

to AUK, as evidenced by the Gd/Yb_N ratios (Fig. 3.5f) and extended trace elements patterns (Fig. 3.6a, b).

Tholeiitic basalts represent ~36% of the dataset, while tholeiitic intermediate volcanic rocks are very rare (0.5%, Table 3.2). The geochemical ratios of these groups are comparable to the Primitive Mantle values (Sun and McDonough, 1989) and average Oceanic Plateaus Basalts (Pearce et al., 2021). Their trace element profiles are typically flat, characterized by low Th concentrations (Fig. 3.6c, d).

Table 3.2 Geochemical groups in the Stoughton-Roquemaure assemblage

Geochemical group	***Percentage of samples***
Ultramafic compositions (3.6%)	
Komatiites	1.0
Komatiitic basalts	2.6
Mafic to intermediate compositions (86.5%)	
Tholeiitic basalts	37.1
Tholeiitic intermediate	0.5
Medium-Th basalts	8.1
High-Th basalts	19.1
Low-Zr basalts	0.4
Transitional intermediate	4.2
Calc-alkaline intermediate	17.1
Felsic compositions (9.9%)	
Transitional felsic	0.7
High-Yb rhyolites	0.5
Low-Yb Rhyolites	6.3
Calc-alkaline felsic	2.4
Total	100

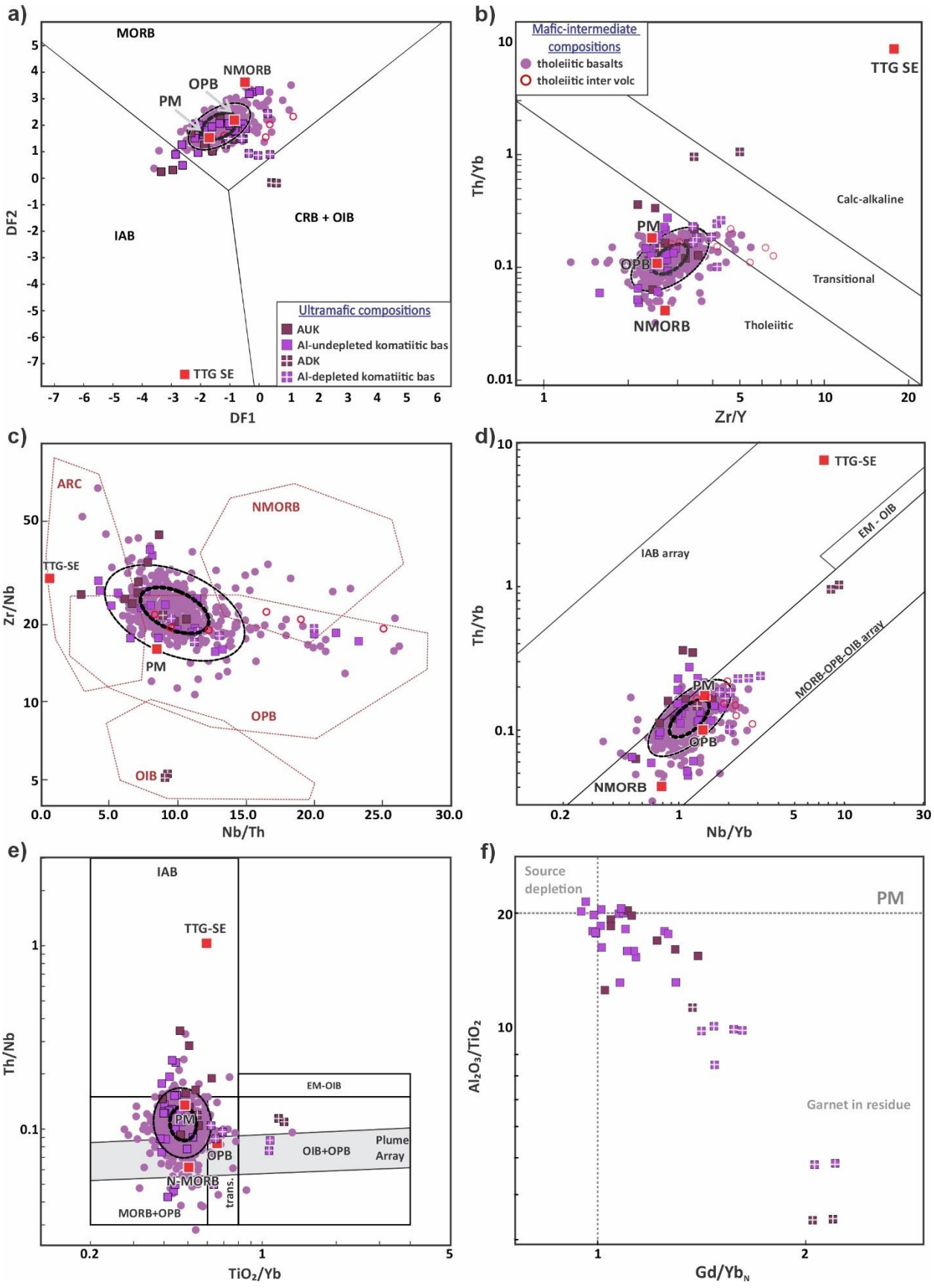
a)
MORB
NMORB
OPB
PM
IAB
CRB + OIB
Ultramafic compositions
AUK
Al-undepleted komatiitic bas
ADK
Al-depleted komatiitic bas
TTG SE
DF2
DF1
b)
Mafic-intermediate compositions
tholeiitic basalts
tholeiitic inter volc
TTG SE
Calc-alkaline
Transitional
Tholeiitic
PM
OPB
NMORB
Th/Yb
Zr/Y
c)
ARC
NMORB
TTG-SE
PM
OPB
OIB
Zr/Nb
Nb/Th
d)
TTG-SE
IAB array
EM - OIB
MORB-OPB-OIB array
PM
OPB
NMORB
Th/Yb
Nb/Yb
e)
IAB
TTG-SE
EM-OIB
PM
OPB
OIB+OPB
Plume Array
N-MORB
trans.
MORB+OPB
Th/Nb
TiO2/Yb
f)
Source depletion
PM
Garnet in residue
Al2O3/TiO2
Gd/YbN

Figure 3.5 (previous page) Trace element diagrams for tholeiitic affinity rocks, including komatiites, komatiitic basalts, tholeiitic basalts, and tholeiitic intermediate rocks. (a) DF1 vs DF2 diagram from Agrawal et al. (2008) using DF1 = 1.7517 $\log_e$ (Sm/Th) – 1.9508 $\log_e$ (Yb/Th) + 1.9573 $\log_e$ (Nb/Th) – 5.0928; DF2 = –2.2412 $\log_e$ (Sm/Th) + 2.2060 $\log_e$ (Yb/Th) + 1.2481 $\log_e$ (Nb/Th) – 0.8243. MORB: mid-ocean ridge basalt, IAB: island-arc basalt, CRB: continental-rift basalt, OIB: oceanic island basalt. Red squares show the following averages: normal MORB and primitive mantle (PM) from Sun and McDonough (1989), Oceanic plateau basalts (OPB) from Pearce et al. (2021) and SE Superior Province TTG from Mole et al. (2021). (b) Zr/Y vs Th/Yb diagram of Ross and Bédard (2009). (c) Zr/Nb vs Nb/Th after Condie (2005). ARC: active margin (Arc) compositions, other abbreviations as above. (d) Th/Yb vs Nb/Yb diagram of Pearce et al. (2021). EM is enriched mantle, other abbreviations as above. (e) Th/Nb vs TiO_2/Yb. Pearce et al. (2021). (f) Al_2O_3 /TiO_2 vs Gd/Yb_N (normalized to Primitive Mantle).

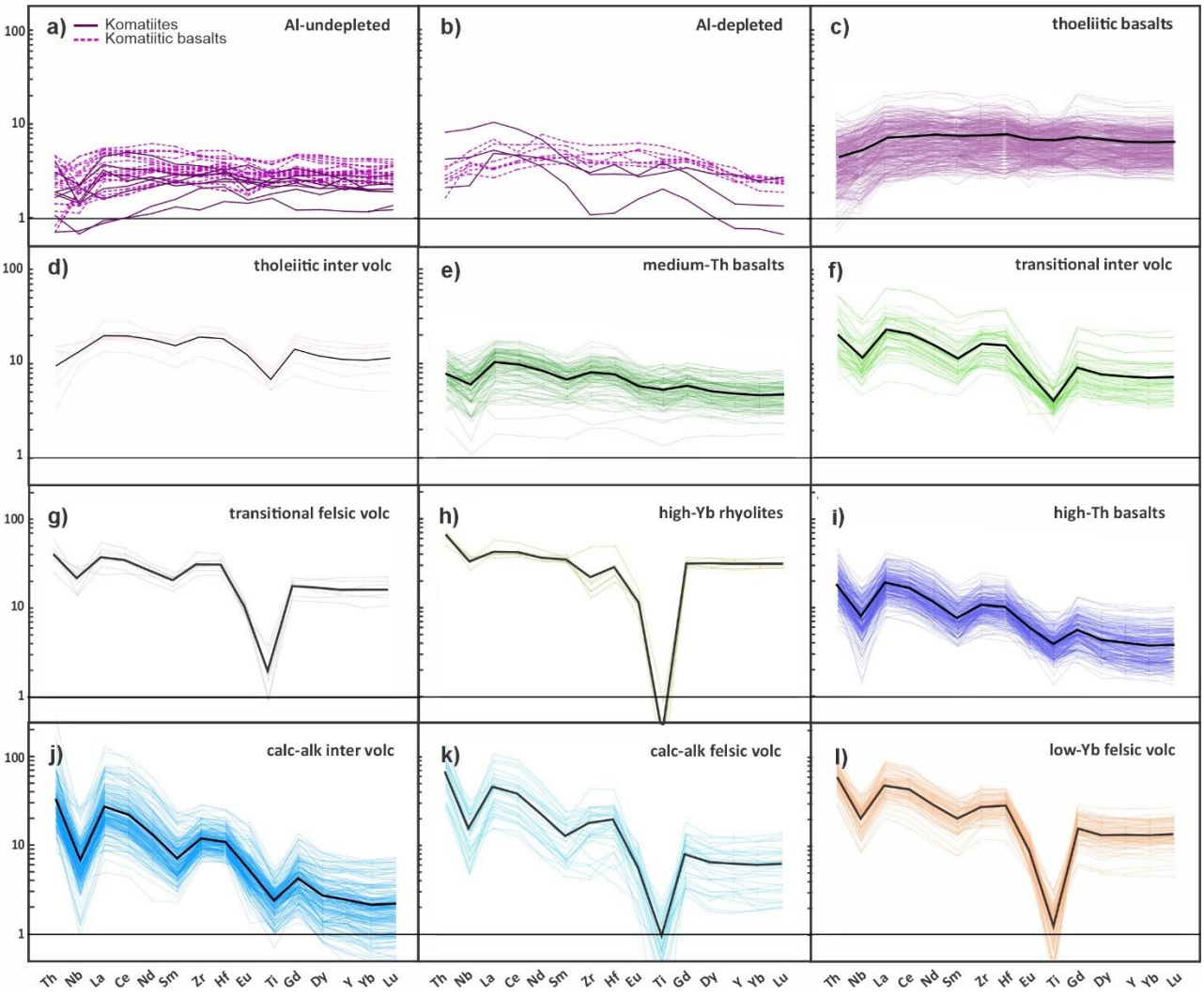

Figure 3.6 Extended trace element profiles for geochemical groups in the S-R assemblage (a-l), normalized to Primitive Mantle (Sun and McDonough, 1989). Black lines indicate group averages.

3.5.4 Transitional affinity

Medium-Th basalts and transitional intermediate volcanic rocks exhibit moderate LREE fractionation, moderate negative Nb anomalies, and slightly higher Th concentrations (Fig. 3.6e,

f). These groups occupy the transitional zones between tholeiitic-dominated and calc-alkaline-dominated fields. For instance, between MORB and Island Arc basalts (Agrawal, 2008; Fig. 3.7a), between the Oceanic Plateau Basalts and arc basalts (Condie, 2005; Fig. 3.7c) or between the mantle array and the island-arc array (Pearce et al., 2021; Fig. 3.7d, e).

Transitional felsic volcanic rocks exhibit higher trace element concentrations than their mafic to intermediate counterparts, except for Ti, with high-Yb rhyolites displaying even higher concentrations (Fig. 3.6g, h). Transitional felsic samples mostly plot in the FIIIa field of Hart et al. (2004), whereas high-Yb rhyolites plot outside defined fields with FIV-like La/Yb_N ratios and FIIIb-like Yb_N values (Fig. 3.7f).

3.5.1 Calc-alkaline affinity

High-Th basalts and calc-alkaline intermediate volcanic rocks align predominantly along island-arc or arc arrays in various diagrams (Fig. 3.7a, c, d, e). Their extended trace element patterns exhibit fractionated REE profiles, elevated Th concentrations, and pronounced negative Nb anomalies (Fig. 3.6i, j).

Low-Yb felsic rocks plot mostly in the FIIIa field of Hart et al. (2004), while calc-alkaline felsic rocks extend into the FII and FI fields (Fig. 3.7f). Their fractionated REE profiles exhibit moderate to high Th enrichment and negative Nb anomalies (Fig. 3.6k, l).

3.5.2 Geographic distribution of geochemical groups

Tholeiitic basalts predominate in many areas of the S-R assemblage (Fig. 3.8a). The following stratigraphic units are dominated by tholeiitic basalts: S-R, Catherine and the Vanier-Dalet-Poirier groups as well as Clermont-Disson and Bruneau formations (Fig. 3.8b). Komatiitic samples, including komatiitic basalts, are particularly abundant in the S-R Group, forming a distinct NNW-SSE distribution; some are also found in the Vanier-Dalet-Poirier Group and the Catherine Group.

Transitional to calc-alkaline magmatic affinities are most prevalent in the northern part of the S-R assemblage and near Cochrane in Ontario (Fig. 3.8a). The Dussieux Formation provides a good example, as its rocks display signatures that are almost entirely calc-alkaline (Figs 3.8a, b).

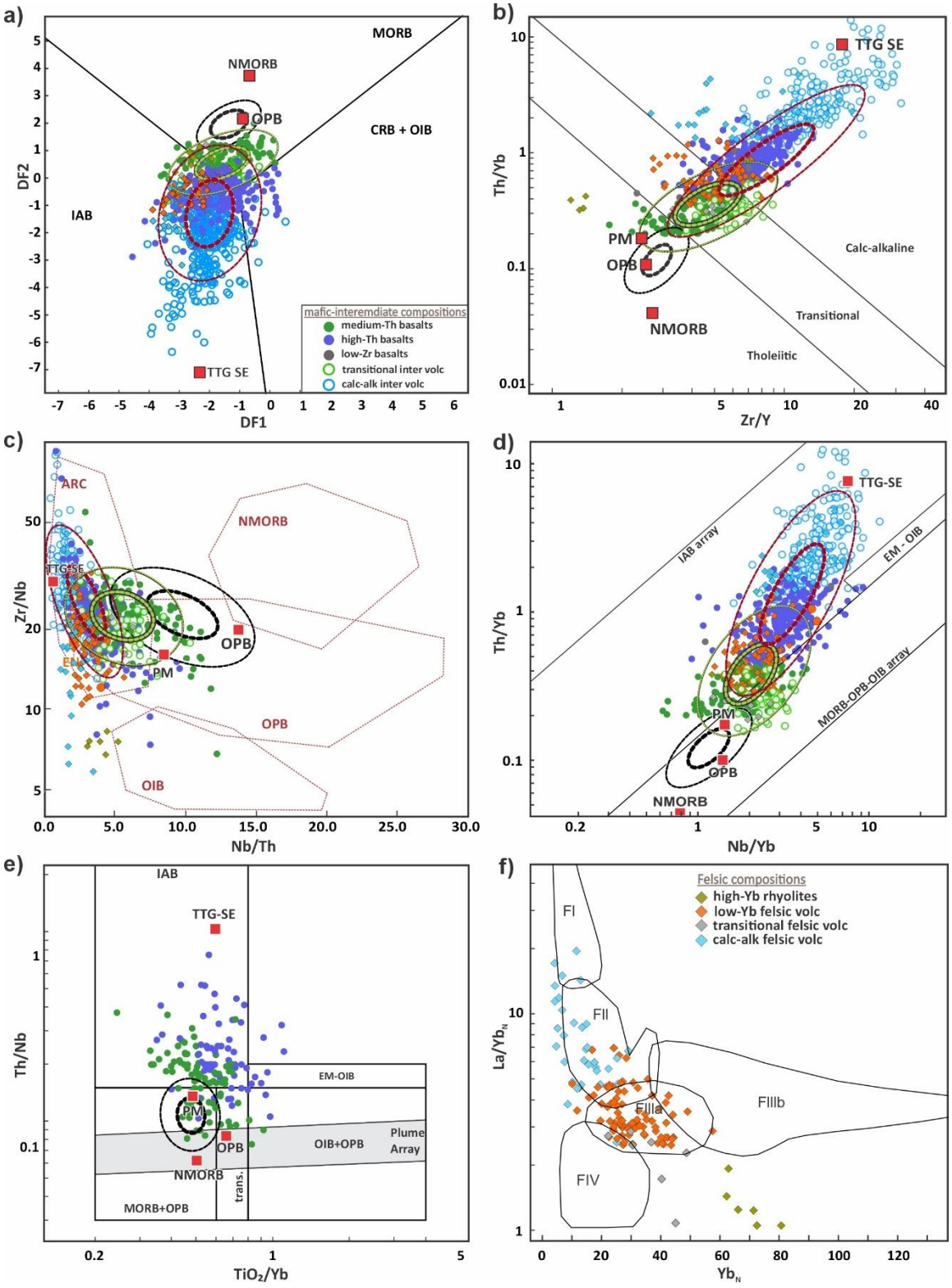

Figure 3.7 Trace element diagrams for transitional to calc-alkaline geochemical groups. (a) DF1 vs. DF2 (Agrawal et al., 2008; see Fig. 3.5). (b) Zr/Y vs. Th/Yb (Ross and Bédard, 2009). (c) Zr/Nb vs. Nb/Th (Condie, 2005; see Fig. 3.5). (d) Th/Yb vs. Nb/Yb (Pearce et al., 2021). (e) Th/Nb vs. TiO_2/Yb (Pearce et al., 2021). (f) La/Yb^N vs. Yb^N for felsic rocks (Hart et al., 2004).

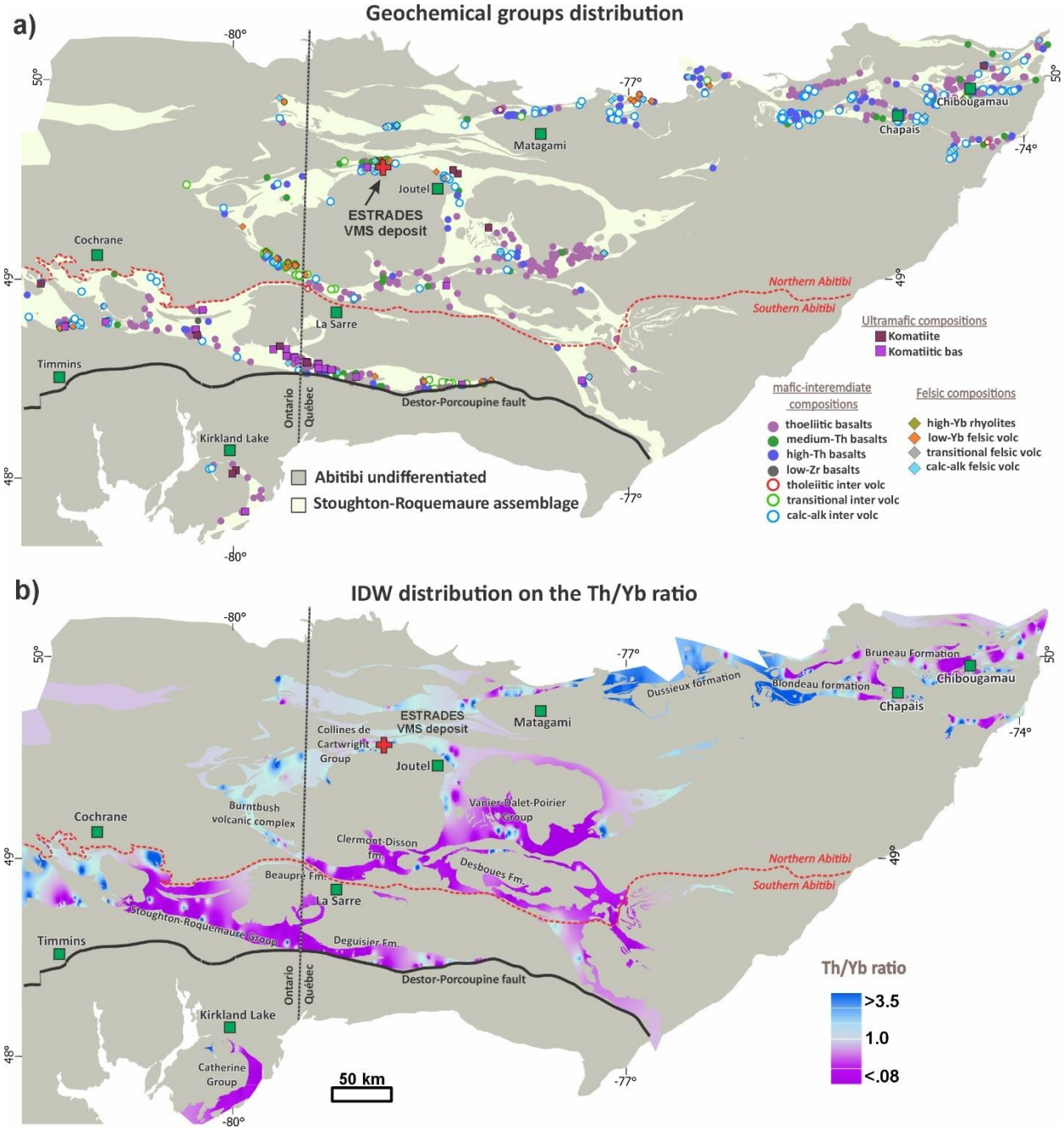

Figure 3.8 Geographic distribution of S-R geochemical groups. (a) Individual samples. (b) Inverse distance weighting (IDW) distribution on the Th/Yb ratio from whole-rock analysis. Map projection: Lambert Conformal Conic. Datum: North American 1983 CSRS. Coordinate system: Lat-Lon.

3.5.3 Primary magmas

Primary magmas were successfully calculated for 25 of the 69 samples considered. The rest of the 69 were predominantly flagged as having a 'pyroxenite source', with a few identified as 'volatile peridotite source'.

The composition of the primary magmas in terms of MgO, FeO and Al_2O_3, together with their mantle potential temperature (T_P), as calculated with PRIMELT3, broadly reveal two clusters of calculated primary magmas (Fig. 3.9). The first cluster, primarily associated with Al-depleted komatiites samples (ADK) with a few komatiitic basalts and basalts, yields primary magmas with an average composition of 23.8 ± 1.4 (2σ) wt.% MgO and an average T_P of 1658 ± 33°C (2σ). The second cluster corresponds to Al-undepleted komatiites (AUK) and most komatiitic basalts and tholeiitic basalts, with primary magmas averaging 20.1 ± 1.4 (2σ) wt.% MgO and a T_P of 1565 ± 87°C (2σ). All primary magmas calculated share a similar magnesium number of 92.1 ± 0.8.

3.5.3.1 Olivine line of control for primary magmas

Two primary magmas were selected to construct liquid lines of descent (LLDs) in MCS at 0.15 GPa under anhydrous conditions. These magmas correspond to samples from the S-R Group, as analyzed by Dostal and Mueller (2013). They are representative of the average compositions of the AUK and ADK clusters described earlier. This approach provides an alternative framework for analyzing the phase equilibria of the calculated primary magmas using the thermodynamic database from MELTS (Ghiorso and Sack, 1995; Ghiorso et al., 2002; Gualda et al., 2012) that the MCS uses. PRIMELT3, in contrast, calculates the primary composition by incrementally adding olivine to mantle-derived compositions.

The results indicate that the LLDs crystallize olivine until ~13 wt% MgO, after which orthopyroxene and plagioclase begin to crystallize. These LLDs closely align with observed sample compositions, depending on whether they originate from ADK or AUK sources. The AUK LLD's show higher Al_2O_3 and lower FeO compared to ADK and most of the S-R ultramafic samples follow this trend. In general, komatiitic compositions remain close to their primary magmas and require ~20% olivine removal from a calculated primary magma with 20 wt% MgO to reach basaltic compositions, according to MCS calculations (Fig. 3.9a, b).

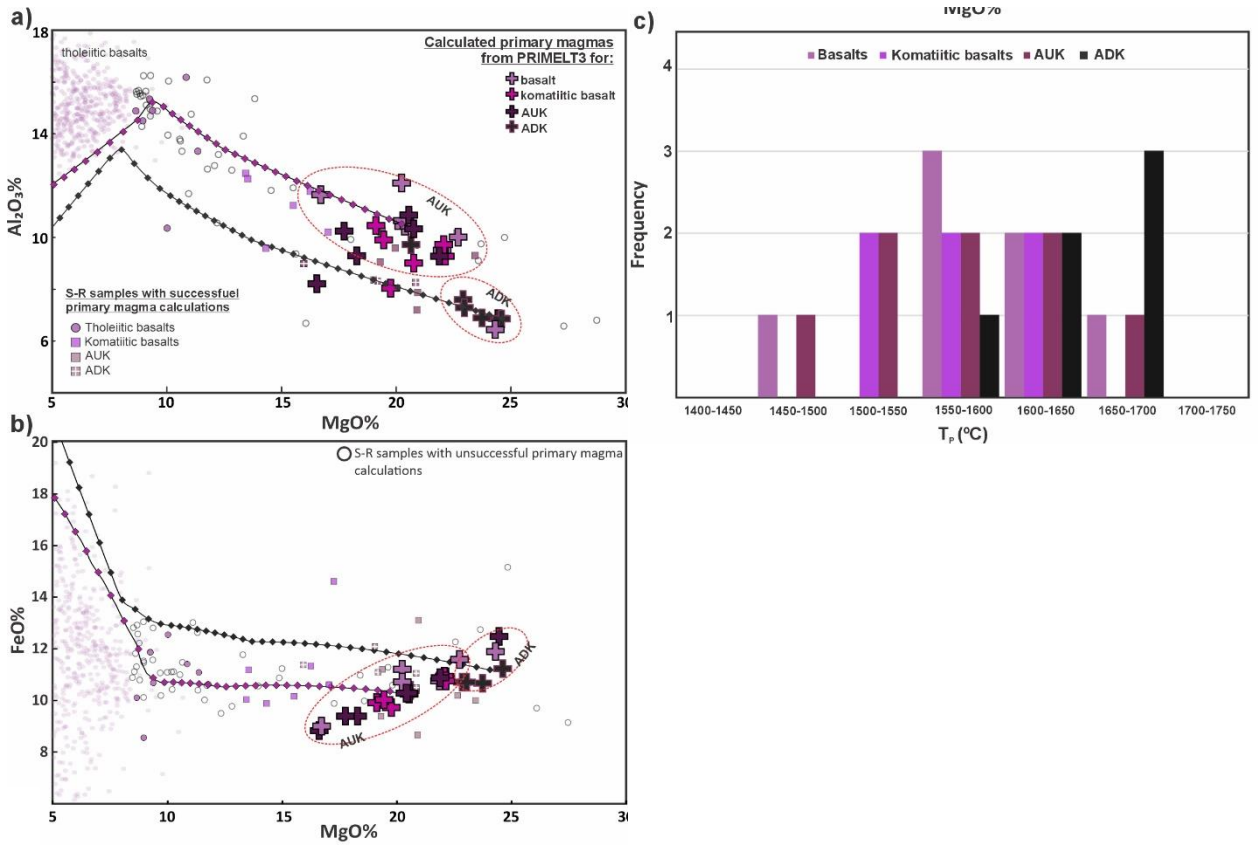

Figure 3.9 Composition and mantle potential temperature of primary magmas. (a–b) MgO, Al_2O_3, and FeO contents of primary magmas derived from mafic to ultramafic compositions (crosses), with liquid lines of descent (LLD) for AUK (purple diamonds) and ADK (black diamonds)) based on representative S-R samples (Roq 95-15 and Roq 95-17 from Dostal and Mueller, 2013). (c) Summary of calculated mantle potential temperatures (TP) for primary magmas, classified by their source compositions

3.5.4 Fractional crystallization models (major elements)

FC models attempt to explain the range of tholeiitic basalt behaviours starting with a single magma source at 11.3 wt. % MgO. In the 0.1% dissolved water content models at 0.15 and 0.3 GPa (Fig. 3.10a, b, c, d), corresponding to upper crustal conditions (~6-12 km), Fe-Ti enrichment and declining Al_2O_3 concentrations develop as MgO decreases. Those models approximately bracket the upper range of Fe-Ti enrichment and the lower range of Al_2O_3 concentrations in the tholeiitic basalt samples. Initially, at high temperatures, olivine forms, although plagioclase and clinopyroxene soon dominate the crystallizing phases (Fig. 3.10e, f). At ~3.5 wt% MgO when Fe-Ti is saturated the magma precipitates oxides.

In contrast, FC models with 1.0% water at the same low pressures largely suppress Fe-Ti enrichment and yield higher Al_2O_3 concentrations. The former effect is due to olivine fractionation, and the latter to delayed plagioclase formation. This behaviour is consistent with hydrated magmas (e.g., Sisson and Grove, 1993; Zimmer et al., 2010) (Figs. 3.10a, e, f).

Generally similar LLD behaviours are observed at 0.6 GPa (~18 km, middle crust). The 0.1% water model still shows Fe-Ti enrichment, but plagioclase starts to crystalize only at about 6% MgO, so it does not bracket the lowest Al_2O_3 contents on figure 3.10c like the lower pressure models do. The 1% H_2O, 0.6 GPa model creates even higher Al_2O_3 contents since clinopyroxene is enhanced while plagioclase formation is delayed. Also, the 1.0% water models produce liquids richer in silica as MgO decreases for the 0.15, 0.3 and 0.6 GPa pressures.

At higher pressures (1 and 2 GPa, ~34-64 km, lower crust to mantle depths), significant garnet formation occurs, up to 23% of the mass fraction in the 1.0 GPa models and up to 38% in the 2.0 GPa, similar for both water contents (Fig. 3.10h, i). The Ti inflection points of the tholeiitic basalts are completely missed by the 0.1% water models at these high pressures, and the Al_2O_3 contents are much higher in the models than in most tholeiitic basalt samples for a certain MgO content (>4% MgO).

3.5.5 Assimilation-fractional crystallization (AFC) models (major elements)

Since the FC models at 0.3 and 0.6 GPa with 0.1-1% dissolved water bracketed the tholeiitic basalt compositions reasonably well in terms of TiO_2, Al_2O_2 and MgO, we use the same conditions for the AFC models. These models indicate that a tholeiitic basalt magma can assimilate 23% (0.3 GPa) to 32% (0.6 GPa) of TTG wall rock. In the 0.1% H_2O model, assimilation initiates when the system is at ~3.5 wt% MgO for 0.3 GPa, while at 0.6 GPa, it begins at ~8 wt% MgO (Fig. 3.11a). Except for the 0.1% water model at 0.3 Gpa, Fe-Ti depletions are observed for the LLD's in the AFC models (Fig. 3.11a, b). These AFC models better explain the $Fe_2O_3^t$ and SiO_2 contents of the transitional and calc-alkaline groups and allow higher Al_2O_3 concentrations at the same pressures (Fig. 3.11c).

3.5.6 Mixing models (major elements)

The 4:1 mixing model, where the mafic magma dominates, yields basaltic andesite compositions with ~52% SiO_2 and 6.9% MgO (Fig. 3.11d). The 1:1 model generates an andesitic magma with ~58 wt% SiO_2 and 3.8 wt% MgO (Fig. 3.11d). The 1:4 mixing model, where the TTG melt is dominant, results in an andesitic composition around 62% SiO_2 and 2 wt% MgO. Subsequent fractional crystallization of the resulting mixture exhibits no moderate Al_2O_3 contents and no Fe-Ti enrichments (Fig. 3.11c).

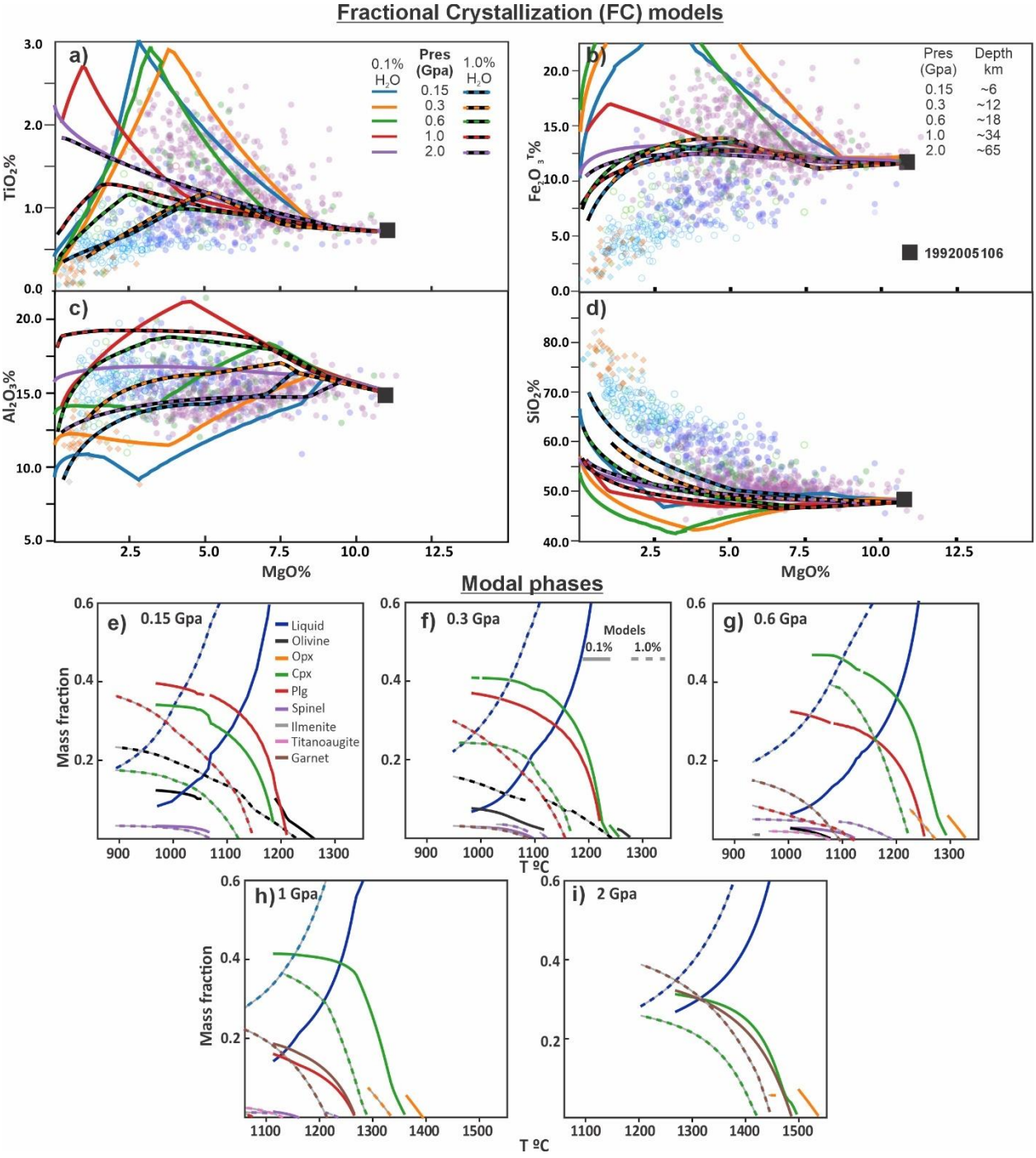

Figure 3.10 Fractional crystallization (FC) models. (a–d) LLD models for sample 1992005106 at two water concentrations (0.1% and 1.0% H_2O) and varying pressures (0.15, 0.3, 0.6, 1, 2 GPa), plotted as TiO_2, Al_2O_3, $Fe_2O_3^T$, and SiO_2 vs. MgO. (e–i) Mass fraction of phases in the LLD models corresponding to (a–d). Depth estimations from Sun et al. (2021).

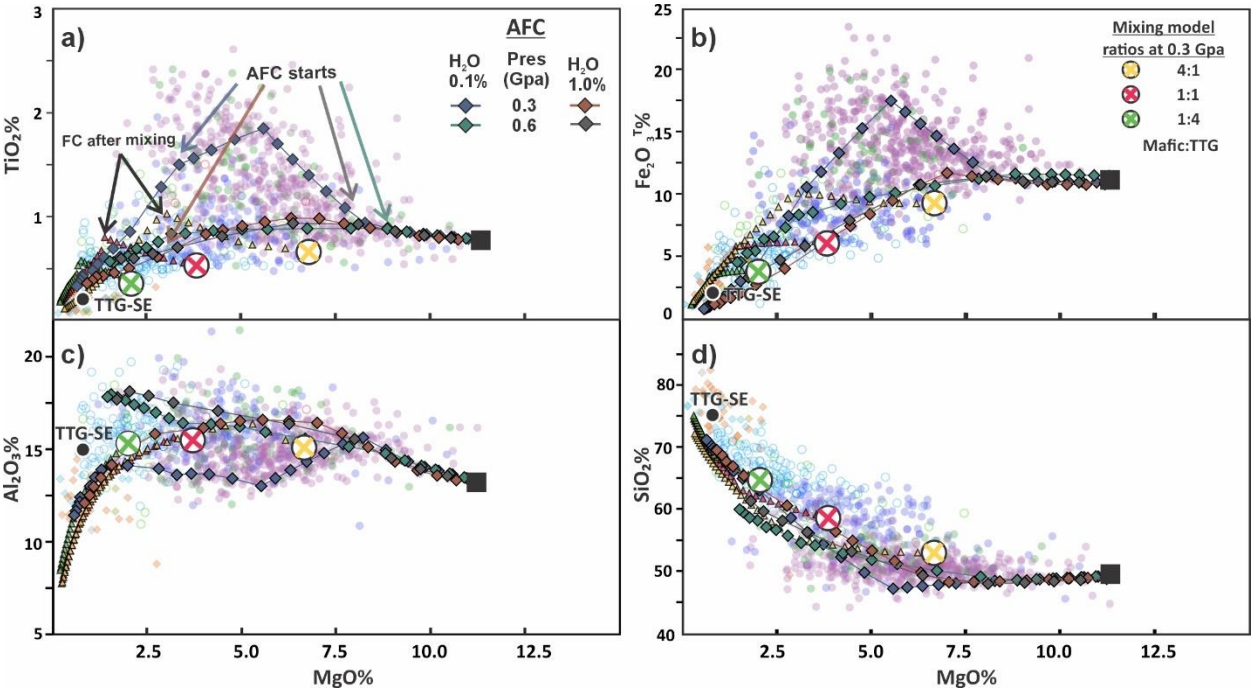

Figure 3.11 AFC and magma mixing models (a-d) displayed in TiO2, Al2O3, Fe2O3T, SiO2 versus MgO diagrams (see text).

3.5.7 Trace element behaviour of FC, AFC and mixing models

We looked at some of the same petrogenetic models from a trace element perspective (Fig. 3.12). Using the FC model with 0.1% water and 0.15 Gpa pressure as an example, reaching the right edge of the tholeiitic basalt field on figure 3.12a requires forming and separating ~76% crystals (5.4% ol, 41.2% cpx, 28.3% plg, 2.1% spn) leaving 24% liquid remaining. Reaching the most evolved tholeiitic intermediate sample requires another ~7% crystallisation relative to the original magma mass.

The trace element behaviour of AFC models shows enrichment in Th and LREE as assimilation begins. This causes the models to progressively evolve from tholeiitic basalts to calc-alkaline felsic compositions, crossing most of the other groups but missing the lower Th/Yb felsic groups in the Th/Yb vs Zr/Ti diagram (Fig. 3.12a). The AFC models evolve from tholeiitic affinities to calc-alkaline affinities in the Ross and Bedard (2009) diagram (Fig. 3.12b) and shift from the mantle array to the island arc basalt field in the Pearce et al. (2021) diagrams (Fig. 3.12c, d). A comparison of extended trace element profiles based on the 0.1% water AFC model at 0.6 Gpa shows that ~4% assimilation generates a similar profile to the average medium-Th basalts, whereas ~16 % and 27% assimilation generates high-Th basalts and intermediate calc-alkaline groups, respectively (Fig. 3.12e, f)

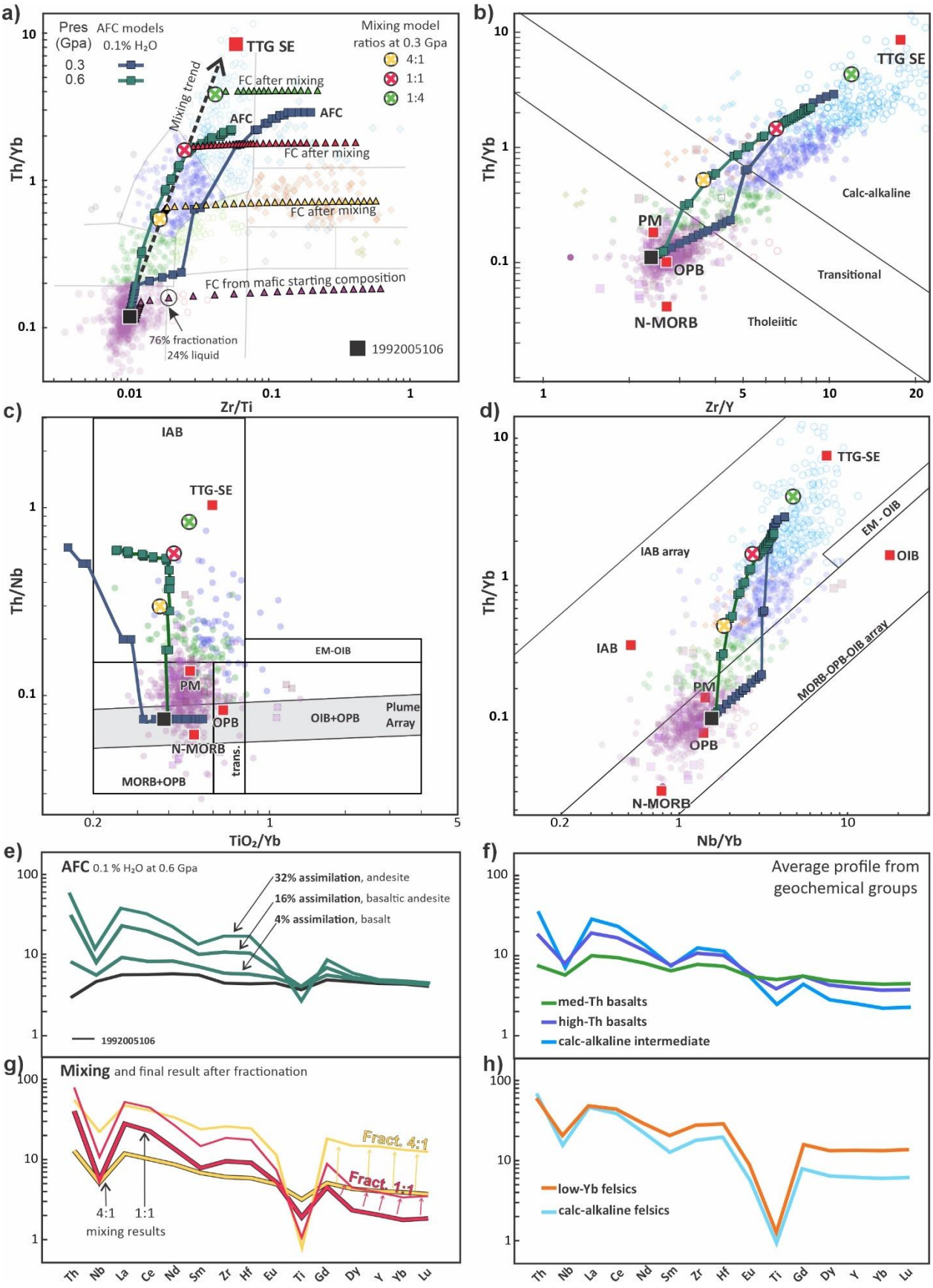
a)
Pres (Gpa)
AFC models 0.1% H2O
0.3
0.6
Mixing model ratios at 0.3 Gpa
4:1
1:1
1:4
TTG SE
Mixing trend
FC after mixing
AFC
AFC
FC after mixing
FC after mixing
FC from mafic starting composition
76% fractionation
24% liquid
1992005106
Th/Yb
Zr/Ti
b)
TTG SE
Calc-alkaline
PM
OPB
Transitional
N-MORB
Tholeiitic
Th/Yb
Zr/Y
c)
IAB
TTG-SE
EM-OIB
PM
OPB
OIB+OPB
Plume Array
N-MORB
trans.
MORB+OPB
Th/Nb
TiO2/Yb
d)
TTG-SE
IAB array
EM - OIB
OIB
IAB
PM
OPB
MORB-OPB-OIB array
N-MORB
Th/Yb
Nb/Yb
e)
AFC 0.1 % H2O at 0.6 Gpa
32% assimilation, andesite
16% assimilation, basaltic andesite
4% assimilation, basalt
1992005106
f)
Average profile from geochemical groups
med-Th basalts
high-Th basalts
calc-alkaline intermediate
g)
Mixing and final result after fractionation
Fract. 4:1
Fract. 1:1
4:1
1:1
mixing results
Th Nb La Ce Nd Sm Zr Hf Eu Ti Gd Dy Y Yb Lu
h)
low-Yb felsics
calc-alkaline felsics
Th Nb La Ce Nd Sm Zr Hf Eu Ti Gd Dy Y Yb Lu

Figure 3.12 (previous page) Various petrogenetic models in trace element space. (a-d) AFC (0.1% H_2O) and mixing models across different trace element diagrams. A simple FC model is also shown in (a) for tholeiitic basalts (0.1% H_2O at 0.15 GPa, purple triangles), as well as FC starting from various mixed magmas (yellow, red and green triangles). (e, g) Different model outputs in extended trace element diagrams. (f, h) Average extended trace element profiles for selected geochemical groups.

The mixing models in the 4:1 scenario produce compositions that fall between the boundaries of the medium-Th and high-Th groups, while the 1:1 mixing scenario yields a composition in the upper limit of high-Th basalts (Fig 3.12a, g). Further fractional crystallization of these mixed magmas as exemplified in the Zr/Ti vs Th/Yb diagram (Fig. 3.12a) produces low-Yb felsic compositions that are also similar comparing their extended trace element diagram (Fig. 3.12g, h).

3.6 Discussion

The S-R assemblage is the most voluminous volcanic assemblage in the Abitibi greenstone belt by surface area (16 000 km^2 or ~34% of the volcanic coverage) with the faster emplacement time (~3 m.y.). Traditionally, the understanding of this assemblage has centered on zones like the S-R group (Fig. 3.8), recognized for its classic komatiite-tholeiite association often linked to mantle plume activity in the literature (e.g., Dostal and Mueller, 1997; 2013; Sproule et al., 2002; Thurston, 2015). However, extending the geochemical compilation to the entire assemblage reveals that, although tholeiitic basalts dominate and komatiitic rocks are present, transitional to calc-alkaline affinities were produced during the same magmatic event, revealing a greater complexity than anticipated (Table 3.2; Figs. 3.3, 3.8).

The injection of hot, mantle-derived basalts into pre-existing TTG-like crust produces complex magmatic systems. These systems account for much of the geochemical variability in the S-R assemblage, particularly among samples with transitional to calc-alkaline affinities, where processes such as assimilation-fractional-crystallization might have occurred. Alternatively, the coexistence of TTG magmatism during S-R emplacement may have facilitated direct magma mixing with mantle-derived magmas.

3.6.1 Mantle thermal state and voluminous magmatism

The large-scale and rapid emplacement of the S-R assemblage suggests a highly efficient mechanism for magma production and delivery to the crust. Several factors likely contributed to this efficiency, including elevated mantle potential temperatures (T_P), prolonged decompression,

and the presence of volatiles (H_2O, CO_2) in the mantle source (Sobolev et al., 2011; Xie et al., 2016). Understanding the interplay of these factors is key to explaining the S-R magmatic events.

Evidence for high mantle temperatures in the Abitibi greenstone belt comes from komatiites, reported in the earlier Pacaud (2750–2735 Ma) and Deloro (2734–2724 Ma) assemblages, as well as the subsequent Kidd-Munro (2720–2710 Ma) and Tisdale (2710–2704 Ma) assemblages (Houlé et al., 2017). However, detailed T_P calculations have only been presented for the Alexo and Pyke Hill komatiites, which are part of the Kidd-Munro assemblage. Arndt (1986) initially proposed a primary magma with 28.2% MgO (Mg# of 94.1) modeled by adding 1% olivine (Fig. 3.13a, b). Later, Sobolev et al. (2016) used olivine inclusions to obtain a primary magma with 30% MgO (Mg# of 94.7) and a T_P of 1730 ± 50°C (Fig. 3.13a, b). Recently, Herzberg (2022), using PRIMELT3, calculated a primary magma with 27.6% MgO (Mg# of 94.5) and a T_P of 1750 ± 42°C. Despite differences in method, these three Kidd-Munro assemblage estimates are broadly consistent, and comparable to T_P values from other Archean komatiite localities, such as Belingwe, Barberton, Yilgarn, and Pilbara, where temperatures ranged from 1740°C to 1900°C (Herzberg et al., 2010; Sossi et al., 2016; Herzberg, 2022). Our T_P estimates for S-R magmas are 100–150°C lower than those of the Alexo and Pyke Hill komatiites and correspond to less magnesian magmas (Fig. 3.13a, b). This suggests that a high mantle potential temperature is not the sole factor.

Decompression melting is one of the most influential factors in generating large magma volumes. In the S-R context, the presence of major tectonic structures, like the precursors to the Destor-Porcupine fault zone (Poulsen, 2017), along with evidence for a thinner crust in the central zones (Faure et al., 2011; Mole et al., 2021), would have significantly enhanced melt production by facilitating mantle ascent. It is possible that the center of the thermal anomaly was located within these structurally favorable zones, a hypothesis supported by our spatial geochemical analysis (see Section 3.5.6).

Furthermore, the presence of volatiles can substantially increase melt fractions. For instance, water reduces the mantle solidus temperature, which enhances melting during partial melting (e.g., Black et al., 2021; Herzberg, 2022). Sobolev et al. (2016) showed that the Kidd-Munro komatiites originated from a hydrated mantle source. Although direct water-content estimates for S-R volcanics are lacking, our models require the incorporation of reasonable H_2O concentrations to explain the major element variability in the tholeiitic basalts, indirectly suggesting the presence of volatiles in the S-R parental magmas.

Collectively, the voluminous magmatism of the S-R assemblage appears to be the result of a confluence of these factors. The temperature difference between the S-R magmas and the Kidd-Munro komatiites strongly suggests an evolving thermal anomaly beneath the Abitibi greenstone belt. This evolving history leads to two possible scenarios. In the first, a single, long-lived, belt-wide thermal anomaly was responsible for all of the Abitibi greenstone belt sub-alkaline volcanism, with its peak in magma production reached during the S-R timeframe before waning in subsequent assemblages (e.g., Dostal and Mueller, 2013). Alternatively, if distinct thermal anomalies drove each assemblage's emplacement (e.g., Sproule et al., 2002), conditions during the S-R event were uniquely favorable for more voluminous volcanism.

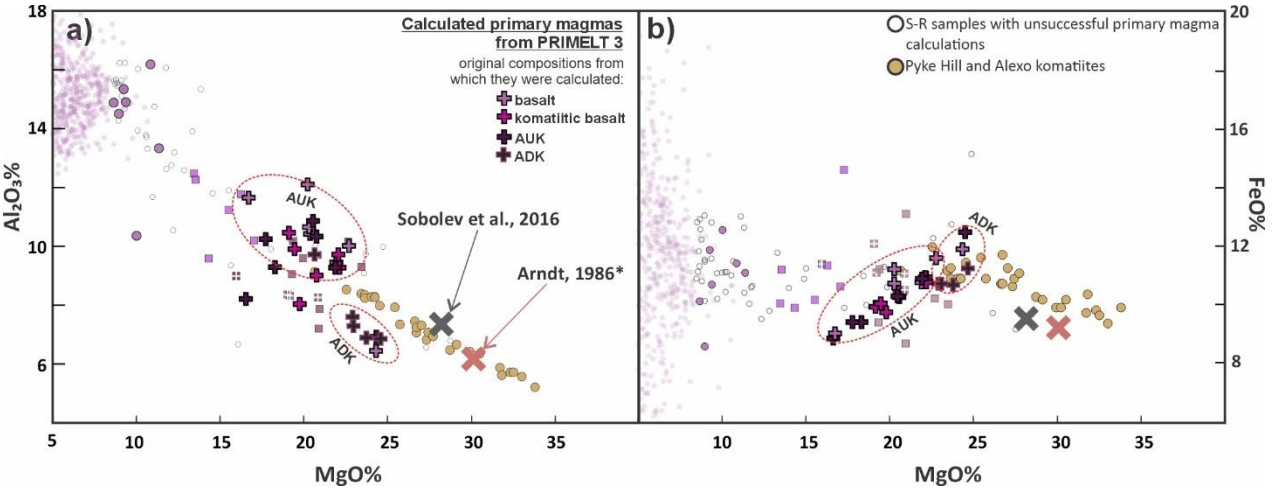

Figure 3.13 (a–b) MgO, Al_2O_3, and FeO contents of S-R primary magmas compared with primary magma calculations for the Pyke Hill and Alexo komatiites (marked with 'X'). Komatiites compositions (yellow circles) from Puchtel et al. (2009). *Primary magma calculations based on Arndt (1986), which suggest that adjusting to Mg# 94.5 would approximate the sample to primary magma composition. In this study, primary magma was calculated using the olivine addition method in PRIMELT3.

3.6.2 Magmatic processes in the crust

3.6.2.1 Fractional crystallization (FC) in tholeiitic basalts

Petrogenetic modeling indicates that fractional crystallization (FC) played a significant role in the evolution of S-R tholeiitic magmas under varying pressures and water contents. Models using a single starting composition with 0.1% and 1.0% water content at 0.15 to 0.6 GPa reveal distinct trends: strong Fe-Ti enrichment (Fig. 3.10a, b) and lower Al_2O_3 (Fig. 3.10c) concentrations are associated with low-water magmas, whereas higher Al_2O_3 and suppressed Fe-Ti enrichment

occur in more hydrated magmas. This behaviour, particularly in the 0.15 and 0.3 GPa models, is largely controlled by the fractionation of major phases (see section 3.5.8).

At higher pressures (>0.6 GPa), Al_2O_3 concentrations in low-water magmas are primarily controlled by clinopyroxene formation (Fig. 3.10e-f). Furthermore, under these conditions, the 1.0% water model stabilizes garnet, which becomes a major phase at 1–2 GPa. Garnet typically retains HREE, modifying the trace element profiles and affecting ratios such as TiO_2/Yb (Fig. 3.5e). This is not observed in tholeiitic basalts which, along with major oxide patterns, constrains the FC process under 0.6 GPa. In summary, mantle-derived precursor magmas for tholeiitic basalts spent some time crystallizing in the middle to upper crust, without significant contamination showing up in the trace element patterns at least from something like a TTG-like crust. While up to ~75% crystal fractionation is required to reach the right side of the tholeiitic basalt field (Fig. 3.12a), more extensive FC leading to intermediate or even felsic tholeiitic compositions was very rare within the S-R assemblage.

3.6.2.2 Assimilation-fractional crystallization (AFC)

Our AFC models explain Fe-Ti depletion patterns as MgO decreases (Fig. 3.11) and the 'main trend' linking tholeiitic basalts with calc-alkaline intermediate rocks in trace element space (Fig. 3.12a, b). This suggests that an initial tholeiitic magma could progressively acquire a calc-alkaline signature by assimilating increasing amounts of a TTG-like crust. TTG suites are normally hydrated intermediate to felsic magmas with some of them displaying high LREE and low HREE contents (e.g., Moyen and Martin, 2012), providing a suitable contaminant. At greater depths, where wall rock temperatures increase, assimilation occurs earlier in the system, allowing the magma to maintain its mafic character while displaying a calc-alkaline trace element pattern, as observed in the 0.6 GPa models (~600°C for the wall rock; Figs. 3.11, 3.12). Assimilating just 16% of the wall rock is sufficient to transform tholeiitic magmas into compositions resembling high-Th basalts (Fig. 3.12e, f).

The endmember product of the 0.3 GPa AFC model is a felsic composition (~70% SiO_2) with trace element signatures similar to the calc-alkaline felsic group in our classification (Fig. 3.12a). These compositions align with FI-FII rhyolites on the Hart et al. (2004) diagram (Fig. 3.7f), traditionally attributed to partial melts formed at depths of >30 km and >10 km, respectively. However, our models suggest such compositions can also result from evolved magmatic systems involving the assimilation of tholeiitic magma with TTG-like crust at mid- to upper-crustal depths, i.e. trace elements in felsic volcanic rocks cannot always be used to directly interpret the depth of melting.

3.6.2.3 Magma mixing

For simplicity, our models use an average TTG composition, since the TTG suite origin and evolution is the topic of ongoing research (e.g., Moyen and Laurent, 2018). Accordingly, our magma mixing models combine various proportions of tholeiitic basalt and TTG average melt. A key feature of these magma mixing models is a more significant gain in SiO_2 compared to AFC models, which better explains groups such as the calc-alkaline intermediate volcanic rocks (Fig. 3.11d, 3.12a, b, g). They also are generally as successful as the AFC models at explaining trace element patterns in the transitional to calc-alkaline groups, including felsic compositions when post-mixing FC is considered (Fig. 3.12). So instead of the TTG endmember being an older solid crust, it could also be a second magma, generated separately from the tholeiitic basalt endmember, and mixed with it *en route* to the surface. Intrusive equivalents of such felsic magmas are documented within the S-R assemblage, for example, the Joutel Complex of the Vanier–Dalet–Poirier Group (2721 ± 0.7 Ma; Legault et al., 2002). Numerous studies propose that TTG magmas originate from a mafic parental source, either via fractionation of hydrous basalts or partial melting of metabasalts. The latter process can be initiated by various geodynamic mechanisms, such as remelting at the base of a thick mafic crust or melting of a delaminated slab via dripduction. For a comprehensive review of the different models for TTG magmatic suite origin, see Moyen and Martin (2012) and Moyen and Laurent (2018).

3.6.3 Spatial variations

The spatial distribution of magma compositions within the S-R assemblage provides key insights into the crustal architecture that influenced the volcanic event. The central and southern zones are dominated by relatively uncontaminated tholeiitic compositions, and komatiites are most abundant here, particularly in west-east elongated formations around the Destor-Porcupine fault zone (e.g., the Stoughton-Roquemaure Group and the Deguisier Formation; Fig. 3.8). This geographic pattern provides strong evidence for the hypothesis presented in Section 5.1: that the thermal event was centered on this region, where pre-existing tectonic structures and thinner crust (Faure et al., 2011; Mole et al., 2021) provided a preferential pathway for the rapid ascent of mantle-derived magmas.

Alternatively, given the extensive FC required to explain the major element variations in tholeiitic rocks, the existing middle to upper crust in the central and southern zones may have had a different geochemical composition (less TTG-like) to that of other areas, so that possible contamination does not readily show up as high Th/Yb ratios and other typical features. Zircon

geochemical proxies further suggest that these central zones (including the Catherine Group, Fig. 3.8b) are characterized by juvenile crust generation, although this finding is not exclusively tied to the S-R timeframe (Mole et al., 2021).

The northern and northwestern regions of the S-R assemblage predominantly display transitional to calc-alkaline geochemical patterns (Fig. 3.8). These signatures are interpreted to reflect interaction with predominant older pre-existing crust, an interpretation supported by regional seismic surveys (Mathieu et al., 2020) and zircon geochemical proxies (Mole et al., 2021, 2022) indicating such crust in this northern area. While the same mantle thermal event probably drove volcanism across the greenstone belt at S-R time (Fig. 3.8), a predominant TTG-like crust in the north likely facilitated contamination. Nevertheless, the occurrence of predominantly tholeiitic units locally within this northern region, such as in the Bruneau formation near Chibougamau (Fig. 3.8), demonstrates that pathways for less contaminated, mantle-derived magmas also existed, implying variability in the extent of crustal interaction or magma ascent routes and/or variability in the composition of existing crust. Alternatively, the presence of the calc-alkaline intermediate group in the north could indicate mixing between a mantle-derived tholeiitic basalt magma and a TTG-like magma.

3.7 Conclusions

The Stoughton-Roquemaure (S-R) assemblage, representing the most voluminous magmatic pulse in the Abitibi greenstone belt, exemplifies the intricate nature of Archean volcanic systems. Our findings demonstrate that its petrogenetic history involved a multifaceted interplay of mantle-derived magmatism and extensive crustal processing. The presence of komatiites, komatiitic basalts, and voluminous tholeiitic basalts, associated with high mantle potential temperatures (T_P 1565 ± 87°C for AUK sources), reveal a significant thermal anomaly, likely plume-related, as the primary driver for S-R magmatism. This voluminous melt production was probably enhanced by lithospheric extension, facilitated by major existing tectonic structures, and potentially by mantle hydration.

Within the crust, S-R magmas underwent diverse evolutionary pathways. Fractional crystallization, primarily at mid- to upper-crustal levels (<0.6 GPa) and influenced by variable magma water contents, accounts for the major and trace element diversity within the tholeiitic basalts prominent in the central and southern regions. However, many S-R magmas, particularly in the northern regions, exhibit transitional to calc-alkaline characteristics. We attribute these signatures to a crustal input, either through (i) interaction with pre-existing TTG-like upper- to mid-

crust during assimilation-fractional crystallization (AFC) or (ii) mixing between a tholeiitic basalt magma and a second, TTG-like magma. These interactions were likely more pronounced in areas with more established crust, contrasting with the rapid ascent of seemingly uncontaminated magmas in central and southern zones.

This study highlights that the geochemical makeup of the S-R assemblage was shaped by the mantle source's thermal state, the regional tectonic framework, and the nature of the existing crust. These insights into the dynamic interplay between mantle-derived magmas and crustal processes contribute to a better understanding of Archean crustal growth and the evolution of Earth's early lithosphere.

3.8 Acknowledgements

We thank Taus Jorgensen for providing GIS data on the Abitibi greenstone belt.

4 BLAKE RIVER GROUP VS STOUGHTON-ROQUEMAURE

BLAKE RIVER GROUP VERSUS STOUGHTON-ROQUEMAURE ASSEMBLAGE : GEOCHEMICAL COMPARISON AND VMS IMPLICATIONS

4.1 Introduction

This chapter aims to compare the geochemical characteristics of the Stoughton-Roquemaure (S-R) assemblage and the Blake River Group (BRG) (Fig. 4.1), based largely on the information presented in chapters 2 and 3. These assemblages were selected for comparison because they represent contrasting extremes in volcanogenic massive sulfide (VMS) deposit endowment. Specifically, the S-R assemblage is among the least VMS-endowed packages, whereas the BRG forms the core of the Blake River assemblage, the most endowed assemblage of the belt.

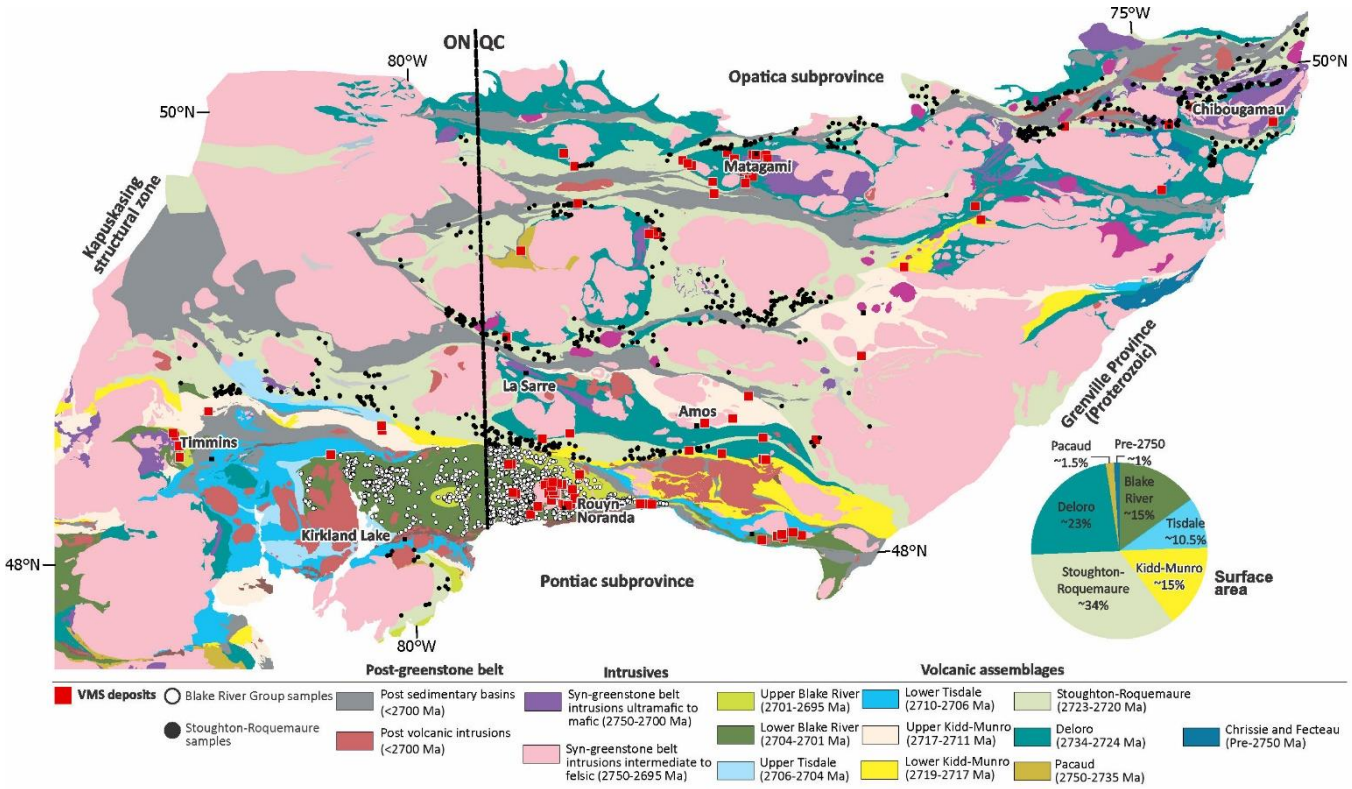

Figure 4.1 Volcanic assemblage map of the Abitibi greenstone belt. Each assemblage surface extent is indicated in the pie chart (modified from Jorgensen and Gibson, 2024).

As seen in chapter 1, Thurston (2015) distinguished two types of volcanic assemblages in greenstone belts, from a geochemical point of view. According to this framework, the Blake River assemblage is characterized by a bimodal (mafic-felsic) volcanic suite ranging from tholeiitic to calc-alkaline. Conversely, the S-R assemblage has traditionally been interpreted predominantly as a komatiite-tholeiite succession (Dostal and Mueller, 1997, 2013; Ayer et al., 2002). However, as documented in Chapter 3 (Vite-Sánchez et al., 2025), several formations within the S-R assemblage exhibit distinctively calc-alkaline geochemical signatures, pointing toward a more complex magmatic evolution than previously recognized. Additionally, the assemblages differ notably in their surface area extent, indirectly reflecting their respective magmatic volume. The S-R assemblage covers approximately 34% of the volcanic rocks in Abitibi belt, whereas the Blake River assemblage accounts for roughly 15% (Mercier-Langevin et al., 2023; Jorgensen and Gibson, 2024). Moreover, the S-R assemblage was emplaced over a relatively short geological timeframe of ~3 m.y., in contrast to the BRG assemblage, whose emplacement spanned ~9 m.y. (Ayer et al., 2002; Thurston et al., 2008).

Previous chapters thoroughly documented the geochemical variability within both the BRG the and S-R assemblage, establishing foundational geochemical groupings. Chapter 2 specifically laid the groundwork for a BRG geochemical classification system, which was subsequently applied to the S-R assemblage, excluding komatiites, in chapter 3. These chapters extensively describe the characteristics of the geochemical groups, although felsic groups from the BRG have not been described in chapter 2 and are therefore presented here.

This chapter highlights key geochemical differences between assemblages, examines the proportions of dominant geochemical groups, assesses their interrelationships, and explores their spatial association with VMS deposits. Ultimately, this comparative approach aims to elucidate petrological processes underlying geochemical variations and evaluate their potential influence on regional VMS fertility.

4.2 Classification of the volcanic rocks

4.2.1 Principal Component Analysis (PCA)

In Chapter 3, mafic to felsic volcanic rocks of the S-R assemblage were classified on a Zr/Ti vs Th/Yb diagram initially developed for the BRG rocks in chapter 2. Figure 4.2 illustrates that principal components 1 (PC1) and 2 (PC2) capture most of the variance in mafic to felsic rocks for both assemblages, accounting for approximately 70% and 19% respectively, similar in both

datasets. Although the vectors point in slightly different directions, the elements Ti, Th, and Yb exert the greatest influence on geochemical variability in both datasets (Fig. 4.2a, b), indicating that the Zr/Ti versus Th/Yb diagram is appropriate in classifying rock types in both assemblages.

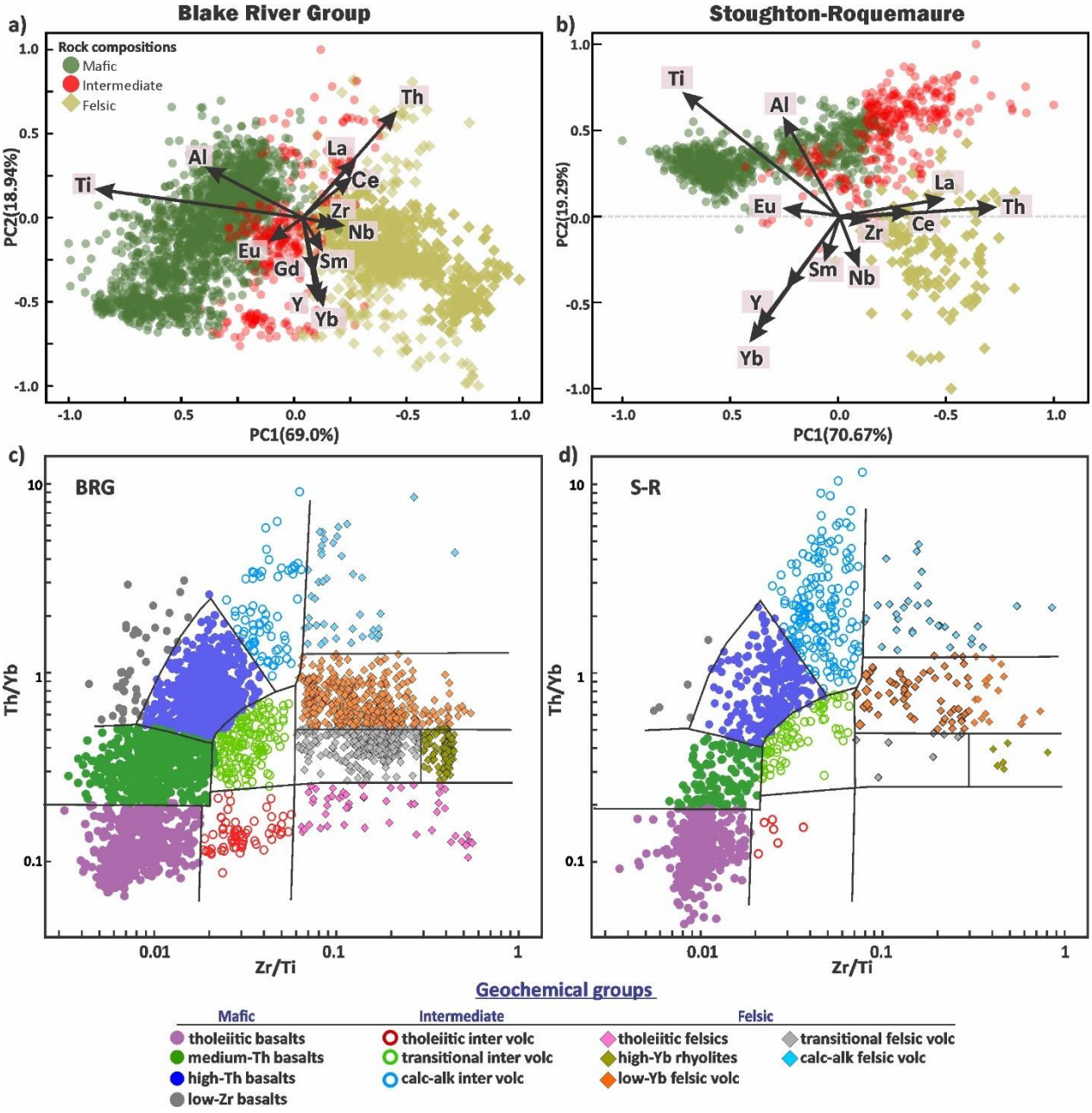

Figure 4.2 Principal Component Analysis for selected immobile elements and classification for the BRG and S-R. (a, b) Principal Component Analysis (PCA) applied to the BRG (a) and S-R (b) datasets using the same suite of elements. (c, d) Zr/Ti vs. Th/Yb classification diagram developed in Chapter 2 and applied to both datasets. In all four plots, all samples are shown except komatiites and komatiitic basalts.

In the BRG (Fig. 4.2a), Ti shows a strong positive alignment with the PC1 axis and exhibits an inverse relationship with Zr. This negative correlation between Ti and Zr is in agreement with

magma fractionation processes (Winchester and Floyd, 1977): mafic samples have negative PC1 and felsic samples have positive PC1 (Fig. 4.2a). PC2 primarily reflects the variability driven by Th and Yb. Specifically, Th correlates closely with light rare earth elements (LREE), whereas Yb correlates with heavy rare earth elements (HREE) and Y. Samples with the highest PC2 values exhibit distinct extended trace element signatures characterized by fractionated REE patterns, significant negative Nb anomalies, and calc-alkaline affinities (see below). Conversely, samples with the lowest PC2 values show unfractionated HREE profiles, minimal Nb anomalies, and tholeiitic signatures. In other words, PC2 – which can be approximated with Th/Yb – corresponds to magmatic affinity (Ross and Bédard, 2009) and crustal influence (Pearce, 2008).

For the S-R assemblage's mafic to felsic rocks, the most prominent elemental vectors again form three main groups pointing in distinct directions: Ti-Al, Th-LREE, Y-Yb (Fig. 4.2b). These vectors are however rotated clockwise by ~30-40° relative to the BRG ones. Again, for the S-R assemblage, Zr/Ti is a reasonable proxy for fractionation whereas Th/Yb represents magmatic affinity or crustal input (chapter 3), although these ratios don't directly correspond to PC1 and PC2, respectively, as they do for the BRG, because of the rotation of vectors.

4.2.2 The Zr/Ti vs Th/Yb diagram

Based on PCA results, mafic to felsic samples in both datasets are plotted on a Zr/Ti vs. Th/Yb (Fig. 4.2c, d), with the S-R komatiites being classified separately (Fig. 4.3a, b). These ratios are widely referenced in the literature (Winchester and Floyd, 1977 Pearce, 1996, 2008; Ross and Bédard, 2009; Pearce et al., 2021), but the specific configuration used here was first introduced in Chapter 2. The BRG geochemical group boundaries were initially guided by the diagrams from Pearce (1996) (Fig. 4.3c) and Ross and Bédard (2009) (Fig. 4.3e), then customized specifically for the BRG dataset based on clustering methodologies described in Chapter 2. The final validation involved extended trace element diagrams.

Instead of creating a different diagram optimized for the S-R assemblage (either using different elemental ratios or the same ones with different fields), the BRG Zr/Ti vs Th/Yb diagram was applied "as is" to the S-R assemblage in chapter 3, after developing the felsic part of the plot (Fig. 4.2d). Using similar fields allows for a direct comparison between the two datasets in terms of proportions of different geochemical groups.

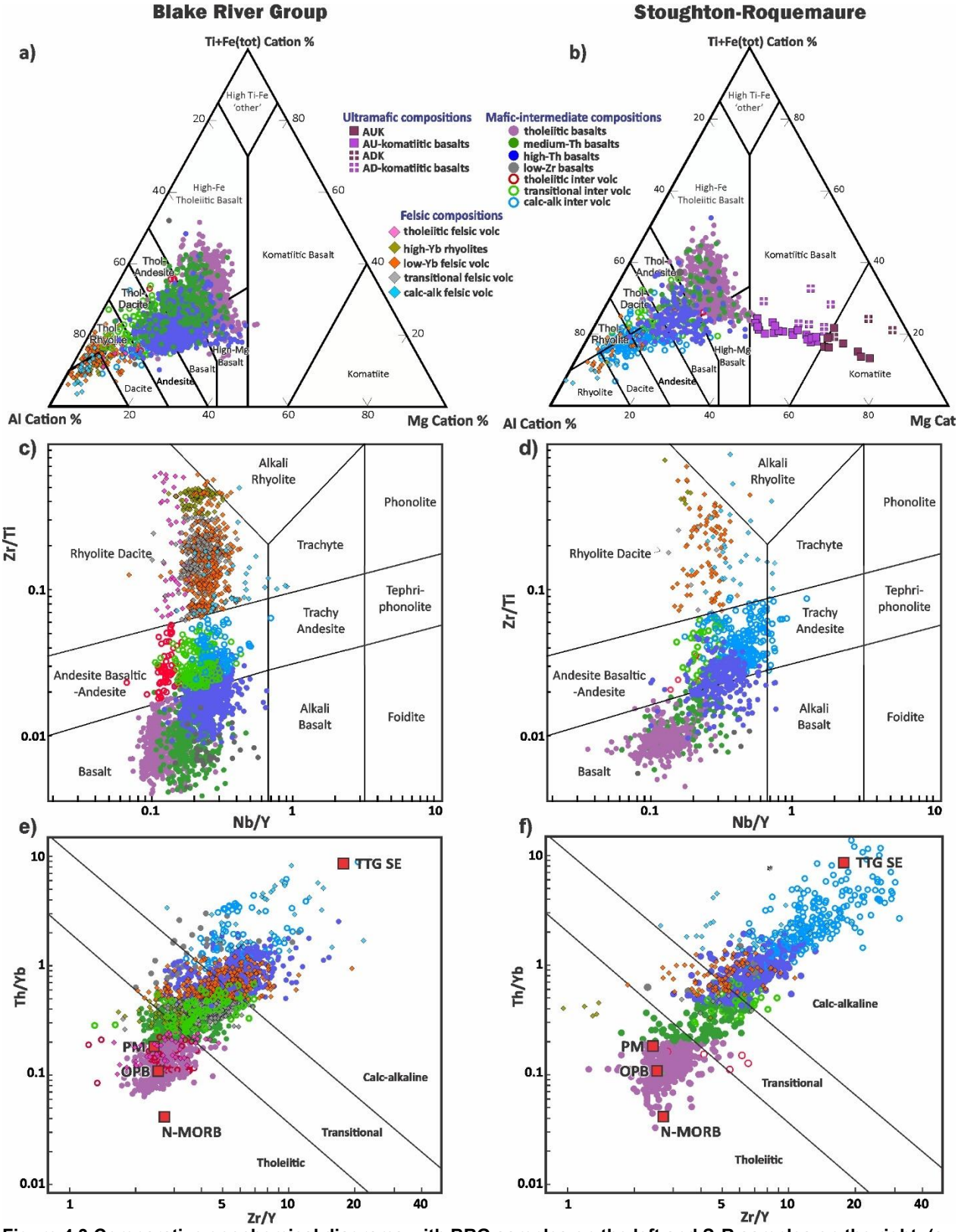

Figure 4.3 Comparative geochemical diagrams with BRG samples on the left and S-R samples on the right. (a, b) Jensen's cation plot for the least-altered samples (Jensen, 1976); (c, d) Zr/Ti vs. Nb/Y classification diagram (Pearce, 1996) on all samples except komatiites and komatiitic basalts; (e, f) Th/Yb vs. Zr/Y magmatic affinity diagram (Ross and Bédard, 2009) on all samples except komatiites and komatiitic basalts.

4.2.3 Extended trace elements and geochemical ratios across assemblages

Average extended trace-element patterns for each geochemical group in the BRG and the S-R assemblage are shown using violin plots (Fig. 4.4). Even though komatiitic magmas were not part of the Zr/Ti vs Th/Yb classification diagram, their extended trace elements profiles are shown for completeness and their relevance with the tholeiitic series (Fig. 4.4a, b). Key geochemical ratios are also shown using box plots (Fig. 4.5), which reinforce the similarities and differences observed among geochemical groups.

The results reveal consistency among mafic compositions including tholeiitic basalts, medium-Th basalts and high-Th basalts (Fig. 4.4c, d, e). For these groups, the BRG and S-R assemblage are barely distinguishable in terms of average extended trace element profiles, confirmed by their ratios distribution (Fig. 4.5). For low-Zr basalts, average profiles have similar shapes, but the average concentrations are higher in the S-R assemblage (Fig. 4f) with higher Nb/Y and La/Sm ratios (Fig. 5e, f). Transitional intermediate volcanic rocks are also similar across assemblages, with minor HREE differences (Fig. 4.4g), also visible in ratios such as La/Yb_N, and La/Sm (Fig. 5c, f).

There is however a notable difference in the intermediate calc-alkaline compositions, with higher trace element concentrations in the BRG samples, especially for HREE (Fig. 4.4h). This is also observable in most geochemical ratios (Fig. 4.5) Tholeiitic intermediate compositions also differ slightly in their average HREE concentrations (Fig. 4.4i) or comparable ratios (Fig. 4.5c-f).

Most felsic groups show some degree of divergence between assemblages. Transitional felsic compositions are generally comparable (Fig. 4.4j) in extended trace elements and geochemical ratios. High-Yb rhyolites from the S-R assemblage and BRG differ in their Zr and Hf contents and LREE segment (Fig. 4.4k) that is also observable in the corresponding ratios (Fig. 4.5). However, the extremely low number of samples in the S-R makes comparison difficult. Tholeiitic felsic compositions are exclusively present in the BRG (Fig. 4.4l). Low-Yb felsic averages show slightly higher trace element concentrations in the S-R assemblage and slight REE fractionation compared to the BRG (Fig. 4.4m), confirmed by geochemical ratios like in La/Yb_N, and La/Sm (Fig. 4.5c, f). Calc-alkaline felsic volcanic rocks show broadly comparable profiles between assemblages, with the main difference being the deeper negative Ti anomaly in the S-R samples (Fig. 4.4n), consistent with their ratio fields (Fig. 4.5).

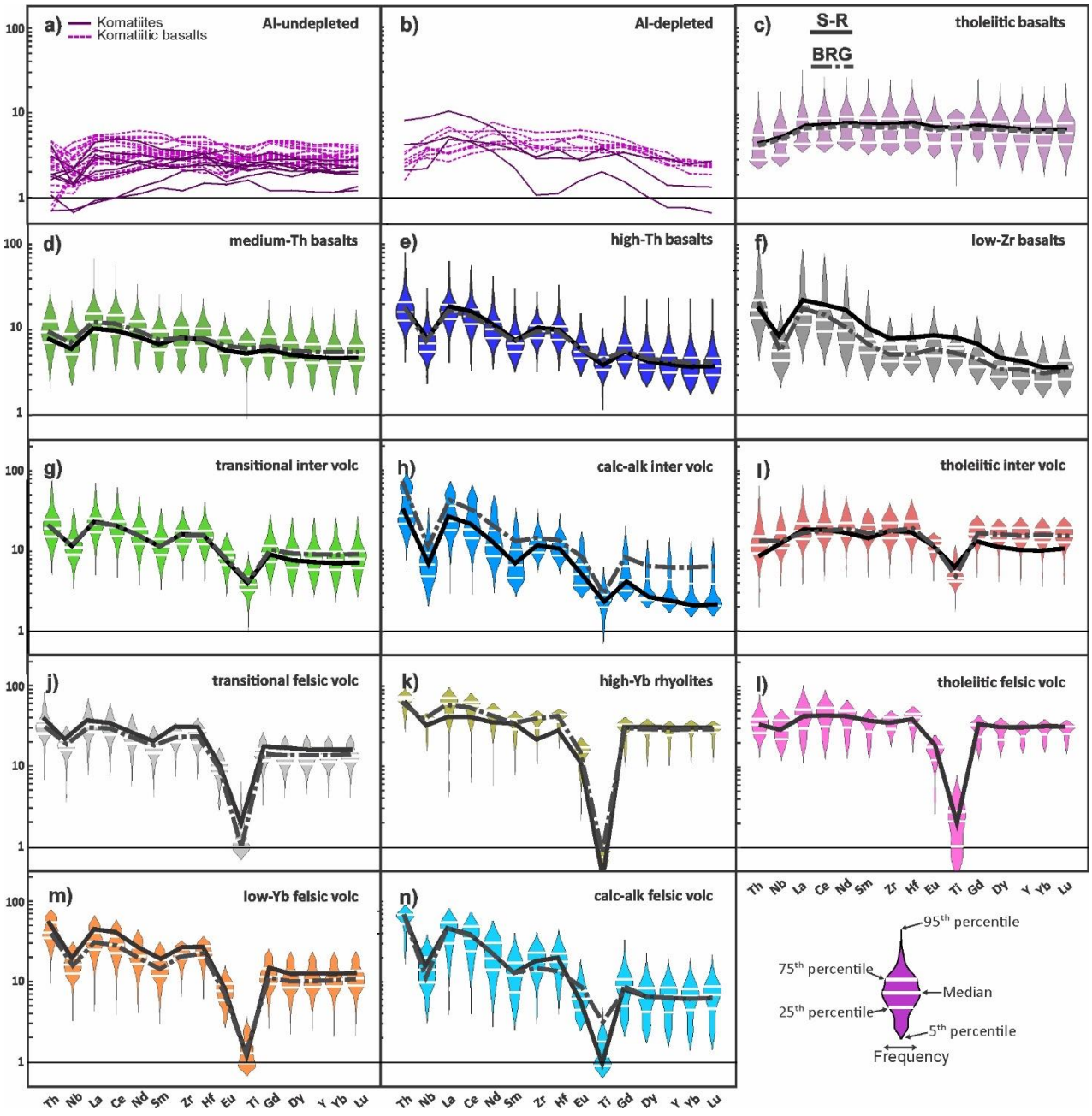

Figure 4.4 Extended trace element diagrams for both BRG and S-R assemblages showing average patterns for each geochemical group (a–n). Violin plots illustrate the data distribution within each group by using BRG and S-R samples. A violin plot combines the features of a box plot (range and quartiles) with a kernel density plot (data modes).

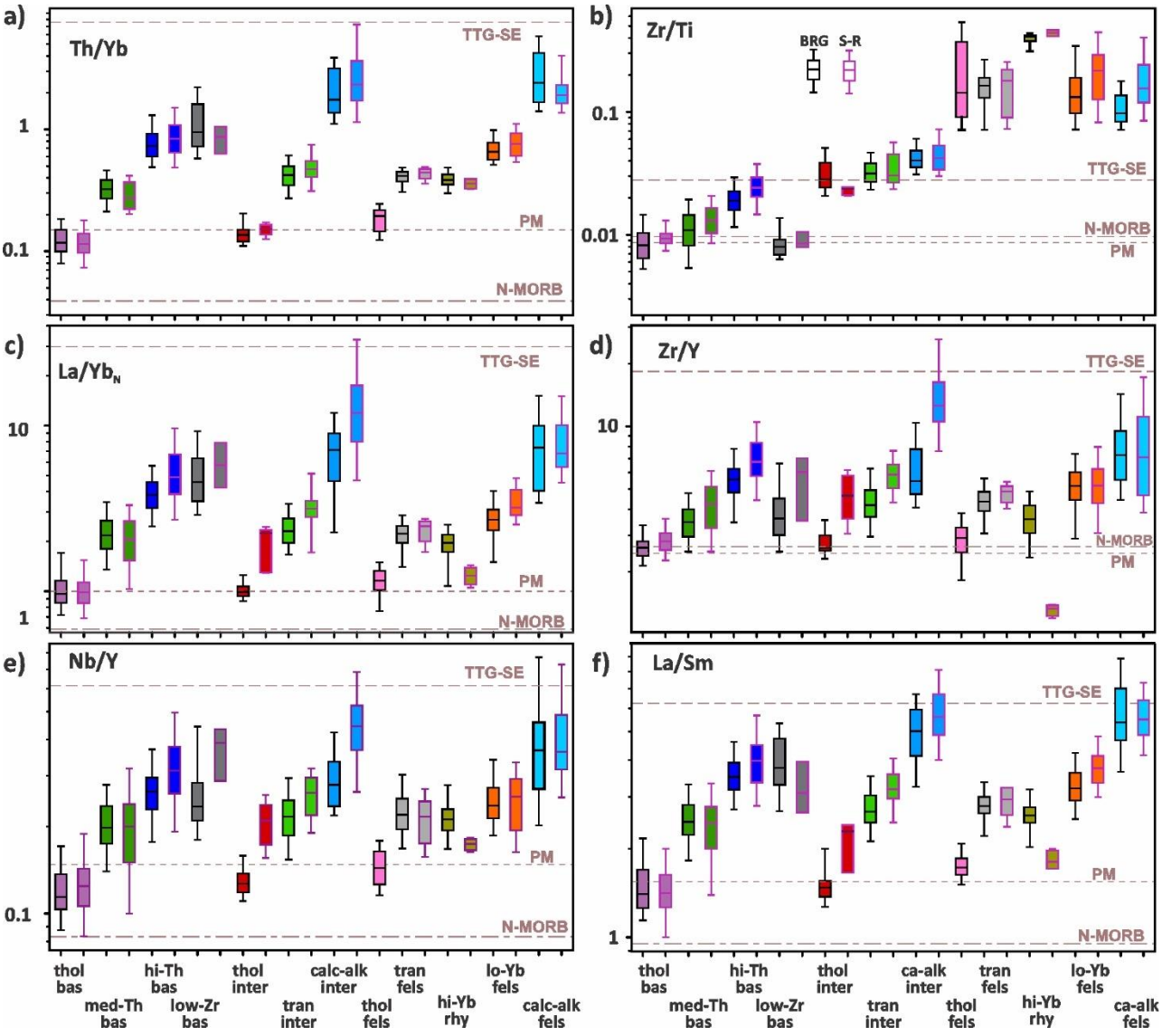

Figure 4.5 Key trace-element ratios for each geochemical group for the BRG and the S-R assemblage. Box plots represent the 90th (max) and 10th (min) percentiles as the error bar and 75^{th,} 50th and 25th percentiles in the main rectangle. They highlight the range and central tendency of the data for both assemblages.

4.2.4 Discriminant diagrams

The BRG and the S-R assemblage show similar overall distributions when individual samples are plotted in both the Agrawal et al. (2008) and Pearce et al. (2021) diagrams, ranging from the MORB field or mantle array to the Island Arc Basalt field or array (Figs. 4.6a-d). One noticeable difference is that the intermediate calc-alkaline group samples extend further towards the TTG average in the S-R assemblage as already described in previous section. However, felsic samples show a different distribution in the Hart et al. (2004) plot (Figs. 4.6e, f). Specifically, the BRG felsic

rocks are more geochemically diverse, with abundant samples in the FIIIa, FIIIb and FIV fields, unlike in the S-R assemblage.

Density plots of the same diagrams provide a different view of these distributions, which sheds additional light. In both assemblages, there are two main clusters represented by the two most abundant groups, tholeiitic basalts and high-Th basalts (Fig. 4.7a-d). Compared to the BRG, the S-R data shows a broader distribution, with a larger proportion of samples having high Th/Yb ratios. Felsic samples from the S-R assemblage tend to display higher La/Yb_N ratios on average, with most plotting in the FII field (Fig. 4.7f), while BRG felsic samples are more concentrated in the FIIIa field (Fig. 4.7e).

In summary, the mafic groups and some intermediate groups are similar enough between assemblages to fully justify using the same Zr/Ti vs Th/Yb diagram on both the BRG and the S-R assemblage. In contrast, some felsic groups and intermediate groups have some geochemical differences between assemblages which indicate nuances in magma petrology but still allow a broad comparison between assemblages based on Zr/Ti vs Th/Yb systematics.

4.3 Felsic groups in the BRG

Felsic groups within the BRG assemblage have not been detailed elsewhere in this thesis, so they are described here. They are listed by increasing Th/Yh ratios.

4.3.1 Tholeiitic felsic volcanic rocks

Tholeiitic felsic samples in the BRG have the lowest Th/Tb ratios (Fig. 4.2c), range from dacite to rhyolite (Fig. 4.3c) and fall largely in the tholeiitic field on the magmatic affinity diagram (Fig. 4.3e). Their extended trace element patterns are flat (Fig. 4.8a), resembling those of their parental tholeiitic mafic magmas (Fig. 4.4c). Tholeiitic felsic samples typically plot within the MORB field on the Agrawal et al. (2008) tectonic discrimination diagram and along the mantle array on the Pearce (2008) diagram (Fig. 4.6a, c). In the Hart et al. (2004) classification, they generally exhibit La/Yb_N ratios characteristic of FIV-type and Yb_N contents similar to FIIIb, plotting mostly out of any defined compositional fields (Fig. 4.6e).

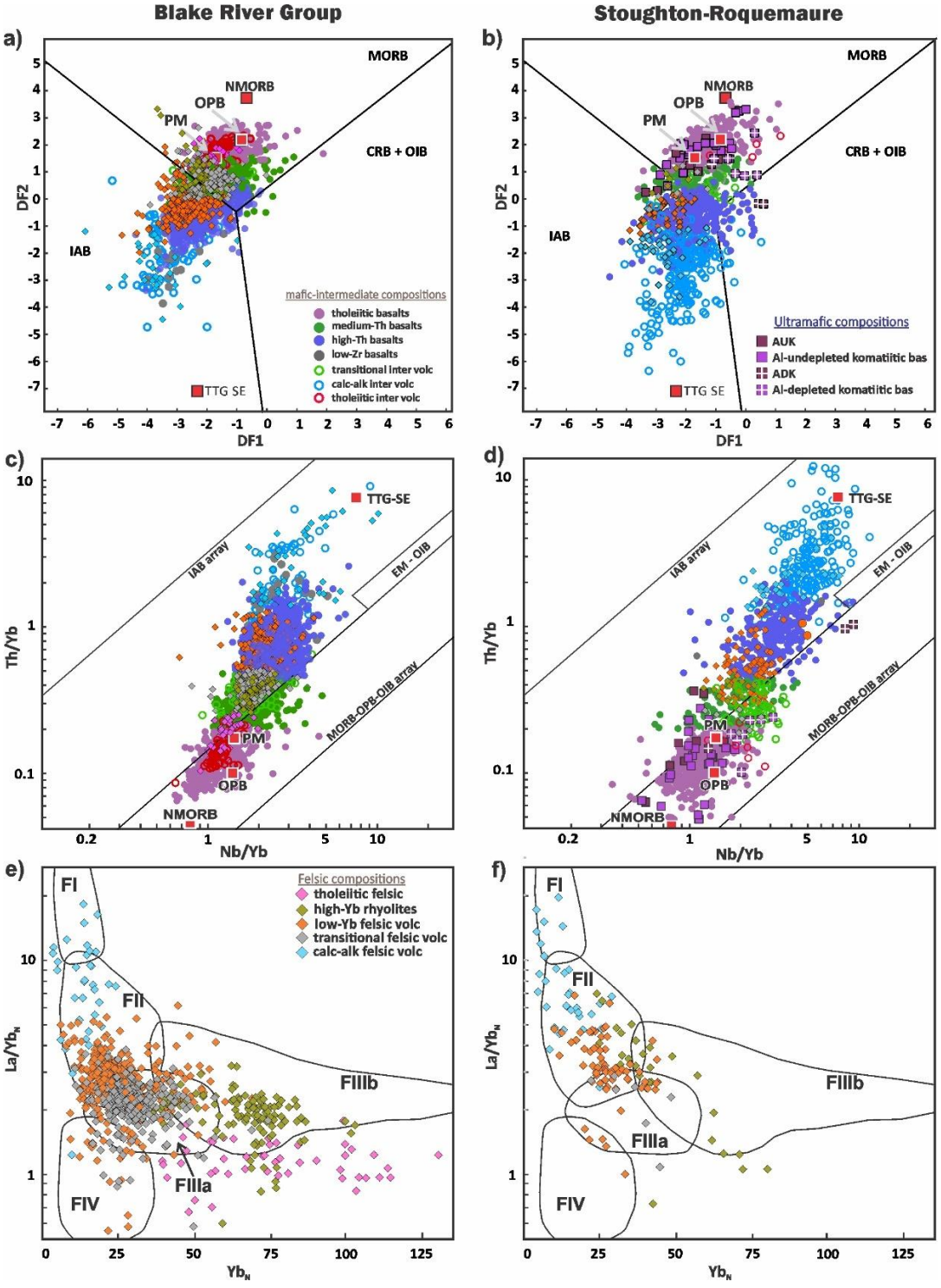

Figure 4.6 Discriminant plots comparing the BRG with the S-R assemblage. (a, b) DF1 vs DF2 diagram from Agrawal et al. (2008) using DF1 = 1.7517 $\log_e$ (Sm/Th) – 1.9508 $\log_e$ (Yb/Th) + 1.9573 $\log_e$ (Nb/Th) – 5.0928; DF2 = –2.2412 $\log_e$ (Sm/Th) + 2.2060 $\log_e$ (Yb/Th) + 1.2481 $\log_e$ (Nb/Th) – 0.8243. MORB: mid-ocean ridge basalt, IAB: island-arc basalt, CRB: continental-rift basalt, OIB: oceanic island basalt. Red squares show the following averages: normal MORB and primitive mantle (PM) from Sun and McDonough (1989), Oceanic plateau basalts (OPB) from Pearce et al. (2021) and SE Superior Province TTG average from Mole et al. (2021). (c, d) Th/Yb vs Nb/Yb diagram of Pearce et al. (2021). EM is enriched mantle, other abbreviations as above. (e, f) La/Yb$_N$ vs YbN diagram for felsic rock classification from Hart et al. (2004).

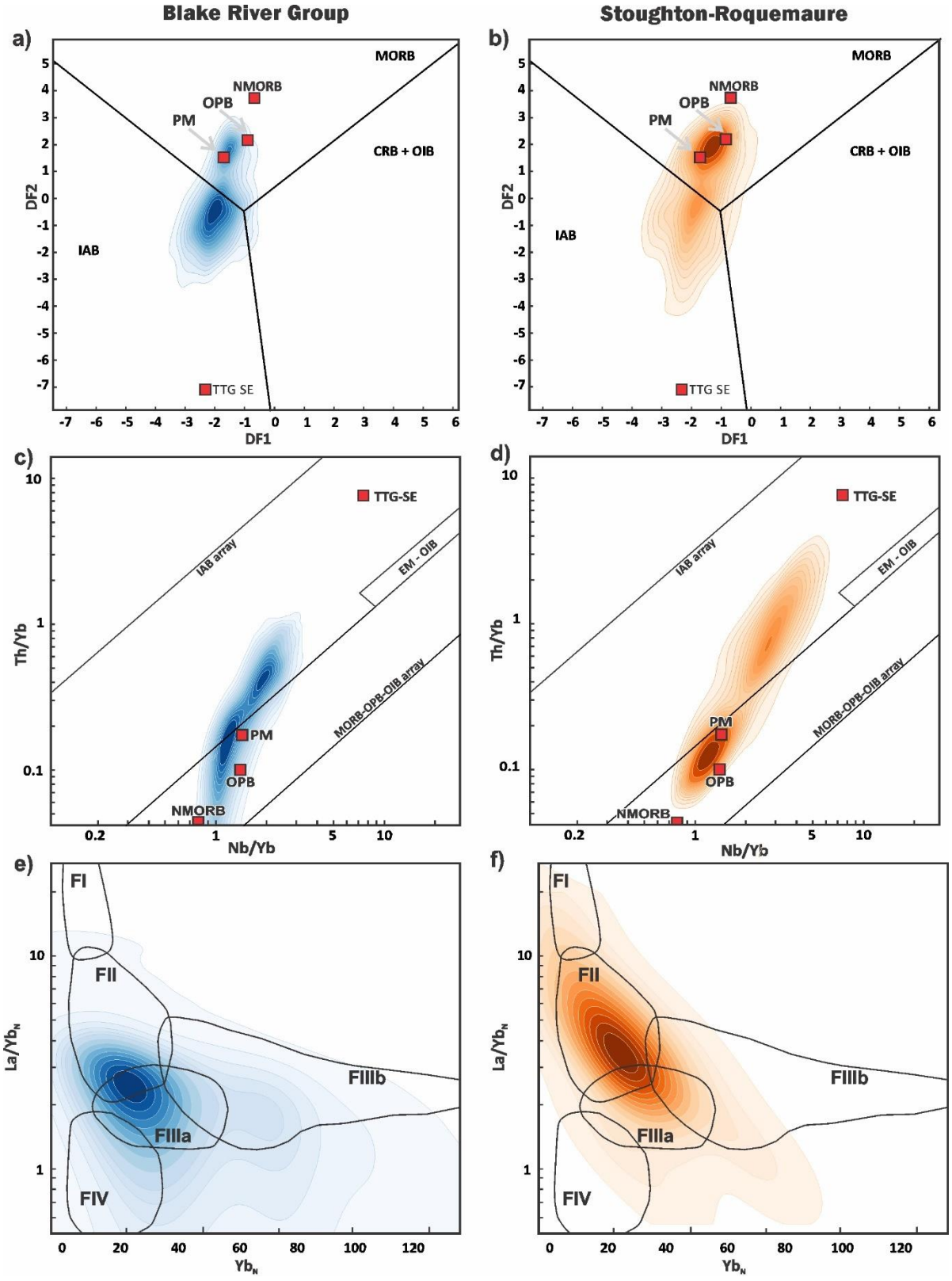

Figure 4.7 . Density plots using the same diagrams as Figure 4.5, showing the distribution of the BRG and S-R datasets (a–f). Density plots are build using the 10th and 90th percentiles in 5% increments. See text for detailed discussion.

4.3.2 Transitional felsic volcanic rocks and High-Yb rhyolites

Transitional felsic rocks and High-Yb rhyolites have similar Th/Tb ratios (Fig. 4.2c). The former ranges from dacite to rhyolite in composition whereas the latter are all rhyolite (Fig. 4.3c). These two groups generally display transitional magmatic affinities (Fig. 4.3e). Both tend to plot between the MORB and IAB (Island Arc Basalt) fields (Agrawal et al., 2008), or just above the mantle array (Pearce, 2008) (Fig. 4.6a, c). Their extended trace element profiles are also similar, characterized by moderate Th concentrations, small negative Nb anomalies, slightly fractionated LREEs, and flat HREEs (Fig. 4.8b, c). High-Yb rhyolites, being more evolved silicic rocks, generally show higher concentrations of incompatible elements and deeper negative Ti anomalies (Fig. 4.8b). In the Hart et al. (2004) diagram, both groups share similar La/Yb_N ratios but different Yb_N concentrations. This makes the transitional felsic rocks plot in the FIIIa field predominantly and the high-Yb rhyolites in the FIIIb field (Fig. 4.6e).

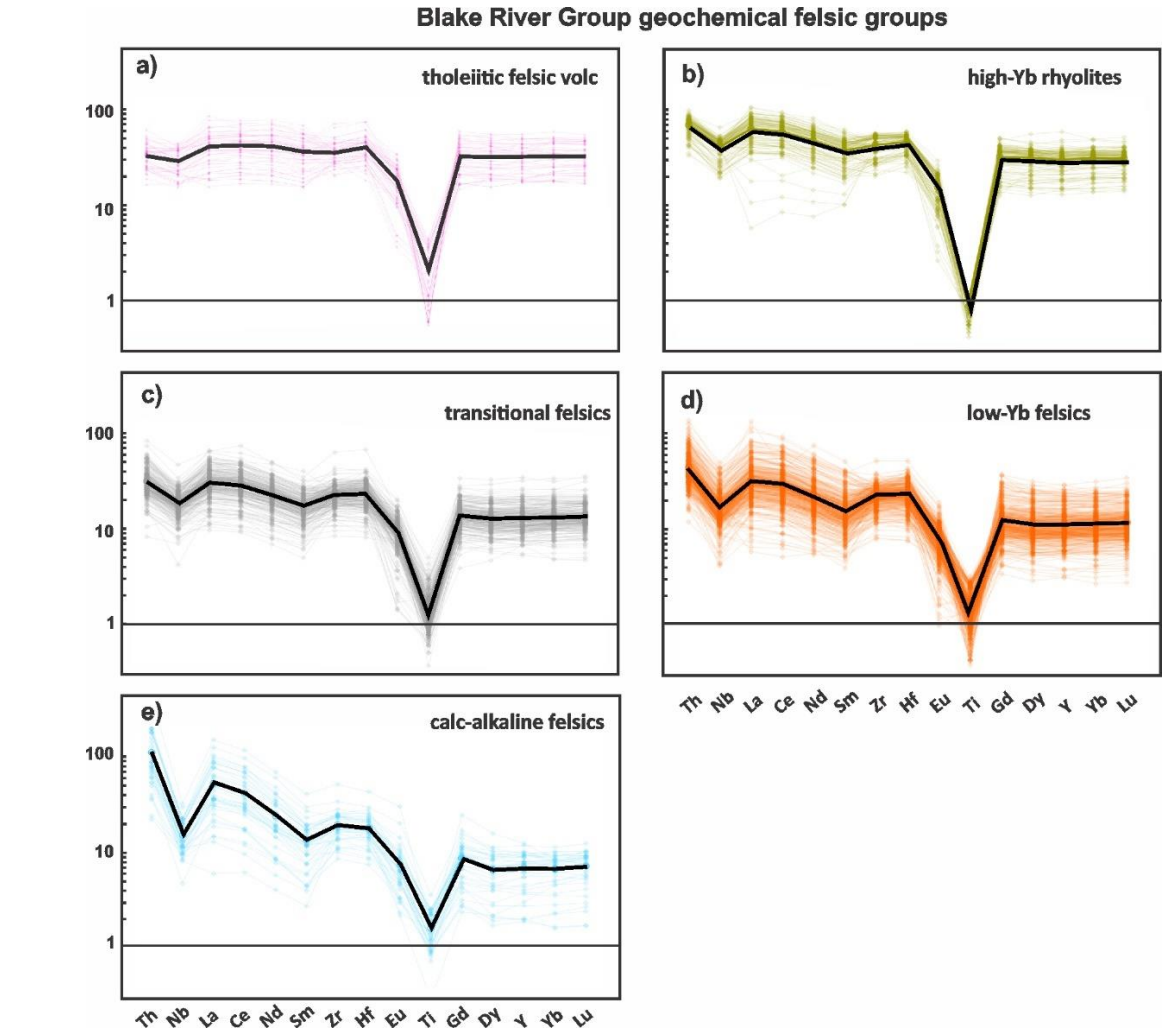

Figure 4.8 Extended trace element diagrams for felsic volcanic rocks from the BRG (a–e).

4.3.3 Low-Yb felsic volcanic rocks

Low-Yb felsic volcanic rocks have un-normalized Th/Yb ratios close to 1 (Fig. 4.2c). They again range from dacite to rhyolite (Fig. 4.3c) but straddle the transitional and calc-alkaline fields (Fig. 4.3e). This group exhibits extended trace element patterns broadly similar to the transitional felsic group but with slightly higher Th concentrations, more pronounced Nb anomalies, and more strongly fractionated LREEs (Fig. 4.8d). The samples plot predominantly within the IAB fields/arrays in discrimination diagrams such as Pearce et al. (2021) and Agrawal et al. (2008) (Fig. 4.6a, c) and distribute mostly between the FIIIa and FII fields (Fig. 4.6a).

4.3.4 Calc-alkaline felsic volcanic rocks

Calc-alkaline felsic rocks have the highest Th/Yb ratios (Fig. 4.2c), range from dacite to rhyolite (Fig. 4.3c), and display largely calc-alkaline affinities (Fig. 4.3e). This group is distinguished by the highest Th contents, deepest Nb anomalies, and the most strongly fractionated LREE patterns among the BRG felsic groups (Fig. 4.8e). In the Agrawal et al. (2008) and Pearce (2008) plots, they are consistently positioned within the IAB field/array, reflecting a classic calc-alkaline magmatic signature (Fig. 4.6a, c). In the Hart et al. (2004) diagram, these samples plot mostly within the FII and FI fields (Fig. 4.6e).

4.4 Proportions of geochemical groups in the BRG and the S-R assemblage

4.4.1 Komatiitic volcanic rocks

Komatiites and komatiitic basalts are absent in the BRG compilation (Figs. 4.3a, 4.9). In the S-R assemblage, ultramafic komatiites account for 1.0% of samples, with an additional 2.6% of samples classified as komatiitic basalts, totaling 3.6% komatiitic samples (Fig. 4.9). These proportions are consistent with previous field-based/map-based estimations suggesting that komatiitic rocks make up approximately 4% of the S-R assemblage (Sproule et al., 2002; Dostal and Mueller, 2013).

4.4.2 Mafic volcanic rocks

Mafic groups summed together represent over 60% of samples in both the BRG and the S-R assemblage, and are slightly more abundant in the latter (Fig. 4.9). Tholeiitic basalts dominate

the S-R assemblage but are only the third-most abundant group in the BRG, signaling a major difference between assemblages, the implication of which will be discussed later. Another important difference is the proportion of medium-Th basalts, which is rather low in the S-R assemblage, resulting from the presence of two distinct clusters of mafic rocks (Figs. 4.2b, 4.3d), compared to the more continuous distribution of mafic samples in the BRG (Figs. 4.2a, 4.3c). High-Th basalts are fairly abundant in both assemblages and represent the most abundant geochemical group in the BRG.

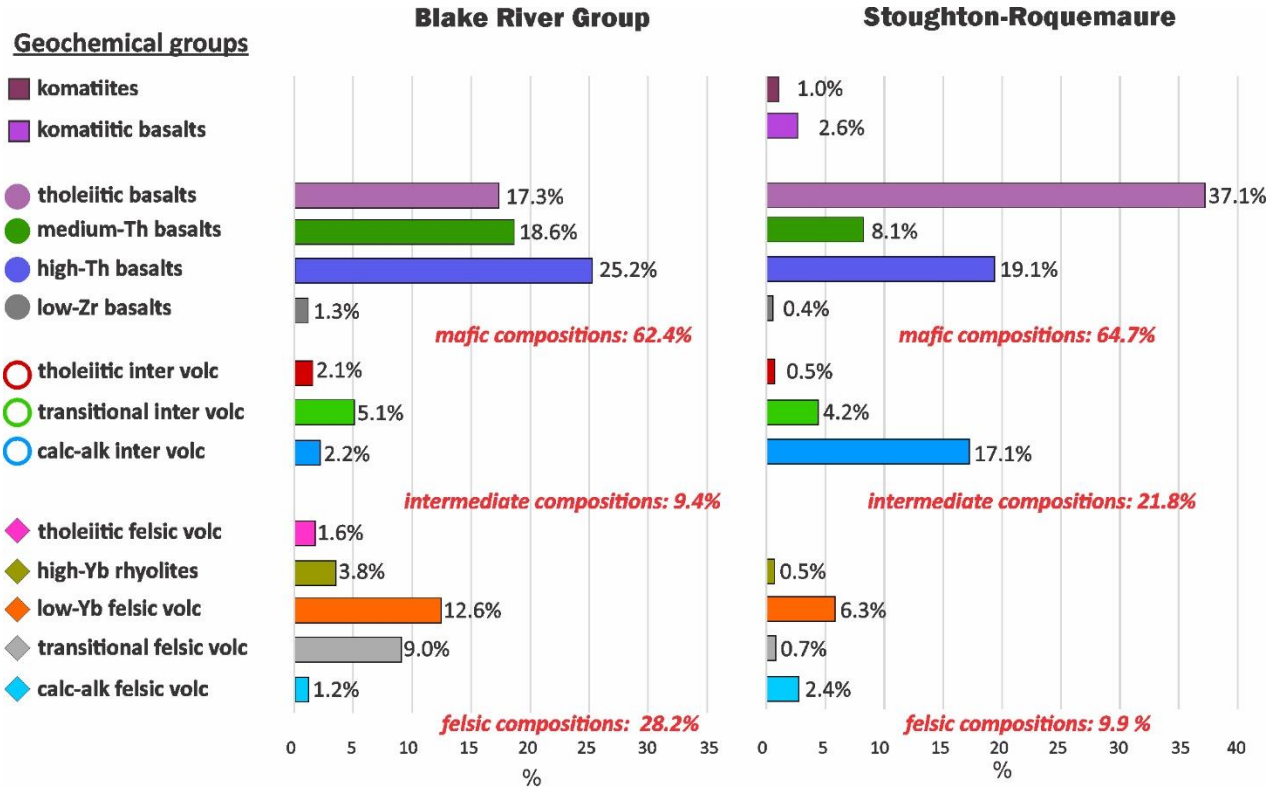

Figure 4.9 Relative abundances of geochemical groups in the BRG and S-R assemblage.

4.4.3 Intermediate volcanic rocks

Intermediate compositions show a marked contrast between the two assemblages. In the S-R, they account for 21.8% of the total number of samples, largely due to the prevalence of calc-alkaline intermediate volcanic rocks (17.1%), followed by transitional intermediate volcanic rocks (4.2%). In contrast, the BRG assemblage contains only 9.4% intermediate samples, dominated by transitional intermediate volcanic rocks (5.1%), with minor contributions from calc-alkaline (2.2%) and tholeiitic intermediate volcanic rocks (2.1%). This disparity signals a bimodal volcanic character in the BRG, with intermediate compositions less abundant than felsic compositions (Fig. 4.9). Whereas in the S-R assemblage, intermediate rocks are more abundant than felsic ones.

The major difference between assemblages in the proportions of calc-alkaline intermediate volcanic rocks is also noteworthy.

4.4.4 Felsic volcanic rocks

Felsic compositions comprise 28.2% of compiled samples of the BRG and 9.9% of samples in the S-R assemblage. Surface exposure data (calculated from Jorgensen and Gibson, 2024) supports these trends, albeit with smaller percentages reflecting oversampling of felsic rocks, especially in the S-R assemblage: 22% of felsic surface in the BRG and less than 4% in the S-R. Regardless of whether the proportion or samples or the surface area is used, the BRG contains a significant felsic component. The most abundant felsic type in the BRG is the low-Yb felsic volcanic rocks (12.6% of samples), followed by transitional felsic volcanic rocks (9.0%), high-Yb rhyolites (3.8%), tholeiitic felsic volcanic rocks (1.6%) and calc-alkaline felsic volcanic rocks (1.2%). This contrasts with the S-R assemblage, where felsic rocks represent only 9.9% of the total number of samples, mostly dominated by low-Yb felsic volcanic rocks (6.3%) and calc-alkaline felsic volcanic rocks (2.4%). Notably, transitional felsic volcanic rocks (0.7%) and high-Yb rhyolites (0.5%) are almost absent in the S-R, and no tholeiitic felsic volcanic rocks are recorded (Fig. 4.9).

4.4.5 Summary of the comparison

In summary, while both assemblages are dominated (>60%) by tholeiitic, medium-Th and high-Th basalts, which remain broadly comparable in their geochemical characteristics, although their relative abundances vary between the two. A major difference is the presence of komatiitic rocks and the abundance of tholeiitic basalts in the S-R assemblage. The S-R assemblage also displays a progressive decline in abundance from mafic to felsic compositions with a strong presence of calc-alkaline intermediate volcanic rocks (nearly 8 times more abundant than in the BRG). In contrast, the BRG shows a distinctly bimodal distribution, characterized by abundant mafic and felsic compositions and a smaller presence of intermediates. The abundant felsic rocks in the BRG are geochemically more diverse than those of the S-R assemblage.

4.5 Geochemical signatures in the main mining zones

There appears to be significant differences in the relative abundance of certain geochemical groups in the main formations that host VMS deposits in the BRG, namely the Noranda, Bousquet, and Horne formations, compared with the overall BRG composition (Fig. 4.10). Similarly, the

Estrades deposit area in the S-R assemblage appears to show different proportions of some geochemical groups compared with the overall assemblage, which hints at a potential relationship between the presence of some units and VMS deposits.

In the BRG, VMS-hosting formations tend to have more abundant felsic samples than the BRG as a whole. For example, the Noranda formation has nearly 60% felsic samples in our dataset (Fig. 4.9a) whereas the Horne formation has nearly 50% felsic samples (Fig 4.10c).

Within the ***Noranda Formation***, medium-Th basalts (19.6%) slightly outnumber high-Th basalts (15.5%) as the dominant mafic compositions (Fig. 4.10a). Tholeiitic basalts are absent. Transitional intermediate rocks are present in minor proportions (4.7%). Among felsic compositions, three dominant groups are identified: transitional felsic volcanic rocks (21.5%), high-Yb rhyolites (19.2%), and low-Yb felsic rocks (18.3%).

The ***Bousquet Formation*** is characterized by a much greater abundance of calc-alkaline compositions and a significant presence of intermediate compositions (Fig. 4.10b). High-Th basalts (21%) and low-Zr basalts (21.7%) dominate over medium-Th basalts (12.3%). The 21.7% occurrence of low-Zr basalts is particularly anomalous, given their 1.3% representation in the BRG overall. Again, tholeiitic basalts are absent. Calc-alkaline intermediate rocks represent nearly 20% in the Bousquet formation compared to about 2% in the BRG overall, and are dominant over transitional intermediate units (2.9%). Calc-alkaline felsic compositions are dominant (13%) in the Bousquet formation, followed by high-Yb felsic volcanic rocks (5.8%) and transitional felsic volcanic rocks (3.6%). The proportion of calc-alkaline felsic volcanic rocks in the Bousquet formation is more than 10 times the proportion in the BRG overall, highlighting – along with other aspects noted above – the formation's geochemical distinctiveness.

*The **Horne formation**, or **Horne block,*** is a volcaniclastic-dominated package composed mainly of felsic compositions with abundant volcaniclastic rocks (Monecke et al., 2008; Krushnisky et al., 2023, and references therein). The mafic compositions recorded in our database for this block likely represent at least in part mafic intrusions that fed the overlying volcanic units/flows, although they are labeled as "volcanic" in the database. Therefore, these mafic rocks may not represent a major volcanic component in the Horne block. In our dataset, all of the felsic rocks are of the low-Yb type (Fig. 4.10c), which is also the most abundant felsic group in the BGR overall. Results from Krushnisky et al. (2023) show that the compositions are mainly FII to FIIa types, which precisely correspond to the low-Yb felsic group, thus confirming our findings.

In comparison, less endowed areas of the BRG also deviate from the overall group composition but in distinct ways. For example, the Lower Blake River in the western part of the BRG has a large proportion of tholeiitic basalts (Chapter 2), whereas the Upper Blake River is dominated by high-Th basalts (Fig. 4.10d). Both divisions have lesser proportions of felsic rocks than the eastern part of the BRG, which are particularly well exposed in Quebec. The Rouyn–Pelletier formation, with only two known VMS showings, shares a mafic and intermediate composition pattern similar to that of the Noranda formation, but with minor contributions from tholeiitic mafic and felsic suites (Fig. 4.10e), which are absent in the VMS-bearing Noranda formation.

Samples from the **Estrades zone** of the S-R assemblage generally shows a dominance of medium-Th basalts with minor contributions of tholeiitic basalts and high-Th basalts (Fig. 4.10f). Minor contributions of transitional and calc-alkaline intermediate rocks are also present. The felsic portion, much greater than in the overall S-R assemblage, is dominated by low-Yb felsic volcanic rocks, with minor contributions of high-Yb rhyolite and calc-alkaline felsic compositions, and a minimal presence of transitional felsic volcanic rocks.

In summary, VMS mining camps in both assemblages generally lack significant tholeiitic signatures across the mafic to felsic spectrum. The dominant mafic components in these VMS-fertile zones are typically medium-Th and high-Th basalts, although the abundance of low-Zr basalts is unique to the Bousquet formation. Intermediate compositions are present in moderate proportions, particularly the transitional and calc-alkaline types, notably in the Bousquet formation and the Estrades deposit host succession. The low-Yb felsic group appears in all studied mining camps, being dominant in the Horne block and the Estrades deposit, and somewhat important in Noranda and Bousquet formations. The remaining felsic groups appear in varying proportions or are absent in certain camps. For instance, calc-alkaline felsic compositions are dominant in the Bousquet formation but minor in the Estrades deposit host succession, and absent in the Noranda formation and the Horne block. Transitional felsic compositions are present in Noranda and Bousquet formations, whereas this group is generally rare in the S-R assemblage as a whole, representing one of the major differences in felsic group distribution between the BRG and the S-R assemblage.

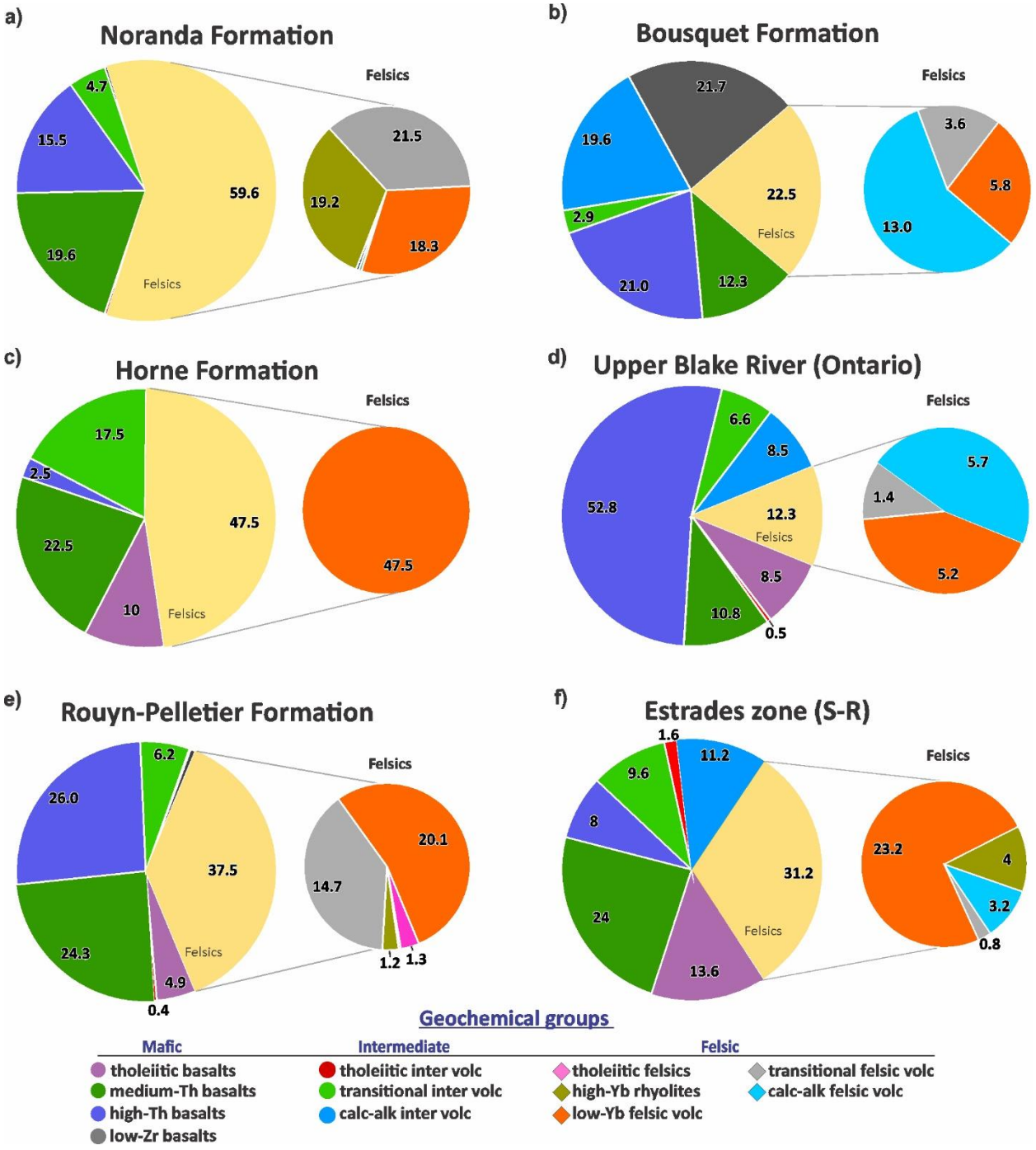

Figure 4.10 Proportions of geochemical groups within specific formations and VMS mining camps across the BRG and S-R assemblage (a-f).

4.6 Discussion

Similarities and differences between the BRG and the S-R assemblage, and the possible petrological process behind it, are discussed in this section. A model for the generation of each assemblage and links between the geochemistry/petrogenesis and VMS-endowment are also discussed below.

4.6.1 Similarities between the BRG and the S-R assemblage: petrogenetic processes

The PCA results (Fig. 4.2a, b) demonstrated that the dominant elements controlling geochemical variability are similar for both datasets (Ti, Th, Yb), despite a vector rotation in the S-R assemblage relative to the BRG. Thus, the studied assemblages were both classified on a Zr/Ti vs Th/Yb diagram initially developed for the BRG (Fig. 4.2c, d), to allow a direct comparison of the proportions of geochemical groups. This diagram showed good results overall because the two assemblages have some common geochemical and petrogenetic characteristics.

In both the BRG and the S-R assemblage, the tholeiitic series (including komatiites in the S-R) represents the least crustally contaminated set of geochemical groups. Although komatiites are absent from the BRG compilation and tholeiitic felsic rocks are not present in the S-R dataset, tholeiitic basalts remain the dominant mafic composition in the S-R and the third most abundant in the BRG. These magmas likely represent partial melting of the asthenospheric mantle with trace element signatures similar to the primitive mantle (Sun and McDonough, 1989), showing very subtle signs of trace-element depletion (see Th/Yb, La/Yb_N, Zr/Y, La/Sm, Fig. 4.5a, c, d, f; 4.6a-d) or high-pressure residual mineralogy (Fig. 3.6e, see the TiO_2/Yb ratio). This is a common characteristic for Archean tholeiites (Barnes et al., 2021) that parallels modern Oceanic Plateau basalts (Kerrich et al., 1999).

Our models suggest that variations in magmatic H_2O content are the principal control on the observed differences in $Fe_2O_3^t$, TiO_2 and Al_2O_3 among the tholeiitic basalts, although crystallization at modestly higher pressures cannot be entirely ruled out (see Chapter 3). Experimental and thermodynamic studies in modern spreading centers demonstrate that major phases (plagioclase, clinopyroxene, Fe–Ti oxides) are substantially more sensitive to changes in H_2O than to plausible variations in pressure or oxygen fugacity, making H_2O the most effective driver of major-element divergence within tholeiitic suites (Danyushevsky, 2001; Husen et al., 2016).

The similarity of tholeiitic basalts across assemblages suggests that the BRG and the S-R assemblage likely have a similar mantle source. Komatiitic volcanic rocks in the S-R assemblage, specially the AUK types, plot in a similar area of the tholeiitic basalts on diverse diagrams (Fig. 4.6a-d), although komatiite petrogenesis is beyond the scope of this thesis.

A shared geochemical 'main trend' across assemblages defines a curved trajectory on the Zr/Ti and Th/Yb plot that links mafic to intermediate rock compositions (Figs. 4.2c, d). This trend likely results from either (i) crustal contamination of the AFC type involving a tholeiitic basalt magma being contaminated by a TTG-like mid- or upper crust or (ii) bulk mixing (magma mixing between a tholeiitic basalt and a TTG magma, or country rock stopping into a mafic chamber). These processes explain the observed enrichment in LREE and Th with increasing Th/Yb and Zr/Ti values consistent with our proposed models (Chapters 2-3), although other processes are also possible and are discussed below (section 4.6.3).

4.6.2 Differences between the BRG and the S-R assemblage: petrogenetic processes

Despite broad similarities, the BRG and the S-R assemblage differ significantly in terms of geochemical group proportions (Fig. 4.9). A first order difference emerges in the PCA (Fig. 4.2) by observing the intermediate rock groups. In the BRG, intermediate compositions cluster between the mafic and felsic fields, with the Ti and Zr vectors suggesting a link through fractionation (and perhaps crustal assimilation). In contrast, many intermediate rocks from the S-R assemblage plot in the NE quadrant, showing no clear connection between mafic or felsic clusters (Fig. 4.2). This suggest different petrogenetic process at work, as discussed below.

The BRG displays a bimodal (mafic-felsic) character with no komatiites, while the S-R assemblage is mafic > intermediate > felsic > komatiitic (Fig. 4.9). The presence of komatiitic rocks in the S-R assemblage indicates a thermal state of the mantle that allowed high degrees of partial melting. In contrast, the BRG represents cooler mantle conditions that still allowed abundant tholeiitic basalt magma generation throughout the BRG history, although in some formations the tholeiitic basalt was modified completely on its way to the surface (see Chapter 2).

The higher abundance of felsic rocks in the BRG, with rarer intermediate compositions (i.e. the bimodal character) is not easily explained. Some researchers suggest that eruptive conditions may have favored the ascent and eruption of basaltic and felsic magmas, while intermediate compositions were also generated but conditions caused them to stall at depth (Kent et al., 2010). Alternatively, the mush model suggests that high-silica magmas are extracted from crystal-rich,

intermediate-composition mushes, which themselves remain trapped in the crust (Bachmann and Bergantz, 2006; Cashman et al., 2017).

The S-R assemblage reveals samples with higher Th/Yb ratios, coming from the calc-alkaline intermediate compositions, which are more abundant in the S-R assemblage and display more pronounced HREE depletion profiles than those of the BRG (Fig. 4.4h, Fig. 4.5a, c, f). In Chapter 3, this group is interpreted to possibly be the extrusive equivalent to a TTG magma. This aligns with Iles et al. (2025), who propose that similar calc-alkaline andesites in the Deloro assemblage represent 70-100% of the TTG endmember in a magma mixing model. Magma mixing might also have been prominent in the S-R assemblage, with calc-alkaline intermediate volcanic rocks representing the erupted TTG endmember. In contrast, the BRG main trend may be better explained by AFC (Chapter 2) as it delineates a continuous trend (Fig. 4.2c) with a larger abundance of medium-Th basalts. In this sense, magma mixing can explain both the greater abundance of intermediate rocks in the S-R assemblage (Fig. 4.9) and their distinct character, separate from felsic rocks in the PCA (Fig. 4.2b).

Another difference is the presence of a volumetrically minor but petrogenetically important tholeiitic fractionation trend in the BRG rocks, characterized by a subhorizontal trend linking tholeiitic basalts, tholeiitic intermediate volcanic rocks and tholeiitic felsic rocks on figure 4.2c. There are only a few tholeiitic intermediate samples in the S-R, and no felsic ones (Fig. 4.2d). In Chapter 2, the tholeiitic fractionation trend of the BRG was interpreted as caused by long-lived magmatic systems capable of fractionating at least 90% of their mass before getting to dacitic compositions.

4.6.3 TTG-like end-member

A brief note on the TTG-like end-member is warranted here. This component is incorporated in our models either as a crustal host in AFC models or as a melt in magma mixing models (see Chapters 2 and 3), consistent with the possibility that existing TTG crust and TTG magmatism were present contemporaneously with the emplacement of the BRG and the S-R assemblage. Indeed, several TTG intrusions overlap temporally with the S-R episode, including the Dauversière pluton (Mortensen, 1993) and the Joutel complex (Legault et al., 2002). Geophysical evidence supports the presence of existing TTG crust (e.g., Benn, 2006; Haugaard et al., 2021; Smith et al., 2023), while other processes contributing to TTG magmatism are discussed below. In this study, the TTG end-member used is taken from the South-East Superior Province average (Mole et al., 2021) and represents a sodic, low-HREE type, one of the most common compositions

in Archean TTG suites (Moyen and Martin, 2012). Nevertheless, other TTG types were not incorporated into our models. Incorporating these additional TTG compositions, like those of the medium and high HREE TTG types (Moyen and Martin, 2012), into comparable modeling approaches could yield alternative geochemical trajectories to explain volcanic groups with transitional magmatic affinities.

TTG magmatism includes a wide range of compositions, but all models agree on a mafic parental source (see Moyen and Martin, 2012; Moyen and Laurent, 2018). One possibility is the partial melting of metabasalts, similarly to the 'adakitic model', where a subducted slab is melted by a hotter Archean mantle (e.g., Martin et al., 2005). Other variations invoke melting at the base of a thick oceanic crust or partial melting of delaminated mafic crust (e.g., Bédard, 2006; Smithies et al., 2009). An alternative explanation proposes that the TTG suite formed instead through fractionation of hydrous mafic magmas where first-order fractionation processes account for much of the chemical variability (e.g., Moyen and Martin, 2012; Laurent et al., 2020).

These processes for TTG generation matter for our study because they could have operated during the formation of both the S-R assemblage and BRG. Contemporaneous TTG magmatism is relevant for magma mixing models, which seem especially important in the S-R assemblage, with its abundant calc-alkaline intermediate volcanic rocks that resemble an erupted TTG-like end-member. Partial melting of existing basalts at considerable depth (in the crust or mantle) would have been triggered by the hotter mantle prevailing during S-R time. While magma mixing also likely occurred in the BRG, its importance lies with the connection with felsic magmatism. For instance, recent work (e.g., Laurent et al., 2020) highlights this connection in the context of transcrustal magmatic systems, bringing the transcrustal magmatic system paradigm into Archean terranes. The details of this paradigm are still a matter of debate and some details are mentioned in the BRG model.

4.6.4 Stoughton-Roquemaure assemblage model

The Abitibi greenstone belt was formed by a series magmatic pulses separated by gaps of no activity where chemical-sedimentary interfaces zones where deposited (Ayer et al., 2002; Thurston et al., 2008). The S-R assemblage occupies the largest surface area of the Abitibi assemblages (Fig. 4.1) and was formed in a short time span (~3 m.y.), thereby representing the largest magmatic pulse in volume, likely with the maximum magma production per million year. Chapter 3 describes a N-S zonation in the abundances of geochemical groups in the S-R assemblage (Fig. 3.8). The abundance of tholeiitic mafic rocks, accompanied by komatiitic rocks,

in the central part of the Abitibi during S-R time, is interpreted as the direct result of mantle-generated magmatism with little crustal input (Fig. 4.11a). Several factors facilitated the magma generation in this context such as the thermal anomaly, the possible presence of volatiles in the mantle, and the presence of inferred major structures that facilitated mantle decompression (see Chapter 3). One such structure may have been the ancestral Destor-Porcupine fault, north of which stratigraphic units like the Stoughton-Roquemaure Group and the Degusier formation (Fig. 3.8) show up to 7 km in thickness of volcanic material (Dostal and Mueller, 1997; MRNF, 2019). A major rift zone in the central Abitibi has also been proposed by Mole et al. (2021, 2022) on the basis of zircons showing juvenile mantle-derived isotopic signatures, although this is not unique to S-R time. Higher degree of partial melting occurred to generate komatiites and komatiitic basalts (Arndt, 1994; Sossi et al., 2016).

The northern and northwestern regions of the S-R, on the other hand, specially the Burntbush complex, the Collines de Cartwrigth Group, and the Dessieux and Blondeau formations (Fig. 3.8), mostly show transitional to calc-alkaline signatures, although tholeiitic basalts are present as well (e.g., Bruneau Formation). The same thermal event occurring in central zone of the Abitibi might have influenced the northern regions, but the mantle-generated magma was commonly either contaminated by the crust and/or mixed with a Th-rich (TTG-like) magma (Fig. 4.11a). Komatiites either were not generated in the north, which was beyond the main plume upflow zone, or any komatiitic magmas were modified beyond recognition on their way to the surface.

Mole et al. (2021) suggest that the flanks of the rift that led to the emplacement of Abitibi volcanic rocks are located in the south and north-northwest regions of the Abitibi where the crust could have been thicker, leaving a central zone with a thinner crust. Pre-existing (thicker?) crust is compatible with geophysical profiles for the northern regions especially in the Chibougamau area (e.g., Mathieu et al., 2020). In the same area, zircon geochemistry also suggest that magmas display an interaction with an older crust (Mole et al., 2021, 2022).

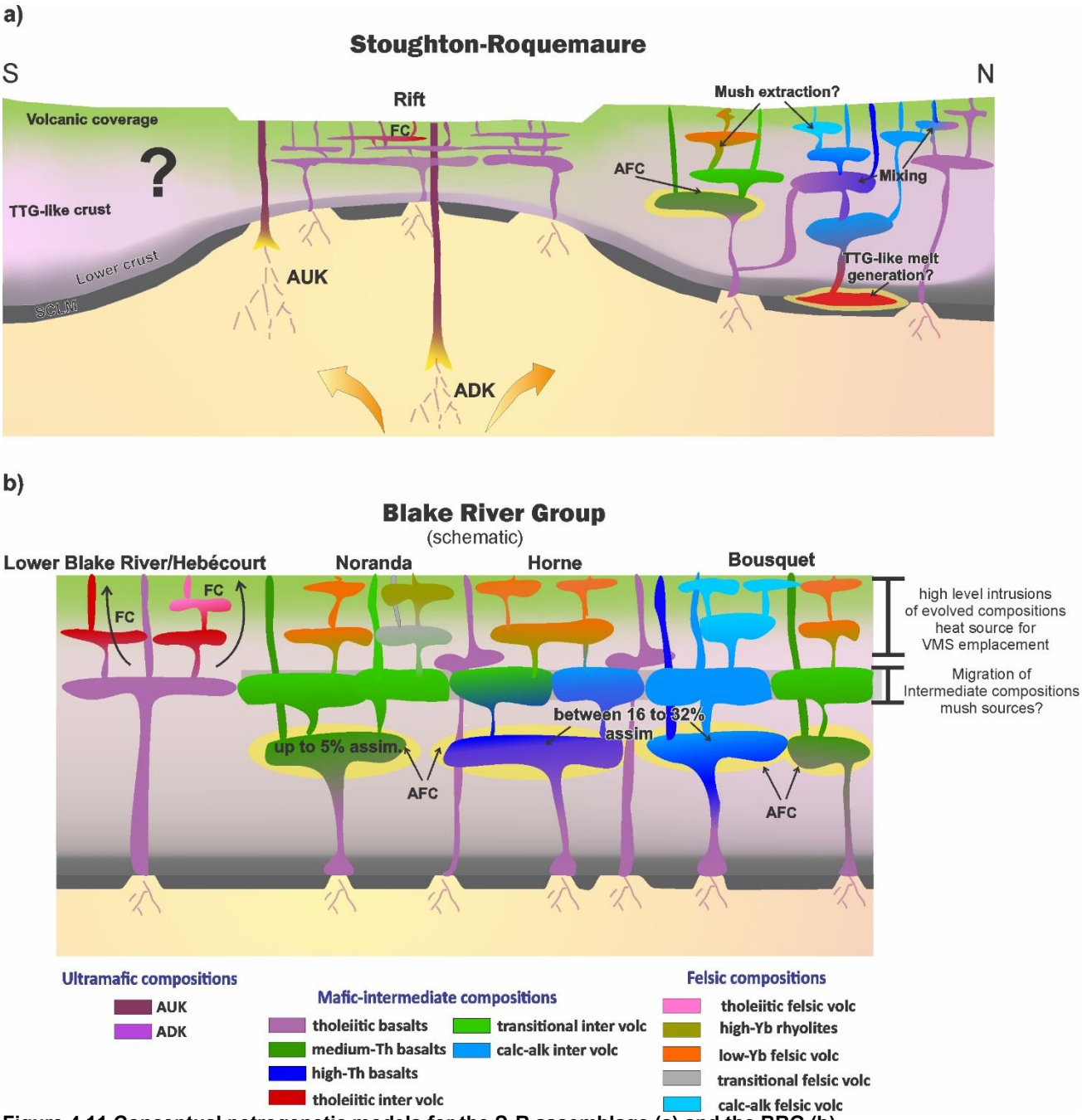

Figure 4.11 Conceptual petrogenetic models for the S-R assemblage (a) and the BRG (b).

Although the development of geochemical signatures indicative of crustal interaction is observed during the S-R emplacement, large proportions of evolved volcanism were not produced (compared with the BRG). The relative abundance of intermediate compositions in the S-R assemblage, reflecting significant contributions from a TTG-like end-member, suggests that magma mixing was a more prevalent process. Modern analogues show that fast and short-lived magmatic systems – controlled by heat flux, crustal structure, and rheology – tend to generate

only limited volumes of evolved magmas, as mafic magmas are rapidly extracted before significant pooling or differentiation can occur (Annen et al., 2025).

4.6.5 Blake River Group model

The Blake River assemblage represents the last major volcanic pulse of the Abitibi but covers less of the 15% of the Abitibi volcanic rocks (Jorgensen and Gibson, 2024; Mercier-Langevin et al. 2023). The BRG is core of the Blake River assemblage. Zircon geochronology and our geochemical compilation shows the BRG starting with mostly tholeiitic successions like the lower Blake River in Ontario and the Hébécourt formation in Quebec (McNicoll et al., 2014). Younger BRG rocks are more geochemically diverse, contain more felsic rocks, and range up to calc-alkaline (Chapter 2).

The emplacement of this last major volcanic pulse occurred after the Abitibi crust had evolved during at least 40 m.y. This might imply a somewhat different petrogenetic scenario for the BRG magmas relative to what happened during S-R time (Fig. 4.11b). Although most geochemical groups occur in both assemblages, the proportions are strikingly different in some cases (Fig. 4.9):

- The BRG lacks komatiitic rocks and has less than half the tholeiitic basalt proportion of the S-R assemblage, making a mantle plume association much less obvious;
- Medium-Th basalts are much more prominent in the BRG; AFC models indicate ~1% assimilation of a TTG-like contaminant to generate their signature. High-Th basalts can be explained with a greater degree of crustal contamination (Chapter 2);
- Calc-alkaline intermediate volcanic rocks are much less abundant in the BRG, which would seem to favour AFC over magma mixing for the BRG;
- The BRG displays ~22% felsic volcanic rocks by surface area (28% by sample proportions) versus the 9% estimated for the whole Blake River assemblage (Jorgensen and Gibson, 2024) and the much smaller proportions in the S-R assemblage (~4% by surface area).

Recent integrated models for Phanerozoic systems indicate that in order to sustain large volumes of silicic volcanism, thermal maturation of the crust and the development of a transcrustal magmatic systems are required (e.g., Annen et al., 2015; Karekas, 2017: Cashman et al., 2017; Humphreys et al., 2025). These systems consist of vertically extensive networks of interlinked crystal-melt-volatile mushes that span from the base of the crust to shallow magma reservoirs (Cashman et al., 2017, and references therein). This model initiates with injections of mafic sills

at the base of the crust that might trigger some melting of the crust. These mafic sills, when thermally equilibrated, form dense crystal mushes that efficiently segregate evolved melts by compaction. These melts might stall in middle crust where they might continue evolving and forming mushes. Those mid-crustal reservoirs might be continually fed by magma recharge that might reset fractionation patterns, creating a dynamic and complex pattern of recharge-mush-extraction and final formation of felsic magmas can happen in the upper crust. This could be a mechanism for the bimodal magmatism observed in the BRG and the scarcity of intermediate compositions as typically the melts extracted from the mushes tend to be a more evolved fraction (see 4.6.2).

Crustal maturation and the development of a complex transcrustal magmatic system require several million years (Karakas et al., 2017; 2019). The ~9 million-year emplacement history of the BRG (McNicoll et al., 2014) likely provided sufficient time for such a system to develop and evolve. This prolonged evolution may also explain the coexistence of different geochemical groups within single formations, as processes such as assimilation–fractional crystallization (AFC) and magma mixing are expected in such settings (Fig. 4.11b). Our models suggest that assimilation is more efficient at greater depths, within middle to lower crustal levels (0.3 to 0.6 GPa; Figs. 3.11, 3.12). Within a transcrustal system, continuous input of mantle-derived magmas can assimilate TTG-like crust to varying degrees.

Higher degrees of assimilation and prolonged evolution are recorded by calc-alkaline groups and some low-Yb felsic compositions, particularly those with higher Th/Yb ratios. In contrast, lower degrees of assimilation, followed by subsequent evolution, are reflected in medium-Th basalts, transitional intermediate rocks, and high-Yb rhyolites. This progression is illustrated in Figure 4.11b, which shows an ascending fractionation path driven by a mush-dominated system. In the early stages, assimilation in the lower crust produces basaltic to basaltic-andesitic magmas, which may erupt directly at this stage, as observed in the field. However, continued ascent may cause magmas to stall and evolve further within the crust, eventually forming mush reservoirs from which evolved felsic or silicic magmas are extracted.

4.6.6 Link between petrogenesis and VMS deposits

In Archean greenstone belts, VMS mineralization is often intimately tied to high-level felsic magmatism (e.g., Lesher et al., 1986; Galley, 2003). Some studies suggest that the Abitibi volcanic sequences were emplaced onto pre-existing TTG crust (Benn, 2006; Haugaard et al., 2020; Smith et al., 2023). In the case of the fertile BRG, there might have been existing TTG-like

crust, plus the presence of at least some of the previous volcanic assemblages underneath, as seen by a komatiite enclave in a BRG gabbro and inherited zircons in BRG volcanic rocks (McNicoll et al., 2014). These features indicate that earlier volcanic assemblages underlie the BRG and may have contributed to its magmatic evolution. In contrast, the older VMS-poor S-R assemblage has less detectable crustal interaction, in the central Abitibi at least.

In addition to the crustal context, the duration of BRG emplacement (9 m.y.), implies a prolonged thermal regime that could have supported the maturation of large-scale magmatic systems. This extended duration would have allowed progressive crustal heating, facilitating the development of vertically integrated melt reservoirs, and the abundant production of felsic volcanic rocks, and well as high-level syn-volcanic intrusions.

Recent crustal reconstructions suggest the existence of a transcrustal structural corridor beneath the BRG (Jorgensen et al., 2022). The coupling of this structural architecture with a thermally mature crust capable of sustaining long-lived silicic magmatism (Cashman et al., 2017) likely enabled the ascent of magmatic and hydrothermal fluids to the upper crust. Together, these conditions would have been favorable for the development of world-class VMS deposits.

In contrast, the single VMS deposit observed in the S-R assemblage (Estrades) is found in the northern part of the belt, where felsic volcanic rocks with transitional to calc-alkaline affinities are more abundant – comparable to BRG compositions. This may be linked to a thicker crust in that region, which promoted crustal assimilation and favored these evolved geochemical signatures. However, the short duration of magmatism (~3 m.y.) in the S-R assemblage and crustal conditions were not suitable to generate mature magmatic systems.

The prevalence of low-Yb felsic volcanic rocks (types FII and FIIIa in the Hart et al., 2004 classification with transitional to calc-lakaline affinities) among VMS-hosting camps in the BRG and the S-R suggests that the petrogenetic processes leading to the generation of this specific type of silicic volcanism are particularly favorable for VMS formation. Their petrogenesis typically involves moderate TTG-like crustal assimilation or inmixing followed by sustained fractional crystallization at relatively low pressure (Chapters 2 and 3). The latter scenario would require the development of magma reservoirs in the mid- to upper crust, which could act simultaneously as (i) sources of high-level intrusions, (ii) the thermal engine for VMS hydrothermal systems, and (iii) reservoirs of metals, including gold. Such magmatic contributions are well documented in calc-alkaline–dominated formations, as exemplified by the gold-rich VMS systems of the Bousquet Formation, where gold enrichment is linked directly to synvolcanic intrusions (e.g., Hannington et al., 2005; Mercier-Langevin et al., 2011; Dubé et al., 2014; Yergeau et al., 2022b). In this sense,

the production of large volumes of evolved felsic magma is a direct consequence of a well-developed transcrustal magmatic system (Cashman et al., 2017; Annen et al., 2025).

VMS-bearing formations differ geochemically from both barren units and their parent assemblages (Fig. 4.11). Interestingly, formations dominated by tholeiitic signatures, especially large volumes of tholeiitic basalts, tend to be barren in the BRG and the S-R. However, notable exceptions exist, such as in the Matagami district (Ross et al., 2014), where tholeiitic felsic rocks host VMS-bearing horizons in the Deloro assemblage (Debreil et al., 2018; Iles et al., 2025). There, thick felsic units such as the Watson Lake Dacite and Rhyolite (up to 1000-1400 m thick; Pilote et al., 2022) are interpreted to result from prolonged fractionation of tholeiitic parental magmas under recharge conditions (Iles et al., 2025). This example reinforces the idea that VMS deposits can occur in association with volcanic rocks from a range of geochemical groups, but that their formation is controlled primarily by the presence of a long-lived, evolved magmatic system capable of generating silicic volcanism, regardless of whether the system exhibits tholeiitic or calc-alkaline affinities. In the Abitibi context, such systems tend to develop transitional to calc-alkaline affinities given the inferred existence of a TTG-like middle crust in many places.

Critically, our results highlight that understanding VMS fertility requires integrating the entire compositional spectrum of volcanic rocks—from mafic through intermediate to felsic—rather than focusing solely on evolved end-members. Although specific mafic and intermediate signatures are not diagnostic on their own, their variability (e.g., medium- and high-Th basalts, low-Zr basalts and transitional to calc-alkaline intermediate compositions) provides essential constraints on crustal interaction and magmatic evolution. When combined with felsic rock geochemistry, these compositions enhance our ability to reconstruct magmatic systems and develop more comprehensive models for VMS targeting. Additionally, recent crustal reconstructions in the Abitibi highlight that Archean VMS clusters often align with trans-crustal feeder structures (Jorgensen et al., 2022) that likely facilitated the ascent and emplacement of magmatic reservoirs. This implies that VMS emplacement is facilitated by a conjunction of factors, including specific magmatic processes and structural controls, and its complete understanding is multidisciplinary.

4.7 Chapter conclusions

This chapter presents a comparative geochemical and petrogenetic analysis of the BRG and the S-R assemblage, with the aim of exemplify the processes controlling VMS endowment in the Abitibi Greenstone Belt. Both assemblages display similar partly principal geochemical trends on a PCA diagram, dominated by Ti, Th, and Yb, supporting the use of a unified classification scheme

(Zr/Ti vs. Th/Yb) to place volcanic rocks into groups. Both assemblages are dominated by tholeiitic and high-Th basalts, but medium-Th basalts are twice as abundant in the BRG. The S-R assemblage shows a progressive decline in abundance from mafic to felsic compositions and is strongly characterized by calc-alkaline intermediate rocks, which are eight times more abundant than in the BRG. In contrast, the BRG exhibits a bimodal mafic-felsic distribution, with a comparatively large felsic component dominated by transitional and low-Yb felsic rocks. Tholeiitic felsic compositions are exclusive to the BRG, while transitional felsic volcanic rocks are nearly absent in the S-R assemblage.

Felsic volcanism – especially of the low-Yb type – is more prevalent in VMS-hosting regions. Their geochemical signatures are more related to moderate Th/Yb ratios reflecting mostly transitional affinities, observable in the Noranda, Horne and Estrades districts. The Bousquet formation has a more calc-alkaline affinity. Formations dominated by mafic tholeiitic affinities are typically barren in the studied assemblages. However, the dominance of tholeiitic magmatism in the initial formations and its recurrence throughout most BRG units suggests a single asthenospheric source for all basalts, with various intensities of crustal modification. This study shows that integrating mafic to intermediate compositions is also essential reconstructing magmatic evolution and assessing VMS potential.

The evidence suggests that the development of long-lived, thermally mature, transcrustal magmatic systems is a key condition for generating large volumes of evolved felsic magma and associated upper-crustal hydrothermal systems conducive to VMS formation. The extended magmatic duration (~9 m.y.) of the BRG allowed for crustal maturation and the establishment of such systems, likely aided by structural focusing via transcrustal feeders. In contrast, the short-lived nature of the S-R pulse (~3 m.y.) limited its VMS potential, even though rocks with similar geochemical signatures are present (albeit in different proportions).

The findings of this study emphasize that VMS fertility is not controlled by geochemistry alone but results from the interplay between magmatic evolution and structural architecture. These insights into the contrasting evolution of barren and endowed assemblages may inform future mineral exploration strategies and provide a framework for targeting VMS deposits in Archean terrains.

5 GENERAL CONCLUSIONS

This study has investigated the geochemical diversity of the VMS-endowed Blake River Group (BRG) and that of the poorly endowed Stoughton-Roquemaure (S-R) assemblage, using whole-rock geochemistry and petrogenetic modeling. Over 4000 volcanic rocks analyses were compiled, from ultramafic to felsic compositions. A unified classification scheme based on immobile-element ratios (Zr/Ti vs Th/Yb) was developed, guided by principal component analysis (PCA). Twelve geochemical groups (plus four komatiitic groups for the S-R assemblage) were defined, allowing a comparison between assemblages. Mining zones were also compared with unmineralized areas. These insights help identify the petrological conditions that may explain the differential metal endowment observed in the AGB.

In this chapter, I summarize the main points of each core chapter (chapters 2, 3 and 4). I then further discuss petrological insights about each assemblage and the link with VMS endowment. Finally, I offer suggestions for future work.

5.1 Summary of the main findings in the thesis

Chapter 2. Mafic to intermediate volcanic rocks of the Blake River Group, Abitibi greenstone belt, Canada: Geochemistry, petrogenesis and relation with VMS deposits

- The BRG hosts 357 Mt of VMS deposits (as to 2018 estimations) and was emplaced between 2704 to 2695 Ma. This is the best endowed area in the AGB in terms of VMS deposits, including several world-class gold-rich VMS deposits.
- The chapter focuses on mafic to intermediate volcanic rocks in the BRG; it lays the foundation for the geochemical classification scheme. A Zr/Ti vs Th/Yb diagram was developed after exploring the data via PCA and clustering techniques.
- Seven initial geochemical groups identified on the Zr/Ti vs Th/Yb diagram for mafic to intermediate volcanic rocks, and checked on other diagrams including extended trace element plots: tholeiitic basalts, medium-Th basalts, high-Th basalts and low-Zr basalts, and tholeiitic, transitional and calc-alkaline intermediate volcanic rocks.
- Tholeiitic basalts, medium-Th basalts, and high-Th basalts dominate, but beyond the mafic to intermediate rocks investigated in this chapter, a significant proportion of felsic rocks also occurs in the BRG, making it bimodal (mafic-felsic) in composition.

- Fractional crystallization (FC) models at 0.25 GPa suggest that variations in H_2O content (0-1.2 % H_2O) account for most tholeiitic trends on Harker diagrams; up to 75% crystallization is required to reach intermediate compositions.
- Assimilation-fractional crystallisation (AFC) models indicate that ~1% crustal assimilation produces medium-Th basalts, while >2.5% crustal assimilation is needed for high-Th basalts.
- The BRG's informal geological formations vary in composition: tholeiitic basalt-dominated units tend to be barren, while VMS-hosting formations (e.g., Noranda, Bousquet) contain <2% tholeiitic basalt and are dominated by transitional to calc-alkaline groups (medium-Th basalts, high-Th basalts, transitional and calc-alkaline intermediate volcanic rocks, and low-Zr basalts).
- Stratigraphic analyses in the Noranda formation link peaks in Th/Yb ratios to VMS bearing horizons.

Chapter 3. Petrogenetic insights on the largest volcanic pulse in the Archean Abitibi greenstone belt, Canada: the Stoughton-Roquemaure assemblage

- The S-R assemblage contains about a third of the volcanic rocks in the AGB by surface area, yet it was emplaced within only 3 m.y. (2723-2720 Ma), making it the largest and likely most intense volcanic pulse in the AGB. It contains only one small VMS deposit, meaning it is a very poorly endowed assemblage considering its volume.
- The BRG geochemical classification method, extended to include felsic compositions, was applied to the S-R assemblage dataset.
- Nearly all of the mafic to felsic geochemical groups found in the BRG are also present in the S-R assemblage. In addition, the S-R assemblage also contains komatiitic rocks.
- The proportions of geochemical groups are however different in the two assemblages; in the S-R case, tholeiitic basalts are much more abundant, almost double at 37.1%.
- Using PRIMELT3 on high-Mg tholeiitic basalts and on komatiitic samples, two clusters of mantle potential temperature (T_P) were estimated: 1658 ± 33°C and 1565 ± 87°C, indicating a mantle plume influence during emplacement.
- More extensive FC modeling was done to better constrain crystallisation pressures (depths) for the tholeiitic basalts. At >0.6 GPa, garnet stabilizes, but the modeled major and trace elements do not correspond well to the analyzed samples and trends. Instead,

the best FC models are at 0.15 to 0.6 GPa, or about 6 to 16 km depth, corresponding to the upper- to mid-crust.

- AFC modeling demonstrated that assimilation is more efficient at depth, producing strong crustal signatures even in relatively mafic compositions.
- Magma mixing between high-Mg tholeiitic basalt and TTG-like melt was modeled using three endmember proportions (25%, 50% and 75% of TTG). The resultant mixtures were then fractionated to felsic compositions. These models are useful to reproduce the observed compositional spectrum.
- The abundance of calc-alkaline intermediate compositions in the S-R assemblage, displaying strongly depleted and fractionated HREE patterns, is interpreted as evidence that these magmas are closely related to the TTG endmember.
- A geochemical zonation is observed in the S-R assemblage: the central and southern zones are tholeiitic-dominated (including the komatiitic samples); whereas the northern and northwestern sectors contain more transitional to calc-alkaline signatures.
- The only formal VMS deposit in the S-R is located in the northwest, in an area where transitional compositions dominate.
- S-R magmatism appears to have been influenced by both mantle conditions and structural settings. T_P estimates support a mantle plume model, with abundant magmatism concentrated along the precursor to the Destor-Porcupine fault system, where decompression was facilitated. This same area hosts abundant tholeiitic basalts and komatiitic rocks (e.g., Stoughton-Roquemaure Group and Deguisier formation).
- In contrast, the northern sector, with a potentially thicker crust, promoted more interaction between mantle-derived magmas and the crust, resulting in more complex (transitional/calc-alkaline) signatures.

Chapter 4. Blake River Group versus Stoughton-Roquemaure assemblage: geochemical comparison and VMS implications

- This chapter integrates findings from the BRG and S-R assemblage to produce two schematic petrological models and a comparative analysis of their VMS potential.
- Independent PCA of both assemblages confirms that the same elements control geochemical variance, validating the unified classification scheme.
- Similar geochemical groups occur in both assemblages but with different proportions.
- Both the BRG and the S-R assemblage are dominated by tholeiitic basalts and high-Th basalts, though medium-Th basalts are twice as abundant in the BRG.

- The BRG exhibits a bimodal mafic-felsic pattern, with ~28% felsic rocks; it contains tholeiitic felsic compositions which are absent in the S-R assemblage.
- The S-R contains about 4% komatiitic samples, then shows a mafic > intermediate > felsic pattern.
- The S-R assemblage has an abundance of intermediate calc-alkaline volcanic rock compositions (~17%), which are eight times more abundant there than in the BRG; one hypothesis is that this group represents the end-member TTG magma (in the mixing models) that basically erupted on the sea floor.
- Mafic to felsic compositions in VMS-bearing formations studied lack tholeiitic signatures and are dominated by transitional to calc-alkaline groups.
- Evolved felsic rocks (especially low-Yb types) are common in endowed zones (Noranda, Horne, Estrades). Calc-alkaline felsic rocks are slightly more abundant in the Bousquet formation.
- The S-R assemblage might have formed in a setting analogous to modern oceanic plateaus – abundant but short-lived mantle-derived magmatism with limited crustal processing. This does not seem conducive to VMS generation in the AGB.
- In contrast, the BRG shows sustained, lower-flux magmatism over ~9 m.y. This allowed the crust to thermally mature and develop a transcrustal magmatic system capable of generating evolved felsic magmas and related intrusions – the thermal engines required for VMS formation.

5.2 Petrological insights about VMS endowment

By examining the magmatic framework over time, we identified significant variability and contrasting geochemical signatures between the BRG and S-R assemblage. The way these signatures are distributed highlights the complexity of Archean magmatic systems and sets them apart from modern tectonic environments, where geochemical patterns are typically used to directly infer tectonic settings. In present-day systems, similar arc-like geochemical traits – particularly those resembling the calc-alkaline signatures identified in this study – are generally linked to long-lived, stable arc settings (e.g., Moyen and Laurent, 2018). In contrast, our geochemical modeling suggests that the diversity observed in the Abitibi assemblages results from interactions between mantle-derived magmas (tholeiitic basalts) and a TTG-like end member, acting both as pre-existing contaminant (assimilation) and as a coeval TTG melt (mixing) generated during volcanism.

This interaction underscores the remarkable complexity of the magmatic systems required to sustain such processes and to generate the evolved felsic compositions we observe today. In the case of the BRG, I argue that its bimodal magmatism, prolonged magmatic activity during emplacement, and the influence of deep transcrustal structures (Jorgensen et al., 2022) played a central role in shaping its exceptional VMS endowment. Although BRG magmatism is less volumetrically extensive than that of the S-R assemblage – ranking third in areal coverage within the Abitibi, alongside the Kidd-Munro assemblage – the fact that magmatic activity persisted for nearly nine million years strongly points to the development of a transcrustal magmatic system.

This interpretation aligns with recent models of magmatic system evolution (e.g., Cashman et al., 2017; Karakas et al., 2017; Annen et al., 2025), which indicate that generating large volumes of evolved felsic magmas requires a transcrustal magmatic architecture. Such systems begin with the intrusion of mantle-derived magmas into the crust, followed by repeated episodes of magma extraction feeding mid-crustal intrusions where magmas stall, differentiate, and evolve. Over time, these reservoirs become the sources from which felsic magmas are extracted and give rise to high-level intrusions that act as thermal engines driving VMS deposition.

Ultimately, the persistent association between felsic magmatism and VMS deposits in the Archean reflects a prolonged and intricate magmatic history. Long-lived magmatism provided the thermal and compositional conditions necessary to produce abundant felsic magmas, which, in turn, played a fundamental role in enhancing the metallogenic fertility of the BRG.

5.3 Future directions

Some of the foundations established in this study are already being applied in ongoing work, such as that of Iles et al. (2025), who are focusing on understanding the remaining assemblages of the AGB. Their research will address key questions about additional geochemical signatures that our models could not fully explain, potentially refining or expanding the interpretations presented here. For example, different TTG compositions should be examined as contaminants or melts. This may reveal additional magmatic trends or hybridization pathways. Integrating these TTG variants into future modeling efforts could provide a more complete understanding of crust–mantle interactions and help identify magmatic processes that distinguish fertile from barren volcanic sequences.

The transcrustal magmatic system model adopted in this study typically integrates both intrusive and volcanic components. However, a critical future direction lies in better understanding the relationship between syn-volcanic intrusive systems and the associated volcanic compositions.

Integrating geochemical and petrological insights from intrusive magmatism with those from volcanic rocks could provide a more comprehensive understanding of Archean magmatic systems and, by extension, the processes driving metal endowment.

Finally, the insights gained from this study also contribute to broader questions about the nature of Archean tectonics. Future work should explore whether the magmatic and geodynamic processes observed are more comparable to modern-style plate tectonics or better align with alternative geodynamic models, such as the stagnant-lid hypothesis (e.g., Bédard, 2018).

6 REFERENCES

Agrawal, S., Guevara, M., and Verma, S.P., 2008. Tectonic Discrimination of Basic and Ultrabasic Volcanic Rocks through Log-Transformed Ratios of Immobile Trace Elements. International Geology Review. 50, 1057-1079.

Aitchison, J., 1986. The Statistical Analysis of Compositional Data. London, Chapman and Hall.

Albarède, F., 1995. Introduction to geochemical modeling, Cambridge University Press.

Allard, G.O., Caty, J.L., and Gobeil, A. 1985. The Archean supracrustal rocks of the Chibougamau area. In: Ayres, L.D., Thurston, P.D., Card, K.D. and Weber, W. (eds). Evolution of Archean Supracrustal Sequences. Geological Association of Canada; Special Paper 28, 55–63.

Anhaeusser, C.R., 2014. Archaean greenstone belts and associated granitic rocks – a review. Journal of African Earth Sciences, 100, 684-732.

Annen, C., 2009., From plutons to magma chambers: Thermal constraints on the accumulation of eruptible silicic magma in the upper crust. Earth and Planetary Science Letters, 284, 409–416.

Annen, C., Blundy, J.D., Leuthold, J. and Sparks, R.S.J., 2015. Construction and evolution of igneous bodies: Towards an integrated perspective of crustal magmatism. Lithos, 230, 206-221.

Annen, C., Weinberg, R.F., Moyen, J.F. and Cazabet, R., 2025. A complex system approach to magmatism. Nature Reviews Earth and Environment, 6, 535–548.

Arndt, N.T., 1986. Differentiation of komatiite flows. Journal of Petrology, 27, 279-301.

Arndt, N.T., 1994. Chapter 1 Archean Komatiites. Developments in Precambrian Geology, 11, 11-44.

Arndt, N.T., and Jenner, G. A., 1986. Crustally contaminated komatiites and basalts from Kambalda, Western Australia. Chemical geology, 56, 229-255.

Asimow, P.D. and Ghiorso, M.S., 1998. Algorithmic modifications extending MELTS to calculate subsolidus phase relations. American Mineralogist, 83, 1127-1132.

Ayer, J., Amelin, Y., Corfu, F., Kamo, S., Ketchum, J., Kwok, K., and Trowell, N., 2002. Evolution of the southern Abitibi greenstone belt based on U–Pb geochronology: autochthonous volcanic construction followed by plutonism, regional deformation and sedimentation. Precambrian Research, 115, 63–95.

Ayer, J., Thurston, P., Bateman, R., Dube, B., Gibson, H., Hamilton, M., Hathway, B., Hocker, S. M., Houlé, M., Hudak, G., Ispolatov, V., Lafrance, B., Lesher, M., MacDonald, P.J., Peloquin, A., Piercey, S., Reed, L. E., and Thompson, P. H., 2005. Overview of results from the greenstone architecture project: discover Abitibi initiative. Ontario Geological Survey. Open File Report 6154.

Ayer, J.A., Dubé, B., Goodfellow, W.D., Ross, P.-S., Bleeker, W., Taylor, B.E., ... Van Breemen, O., 2007. The Abitibi Greenstone Belt: Update of the Precambrian geoscience section program, the targeted geoscience initiative III Abitibi and deep search projects; In Summary of field work and other activities 2007. Ontario Geological Survey. Open File Report 6213.

Bachmann, O., and Bergantz, G.W., 2006. Gas percolation in upper-crustal silicic crystal mushes as a mechanism for upward heat advection and rejuvenation of near-solidus magma bodies. Journal of Volcanology and Geothermal research, 149, 85-102.

Barnes, S.J. and Van Kranendonk, M.J., 2014. Archean andesites in the east Yilgarn craton, Australia: Products of plume-crust interaction? Lithosphere, 6, 80-92.

Barnes, S.J., Williams, M., Smithies, R.H., Hanski, E., and Lowrey, J.R., 2021. Trace element contents of mantle-derived magmas through time. Journal of Petrology 62 , article p.egab024.

Barrett, T.J. and MacLean, W.H., 1994. Mass changes in hydrothermal alteration zones associated with VMS deposits of the Noranda area. Exploration and Mining Geology, 3, 131-160.

Barrett, T. J., Ayer, J. A., Ordóñez-Calderón, J. C. and Hamilton, M. A., 2013. Geological mapping and compilation of the Burntbush–Normétal volcanic belt, Abitibi greenstone belt, Ontario–Quebec. Ontario Geological Survey, Miscellaneous Release—Data 299.

Barrie, C. T., 1999. The Kidd–Munro extension project: Geology of the Munro north area; in Summary of Field Work and Other Activities 1999. Ontario Geological Survey. Open File Report 6000.

Barrie, C. T., and Hannington, M. D., 1999. Classification of volcanic-associated massive sulfide deposits based on host-rock composition. Reviews in Economic Geology 8, 1-11.

Bédard, J.H., 2006. A catalytic delamination-driven model for coupled genesis of Archaean crust and sub-continental lithospheric mantle. Geochimica et Cosmochimica Acta, 70, 1188-1214.

Bédard, J.H., 2018. Stagnant lids and mantle overturns: Implications for Archaean tectonics, magma genesis, crustal growth, mantle evolution, and the start of plate tectonics. Geoscience Frontiers 9, 19-49.

Bédard, J.H., 2024. A gradual Proterozoic transition from an unstable stagnant lid to the modern plate tectonic system. Journal of the Geological Society, 181, 2024-023.

Bédard, J.H., and Harris, L.B., 2014. Neoarchean disaggregation and reassembly of the Superior craton. Geology, 42, 951-954.

Bédard, J.H., Harris, L.B., and Thurston, P.C., 2013. The hunting of the snArc. Precambrian Research. 229, 20-48.

Benn, K., 2006. Tectonic delamination of the lower crust during Late Archean collision of the Abitibi-Opatica and Pontiac terranes, Superior Province, Canada. American Geophysical Union. Geophysical Monograph 164, 267-282.

Benn, K. and Moyen, J.F., 2008. The Late Archean Abitibi-Opatica terrane, Superior Province: A modified oceanic plateau. In: Condie, K.C. Pease V. (eds) When Did Plate Tectonics Begin on Planet Earth? Geological Society of America, 440, 173-197.

Berger, B.R., Ayer, J.A., McNicoll, V.J., and Bleeker, W., 2007. The Kidd–Munro project: Stratigraphy of the Kidd–Munro Assemblage in Prosser township and area based on geology, geochemistry and new geochronology; in Summary of Field Work and Other Activities 2007. Ontario Geological Survey. Open File Report 6213.

Black, B.A., Karlstrom, L., and Mather, T.A., 2021. The life cycle of large igneous provinces. Nature Reviews Earth and Environment, 2, 840–857.

Bohrson, W.A., Spera, F.J., Ghiorso, M.S., Brown, G.A., Creamer, J.B. and Mayfield, A., 2014. Thermodynamic model for energy-constrained open-system evolution of crustal magma bodies undergoing simultaneous recharge, assimilation and crystallization: The magma chamber simulator. Journal of Petrology, 55, 1685-1717.

Bohrson, W.A., Spera, F.J., Heinonen, J.S., Brown, G.A., Scruggs, M.A., Adams, J.V., Takach, M.K., Zeff, G., and Suikkanen, E., 2020. Diagnosing open-system magmatic processes using the Magma Chamber Simulator (MCS): part I—major elements and phase equilibria. Contributions to Mineralogy and Petrology, 175, article 104.

Capdevila, R., Goodwin, A.M., Ujike, O. and Gorton, M.P., 1982. Trace-element geochemistry of Archean volcanic rocks and crystal growth in southwestern Abitibi Belt, Canada. Geology, 10, 418-422.

Card, K., 1990. A review of the Superior Province of the Canadian Shield, a product of Archean accretion. Precambrian Research, 48, 99-156.

Card, K., and Ciesielski, A., 1986. DNAG# 1. Subdivisions of the Superior province of the Canadian shield. Geoscience Canada, 13, 5-13.

Cashman, K. V., Sparks, R. S. J., and Blundy, J. D., 2017. Vertically extensive and unstable magmatic systems: a unified view of igneous processes. Science, 355, article eaag3055.

Chown, E.H., Daigneault, R., Mueller, W. and Mortensen, J.K., 1992. Tectonic evolution of the northern volcanic zone, Abitibi belt, Quebec. Canadian Journal of Earth Sciences, 29, 2211-2225.

Condie, K.C., 1986. Origin and early growth rate of continents: Precambrian Research, 32, 261-278.

Condie, K.C., 2005. High field strength element ratios in Archean basalts: a window to evolving sources of mantle plumes? Lithos, 79, 491–504.

Corfu, F., 1993. The evolution of the southern Abitibi greenstone belt in light of precise U-Pb geochronology. Economic Geology, 88, 1323–1340.

Couture, J.F. and Goutier, J., 1996. Métallogénie et évolution tectonique de la région de Rouyn-Noranda. Ministère des Ressources naturelles du Québec, MB 96-06, 102.

Cox, D.P., and Singer, D.A., 1986. Mineral deposit models. USGS Bulletin 1693,189-188.

Daigneault, R., Mueller, W.U. and Chown, E.H., 2002. Oblique Archean subduction: accretion and exhumation of an oceanic arc during dextral transpression, Southern Volcanic Zone, Abitibi Subprovince Canada. Precambrian Research, 115, 261-290.

Daigneault, R., Mueller, W., and Chown, E., 2004. Abitibi greenstone belt plate tectonics: the diachronous history of arc development, accretion and collision. Developments in Precambrian Geology, 12, 88-103.

Danyushevsky, L.V., 2001. The effect of small amounts of H2O on crystallisation of mid-ocean ridge and backarc basin magmas. Journal of Volcanology and Geothermal Research, 110, 265-280.

Daoudene, Y., Tremblay, A., Ruffet, G. and Leclerc, F., 2022. The Abitibi-Opatica transition, Superior Province, Quebec, Canada: structural analysis, 40Ar/39Ar thermochronology and implications for Archean tectonics. Precambrian Research, 379, 106803.

David, J., Davis, D. W., Dion, C., Goutier, J., Legault, M., and Roy, P., 2007. Datations U-Pb effectuées dans la Sous-province de l'Abitibi en 2005-2006. Ministère des Ressources naturelles et de la Faune, Québec. Report number: RP 2007-01.

David, J., McNicol, V., Simard, M., Bandyayera, D., Hammouche, H., Goutier, J., Pilote, P., Rhéaume, P., Leclerc, F., and Dion, C. 2011. Datations effectuées dans les provinces du Supérieur et de Churchill en 2009−2010. Ministère des Ressources naturelles et de la Faune. Report number: RP 2011-02.

Davis, D.W., David, J., Dion, C., Gonfler, J., Bandyayera, D., Rhéaume, P., and Roy, P., 2005. Datations U-Pb effectuées en support aux travaux de cartographie géologique et de compilation géoscientifique du SGNO (2003-2004). Ministère des Ressources naturelles et de la Faune. Report number: RP 2005-02.

Davis, D.W., Simard, M., Hammouche, H., Bandyayera, D., Goutier, J., Pilote, P., Leclerc, F., and Dion, C., 2014. Datations U-Pb effectuées dans les provinces du Supérieur et de Churchill en 2011-2012. Ministère des Ressources naturelles et de la Faune. Report number: RP 2014-05.

De Campos, C.P., Perugini, D., Ertel-Ingrisch, W., Dingwell, D.B., and Poli, G., 2011. Enhancement of magma mixing efficiency by chaotic dynamics: an experimental study. Contributions to Mineralogy and Petrology, 161, 863–881.

De Rosen-Spence, A.F., 1976. Stratigraphy, Development and Petrogenesis of the Central Noranda Volcanic Pile, Noranda, Quebec. Ph.D. Thesis, Univ. of Toronto, 116 pp.

Debreil, J.-A., 2014, Évolution volcanologique et chimico-stratigraphique du district minier de Matagami, Sous-province de l'Abitibi, Québec: Unpublished PhD thesis, Quebec City, Canada, Institut national de la recherche scientifique, 279.

Debreil, J.A., Ross, P.-S. and Mercier-Langevin, P., 2018. The Matagami district, Abitibi Greenstone Belt, Canada: volcanic controls on Archean volcanogenic massive sulfide deposits associated with voluminous felsic volcanism. Economic Geology, 113, 891-910.

Dimroth, E., Imreh, L., Goulet, N. and Rocheleau, M., 1983. Evolution of the south-central segment of the Archean Abitibi belt, Quebec. Part II: Tectonic evolution and geomechanical model. Canadian Journal of Earth Sciences, 20,1355-1373.

Dostal, J., and Mueller, W.U., 1997. Komatiite Flooding of A Rifted Archean Rhyolitic Arc Complex: Geochemical Signature and Tectonic Significance of the Stoughton-Roquemaure Group, Abitibi Greenstone Belt, Canada. The Journal of Geology, 105, 545–564.

Dostal, J., and Mueller, W.U., 2013. Deciphering an Archean mantle plume: Abitibi greenstone belt, Canada. Gondwana Research, 23, 493–505.

Dubé, B., and Mercier-Langevin, P., 2020. Chapter 32: Gold Deposits of the Archean Abitibi Greenstone Belt, Canada. In: Sillitoe, R. H., Goldfarb, R. J., Robert, F., Simmons, S. F. (eds) Geology of the World's Major Gold Deposits and Provinces. Society of Economic Geologists 23, 669–708.

Dubé, B., Mercier-Langevin, P., Hannington, M., Lafrance, B., Gosselin, G., and Gosselin, P., 2007a. The LaRonde Penna world-class Au-rich volcanogenic massive sulfide deposit, Abitibi, Québec: Mineralogy and geochemistry of alteration and implications for genesis and exploration. Economic Geology, 102, 633-666.

Dubé, B., Gosselin, P., Mercier-Langevin, P., Hannington, M., and Galley, A., 2007b. Gold-rich volcanogenic massive sulphide deposits. In: Goodfellow, W.D. (Ed) Mineral deposits of Canada: a synthesis of major deposits types, district metallogeny, the evolution of geological provinces, and exploration methods. Geological Association of Canada, Mineral Deposits Division, Special Publication 5, 75-94.

Dubé, B., Mercier-Langevin, P., Kjarsgaard, I., Hannington, M., Bécu, V., Côté, J., Moorhead, J., Legault, M., and Bédard, N., 2014. The Bousquet 2-Dumagami world-class Archean Au-rich volcanogenic massive sulfide deposit, Abitibi, Quebec: Metamorphosed submarine advanced argillic alteration footprint and genesis. Economic Geology, 109, 121-166.

Dufek, J., and Bergantz, G.W., 2005. Lower crustal magma genesis and preservation: a stochastic framework for the evaluation of basalt–crust interaction. Journal of Petrology, 46, 2167-2195.

Eakins, P.R., 1972, Roquemaure Township: Quebec Dep Nat. Res. Geol. Rept. 150, 69.

Eckstrand, O. R., Sinclair, W., and Thorpe, R., 1995. Geology of Canadian mineral deposit types, Geological Survey of Canada 8.

Fassbender, M.L., Hannington, M., Stewart, M., Brandl, P.A., Baxter, A.T., and Diekrup, D., 2023. Geochemical Signatures of Felsic Volcanic Rocks in Modern Oceanic Settings and Implications for Archean Greenstone Belts. Economic Geology, 118, 319-345.

Fassbender, M.L., Hannington, M.D., Baxter, A.T., Diekrup, D., Stewart, M. and Brandl, P.A., 2024. Geochemical signatures of mafic volcanic rocks in modern oceanic settings and implications for Archean mafic magmatism. Economic Geology, 119, 445-470.

Faure, S., Godey, S., Fallara, F. and Trépanier, S., 2011. Seismic architecture of the Archean North American mantle and its relationship to diamondiferous kimberlite fields. Economic Geology, 106, 223-240.

Feig, S.T., Koepke, J., and Snow, J.E., 2006. Effect of water on tholeiitic basalt phase equilibria: an experimental study under oxidizing conditions. Contributions to Mineralogy and Petrology 152, 611-638.

Fowler, A.D., and Jensen, L.S., 1989. Quantitative trace-element modelling of the crystallization history of the Kinojévis and Blake River groups, Abitibi Greenstone Belt, Ontario. Canadian Journal of Earth Sciences, 26, 1356-1367.

Franklin, J.M., Lydon, J.W., and Sangster, D.F., 1981. Volcanic-associated massive sulfide deposits. In: Skinner, B. J. (Ed). Seventy-Fifth Anniversary Volume. Economic Geology Publishing Company, 485-627.

Franklin, J., Gibson, H., Jonasson, I., and Galley, A., 2005. Volcanogenic massive sulfide deposits. In: Hedenquist, J. W., Thompson, J. F. H., Goldfarb, R. J., Richards, J. P. (eds). One Hundredth Anniversary Volume. Society of Economic Geologists, 523-560.

Frost, B.R., Lindsley, D.H. and Andersen, D.J., 1988. Fe-Ti oxide-silicate equilibria; assemblages with fayalitic olivine. American Mineralogist, 73, 727-740.

Gaboury, D., and Daigneault, R., 1999. Evolution from sea floor-related to sulfide-rich quartz vein-type gold mineralization during deep submarine volcanic construction; the Geant Dormant gold mine, Archean Abitibi Belt, Canada. Economic Geology, 94, 3–22.

Galley, A. G., 2003. Composite synvolcanic intrusions associated with Precambrian VMS-related hydrothermal systems. Mineralium Deposita, 38, 443-473.

Galley, A.G., Hannington, M. D., and Jonasson, I., 2007. Volcanogenic massive sulphide deposits. In: Goodfellow, W.D. (Ed) Mineral deposits of Canada: a synthesis of major deposits types, district metallogeny, the evolution of geological provinces, and exploration methods, Geological Association of Canada, Mineral Deposits Division, Special Publication 5, 141-161.

Galley, A.G., and Lafrance, B., 2014. Setting and evolution of the Archean synvolcanic Mooshla Intrusive Complex, Doyon-Bousquet-LaRonde mining camp, Abitibi greenstone belt: Emplacement history, petrogenesis, and implications for Au metallogenesis. Economic Geology, 109, 205-229.

Gélinas, L. and Ludden, J.N., 1984. Rhyolitic volcanism and the geochemical evolution of an Archaean central ring complex: the Blake River Group volcanics of the southern Abitibi belt, Superior province. Physics of the Earth and Planetary Interiors, 35, 77-88.

Gélinas, L., Mellinger, M. and Trudel, P., 1982. Archean mafic metavolcanics from the Rouyn–Noranda district, Abitibi Greenstone Belt, Quebec. 1. Mobility of the major elements. Canadian Journal of Earth Sciences, 19, 2258-2275.

Gélinas, L., Trudel, P., and Hubert, C., 1984. Chemostratigraphic division of the Blake River Group, Rouyn–Noranda area, Abitibi, Quebec. Canadian Journal of Earth Sciences, 21, 220-231.

Ghiorso, M.S., and Sack, R.O., 1995. Chemical mass transfer in magmatic processes IV. A revised and internally consistent thermodynamic model for the interpolation and extrapolation of liquid-solid equilibria in magmatic systems at elevated temperatures and pressures. Contributions to Mineralogy and Petrology, 119, 197–212.

Ghiorso, M.S. and Gualda, G.A., 2015. An H_2O–CO_2 mixed fluid saturation model compatible with rhyolite-MELTS. Contributions to Mineralogy and Petrology, 169, article 53.

Ghiorso, M. S., Hirschmann, M.M., Reiners, P.W., and Kress, V.C., 2002. The pMELTS: A revision of MELTS for improved calculation of phase relations and major element partitioning related to partial melting of the mantle to 3 GPa. Geochemistry, Geophysics, Geosystems, 3, 1–35.

Gibson, H., Watkinson, D.H. and Comba, C.D.A., 1983. Silicification; hydrothermal alteration in an Archean geothermal system within the Amulet Rhyolite Formation, Noranda, Quebec. Economic Geology, 78, 954-971.

Gibson, H., 1989. The Mine Sequence of the Central Noranda Volcanic Complex: Geology, Alteration, Massive Sulphide Deposits and Volcanological Reconstruction. PhD thesis, Carleton University, Ottawa.

Gibson, H., and Watkinson, D., 1990. Volcanogenic massive sulphide deposits of the Noranda cauldron and shield volcano, Quebec. Canadian Institute of Mining and Metallurgy 43, 119-132.

Gibson, H., Morton, R.L., and Hudak, G.J., 1999. Submarine volcanic processes, deposits, and environments favorable for the location of volcanic-associated massive sulfide deposits. In: Barrie, T., Hannington M. D., (eds). Volcanic Associated Massive Sulfide Deposits: Processes and Examples in Modern and Ancient Settings. Society of Economic Geologists 8, 13-51.

Gibson, H., Galley, A., and Goodfellow, W., 2007. Volcanogenic massive sulphide deposits of the Archean, Noranda District, Quebec. In: Goodfellow, W.D. (Ed) Mineral deposits of Canada: a synthesis of major deposits types, district metallogeny, the evolution of geological provinces, and exploration methods, Geological Association of Canada, Mineral Deposits Division, Special Publication 5, 533-552.

Gifkins, C.C., Herrmann, W., and Large, R.R., 2005. Altered volcanic rocks: a guide to description and interpretation. Centre for Ore Deposit Research.

Goodwin, A.M., 1982. Archean volcanoes in southwestern Abitibi belt, Ontario and Quebec: form, composition, and development. Canadian Journal of Earth Sciences, 19, 1140-1155.

Goodwin, A.M. and Smith, I.E.M., 1980. Chemical discontinuities in Archean metavolcanic terrains and the development of Archean crust. Precambrian Research, 10, 301-311.

Gorman, B.E., Pearce, T.H. and Birkett, T.C., 1978. On the structure of Archean greenstone belts. Precambrian Research, 6, 23-41.

Goutier, J., 1997. Géologie de la région de Destor (32D/07-200-0201). Ministère des Ressources naturelles, Québec. Report number : RG 96-13.

Goutier, J., and Melançon, M., 2007. Compilation géologique de la Sous-province de l'Abitibi (version préliminaire). Ministère des Ressources naturelles et de la faune. Report number: RP 2010-04.

Goutier, J., Rhéaume, P., and Davis, D. W., 2004. Géologie de la région du lac Olga (32F/14). Ministère de l'Énergie et des Ressources naturelles. Report number: RG 2005-05.

Gualda, G.A.R., Ghiorso, M.S., Lemons, R.V., and Carley, T.L., 2012. Rhyolite-MELTS: a modified calibration of MELTS optimized for silica rich, fluid-bearing magmatic systems. Journal of Petrology, 53, 875–890.

Hannington, M.D., de Ronde, C.D., and Petersen, S., 2005. Sea-floor tectonics and submarine hydrothermal systems. In Hedenquist, J. W., Thompson, J. F. H., Goldfarb, R. J., Richards, J.P. (eds). One Hundredth Anniversary Volume. Society of Economic Geologists, 111-142.

Hannington, M.D., Poulsen, K.H., Thompson, J.F.H., and Sillitoe, R.H., 1997. Volcanogenic gold in the massive sulfide environment. In: Barrie, C. T., Hannington, M. D., (eds). Volcanic Associated Massive. Society of Economic Geologists 8, 325–356.

Hart, T.R., Gibson, H., and Lesher, C.M., 2004. Trace element geochemistry and petrogenesis of felsic volcanic rocks associated with volcanogenic massive Cu-Zn-Pb sulfide deposits. Economic Geology, 99, 1003–1013.

Hannington, M.D., Galley, A.G., Herzig, P. and Petersen, S., 1998. Comparison of the TAG mound and stockwork complex with Cyprus-type massive sulfide deposits. In: Proceedings of the Ocean Drilling Program: Scientific Results, 158, 389-415.

Haugaard, R., Della Justina, F., Roots, E., Cheraghi, S., Vayavur, R., Hill, G., Snyder, D., Ayer, J., Naghizadeh, M., and Smith, R., 2021. Crustal-scale geology and fault geometry along the gold-endowed Matheson transect of the Abitibi Greenstone Belt. Economic Geology 116, 1053-1072.

Heinonen, J.S., Bohrson, W.A., Spera, F. J., Brown, G.A., Scruggs, M.A., and Adams, J.V., 2020. Diagnosing open-system magmatic processes using the Magma Chamber Simulator (MCS): part II—trace elements and isotopes. Contributions to Mineralogy and Petrology, 175, article 105.

Herzberg, C., 2022. Understanding the Paleoproterozoic Circum-Superior Large Igneous Province constrains the thermal properties of Earth's mantle through time. Precambrian Research, 375, article 106671.

Herzberg, C., and Asimow, P.D., 2015. PRIMELT3 MEGA.XLSM software for primary magma calculation: Peridotite primary magma MgO contents from the liquidus to the solidus. Geochemistry, Geophysics, Geosystems, 16, 563–578.

Herzberg, C., and O'Hara, M.J., 2002. Plume-Associated Ultramafic Magmas of Phanerozoic Age. Journal of Petrology, 43, 1857–1883.

Herzberg, C., Condie, K., and Korenaga, J., 2010. Thermal history of the Earth and its petrological expression. Earth and Planetary Science Letters, 292: 79–88.

Herzberg, C., Asimow, P.D., and Hernández-Montenegro, J.D., 2023. The Meaning of Pressure for Primary Magmas: New Insights From PRIMELT3-P. Geochemistry Geophysics Geosystems, 24, article e2022GC010657.

Hildreth, W., and Moorbath, S., 1988. Crustal contributions to arc magmatism in the Andes of Central Chile. Contributions to Mineralogy and Petrology, 98, 455-489.

Holder, R M., Viete, D.R., Brown, M., and Johnson, T.E., 2019. Metamorphism and the evolution of plate tectonics. Nature, 572, 378–381.

Hollis, S.P., Yeats, C.J., Wyche, S., Barnes, S.J., Ivanic, T.J., Belford, S.M., Davidson, G.J., Roache, A.J. and Wingate, M.T.D., 2015. A review of volcanic-hosted massive sulfide (VHMS) mineralization in the Archaean Yilgarn Craton, Western Australia: Tectonic, stratigraphic and geochemical associations. Precambrian Research, 260,113-135.

Hotelling, H., 1933. Analysis of a complex of statistical variables into principal components. Journal of Educational Psychology, 24, 417.

Houlé, M.G., Lesher, C.M., and Préfontaine, S., 2017. Physical Volcanology of Komatiites and Ni-Cu-(PGE) Deposits of the Southern Abitibi Greenstone Belt. In: Monecke, T., Mercier-Langevin, P., Dubé, B. (eds). Archean Base and Precious Metal Deposits, Southern Abitibi Greenstone Belt, Canada. Reviews in Economic Geology. 19, 103–132.

Hubert, C., Trudel, P. and Gélinas, L., 1984. Archean wrench fault tectonics and structural evolution of the Blake River Group, Abitibi Belt, Quebec. Canadian Journal of Earth Sciences, 21, 1024-1032.

Humphreys, M.C., Namur, O., Bohrson, W.A., Bouilhol, P., Cooper, G.F., Cooper, K.M., Huber, C., Lissenberg, C. J., Morgado, E. and Spera, F. J., 2025. Crystal mush processes and crustal magmatism. Nature Reviews Earth & Environment, 6, 401–416.

Husen, A., Almeev, R.R. and Holtz, F., 2016. The effect of H_2O and pressure on multiple saturation and liquid lines of descent in basalt from the Shatsky Rise. Journal of Petrology, 57, 309-344.

Huston, D. L., Pehrsson, S., Eglington, B.M., and Zaw, K., 2010. The geology and metallogeny of volcanic-hosted massive sulfide deposits: Variations through geologic time and with tectonic setting. Economic Geology, 105, 571-591.

Iles, K.A., Ross, P.-S. and Vite-Sánchez, O., 2025. The interplay of crystal fractionation, magma recharge, assimilation and mixing in Archean volcanic systems revealed in the geochemical diversity of the Deloro assemblage, Abitibi Greenstone Belt. Lithos, 514-515, article 108161.

Irvine, T.N., and Baragar, W.R.A., 1971. A guide to the chemical classification of the common volcanic rocks. Canadian Journal of Earth Sciences, 8, 523–548.

Ishikawa, Y., Sawaguchi, T., Iwaya, S., and Horiuchi, M., 1976. Delineation of prospecting targets for kuroko deposits basedon modes of volcanism of underlying dacite and alteration halos. Mining Geology, 26, 105-117.

Jenner, G.A., 1996. Trace element geochemistry of igneous rocks: geochemical nomenclature and analytical geochemistry. In: Wyman, D.A. (Ed). Trace element geochemistry of volcanic rocks: applications for massive sulphide exploration. Geological Association of Canada, 51-77.

Jensen, L.S., 1976. A New Cation Plot for Classifying Subalkalic Volcanic Rocks. Ontario Division of Mines. Report number: Miscellaneous Paper, 66.

Jolliffe, I.T., and Cadima, J., 2016. Principal component analysis: a review and recent developments. Philosophical transactions of the royal society A: Mathematical, Physical and Engineering Sciences, 374, article 20150202.

Jolly, W., 1978. Metamorphic history of the Archean Abitibi belt. In: Fraser, J. A., Heywood, W. W. (eds.). Metamorphism in the Canadian Shield. Geological Survey of Canada, 78- 10, 63-78.

Jorgensen, T.R.C. and Gibson, H.L., 2024. Lithological compilation of the Abitibi subprovince, Superior Province, Canada. Metal Earth Project, Mineral Exploration Research Centre. https://metalearth.files.com/f/81ca7963c83475a6. [Accessed 1st June 2024].

Jorgensen, T.R., Gibson, H., Roots, E.A., Vayavur, R., Hill, G.J., Snyder, D.B., and Naghizadeh, M., 2022. The implications of crustal architecture and transcrustal upflow zones on the metal endowment of a world-class mineral district. Scientific Reports, 12, 1-10.

Juster, T.C., Grove, T.L., and Perfit, M.R., 1989. Experimental constraints on the generation of FeTi basalts, andesites, and rhyodacites at the Galapagos Spreading Center, 85 W and 95 W. Journal of Geophysical Research, 94, 9251-9274.

Karakas, O., Degruyter, W., Bachmann, O., and Dufek, J., 2017. Lifetime and size of shallow magma bodies controlled by crustal-scale magmatism. Nature Geoscience, 10, 446–450.

Karakas, O., Wotzlaw, J. F., Guillong, M., Ulmer, P., Brack, P., Economos, R., Bergantz, G.W., Sinigoi, S., and Bachmann, O., 2019. The pace of crustal-scale magma accretion and differentiation beneath silicic caldera volcanoes. Geology, 47, 719-723.

Kent, A.J., Darr, C., Koleszar, A.M., Salisbury, M.J., and Cooper, K.M., 2010. Preferential eruption of andesitic magmas through recharge filtering. Nature geoscience, 3, 631-636.

Kerrich, R., Wyman, D., Fan, J., and Bleeker, W., 1998. Boninite series: low Ti-tholeiite associations from the 2.7 Ga Abitibi greenstone belt: Earth and Planetary Science Letters, 164, 303-316.

Kerrich, R., Polat, A., Wyman, D., and Hollings, P., 1999. Trace element systematics of Mg-, to Fe-tholeiitic basalt suites of the Superior Province: implications for Archean mantle reservoirs and greenstone belt genesis. Lithos, 46, 163–187.

Kerrich, R., Polat, A., and Xie, Q., 2008. Geochemical systematics of 2.7 Ga Kinojevis Group (Abitibi), and Manitouwadge and Winston Lake (Wawa) Fe-rich basalt–rhyolite associations: Backarc rift oceanic crust? Lithos, 101, 1-23.

Krushnisky, A., Mercier-Langevin, P., Ross, P.-S., Goutier, J., McNicoll, V., Moore, L., Monecke, T., and Pilote, C., 2023. Geology and Controls on Gold Enrichment at the Horne 5 Deposit and Implications for the Architecture of the Gold-Rich Horne Volcanogenic Massive Sulfide Complex, Abitibi Greenstone Belt, Canada. Economic Geology, 118, 285-318.

Lacroix, S., 1994. Géologie de la partie ouest du sillon Harricana-Turgeon, Abitibi. Ministère des Ressources naturelles du Québec. Report number: MB 94-54.

Lafrance, B., Moorhead, J., and Davis, D. W., 2003. Cadre géologique du camp minier de Doyon-Bousquet-LaRonde. Ministère des Ressources naturelles, de la Faune et des Parcs, Québec. Report number: EP 2002-07.

Lafrance, B., Mueller, W. U., Daigneault, R., and Dupras, N., 2000. Evolution of a submerged composite arc volcano: volcanology and geochemistry of the Normétal volcanic complex, Abitibi greenstone belt, Québec, Canada. Precambrian Research, 101, 277–311.

Laflèche, M.R., Dupuy, C. and Bougault, H., 1992a. Geochemistry and petrogenesis of Archean mafic volcanic rocks of the southern Abitibi Belt, Québec. Precambrian Research, 57, 207-241.

Lafleche, M.R., Dupuy, C. and Dostal, J., 1992b. Tholeiitic volcanic rocks of the late Archean Blake River Group, southern Abitibi greenstone belt: origin and geodynamic implications. Canadian Journal of Earth Sciences, 29, 1448-1458.

Lang, M., Zhang, Z., Chen, Z., Cheng, Z., Santosh, M. and Kusky, T.M., 2023. Classification and nomenclature of volcanic rocks using immobile elements: a novel approach based on big data analysis. Lithos, 454, p.107274.

Large, R.R., Gemmell, J.B., Paulick, H., and Huston, D.L., 2001. The alteration box plot: A simple approach to understanding the relationship between alteration mineralogy and lithogeochemistry associated with volcanic-hosted massive sulfide deposits. Economic Geology, 96, 957-971.

Laumonier, M., Scaillet, B., Pichavant, M., Champallier, R., Andujar, J., and Arbaret, L., 2014. On the conditions of magma mixing and its bearing on andesite production in the crust. Nature Communications, 5, article 5607.

Laurent, O., Björnsen, J., Wotzlaw, J.F., Bretscher, S., Pimenta Silva, M., Moyen, J.F., Ulmer, P. and Bachmann, O., 2020. Earth's earliest granitoids are crystal-rich magma reservoirs tapped by silicic eruptions. Nature Geoscience, 13, 63-169.

Leclair, A., Berclaz, A., and David, J., 2004. The northeastern Superior Province in Quebec's far north: A Regional Synthesis. In: LITHOPROBE-The Celebratory Conference 2004, 12-15.

Leclerc, F., Bédard, J.H., Harris, L.B., McNicoll, V.J., Goulet, N., Roy, P., and Houle, P., 2011. Tholeiitic to calc-alkaline cyclic volcanism in the Roy Group, Chibougamau area, Abitibi Greenstone Belt—revised stratigraphy and implications for VHMS exploration. Canadian Journal of Earth Sciences, 48, 661-694.

Leclerc, F., Harris, L.B., Bédard, J.H., Van Breemen, O. and Goulet, N., 2012. Structural and Stratigraphic Controls on Magmatic, Volcanogenic, and Shear Zone-Hosted Mineralization in

the Chapais-Chibougamau Mining Camp, Northeastern Abitibi, Canada. Economic Geology, 107, 963-989.

Legault, M., Gauthier, M., Jébrak, M., Davis, D. W., and Baillargeon, F., 2002. Evolution of the subaqueous to near-emergent Joutel volcanic complex, Northern Volcanic Zone, Abitibi Subprovince, Quebec, Canada. Precambrian Research, 115, 187–221.

Lesher, C.M., Goodwin, A. M., Campbell, I.H., and Gorton, M.P., 1986. Trace-element geochemistry of ore-associated and barren, felsic metavolcanic rocks in the Superior Province, Canada. Canadian Journal of Earth Sciences, 23, 222-237.

Lydon, J.W., 1996. Characteristics of volcanogenic massive sulphide deposits: Interpretations in terms of hydrothermal convection systems and magmatic hydrothermal systems. Boletin Geologico y Minera, 107, 215-264.

MacLean, W., and Barrett, T., 1993. Lithogeochemical techniques using immobile elements. Journal of Geochemical Exploration, 48, 109-133.

MacLean, W.H. and Kranidiotis, P., 1987. Immobile elements as monitors of mass transfer in hydrothermal alteration; Phelps Dodge massive sulfide deposit, Matagami, Quebec. Economic Geology, 82, 951-962.

MacLeod, C.J., Johan Lissenberg, C., and Bibby, L.E., 2013. “Moist MORB” axial magmatism in the Oman ophiolite: The evidence against a mid-ocean ridge origin. Geology, 41, 459-462.

Mahalanobis, P.C., 1936. Reprint: “On the Generalised Distance in Statistics.” 2018. Sankhyā: The Indian Journal of Statistics, Series A80, 1-7.

Martin, H., Smithies, R.H., Rapp, R., Moyen, J.F., and Champion, D., 2005. An overview of adakite, tonalite–trondhjemite–granodiorite (TTG), and sanukitoid: relationships and some implications for crustal evolution. Lithos, 79, 1-24.

Mathieu, L., Snyder, D.B., Bedeaux, P., Cheraghi, S., Lafrance, B., Thurston, P., and Sherlock, R., 2020. Deep into the Chibougamau area, Abitibi Greenstone Belt: structure of a neoarchean crust revealed by seismic reflection profiling. Tectonics, 39, article e2020TC006223.

McNicoll, V., Goutier, J., Dubé, B., Mercier-Langevin, P., Ross, P.-S., Dion, C., Monecke, T., Legault, M., Percival, J., and Gibson, H., 2014. U-Pb geochronology of the Blake River Group, Abitibi greenstone belt, Quebec, and implications for base metal exploration. Economic Geology, 109, 27-59.

MER-OGS, 1984. Lithostratigraphic map of the Abitibi subprovince: Ontario Geological Survey and Ministère de l’Énergie et des Ressources, Québec.

Mercier-Langevin, P., Dubé, B., Hannington, M. D., Richer-Laflèche, M., and Gosselin, G., 2007a. The LaRonde Penna Au-rich volcanogenic massive sulfide deposit, Abitibi greenstone belt, Quebec: Part II. Lithogeochemistry and paleotectonic setting. Economic Geology, 102, 611-631.

Mercier-Langevin, P., Dubé, B., Lafrance, B., Hannington, M., Galley, A., Moorehead, J., and Gosselin, P., 2007b. Metallogeny of the Doyon-Bousquet-LaRonde mining camp. Abitibi

Greenstone belt, Quebec. In: Goodfellow, W.D. (Ed) Mineral deposits of Canada: a synthesis of major deposits types, district metallogeny, the evolution of geological provinces, and exploration methods, Geological Association of Canada, Special Publication 5, 673-702.

Mercier-Langevin, P., Hannington, M.D., Dubé, B., and Bécu, V., 2011a. The gold content of volcanogenic massive sulfide deposits. Mineralium Deposita, 46, 509-539.

Mercier-Langevin, P., Goutier, J., Ross, P.-S., McNicoll, V., Monecke, T., Dion, C., Dubé, B., Thurston, P., Bécu, V., and Gibson, H., 2011b. The Blake River Group of the Abitibi greenstone belt and its unique VMS and gold-rich VMS endowment. Geological Survey of Canada. Open File 6869.

Mercier-Langevin, P., Houlé, M.G., Dubé, B., Monecke, T., Hannington, M.D., Gibson, H., and Goutier, J., 2012. A Special Issue on Archean Magmatism, Volcanism, and Ore Deposits: Part 1. Komatiite-Associated Ni-Cu-(PGE) Sulfide and Greenstone-Hosted Au Deposits: Preface. Economic Geology, 107, 745-753.

Mercier-Langevin, P., Gibson, H.L., Hannington, M.D., Goutier, J., Monecke, T., Dubé, B., and Houlé, M. G., 2014. A special issue on Archean magmatism, volcanism, and ore deposits: part 2. Volcanogenic massive sulfide deposits preface. Economic Geology, 109, 1-9.

Mercier-Langevin, P., Dubé, B., Houlé, M.G., Bécu, V., Sappin, A., Pilote, J., and Castonguay, S., 2023. Metallogeny of the Abitibi Greenstone Belt, Canada. In: Decrée (Ed). Metallic Resources 2, 63-141.

Migdisov, A., Williams-Jones, A.E., Brugger, J. and Caporuscio, F.A., 2016. Hydrothermal transport, deposition, and fractionation of the REE: Experimental data and thermodynamic calculations. Chemical Geology, 439, 13-42.

Mole, D., Thurston, P., Marsh, J., Stern, R., Ayer, J., Martin, L., and Lu, Y., 2021. The formation of Neoarchean continental crust in the south-east Superior Craton by two distinct geodynamic processes. Precambrian Research, 356, article 106104.

Mole, D., Frieman, B.M., Thurston, P.C., Marsh, J.H., Jorgensen, T.R.C., Stern, R.A., Martin, L.A.J., Lu, Y.J., and Gibson, H.L., 2022. Crustal architecture of the south-east Superior Craton and controls on mineral systems. Ore Geology Reviews, 148, article 105017.

Monecke, T., Petersen, S. and Hannington, M.D., 2014. Constraints on water depth of massive sulfide formation: evidence from modern seafloor hydrothermal systems in arc-related settings. Economic Geology, 109, 2079-2101.

Monecke, T., Gibson, H., Dubé, B., Laurin, J., Hannington, M., and Martin, L., 2008. Geology and volcanic setting of the Horne deposit, Rouyn-Noranda, Quebec: initial results of a new research project. Natural Resources Canada. Report number: Current Research 2008-9.

Monecke, T., Mercier-Langevin, P., Dubé, B., and Frieman, B., 2017. Geology of the Abitibi greenstone belt. Archean base and precious metal deposits, southern Abitibi greenstone belt, Canada. In: Monecke, T., Mercier-Langevin, P., Dubé, B. (Eds), Archean base and precious metal deposits, southern Abitibi greenstone belt, Canada. Reviews in Economic Geology 19, 7-49.

Morin, D., Jébrak, M., Bardoux, M. and Goulet, N., 1993. Pontiac metavolcanic rocks within the Cadillac tectonic zone, McWatters, Abitibi belt, Quebec. Canadian Journal of Earth Sciences, 30,1521-1531.

Morton, R.L., and Franklin, J.M., 1987. Two-fold classification of Archean volcanic-associated massive sulfide. Economic Geology, 82, 1057-1063.

Mosier, D.L.B., Singer, V.I., and Donald, A., 2009. Volcanogenic massive sulfide deposits of the world: Database and grade and tonnage models. U.S. Geological Survey. Open File Report 2009-1034.

Moyen, J.F. and Martin, H., 2012. Forty years of TTG research. Lithos, 148, 312-336.

Moyen, J.F. and Laurent, O., 2018. Archaean tectonic systems: A view from igneous rocks. Lithos, 302, 99-125.

MRNF, Ministère des Ressources naturelles et des Forêts. 2019. Formation de Deguisier. Lexique Stratigraphique Du Québec. https://gq.mines.gouv.qc.ca/lexique-stratigraphique/province-du-superieur/formation-de-deguisier/. [Accesed 9 Mar. 2025]

MRNF, Ministère des Ressources naturelles et des Forêts. 2022a. Groupe de Stoughton-Roquemaure. Lexique Stratigraphique Du Québec. from https://gq.mines.gouv.qc.ca/lexique-stratigraphique/province-du-superieur/groupe-de-stoughton-roquemaure/. [Accesed July 4, 2024]

MRNF, Ministère des Ressources naturelles et des Forêts. 2022b. Formation de Desboues. Lexique Stratigraphique Du Québec. https://gq.mines.gouv.qc.ca/lexique-stratigraphique/province-du-superieur/formation-de-desboues/. [Accesed 9 Mar. 2025]

MRNF, Ministère des Ressources naturelles et des Forêts. 2022c. Formation de Clermont-Disson. Lexique stratigraphique du Québec. https://gq.mines.gouv.qc.ca/lexique-stratigraphique/province-du-superieur/formation-de-clermont-disson/. [Accesed 9 Mar. 2025]

MRNF, Ministère des Ressources naturelles et des Forêts. 2024a. Formation de Bruneau. Lexique Stratigraphique Du Québec. https://gq.mines.gouv.qc.ca/lexique-stratigraphique/province-du-superieur/groupe-de-stoughton-roquemaure/. [Accesed 9 Mar. 2025]

MRNF, Ministère des Ressources naturelles et des Forêts. 2024b Formation de Blondeau. Lexique stratigraphique du Québec. https://gq.mines.gouv.qc.ca/lexique-stratigraphique/province-du-superieur/formation-de-blondeau. [Accesed August 4, 2024]

Mueller, W.U., Daigneault, R., Mortensen, J.K. and Chown, E.H., 1996. Archean terrane docking: upper crust collision tectonics, Abitibi greenstone belt, Quebec, Canada. Tectonophysics, 265, 27-150.

Nesbitt, R.W., Sun, S.S., and Purvis, A.C., 1979. Komatiites: geochemistry and genesis. The Canadian Mineralogist, 17, 165–186.

Oliver, J., Ayer, J., Dubé, B., Aubertin, R., Burson, M., Panneton, G., Friedman, R. and Hamilton, M., 2011. Structure, stratigraphy, U-Pb geochronology, and alteration characteristics of gold

mineralization at the Detour Lake gold deposit, Ontario, Canada. Exploration and Mining Geology, 20, 1.

Ontario Geological Survey, 2011. 1:250 000 scale bedrock geology of Ontario; Ontario Geological Survey, Report number: Miscellaneous Release–Data 126.

Ordóñez-Calderón J.C., 2013. Stratigraphic and structural investigation in the Burntbush area, district of Cochrane, Abitibi greenstone belt: Implications for mineral exploration. In: summary of field work and other activities 2010. Ontario Geological Survey. Open File Report 6260. 5-3.

O'Neill, H.S.C., 2016. The smoothness and shapes of chondrite-normalized rare earth element patterns in basalts. Journal of Petrology, 57, 1463-1508.

Palin, R.M., Santosh, M., Cao, W., Li, S.S., Hernández-Uribe, D. and Parsons, A., 2020. Secular metamorphic change and the onset of plate tectonics. Earth-Science Reviews, 207, 103172.

Paradis, S., 1990, Stratigraphy, volcanology and geochemistry of the New Vauze-Norbec area, Central Noranda volcanic complex, Québec, Canada: Ph.D. thesis, Ottawa, ON, Carleton University, 695.

Paradis, S., Ludden, J. and Gélinas, L., 1988. Evidence for contrasting compositional spectra in comagmatic intrusive and extrusive rocks of the late Archean Blake River Group, Abitibi, Quebec. Canadian Journal of Earth Sciences, 25, 134-144.

Pawlowsky-Glahn, V., and Egozcue, J.J., 2006. Compositional data and their analysis: an introduction. London, Geological Society, Special Publications, 264, 1-10.

Pearce, J.A., 1983. Role of the sub-continental lithosphere in magma genesis at active continental margins. In: Hawkesworth, C.J., Norry, M.J. (eds.). Continental Basalts and Mantle Xenoliths, Shiva. Cheshire, UK, 230-249.

Pearce, J. A., 1996. A user's guide to basalt discrimination diagrams. In: Wyman, D.A. (Ed.) Trace element geochemistry of volcanic rocks: applications for massive sulphide exploration 1996. Geological Association of Canada, Short Course Notes 12, 79-113.

Pearce, J. A., 2008. Geochemical fingerprinting of oceanic basalts with applications to ophiolite classification and the search for Archean oceanic crust. Lithos, 100, 14-48.

Pearce, J.A., Ernst, R.E., Peate, D.W., and Rogers, C., 2021. LIP printing: Use of immobile element proxies to characterize Large Igneous Provinces in the geologic record. Lithos, 392–393, article 106068.

Pearson, V., and Daigneault, R., 2009. An Archean megacaldera complex: the Blake River Group, Abitibi greenstone belt. Precambrian Research, 168, 66-82.

Pedregosa, F., Varoquaux, G., Gramfort, A., Michel, V., Thirion, B., Grisel, O., Blondel, M., Prettenhofer, P., Weiss, R., Dubourg, V., and Vanderplas, J., 2011. Scikit-learn: Machine learning in Python. Journal of machine Learning Research, 12, 2825-2830.

Péloquin, A.S., Verpaelst, P., Ludden, J.N., Dejou, B. and Gaulin, R., 2001. Stratigraphie de la partie ouest du Groupe de Blake River (Sous-province de l'Abitibi). Ministère des Ressources naturelles du Québec, ET 98-03, 98-03.

Péloquin, A.S., Piercey, S.J. and Hamilton, M.A., 2008. The Ben Nevis volcanic complex, Ontario, Canada: part of the late volcanic phase of the Blake River Group, Abitibi Subprovince. Economic Geology, 103, 1219-1241.

Percival, J., Mortensen, J., Stern, R., Card, K., and Bégin, N., 1992. Giant granulite terranes of northeastern Superior Province: the Ashuanipi complex and Minto block: Canadian Journal of Earth Sciences, 29, 2287-2308.

Percival, J., Sanborn-Barrie, M., Skulski, T., Stott, G., Helmstaedt, H., and White, D., 2006. Tectonic evolution of the western Superior Province from NATMAP and Lithoprobe studies. Canadian Journal of Earth Sciences, 43, 1085-1117.

Percival, J.A., Skulski, T., Sanborn-Barrie, M., Stott, G.M., Leclair, A.D., Corkery, M.T., and Boily, M., 2012. Geology and tectonic evolution of the Superior Province, Canada. In Tectonic Styles in Canada: The LITHOPROBE Perspective. Geological Association of Canada, Special Paper 49, 321–378.

Perugini, D., and Poli, G., 2012. The mixing of magmas in plutonic and volcanic environments: Analogies and differences. Lithos, 153, 261–277.

Piercey, S.J., 2010. An overview of petrochemistry in the regional exploration for volcanogenic massive sulphide (VMS) deposits. Geochemistry: Exploration, Environment, Analysis, 10, 119–136.

Piercey, S.J., 2011. The setting, style, and role of magmatism in the formation of volcanogenic massive sulfide deposits. Mineralium Deposita, 46, 449-471.

Piercey, S.J., Chaloux, E.C., Péloquin, A.S., Hamilton, M.A. and Creaser, R.A., 2008. Synvolcanic and younger plutonic rocks from the Blake River Group: Implications for regional metallogenesis. Economic Geology, 103,1243-1268.

Piercey, S. J., Peter, J. M. and Herrington, R.J., 2015. Zn-rich volcanogenic massive sulphide (VMS) deposits. Current perspectives on zinc deposits, 37-57.

Piercey, S. J., Hinchey, J.G. and Sparkes, G.W., 2023. Volcanogenic massive sulfide (VMS) deposits of the Dunnage Zone of the Newfoundland Appalachians: setting, styles, key advances, and future research. Canadian Journal of Earth Sciences, 60, 1104-1142.

Pilote, P., McNicoll, V., Daigneault, R., and Moorhead, J., 2009. Géologie et nouvelles corrélations dans la partie ouest du Groupe de Malartic et dans le Groupe de Kinojévis, Québec. Ministère de l'Énergie et des Ressources naturelles, Québec. Report number: MB 2009-09, 55-60.

Polat, A., and Kerrich, R., 2001. Magnesian andesites, Nb-enriched basalt-andesites, and adakites from late-Archean 2.7 Ga Wawa greenstone belts, Superior Province, Canada: implications for late Archean subduction zone petrogenetic processes: Contributions to Mineralogy and Petrology, 141, 36-52.

Poulsen, K.H., 2017. The Larder Lake-Cadillac Break and Its Gold Districts. In: Monecke, T., Mercier-Langevin, P., Dubé, B. (eds). Archean base and precious metal deposits, southern Abitibi greenstone belt, Canada. Reviews in Economic Geology, 19, 133–167.

Poulsen, K.H., Robert, F., and Dubé, B., 2000. Geological classification of Canadian gold deposits. Geological Survey of Canada. Bulletin 540.

Powell, W.G., Carmichael, D.M. and Hodgson, C.J., 1995. Conditions and timing of metamorphism in the southern Abitibi greenstone belt, Quebec. Canadian Journal of Earth Sciences, 32, 787-805.

Puchtel, I.S., Walker, R.J., Brandon, A.D., and Nisbet, E.G., 2009. Pt–Re–Os and Sm–Nd isotope and HSE and REE systematics of the 2.7Ga Belingwe and Abitibi komatiites. Geochimica Et Cosmochimica Acta, 73, 6367–6389.

Rogers, R., Ross, P. -S., Goutier, J., and Mercier-Langevin, P., 2014. Using physical volcanology, chemical stratigraphy, and pyrite geochemistry for volcanogenic massive sulfide exploration: An example from the Blake River Group, Abitibi Greenstone Belt. Economic Geology, 109, 61-88.

Rollinson, H., and Pease, V., 2021. Using Geochemical Data. Cambridge University Press.

Ross, P.-S., and Bédard, J.H., 2009. Magmatic affinity of modern and ancient subalkaline volcanic rocks determined from trace-element discriminant diagrams. Canadian Journal of Earth Sciences, 46, 823–839.

Ross, P.-S., and Mercier-Langevin, P., 2014. Igneous rock associations 14. The volcanic setting of VMS and SMS deposits: A review. Geoscience Canada, 41, 365-377.

Ross, P.-S., Goutier, J., Mercier-Langevin, P., and Dubé, B., 2011a. Basaltic to andesitic volcaniclastic rocks in the Blake River Group, Abitibi Greenstone Belt: 1. Mode of emplacement in three areas. Canadian Journal of Earth Sciences, 48, 728-756.

Ross, P.-S., McNicoll, V., Goutier, J., Mercier-Langevin, P., and Dubé, B., 2011b. Basaltic to andesitic volcaniclastic rocks in the Blake River Group, Abitibi Greenstone Belt: 2. Origin, geochemistry, and geochronology. Canadian Journal of Earth Sciences, 48, 757-777.

Ross, P.-S., McNicoll, V. J., Debreil, J. A. and Carr, P., 2014. Precise U-Pb geochronology of the Matagami mining camp, Abitibi greenstone belt, Quebec: Stratigraphic constraints and implications for volcanogenic massive sulfide exploration. Economic Geology, 109, 89-101.

Scott, C.R., Mueller, W.U., and Pilote, P., 2002. Physical volcanology, stratigraphy, and lithogeochemistry of an Archean volcanic arc: evolution from plume-related volcanism to arc rifting of SE Abitibi Greenstone Belt, Val d'Or, Canada: Precambrian Research, 115, 223-260.

Shanks, W.C., and Thurston, R., 2012. Volcanogenic massive sulfide occurrence model. U. S. Geological Survey. Report number: 2010–5070—C.

SIGEOM 2022. Système d'information géominière (SIGEOM). http://sigeom.mines.gouv.qc.ca. [Accesed July 30, 2022]

Sinclair, W.D., 1971. A volcanic origin for the No. 5 zone of the Horne mine, Noranda, Quebec. Economic Geology, 66, 1225-1231.

Sisson, T.W., and Grove, T.L., 1993. Experimental investigations of the role of H2O in calc-alkaline differentiation and subduction zone magmatism. Contributions to Mineralogy and Petrology, 113, 143-166.

Smith, I.E.M., 1980. Geochemical evolution in the Blake River Group, Abitibi greenstone belt, Superior province. Canadian Journal of Earth Sciences, 17, 1292-1299.

Smith, R.S., Naghizadeh, M., Cheraghi, S., Adetunji, A., Vayavur, R., Eshaghi, E., Hill, G.J., Snyder, D., Roots, E.A., Justina, F.D., and Fam, H.J.A., 2023. Geophysical transects in the Abitibi greenstone belt of Canada from the mineral-exploration-oriented Metal Earth project. The Leading Edge, 42, 245-255.

Smithies, R.H., Champion, D.C., and Van Kranendonk, M.J. 2009. Formation of Paleoarchean continental crust through infracrustal melting of enriched basalt. Earth and Planetary Science Letters, 281, 298-306.

Sobolev, A.V., Asafov, E.V., Gurenko, A.A., Arndt, N.T., Batanova, V.G., Portnyagin, M.V., Garbe-Schönberg, D., and Krasheninnikov, S.P., 2016. Komatiites reveal a hydrous Archaean deep-mantle reservoir. Nature, 531, 628–632.

Sobolev, S.V., Sobolev, A.V., Kuzmin, D.V., Krivolutskaya, N.A., Petrunin, A.G., Arndt, N.T., Radko, V.A. and Vasiliev, Y.R., 2011. Linking mantle plumes, large igneous provinces and environmental catastrophes. Nature, 477, 312-316.

Sossi, P.A., Eggins, S.M., Nesbitt, R.W., Nebel, O., Hergt, J. M., Campbell, I.H., O'Neill, H.C., Van Kranendonk, M., and Davies, D.R., 2016. Petrogenesis and geochemistry of Archean komatiites. Journal of Petrology, 57, 147–184.

Sparks, R.S.J., and Marshall, L.A., 1986. Thermal and mechanical constraints on mixing between mafic and silicic magmas. Journal of Volcanology and Geothermal Research, 29, 99-124.

Spera, F.J., Schmidt, J.S., Bohrson, W.A., and Brown, G.A., 2016. Dynamics and thermodynamics of magma mixing: Insights from a simple exploratory model. American Mineralogist, 101, 627–643.

Spooner, E.T.C., and Bray, C.J., 1977. Hydrothermal fluids of seawater salinity in ophiolitic sulphide ore deposits in Cyprus. Nature, 266, 808-812.

Sproule, R.A., Lesher, C.M., Ayer, J. A., Thurston, P. C., and Herzberg, C. T., 2002. Spatial and temporal variations in the geochemistry of komatiites and komatiitic basalts in the Abitibi greenstone belt. Precambrian Research, 115, 153-186.

Sterckx, S., 2018. Géochimie des roches volcaniques archéennes du Groupe de Blake River, ceinture de roches vertes de l'Abitibi, Québec. MSc thesis, Institut national de la recherche Scientifique.

Stewart, M. S., Hannington, M. D., Emberley, J., Baxter, A.T., Krätschell, A., Petersen, S., Brandl, P.A., Anderson, M.O., Mercier-Langevin, P., Mensing, R., Breker, K., and Fassbender, M. L.,

2022. A new geological map of the Lau Basin (southwestern Pacific Ocean) reveals crustal growth processes in arc-backarc systems. Geosphere, 18, 910-943.

Sun, S.S., and McDonough, W.F., 1989. Chemical and isotopic systematics of oceanic basalts: implications for mantle composition and processes. Geological Society, London, Special Publications, 42, 313-345.

Sun, G., Liu, S., Cawood, P.A., Tang, M., van Hunen, J., Gao, L., Hu, Y. and Hu, F., 2021. Thermal state and evolving geodynamic regimes of the Meso-to Neoarchean North China Craton. Nature Communications, 12, article 3888.

Sutton, J., Gibson, H., and Jorgensen, T., 2017. Volcanic stratigraphy and intrusions in the Renault–Dufresnoy and Duprat–Montbray formations: implications for metal endowment in the lower Blake River group, Rouyn-Noranda, Quebec. Mineral Exploration Research Centre. Report: MERC-ME2017-011.

Thurston, P.C., 2015. Igneous Rock Associations 19. Greenstone Belts and Granite-Greenstone Terranes: Constraints on the Nature of the Archean World. Geoscience Canada, 42, 437-484.

Thurston, P.C., Ayer, J.A., Goutier, J., and Hamilton, M.A., 2008. Depositional gaps in Abitibi greenstone belt stratigraphy: A key to exploration for syngenetic mineralization. Economic Geology, 103, 1097-1134.

Tourigny, G., Hubert, C., Brown, A.C. and Crépeau, R., 1988. Structural geology of the Blake River Group at the Bousquet mine, Abitibi, Quebec. Canadian Journal of Earth Sciences, 25, 581-592.

Vite-Sánchez, O., Ross, P. -S., and Mercier-Langevin, P., 2024. Mafic to intermediate volcanic rocks of the Blake River Group, Abitibi greenstone belt, Canada: Geochemistry, petrogenesis and relation with VMS deposits. Precambrian Research, 404, article 107331.

Vite-Sánchez, O., Ross, P. -S., Mercier-Langevin, P. and Iles, K., 2025. Petrogenetic insights on the largest volcanic pulse in the Archean Abitibi greenstone belt, Canada: the Stoughton-Roquemaure assemblage. Canadian Journal of Earth Sciences, 62, 1515-1536.

Walter, M.J., 1998. Melting of garnet peridotite and the origin of komatiite and depleted lithosphere. Journal of Petrology, 39, 29-60.

Winchester, J.A., and Floyd, P.A., 1977. Geochemical discrimination of different magma series and their differentiation products using immobile elements. Chemical Geology, 20, 325-343.

Wyman, D.A., 1999. A 2.7 Ga depleted tholeiite suite: evidence of plume-arc interaction in the Abitibi greenstone belt, Canada. Precambrian Research, 97, 27-42.

Wyman, D. and Kerrich, R., 2009. Plume and arc magmatism in the Abitibi subprovince: implications for the origin of Archean continental lithospheric mantle. Precambrian Research, 168, 4-22.

Wyman, D., and Kerrich, R., 2010. Mantle plume–volcanic arc interaction: consequences for magmatism, metallogeny, and cratonization in the Abitibi and Wawa subprovinces, Canada. Canadian Journal of Earth Sciences, 47, 565-589.

Wyman, D.A., Kerrich, R. and Polat, A., 2002. Assembly of Archean cratonic mantle lithosphere and crust: plume–arc interaction in the Abitibi–Wawa subduction–accretion complex. Precambrian Research, 115, 37-62.

Yergeau, D., Mercier-Langevin, P., Dubé, B., Malo, M., and Savoie, A., 2022a. The Westwood deposit, southern Abitibi greenstone belt, Canada: An Archean Au-rich polymetallic magmatic-hydrothermal system – Part I. Volcanic architecture, deformation, and metamorphism. Economic Geology, 117, 545-575.

Yergeau, D., Mercier-Langevin, P., Dubé, B., McNicoll, V., Jackson, S., Malo, M., and Savoie, A., 2022b. The Westwood deposit, southern Abitibi greenstone belt, Canada: An Archean Au-rich polymetallic magmatic-hydrothermal system – Part 2. Hydrothermal alteration, mineralization, and geological model. Economic Geology, 117, 577-608.

Zhang, Q., Machado, N., Ludden, J.N. and Moore, D. 1993. Geotectonic constraints from U-Pb ages for the Blake River Group, the Kinojevis Group and the Normétal Mine area, Abitibi, Quebec. Geological Association of Canada–Mineralogical Association of Canada. Annual Meeting, program with Abstracts, 18, 114.

Zimmer, M.M., Plank, T., Hauri, E. H., Yogodzinski, G.M., Stelling, P., Larsen, J., and Nye, C. J., 2010. The role of water in generating the calc-alkaline trend: new volatile data for Aleutian magmas and a new tholeiitic index. Journal of Petrology, 51, 2411-2444.